Universidade do Minho
Escola de Engenharia

Ana Vanessa Fernandes Ferreira

Monitoring Human Neutrophil Elastase (HNE) in chronic wounds

março de 2018

Ana Vanessa Fernandes Ferreira **Monitoring Human Neutrophil Elastase (HNE) in chronic wounds**

UMinho|2018

SEVENTH FRAMEWORK PROGRAMME
InFact
TecMinho
CENTRE OF BIOLOGICAL ENGINEERING
FCT Fundação para a Ciência e a Tecnologia
LUSO-AMERICAN FOUNDATION

Universidade do Minho
Escola de Engenharia

Ana Vanessa Fernandes Ferreira

Monitoring Human Neutrophil Elastase (HNE) in chronic wounds

Tese de Doutoramento em Engenharia Química e Biológica

Trabalho efetuado sob a orientação do
Professor Doutor Artur Cavaco Paulo
e da
Doutora Joana Marques da Cunha

março de 2018

DECLARAÇÃO

Nome:
Ana Vanessa Fernandes Ferreira

Endereço eletrónico: anavfferreira@gmail.com

Título da Tese de Doutoramento:
Monitoring Human Neutrophil Elastase (HNE) in chronic wounds

Orientadores:
Professor Doutor Artur Cavaco Paulo
Doutora Joana Marques da Cunha

Ano de conclusão: 2018

Designação do Doutoramento:
Programa Doutoral em Engenharia Química e Biológica

DE ACORDO COM A LEGISLAÇÃO EM VIGOR, NÃO É PERMITIDA A REPRODUÇÃO DE QUALQUER PARTE DESTA TESE/TRABALHO

Universidade do Minho, 29/03/2018

Assinatura: Ana Vanessa Fernandes Ferreira

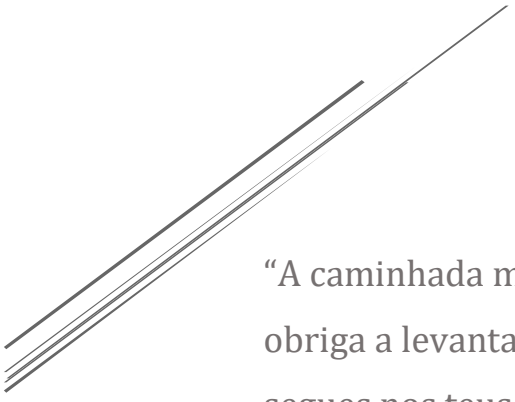
STATEMENT OF INTEGRITY

I hereby declare having conducted my thesis with integrity. I confirm that I have not used plagiarism or any form of falsification of results in the process of the thesis elaboration. I further declare that I have fully acknowledged the Code of Ethical Conduct of the University of Minho.

University of Minho, 29/03/2018

Full name: Ana Vanessa Fernandes Ferreira

Signature: Ana Vanessa Fernandes Ferreira



"A caminhada mais difícil não é a que te obriga a levantar o pó da estrada, mas a que segues nos teus sonhos."– **Luís Ferreira**

À minha avó

À minha família

The research described in this thesis was done within the Bioprocess and Bionanotechnology Research Group, Centre of Biological Engineering, University of Minho,Portugal.

This research was financially supported by the European project INFACT – Functional materials for fast diagnosis of wound infection (FP7-NMP-2013-SME-7 - Grant agreement no. 604278). Financial support was also given by the Portuguese Foundation for Science and Technology (FCT) through the Ph.D. grant SFRH/BD/113247/2015.



AGRADECIMENTOS

Esta tese representa uma etapa na minha vida profissional, mas também a nível pessoal. Todo este desafio não seria possível sem a colaboração das pessoas que me ajudaram a concretizá-lo, que me acompanharam e encorajaram ao longo deste percurso.

Começo por agradecer ao meu supervisor, Professor Dr. Artur Cavaco Paulo, pela oportunidade de ingressar em doutoramento e neste projeto de investigação, por ter confiado e acreditado nas minhas capacidades e no meu potencial. Pelo seu apoio e incentivo nestes anos. Estou muito grata pela oportunidade de ter participado num projeto europeu (INFACT) com um impacto tão importante para a sociedade. A oportunidade de estar envolvida neste projeto deu-me uma visão mais definida da investigação, não só em relação à investigação que se faz a nível europeu mas também em termos empresariais e industriais. Obrigado a todos os parceiros do projeto, pelas reuniões e discussão de ideias, pelo convívio e pelo reconhecimento das minhas capacidades. Obrigada pela oportunidade em participar em reuniões e conferências científicas, onde pude apresentar o meu trabalho e discutir ideias com excelentes investigadores com backgrounds científicos, e pelo privilégio em conhecer outros lugares e outras culturas, cujas experiências estarão sempre presentes comigo.

Obrigada à Fundação para a Ciência e Tecnologia e à Tecminho pelo financiamento da minha bolsa de doutoramento (SFRH/BD/113247/2015). Ao projeto da comissão europeia INFACT (FP7-NMP-2013-SME-7 - Grant agreement no. 604278) e à Tecminho pelo financiamento do meu trabalho. À Fundação Luso-americana para o Desenvolvimento (FLAD) pela bolsa de participação em conferências internacionais nos EUA. Obrigada à instituição de investigação Centro de Engenharia Biológica, bem como à Universidade do Minho, Escola de Engenharia e Departamento de Engenharia Biológica por proporcionar as condições necessárias e apoio ao desenvolvimento do meu trabalho.

Quero agradecer de forma muito especial, à minha orientadora, Dra. Joana Cunha, pelo apoio constante na orientação deste projeto, pela disponibilidade e ajuda. Obrigada por todos os conselhos, pela companhia nas viagens, pelas conversas e partilha de experiências, que me ajudaram e ajudarão no futuro. A forma como te dedicas ao trabalho, o teu espirito crítico, a forma como procuras as respostas sem nunca desistir deram-me um rumo ao longo deste trabalho que irei usar ao longo da minha vida.

À Dra. Teresa Matamá, pelo suporte e apoio na integração em biologia molecular. Obrigada pelas vezes em que ficávamos a trocar ideias, pelos conselhos e dicas. Mas principalmente obrigada pela compreensão e pela motivação constante.

Ao Dr. Artur Ribeiro, pelos conselhos e apoio técnico da sua especialidade, pelo seu apoio e orientação no fim deste trabalho. Obrigada pelas tuas sugestões, contributos essenciais e discussão de ideias que estiveram presentes no percurso deste trabalho.

Ao José Egipto, pelo seu trabalho em dinâmica molecular. Obrigada pela paciência e boa disposição. Obrigada pelo teu contributo com as simulações, tendo-me ajudado a entender mais o meu trabalho, e a permitir uma melhor discussão.

Não podia deixar de agradecer a todas as pessoas do meu grupo de trabalho de investigação Bioprocessos e Bionanotecnologia (BBRG), aos meus colegas da Plataforma de Biologia Molecular Sintética (PBMS) e a todas as pessoas do Departamento de Engenharia Biológica que contribuíram de alguma forma a este trabalho. Um agradecimento especial à Débora e à Carla, que me receberam muito bem na plataforma, e que junto com a Diana e a Sara, ajudaram-me a ambientar no DEB. Obrigada a todos os membros do meu laboratório pelo companheirismo e apoio científico. Em especial, ao Bruno, à Cristiana, à Diana, à Joana, à Teresa, à Célia, ao Nuno, ao Zé, à Tarsila, à Maritza e à Catarina, obrigada pelas conversas, pelos bolos e pães, pelos almoços e lanches, por ajudarem-me a espairecer e a manter sempre o ânimo. Obrigada a todos os meus colegas BBRG por contribuírem para um excelente ambiente de trabalho, profissional, empenhado, mas também divertido, permitindo-me sempre estar "à vontade" no trabalho.

Obrigada a todos os membros do Braga Toastmasters que me acompanharam e incentivaram nestes anos. Obrigada pela amizade, pelo improviso, pelas conversas e motivação constante. Embora agora tenha pouca oportunidade em estar presente nas nossas sessões, todos os momentos e as aprendizagens ficaram sempre comigo.

A todos os meus amigos, pela amizade e apoio durante estes anos. Obrigada por toda a saga que passamos juntos, por todas as histórias que davam muitos livros. Obrigada à Xana, ao Mário, ao Rui, à Luísa, à Sara, à Cláudia, à Joana, à Elísia, à Cristina, ao Pedro, ao Ruben, à Andreia, à Bete, à Débora, ao Rui, à Diana, ao Paulo, pelos risos e momentos divertidos, pelos desabafos, por me ajudarem a viver além do trabalho, por me chamarem à atenção, pelos conselhos, por tudo; em geral, por me aturarem todos estes anos. Obrigado a todos aqueles que embora não tenhamos tanto contacto como gostaríamos estiveram sempre presentes comigo. Obrigada por

todo o carinho e paciência, por me ajudarem nos momentos mais difíceis, e por serem a razão de muitos momentos de felicidade.

Agradeço imenso à minha família, aos meus maravilhosos pais e à minha querida irmã, por todo o apoio, paciência e amor incondicional. Obrigada por me incentivarem a querer sempre mais e a dar sempre o meu melhor. Pai, obrigada pelos conselhos e pelos valores que me transmitiste. Os teus pilares de Humildade, Honestidade e Perseverança permanecerão sempre na minha vida. Obrigada mãe, por eu ser a tua imagem, quer qualidades quer defeitos, não poderia ter escolhido melhor modelo a seguir. Que eu seja a combinação dos dois, mas versão 2.0, com algumas correções de bugs. À minha cara-metade, à minha maravilhosa irmã, obrigada por toda a tua forma de ser. Obrigada mesmo quando me chateias e pedes coisas, e que nos momentos mais importantes estás sempre lá e dizes as coisas mais acertadas e pertinentes. Obrigada por veres sempre o melhor de mim, que também eu tenho muito orgulho em ti. Vocês são as pessoas mais importantes da minha vida, sempre estiveram do meu lado. Tudo o que que fiz, faço e que farei foi graças a vocês, e por essa razão dedico-vos este trabalho. À minha madrinha, aos meus tios, primos e avós pela preocupação e dedicação, por me acompanharem sempre e estarem sempre presentes quando preciso.

Um muito obrigado a todas as pessoas que de alguma forma contribuíram para esta etapa, quer estejam já presentes ou não. Todos os momentos, nestes últimos quatro anos, ficaram-me sempre marcados, os bons e os maus, porque sem eles não seria quem sou hoje.

Muito obrigada de todo o coração!

"Para muitos será uma mão a apontar o céu, mas eu sei que estás a tentar apanhar uma estrela." – **Luís Ferreira**

ABSTRACT

Monitoring Human Neutrophil (HNE) in chronic wounds

The inflammatory response is an important step in wound healing, however if there is an imbalance between the immune response and tissue regeneration, a delay on the healing process will occur, resulting in a chronic wound. Chronic wounds are a significant problem for health care system, accounting for almost 4% of its total budget, and currently increasing. Early detection of incipient wound infection and chronic inflammation reduces the severity of the disease and decreases health care expenses. Currently, it is difficult, expensive and time consuming to accurately assess a wound status, hence, there is an urgent need for a new diagnostic that would give the medical staff a fast and reliable method to determine inflammation/infection of a chronic wound at an early stage. Human neutrophil elastase (HNE) is one of the most abundant proteinases in wounds and its activity was found to be elevated in case of infection and chronic inflammation, making this enzyme a suitable marker for impaired healing.

This PhD thesis intends to explore new strategies for the detection of HNE through the development of chromogenic and fluorogenic sensors that when embedded in a dressing may provide an *in situ* and real-time assessment of the wound status. For that, a specific cleavage sequence for HNE was designed by molecular docking studies and then confirmed *in vitro*. Then, this substrate was associated to chromogenic or fluorogenic detection systems.

Regarding the chromogenic detection systems, two strategies were followed using ultramarine (UM), a GFP-like chromoprotein. The rationale of this approach was to use this protein's ability to regenerate its dark blue colour (hysteresis) upon HNE cleavage, turning it into a switch-on sensor, or to lose its colour upon proteolysis, thus making a switch-off sensor.

In a first attempt to convert ultramarine into a HNE substrate switch was based on a split protein strategy which would signal as a gain of colour sign. We were able to detect an absorbance increase upon HNE cleavage, but this effect was not long lasting due to an instability of the interaction between the signalling and sensing fragments. Indeed, this strategy proved it to be extremely challenging. The main motivation to pursue this work resided in its innovative aspect, as GFP-like chromogenic sensors were never reported. Then, a second strategy was investigated through site-directed mutagenesis of ultramarine. In this latter strategy we were able to obtain sensors with an opposite signal, switch-off. To provide a better understanding regarding UM's chromogenic environment, molecular dynamics studies coupled to protein expression were implemented to each

of the seven produced UM-mutants. Our findings provided new information regarding the effect of certain mutations in UM protein conformation and allowed us to explore its application as a switch sensor. Here, we explored for the first time the development of a colour switch-on sensor based on chromogenic GFP-like proteins. Even though, we were unable to fully accomplish the regeneration of a stable chromophore environment for colour appearance, this work may serve as a starting point for advances in switch-on chromogenic sensors using non-fluorescent GFP-like proteins.

For the fluorogenic detection system, the strategy studied resulted in the successful development of a FRET (Förster resonance energy transfer) peptide to monitor HNE. Upon HNE action, this peptide proved to be more effective than the traditional peptides coupled to fluorophores. Its visual detection was possible using an UV-portable light source. The embedding of this sensor in dressings would provide advantages for its application as a wearable sensor. The methods here used for the FRET-peptide immobilization onto a dressing compromised its detection. However, we envision that with the proper method of integration into a dressing, this FRET peptide could be used as a new strategy of smart materials.

The strategies explored in this thesis can be further investigated and possibly implemented as point-of-care medical devices for wound control. As wound care tools, these devices would allow a prompt detection of chronic wounds, contributing to their proper and effective care and, consequently, granting a better outcome for the millions of people that suffer from non-healing wounds.

RESUMO

Monitorização Elastase neutrofílica humana em feridas crónicas

A resposta inflamatória é um importante passo no processo de cicatrização de feridas. No entanto, desequilíbrios entre a resposta do sistema imunitário e a regeneração celular podem desencadear um atraso significativo no processo de cicatrização, resultando numa ferida crónica. As feridas crónicas apresentam um problema significativo para o sistema de saúde, contabilizando 4% do orçamento total de saúde, sendo que se estima um aumento destes números nas próximas décadas. A deteção antecipada de infeção e inflamação crónica numa ferida reduz a severidade da doença, consequentemente diminuindo o seu impacto nas despesas de saúde. Atualmente, a avaliação do estado de uma ferida de forma exata e precisa é um processo difícil, dispendioso e demoroso. Por esta razão, existe uma necessidade urgente de desenvolvimento de novas ferramentas de diagnóstico que possibilitem a deteção precoce de infeção/inflamação em feridas crónicas de forma rápida e eficaz. A elastase neutrofílica humana (HNE) é uma das proteinases mais abundantes em feridas, estando os seus elevados níveis de atividade em feridas correlacionados com a ocorrência de infeção e inflamação crónica. De facto, esta enzima é considerada um excelente biomarcador para feridas cujo processo de cicatrização se encontra comprometido.

O objetivo principal desta tese de doutoramento foi e exploração de novas estratégias para a deteção da HNE através do desenvolvimento de sensores cromogénicos e fluorogénicos que possam ser incorporados em pensos para feridas, possibilitando uma avaliação *in situ* e em tempo-real do estado da ferida. Para tal, primeiramente desenharam-se sequências de clivagem específicas para HNE cuja afinidade para a enzima foi analisada através de estudos de acoplamento molecular e posteriormente foram confirmados com ensaios *in vitro*. Depois, o substrato foi associado a sistemas de deteção cromogénico ou fluorogénico.

Relativamente aos sistemas de deteção cromogénicos, desenvolveram-se duas estratégias usando a ultramarina (UM), uma cromoproteína do tipo GFP, como substrato sinalizador. A competência desta proteína em regenerar a sua cor azul (devido à capacidade de histerese) permitiu transformá-la num sensor que se liga (switch-on) ou que se desliga (switch-off) após a sua clivagem com a HNE. A primeira tentativa para converter a proteína ultramarina num substrato comutador de sinal para a HNE consistiu na produção de uma proteína segmentada em duas partes que quando em interação resultam num sinal com ganho de cor (sensor switch-on). Após

clivagem com HNE do fragmento substrato, conseguiu-se obter um aumento da absorvância, embora transiente, devido à interação com o fragmento sinalizador. De facto, esta estratégia foi muito desafiante. No entanto, a principal motivação em seguir esta linha de trabalho prendeu-se principalmente com o seu carácter inovador, visto que nunca tinham sido reportados sensores usando proteínas cromogénicas do tipo GFP.

Neste seguimento, explorou-se uma segunda estratégia para o desenvolvimento de substratos sensores switch-on para a HNE através da mutagénese direcionada da proteína ultramarina. Esta abordagem permitiu também obter sensores com o sinal oposto – switch-off. Com o objetivo de melhor compreender as condições que proporcionam o ambiente cromogénico da proteína UM, foram implementados estudos de simulação de dinâmica molecular complementares à expressão das proteínas para cada um dos sete mutantes produzidos. A partir deste trabalho conseguiu-se recolher novos dados acerca do efeito de certas mutações na conformação da proteína UM e possibilitou-nos também explorar a sua aplicação como sensor comutador de sinal.

Nestes trabalhos investigou-se pela primeira vez o desenvolvimento de sensores cromogénicos switch-on baseados em proteínas do tipo GFP. Embora não se tenha conseguido obter a regeneração estável do cromóforo que permite o aparecimento de cor, estes resultados poderão servir como ponto de partida para outros trabalhos em sensores cromogénicos switch-on usando proteínas não fluorescentes do tipo GFP.

Em relação aos sistemas de deteção fluorogénicos, a abordagem explorada resultou no desenvolvimento bem-sucedido de um péptido FRET para monitorização de HNE. Após proteólise, este péptido provou ser mais eficaz do que os tradicionais péptidos fluorescentes (acoplados a fluoróforos). A deteção visual da fluorescência foi possível recorrendo a uma luz UV portátil. A incorporação deste sensor em pensos de feridas trará vantagens relativamente à sua aplicação como sensores *wearable*. Os métodos aqui descritos para a imobilização do péptido FRET em têxteis usados como material de penso comprometeram a deteção do seu sinal. No entanto, prevê-se que a utilização de um método de integração mais apropriado possa permitir a sua aplicação em novas estratégias no desenvolvimento de tecidos inteligentes.

A implementação da investigação aqui descrita em dispositivos médicos para a monitorização do processo de cicatrização de feridas poderá complementar o leque de ferramentas usadas no cuidado das feridas. Estes dispositivos possibilitarão a deteção atempada da cronicidade de uma ferida, contribuindo para o seu cuidado apropriado e eficaz. Consequentemente irá garantir uma melhor qualidade de vida para milhões de doentes que sofrem de feridas de difícil cicatrização.

KEY-WORDS

Wound care; Wound healing; Wound dressings; Chronic wounds; Human Neutrophil Elastase (HNE); Chromogenic sensors; Fluorogenic sensors; GFP-like proteins; Chromoproteins; Ultramarine; Förster resonance energy transfer (FRET).

PALAVRAS-CHAVE

Tratamento de feridas; Cicatrização de feridas; Pensos de feridas; Feridas crónicas, Elastase neutrofílica humana; Sensores cromogénicos; Sensores fluorogénicos; Proteínas tipo-GFP; Cromoproteína; Ultramarina; Transferência de energia por ressonância de Förster (FRET)

TABLE OF CONTENTS

AGRADECIMENTOS xi
ABSTRACT xv
RESUMO xvii
KEY-WORDS xix
PALAVRAS-CHAVE xix
TABLE OF CONTENTS xxi
LIST OF SYMBOLS AND ABBREVIATIONS xxv
LIST OF FIGURES xxix
LIST OF TABLES xxxi
MOTIVATION AND THESIS OUTLINE 1
Scope and objectives 1
Thesis layout 2
CHAPTER I. 5
Abstract 6
I. State-of-the-art in wound healing 7
I.1. Social and economic overview 7
I.2. Historical and clinical overview 9
I.3. Principles of wound healing process 11
Haemostasis – Fibrin clot formation 12
Inflammation – Tissue debridement and phagocytosis 13
Proliferation – Reepithelialisation, formation of granulation tissue and angiogenesis 16
Maturation and remodelling – Wound closure and scar tissue formation 18
I.4. Clinical assessment and its implications 19
I. 4.1. Acute and Chronic wounds 19
I. 4.2. Primary and secondary healing 24
I. 4.3. Clinical indicators of impaired wound healing 25
I. 4.3.1. Biological markers in the wound 27
a) Physiological biomarkers 28
Blood supply 28
Oxygen 29
Temperature and pH 29
Wound moisture (Exudate) 30
b) Histological markers 31

Wound closure and dimensions 31
ECM composition 31
Bioburden and Infection 32
c) Biochemical markers 33
Growth factors and cytokines 33
Proteases and other enzymes 34
I.4.3.2. Human Neutrophil Elastase (HNE) 38
I. 4.3.3.Current methods for biomarkers sensors 41
CHAPTER II. 45
II. HNE-specific chromogenic sensors 46
II. (a) 1. Design of a chromogenic HNE protease sensor based on split-GFP system 47
Abstract 47
II. (a) 1. Introduction 49
II. (a) 2. Materials and Methods 51
Materials and Reagents 51
Instrumentation 51
Methods 52
1. Protein expression and purification 52
2. Molecular docking simulation 53
3. Assessment of the UM-based split proteins as HNE protease sensor 53
II. (a) 3. Results 54
AAPV is the preferred peptide substrate for HNE by molecular docking analysis 54
Production of the split-UM sensor for HNE detection 56
Effect of HNE on split-UM strategy 57
II. (a) 4. Discussion 59
Selection of the sensing substrate to incorporate in HNE sensor 59
Evaluation of the split-UM sensor for HNE detection 61
Field of application 63
II. (a) 5. Supplementary Information 64
Experimental set-up and optimization of the expression of ultramarine (UM) 64
Brief overview on strategies for improving protein solubility applied to UM10 and UM10E11 proteins 65
Optimized protocol for the expression of UM, UM10, E11 and UM10E11 proteins 68
Overview of the HNE recognition sites and active-site 69
Control assay of UM protein with HNE enzyme 70

Investigation of the possible cleavage of UM protein by HNE enzyme, using ExPASy Peptide Cutter software 70

Development of a split-fused UM strategy, based on the UM10E11 recombinant protein 71

II. (b) 2. Model substrates based on ultramarine GFP-like chromoprotein for elastase sensors 73

Abstract 73

II. (b) 1. Introduction 75

II. (b) 2. Materials and Methods 77

Materials and Reagents 77

Instrumentation 77

Methods 77

1. Gene design 77

2. Protein expression and purification 79

3. Assessment of UM mutants as HNE protease sensor 79

4. Structural Bioinformatics 80

4.1. Homology modelling 80

4.2. Molecular dynamics (MD) 80

II. (b) 3. Results and Discussion 82

Overview of ultramarine's structure and site-directed mutagenesis 82

Structure prediction of UM mutants 84

Colour prediction of UM mutants 88

Expression of the designed HNE sensors 90

Switch-off and switch-on sensors in action 93

Understanding disarrangement or establishment of chromophore environment with molecular dynamics 95

II. (b) 4. Conclusion 99

II. (b) 5. Supplementary Information 101

CHAPTER III. 105

III. HNE-specific fluorogenic sensors 107

Abstract 107

III.1. Introduction 109

III.2. Materials and Methods 111

Materials 111

Instrumentation 113

Methods 113

1. HNE activity assessment 113

2. Characterization of synthetic and commercially available HNE substrates and sonochemical immobilization on wound dressings 113
3. Characterization of the FRET-peptides and chemical immobilization using GTA crosslinking 114
III.3. Results 115
In vitro characterization of commercially available fluorogenic HNE substrates sonochemically immobilized on wound dressings 115
In vitro characterization of FRET-peptides for HNE detection 117
In vitro characterization of EDANS/Dabcyl FRET-peptide for HNE detection chemically immobilized on wound dressings 119
III.4. Discussion 121
Analysis of the developed fluorogenic sensors for HNE detection. 121
Improvements and future prospects 124
III.5. Supplementary Information 127
CHAPTER IV. Conclusions 129
IV. Conclusions 131
IV.1. Final Remarks 131
Peptide design with specific HNE cleavage sequences 131
Chromogenic sensor for HNE based on UM-split 132
Chromogenic sensor for HNE based on UM-derived mutants 132
Fluorogenic sensor for HNE 133
IV.2. Future Perspectives 133
REFERENCES 135
APPENDIX 163
Scientific publications 165
Publications in Scientific Meetings 165
Poster Communications 166
Other Communications 166

LIST OF SYMBOLS AND ABBREVIATIONS

ΔG	total Gibbs binding free energy
λAbs_{max}	maximum Absorbance wavelength
λEm_{max}	maximum Emission wavelength
λEx_{max}	maximum Excitation wavelength

A

a.a.	amino acid
a.u.	arbitrary unit
Abs	absorbance
AFC	7-amino-4-ethylcoumarin
AIDS	acquired immunodeficiency syndrome
Ala or A	alanine (a.a.)
ALI	acute lung injury
AMC	7-amino-4-ethylcoumarin
ARDS	acute respiratory distress syndrome
Arg or R	arginine (a.a.)
Asn or N	asparagine (a.a.)
Asp or D	aspartic acid (a.a.)
AST	antibiotic susceptibility testing
AUC	area under the curve

B

bFGF	basic fibroblast growth factor
BPI	bactericidal permeability-increasing proteins
BSA	bovine serum albumin

C

CAP37	cationic antimicrobial proteins of 37kDa
CFP	cyan fluorescent protein
CG	cathepsin G
CN	cyclic neutropenia
$C^{on\text{-}off}$	UM-mutant C designed for a switch-off approach
Cys or C	cysteine (a.a.)
COPD	chronic obstructive pulmonary disease
CP	chromoprotein
CTAB	hexadecyltrimethylammonium bromide
Cys or C	cysteine (a.a.)

D

Dabcyl	4-([4'-dimethulamino)phenyl]azo)benzoyl
DNA	deoxyribonucleic acid

E

E11	11th β-strand of UM protein engineered in an eglin c protein with an HNE cleavage sequence
ECM	extra-cellular matrix
EDANS	*N*-(aminoethyl)-5-naphthalenamine-1-sulfonic acid
EGF	epidermal growth factor
EI	electrospray ionization
ELISA	enzyme-linked immunosorbent assay

F

FAM	5(6)-carboxyfluorescein
FGF	fibroblast growth factor
$F_{on\text{-}off}$	UM-mutant F designed for a switch-off approach
FP	fluorescent protein
FRET	Förster resonance energy transfer

G

GFP11	11th β-strand of GFP protein
GFP1-10	GFP protein engineered without the last 11th β-strand
GFP	green fluorescent protein, isolated from the jellyfish *Aequorea victoria*
Glu or E	glutamic acid (a.a.)
Glp-PV-pNA	pyroglutamate-proline-valine-*p*-nitroaniline
Gly or G	glycine (a.a.)
Gln or Q	glutamine (a.a.)
GTA	glutaraldehyde

H

HAI	hospital-acquired infection
HBO	hyperbaric oxygen
HEPES	4-(2-hydroxyethyl)-1-piperazineethanesulfonic acid
His or H	histidine (a.a.)
HIV	human immunodeficiency virus
HLE	human leukocyte elastase
HNE	human neutrophil elastase
HNPs	human neutrophil peptides
HRSEM	high resolution scanning electron microscope

I

IBs	inclusion bodies
IGF	insulin-like growth factor
IL	interleukin
Ile or I	isoleucine (a.a.)
IPTG	isopropyl-β-d-thiogalactopyranoside

K

kan	kanamycin
KGF	keratinocyte growth factor

L

LB	Luria-Bertani
LC-MS	liquid chromatography-mass spectrometry
Leu or L	leucine (a.a.)
Lys or K	lysine (a.a.)

M

MD	molecular dynamics
MeOSuc	*N*-methoxysuccinyl
Met or M	methionine (a.a.)
MM	molecular mechanics
MMP	matrix metalloproteinase
MPO	myeloperoxidase
MW	molecular weight
MWCO	molecular weight cut off

N

ND	not determined
NE	neutrophil elastase
NETs	neutrophil extracellular traps
NO	nitric oxide
NP	nanoparticle

O

OD	optical density

P

PDB	protein data bank
PDGF	platelet-derived growth factor
PA	polyamide
PEF	polyethylene glycol
pep1	synthetic peptide of the 11th β-strand of UM protein
Phe or F	phenylanine (a.a.)
pI	isoelectric point
PMN	polymorphonuclear neutrophils or leukocytes
*p*Na	*p*-nitroaniline
PR3	proteinase 3
Pro or p	proline (a.a.)
PS	pararosaniline hydrochloride

Q

QM	Quantum Mechanics

R

RMSD	root-mean-square deviation
RMSF	root-mean-square fluctuation
ROS	reactive oxygen species
RT	Room Temperature
Rtms5	GFP-like protein isolated from the reef coral *Montipora efflorescens*

S

SC	*stratum corneum*
SCN	severe congenital neutropenia
SDS	sodium dodecyl sulphate
SDS-PAGE	sodium dodecyl sulfate polyacrylamide gel electrophoresis
Ser or S	serine (a.a.)
split-fused	approach combining UM10 and E11 engineered in the same protein,
UM	UM10E11
split-UM	approach combining UM10 and E11 separated proteins
SUMO	small ubiquitin-like modifier

T

TB	terrific broth
TGF	transforming growth factor
Thr or T	threonine (a.a.)
TIME	tissue, infection/inflammation, moisture and edge
TNF	tumour necrosis factor
t-PA	tissue plasminogen activator
Tris	tris(hydroxymethyl)aminomethane
Trp or W	tryptophan (a.a)
TSF	elongation factor Ts
Tyr or Y	tyrosine (a.a.)

U

U	enzymatic activity unit
UM	ultramarine (UM), an engineered GFP-like protein derived from Rtms5
UM10	UM engineered without the last 11th β-strand
UM10E11	UM10 and E11 portions engineered in a same protein
u-PA	urokinase-type plasminogen activator

V

Val or V	valine (a.a.)
VEGF	vascular endothelial growth factor
VMD	visual molecular dynamics

Y

YFP	yellow fluorescent protein

LIST OF FIGURES

CHAPTER I

Figure I. 1. Representation of the approximated time scale of the wound healing process through the different phases and events. 11
Figure I. 2. Schematic representation of the phases of cutaneous wound healing 12
Figure I. 3. Inflammatory phas 14
Figure I. 4. Proliferation phase 16
Figure I. 5. Classification of ulcers according to the Wound Healing Society..... 20
Figure I. 6. Classification of the healing process. 24
Figure I. 7. Sequence of key-points and interventions for the assessment and management of wounds 26
Figure I. 8. Mechanisms used by neutrophils to control infection: phagocytosis, degranulation and release of neutrophil extracellular traps (NETs) 35
Figure I. 9. Secondary structure catalytic active-site of Human Neutrophil Elastase (HNE) protein. 39

CHAPTER II Subchapter (a)

Figure II. (a) 1. Graphical abstract of the subchapter.. 48
Figure II. (a) 2. Affinity of AAPV peptide to HNE.. 55
Figure II. (a) 3. Bacterial pellets after expression of UM, UM10 and E11 under the optimized laboratorial set-up. 56
Figure II. (a) 4. Efficiency of the split-UM system in detecting HNE and comparison with the mixture of UM10 with the synthetic peptide pep11, in molar ratios of 167:1 or 167:5..... 58

Supplementary Information of CHAPTER II Subchapter (a)

Figure II (a) S 1. Methods used to enhance the solubility of UM10 and UM10E11..... 66
Figure II (a) S 2. Optimized experimental set-up for the expression of split UM-based protein.68
Figure II (a) S 3. Map of the binding sites of HNE, presenting the key amino acids on recognition subsites. 69
Figure II (a) S 4. Absorbance spectrum and SDS-PAGE image of ultramarine before and after incubation with HNE 70
Figure II (a) S 5. Analysis using ExPASy Peptide Cutter software 70
Figure II (a) S 6. Split-fused strategy for HNE sensor..... 71

CHAPTER II Subchapter (b)

Figure II (b) 1. Graphical abstract of the subchapter 74
Figure II (b) 2. Secondary structure of ultramarine (UM) protein and its splay representation 83

Figure II (b) 3. Root-mean-square fluctuation (RMSF) analysis of ultramarine protein (UM) and the seven designed mutants (A-G) 85
Figure II (b) 4. Relative RMSF analysis of seven designed mutants (A-G), in relation to ultramarine protein, considering all residues, residues involved in the chromophore environment, or conserved residues 87
Figure II (b) 5. Expression profiles for ultramarine and the seven UM mutants. 91
Figure II (b) 6. Absorbance profile of UM mutants after incubation with HNE 92
Figure II (b) 7. HNE effect on switch-off and switch-on mutants 94
Figure II (b) 8. Relative RMSF analysis of mutant $C^{on\text{-}off}$ and mutant $F^{off\text{-}on}$ before and after cleavage, in relation to ultramarine, considering all residues, Residues involved in the chromophore environment and the conserved residues 95
Figure II (b) 9. Conformation of mutant $C^{on\text{-}off}$ and $F^{off\text{-}on}$, before and after cleavage. 98

Supplementary Information of CHAPTER II Subchapter (b)

Figure II (b) S 1. β-barrel conformation of each designed variant (A-G), aligned with the original ultramarine protein 102
Figure II (b) S 2. Absorbance spectra for ultramarine before and after addition of HNE..... 103

CHAPTER III

Figure III. 1. Graphical abstract of the chapter..... 108
Figure III. 2. Chemical reaction of the EDANS/Dabcyl FRET-peptide immobilization into a polyamide dressing..... 114
Figure III. 3. Visual assessment of the cotton dressing coated with the HNE substrates..... 115
Figure III. 4. Assessment of the sensitivity of the substrate MeOSuc-AAPV-AFC with different concentrations of HNE, and fluorescence intensity of the dressing material quantified in a fluorimeter..... 116
Figure III. 5. Fluorescence intensity of FAM/Dabcyl-peptide and EDANS/Dabcyl-peptide before and after incubation at 37°C with HNE..... 118
Figure III. 6. FRET-peptides FAM/Dabcyl and EDANS/Dabcyl solutions after incubation with HNE. 119
Figure III. 7. Visual assessment under white light of the resulted PA dressings after immobilization without GTA and with GTA, and under UV light 120

Supplementary Information of CHAPTER III

Figure III. S 1. E-SEM images of non-treated pristine cotton fabric and fabrics treated with ultrasonic waves to incorporate elastase substrate..... 127
Figure III. S 2. Fluorescence spectrum of FAM/Dabcyl-peptide and EDANS/Dabcyl-peptide. 128
Figure III. S 3. Emission spectrum of donor and excitation spectrum of the acceptor of FAM/Dabcyl and EDANS/Dabcyl FRET pairs. 128

LIST OF TABLES

CHAPTER I

Table I. I. Factors that might influence wound healing ability. 23
Table I. II. Biological functions of several enzymes released by neutrophils. 36
Table I. III. Summary of approaches developed to monitor HNE in the wound environment. .. 44

CHAPTER II Subchapter (a)

Table II. (a) I. Summary of the binding free energies involved in the interaction of the peptides with HNE's active site 54

Supplementary Information of CHAPTER II Subchapter (a)

Table II (a) S I. Optimization of culture medium, type and time of induction at 37°C 64
Table II (a) S II. Optimization of incubation temperature and evaluation of the effect of oxygen renewal on ultramarine expression 64
Table II (a) S III. Selection of the culture/flask volume ratio and aeration conditions for the production of dark blue-coloured UM protein 65

CHAPTER II Subchapter (b)

Table II (b) I. Rational for the design of the seven variants of UM with inserted HNE cleavage sequences. 78

Supplementary Information of CHAPTER II Subchapter (b)

Table II (b) S I. Residues involved in the chromophore and conserved residues in ultramarine protein. 101

CHAPTER III

Table III. 1. Chemical information of the used HNE substrates 112

MOTIVATION AND THESIS OUTLINE

Scope and objectives

The work of this PhD thesis was conducted within the project INFACT of the seven framework program of the European Union, which aimed to develop functional materials for fast and reliable diagnosis of wound inflammation/infection. Early detection of an emerging infection or/and of excessive inflammatory response allows the proper management of the wound, as it enables the timely initiation of a treatment strategy, and consequently reduces the severity of the disease. The target of the project was the development of sensors that would detect enzymes released by neutrophils, an immune response to infection, focusing namely on myeloperoxidase, lysozyme and elastase, as they have been reported as biomarkers for impaired healing. This PhD work is focused on the enzyme human neutrophil elastase (HNE), being reported as extremely active in infected wounds and reduced in healing wounds. As the development progresses, the embedding of chromogenic or fluorogenic sensors for HNE or other proteases activity into wearable dressing devices will allow *in situ* and real-time information about the wound status. By simple visualization of the dressing, the medical staff can make an informed decision and apply the most suitable action for proper wound healing.

In this PhD thesis two different detection systems were explored: (1) chromogenic sensors, and (2) fluorogenic sensors. In the first approach, the GFP-like chromoprotein ultramarine was converted into protease switches upon HNE activity; whereas in the second approach, a quencher and fluorophore molecules were paired on opposite ends (FRET) of a specific cleavage sequence for HNE.

The main focus points in this work are:

- Design of the HNE-specific cleavage sequence
- Association of the chromogenic or fluorogenic detection system to the HNE peptide cleavage sequence
- Experimental evaluation of the developed sensor (*in silico* and *in vitro*)
- Embedding of the developed sensor into a wound dressing material
- *In vitro* assessment of the developed sensor dressing as a diagnostic tool

Thesis layout

This thesis is divided into four chapters, being chapters II and III dedicated to reporting of the experimental work. The contents of each chapter are summarized below:

Chapter I. State of the Art in wound healing

The purpose of this chapter was to present a comprehensive overview of the wound healing process, chronic wounds and their current clinical assessment and management. An economic, social and clinical overview regarding wound care as well as some historical facts are presented. It is further explained how chronic wounds arise and how impaired healing can be evaluated and managed. Particular attention is given to the possible biomarkers that can be used for monitoring the wound status, focusing on the enzyme human neutrophil elastase (HNE). This chapter contextualizes the field of application of the subject of this thesis.

The review of these concepts is intended to be submitted for publication as two articles:

Ferreira, A. V., Cunha, J., Cavaco-Paulo, A. Principles of Chronic Wounds – a review.

Ferreira, A. V., Cunha, J., Cavaco-Paulo, A. Biomarkers in wound healing: diagnostics and theranostics.

Chapter II. HNE-specific chromogenic sensors

This chapter describes and exploits the development of chromogenic sensors based on the GFP-like chromoprotein ultramarine. The attempts to convert self-assembling of ultramarine into a HNE switch sensor followed two different strategies, being them reported as two subchapters. Subchapter II (a) presents the split-UM approach for a switch-on sensor and subchapter II (b) reports the development UM-derived mutants to obtain switch-on and switch-off sensors.

The results here described resulted in two articles corresponding to each subchapter:

Ferreira, A. V., Cunha, J., Antunes, E., Ribeiro, A., Matamá, T., Azoia, N., Cavaco-Paulo, A. Design of a chromogenic HNE protease sensor based on split-GFP system, in *Applied Microbiology and Biotechnology*, in submission.

Ferreira, A. V., Cunha, J., Antunes, E., Ribeiro, A., Cavaco-Paulo, A. Novel protease chromogenic sensors based on ultramarine mutants, in *Biomacromolecules*, submitted.

Chapter III HNE-specific fluorogenic sensors

A fluorogenic approach for monitoring HNE was also investigated, being the results presented on this chapter III. It explores the development of a wearable sensor dressing using peptides linked to a fluorophore or to a FRET quenching mechanism. Upon HNE action, the peptide cleavage leads to a fluorescence signal that can be easily detected on the dressing (*in situ*) using a portable UV-light source.

This chapter III is based on the following publication:

> **Ferreira, A. V.**, Perelshtein, I., Perkas, N., Gedanken, A., Cunha, J. and Cavaco-Paulo, A. (2015). Detection of human neutrophil elastase (HNE) on wound dressings as marker of inflammation, in *Applied Microbiology and Biotechnology*, doi: 10.1007/s00253-016-7889-6.

Chapter IV. Conclusions

Chapter IV contains a summarized discussion focused on the contributions of this work towards a better assessment and management of wounds. Brief suggestion for future directions and perspectives are also presented here, describing the work that could be carried out to complement this research.

References and Appendix sections

In the last pages of this thesis the references used along this dissertation are presented. The thesis ends with the appendix section that summarizes the efforts made in the dissemination of this work. It also includes a list of the author's publications in other related fields.

CHAPTER I.

State of the Art in Wound Healing

Abstract

Wound healing involves a complex and highly dynamic series of biological processes, in a series of co-ordinated events. However when disrupted, the wound fails to heal, giving rise to a chronic wound. Chronic wounds are a silent epidemic, representing a major health burden on society and a drain on resources. Management of chronic wounds remains challenging in terms of prevalence, complexity and assessment. Additionally, the lack of fundamental knowledge on the biological processes associated with chronic wounds further intensifies this problem.

Understanding the biochemical changes that occur within a chronic wound as well as development of new strategies for a suitable and effective management and assessment of the wound status may provide a solution, offering hope to patients suffering from this condition. Early recognition of a chronic wound allows a prompt and effective treatment in reducing the negative impacts of these conditions. Herein, we emphasized the need of new strategies for monitoring the wound status, specifically through the detection of Human Neutrophil Elastase (HNE).

Firstly, a brief social, economic, historical and clinical overview is presented on wound care. Then, it explores the general aspects of wound healing and the state-of-the-art on the assessment and management of wounds, including chronic wounds. It focuses essentially on the biological markers that could be used to detect impairing healing. This chapter I concludes with an overview of the current strategies of sensors for wound healing, focusing specifically on the monitoring of HNE.

This chapter is based on the following scientific papers:

Ferreira, A. V., Cunha, J., Cavaco-Paulo, A. Principles of Chronic Wounds – a review, to be submitted.

Ferreira, A. V., Cunha, J., Cavaco-Paulo, A. Biomarkers in wound healing: diagnostics and theranostics, to be submitted.

I. State-of-the-art in wound healing

I.1. Social and economic overview

In developed countries, it is estimated that 1-2% of the population might develop a problematic wound during their lifetime with prospected incidence increasing with age. In developing countries this percentage is likely to be even higher [1–5]. Wound care is a costly burden on society, accounting 4% of the total budget of the health care system worldwide with an annual incidence of 300 million acute wounds in Europe [1,6–8]. The cost burden of treating wounds is expected to rise due to the increasingly elderly population and incidence of obesity, vascular, diabetic and other diseases [1,6,9,10].

Chronic wounds are described as a silent epidemic, often masked and aggravated by comorbid diseases [2,5,6]. Wound care field is often neglected, being deprioritized over other diseases and disorders [5]. The fact that Wound Care is not a defined specialization (instead it is affiliated to several, dermatologists, podiatrists, endocrinologists, vascular surgeons, geriatricians, etc.), many times results in inadequate and inconsistent treatment and uncoordinated prevention, which further aggravates their incidence and prevalence [5]. Early detection of incipient chronic wound reduces the severity of the disease and decreases health care expenses [5,11]. It is estimated that adopting a strategy compiling best practice guidelines for management and prevention of chronic wounds, could reduce the costs of wound management up to 30% [5].

As one of the most billed service in health care, wound treatments consumes up to 30-67% of the nursing care time and approximately 27-60% of the hospital bed resources [1,6,12–15] (values estimated in 2015 for developed European countries). The majority of chronic wounds take a long time to heal, and some remain unresolved for over a year [16]. In developed countries, it is estimated that in a population of 1 million people, approximately 3500 are living with a wound, of which 525 people have had their wound for over a year [16]. Complications likely occur in these wounds, leading to repeated hospital admissions, extended hospital stays or even to a surgical intervention [4,13]. Depending on its severity, the estimated average cost of a chronic wound ranges from 2,500€ to 10,800€ per episode [1,12,17]. In detail, the annual cost in Europe for health care of surgical chronic wounds (in planned interventions) is 1.47-19.1 € billion, for diabetic foot ulcers (common complication of diabetes) is 4-6 € billion and for venous leg ulcers (which occurs mainly in elderly people) is 6.5 € billion [12,17–20]. Wound care costs are averagely distributed as following: hospitalisation (38.6%), antibiotic therapy (11.9%), amputations (8.8%),

revascularisation (5.5%) and other interventions (9.8%), topical treatments (6.5%), consultations and outpatient visits (6.5%), indirect costs (6.3%), orthopaedic appliances (4.5%) and diagnostic procedures and investigation (1.6%) [12,21,22].

Currently, in Europe, majority of wound care (around 70-80%) is conducted within the community (including home care), being predominantly treated by community nurses [14,16]. On average, dressings are typically changed around 3 times per week, which implies the same number of home health care visits [14,16]. Depending on the country, expenses are often paid by the patients, but half of home care costs are funded and regulated by the government, through reimbursed or subsidy plans provided by the social care system or insurance companies [14]. Additionally, the nursing care is also typically provided by the health care system [14]. The prevalence of chronic wounds, coinciding with increased care dependency, reduction of hospital bed resources and growing heath care expenses, has becoming a matter of great concern [14]. Indeed, the increasing demands for wound management services will become unsustainable if the present trend continues [16].

Though difficult to measure, wound care treatment also implies indirect costs on society. These are associated to the patient's inability to work or to engage in social activities and domestic responsibilities, representing loss of income (by the patient or loss of labour productivity by their employer) and extensive welfare, social security or disability payments (by the government and insurance companies) [13,23]. Besides the economic burden, chronic wounds also inflict an immense social impact to society [3,4,24]. As a frequent cause of morbidity and mortality, chronic wounds are much related to stress, frustration, pain, impaired mobility and functioning, poor nutrition or sleep, depression and anxiety. Consequently, patients with chronic ulcers have an unsatisfactory/impaired quality of life [3,4,24–26]. Besides affecting the patient's physical and mental wellbeing, chronic wounds also have a negative psychosocial and cultural impact, being an important cause of social isolation and difficulty in social interactions) [4].

I.2. Historical and clinical overview

The study and treatment of wounds goes back for at least three millennia [27]. In Sumerian times (about 2150 B.C), the early wound care register detailed the use of beer and hot water to wash and clean the wound and bandaging with poultice wine sediments and lizard excrements [28]. In ancient Egypt, according to the Ebers Papyrus (1550 B.C), the wound treatment involved the immediate closure of the wound edges with tape or stiches, placement of a piece of meat in the first day of wounding, and then continuous treatment with salves, such as animal grease, honey, silver or matricaria oil [9,27].

The most accomplished medical researchers in ancient practice were Hippocrates (400 B.C) and Galen of Pergamon (150 A.D). Hippocrates described the importance of the wound exudate, namely the need of draining the pus from the wound, and recognised that "Healing is a matter of time, but it is sometimes also a matter of opportunity" [28]. Galen, that referred wounds as "windows into the body", defined the principle of first and second intention healing [28]. However, up until the 19th century with the advent germ theory, the knowledge and practices applied for wound healing developed slowly [27,28]. At this time, advances made in preventing and controlling infection of wounds revolutionised surgery and improved the wound care [27,28]. Since then, wound healing research and development has progressed in many new ways at a rapid rate [29].

In the last decades, there were some major breakthroughs in the field of wound healing [30]. The emerging of animal model systems allowed the understanding of wound repair mechanisms [30]. However, good chronic wound animal models are challenging because it is difficult to establish a standpoint method for wound repair studies [31]. Still, mammalian models have provided several studies on imaging, and on manipulation or analysis of cellular, genetic and molecular processes of chronic wounds [30]. Nevertheless, the understanding of rapid wound healing can also be achieved using simpler model organisms (*e.g.* invertebrates, fish and amphibians), since they typically heal better and faster than complex organisms, despite being involved the same general mechanisms and molecules [30].

Another spurred development in the field involved the recognition of single-cell wound repair [30]. Recent studies showed that several single-cell elements, such as plasma membrane, are actively repaired through a conserved and similar process of regulated exocytosis, and controlled changes in the cortical cytoskeleton [30]. Heart, lung and nervous system diseases have recently been attributed to muscular dystrophy caused by deficient cell repair [30]. The appreciation of this

phenomenon provides a better understanding of the wound healing process, in acellular and multicellular level [30].

Currently, clinical investigation of the wound healing process focuses on cellular mechanisms, including cell lineages, their functions and mediators [28], but also on the molecular level, namely in the understanding of the complex wound healing cascade [27]. These new approaches consist in the analysis and study of several growth factors, cytokines, proteolytic enzymes (like matrix metalloproteinases and human neutrophil elastase), reactive oxygen species (ROS) and other molecular healing components [27].

Currently, it is very difficult, expensive and time consuming to accurately assess a wound status [9,32,33]. It has been shown that half of patients with non-healing wounds do not show initial clinical signs of infection, and usually do not undergo laboratory testing for confirmation, even though afterwards it shows prevalence of infection as they become chronic [9]. On the other hand, there are other factors that can mislead clinicians to define wounds as infected [9,34]. Especially, when the patient suffers from other diseases, for example peripheral neuropathy, diabetes mellitus, arterial disease [9]. Besides, the mere presence of microorganisms (bioburden) at the wound site may impair wound healing, even in clinically uninfected wounds [9]. For these reason, typical treatment usually implies antimicrobial therapy, even in cases without infection, in order to reduce the bioburden at the wound, avoid infection, and potentially accelerate the healing process [9,34]. Knowledge of the involved pathogens and their prevailing susceptibility should be a prerequisite for prescribing antimicrobials, however that is not only the case, leading to antimicrobial resistance [35]. Antimicrobial therapy can be given systemically or topically with antiseptics, antibiotics or other antimicrobial preparations [9]. Clinicians often avoid prescribing systemic antibiotics, but still topical antimicrobial has also shown to be a threat for antimicrobial resistance; as such, they should only be used in infected wounds [35,36].

Even so, upon diagnosis, the current treatments strategies follow a trial-and-error approach, which is also inefficient, expensive and time-consuming [1,32,33]. This emphasises the need on investing in the research and development on wound assessment, management and treatment [2,10].

I.3. Principles of wound healing process

A wound is defined as a damage or disruption of the anatomic structure and function of the underlying normal tissue [25,37,38]. This can range from a simple break on the integrity of superficial epidermis *strata* to a deeper lesion, extending into subcutaneous structures [3]. Cutaneous wounds may be caused from precise incisions (surgery) or may be instigated by accidents leading to other tissue damages, like burns, contusions, haematomas, laceration, abrasions [38,39], or even as a result of a disease process [3,5]. Regardless of the type of injury or organs involved, the wound repair process occurs in a similar manner in almost all tissues [40].

Normal wound healing is a complex and highly dynamic biological process, involving a bundle of cell variants, cytokines, growth factors and matrix elements [4,41], in a series of co-ordinated events [3,42] (presented in figure I.1). The wound healing process is characterised by four sequential and overlapping phases (schematised in figure I.2): haemostasis, inflammation, proliferation and maturation/remodelling [4,27].

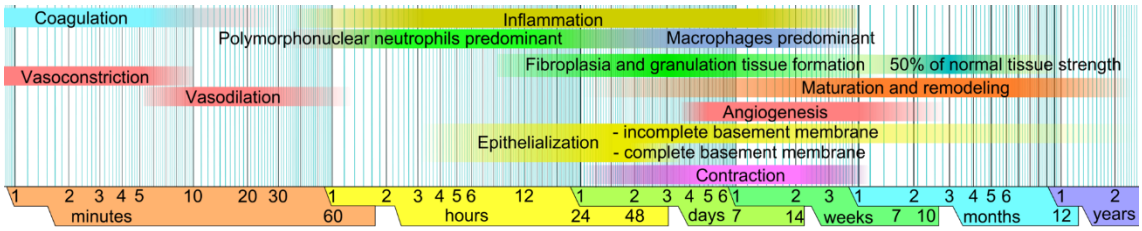


Figure I. 1. Representation of the approximated time scale of the wound healing process through the different phases and events (adapted from Häggström *et al.*, 2014) [43].

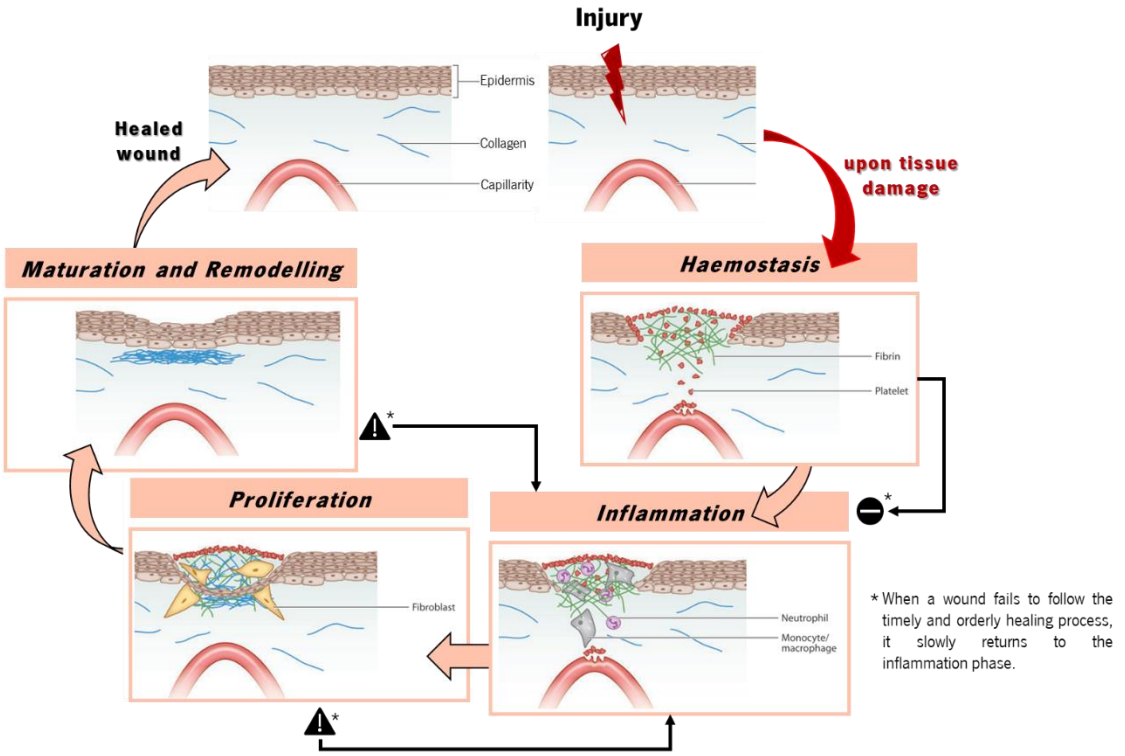


Figure I. 2. Schematic representation of the phases of cutaneous wound healing. Adapted from [30]. In response to an injury, haemostasis process begins to plug the injury hole through platelet activation and coagulation, resulting in the formation of a fibrin clot. The second step, inflammation, allows the elimination of dead tissue cells and invasive pathogenic organisms. Reepithelialisation and granulation tissue formation takes place through proliferation process. Maturation of the new cells and remodelling of the affected tissue layers permits wound closure and final scar tissue formation. When a wound fails to follow the timely and orderly healing process, it slowly returns to the inflammation phase.

Haemostasis – Fibrin clot formation

The initial phase, haemostasis (Figure I.2), occurs within seconds to minutes upon tissue injury [27,44]. This immediate phase is mainly characterised by vasoconstriction and coagulation [30], which help to stop the bleeding and, thus, prevent blood loss (exsanguination) and pathogen intrusion [3,30].

The wound injury causes disruption of the vascular endothelium and exposure of the basal lamina, thus leading to extravasation of blood constituents (haemorrhage) [45]. This initial haemorrhage, exposes platelets to the damaged subendothelium, leading to their aggregation at the wound site and adhesion to the exposed fibrinogen through glycoprotein receptor GpIIp-IIIa

[27,41]. This interaction activates the platelets, causing them to release the contents of their granules, which include cytokines, hormones and chemokines that will ignite the next stages of wound healing [27,41,44].

Upon their activation, platelets release several vasoactive substances, such as catecholamines, serotonin, thromboxane and prostaglandins [27,41], that cause the constriction of the vascular smooth muscle cells in the circular muscle layer [3,30]. This vasoconstriction process is strong enough to significantly reduce or even stop the bleeding, but only momentarily as the bleeding recommences after subsequent passive relaxation caused by hypoxia and acidosis [3]. Vasodilation caused by increased vascular permeability also occurs to allow influx of leukocytes, erythrocytes and plasma proteins, leading to fluid extravasation into the tissue (oedema) [3,27,41]. Several growth factors released by platelets, such as platelet-derived growth factor (PDGF), transforming growth factor-β (TGF-β), epidermal growth factor (EGF), insulin-like growth factor (IGF), fibroblast growth factor (FGF), and others, activate and attract inflammatory cells, predominantly neutrophils, fibroblasts, macrophages and also endothelial cells [3,38].

Platelets aggregation and degranulation at the wound site initiates the formation of an insoluble matrix of platelets and fibrin fibrils, derived by thrombin-mediated cleavage of fibrinogen [30,44]. The resulting mature blood clot, composed of fibrin, fibronectin, vitronectin, von Willibrand factor and thrombospondin [38], temporarily shields the exposed wound tissues [46], and serves as a scaffold for the next phases of healing [40].

Inflammation – Tissue debridement and phagocytosis

The second stage of wound healing – the inflammation phase (figure I.2 and figure I.3) - is essentially defined by the migration and activation of inflammatory cells at the wound site [30,44]. It can be divided into two separate phases, an early phase that occurs within 24-48 hours of injury and a late phase within the following 48-72 hours [38].

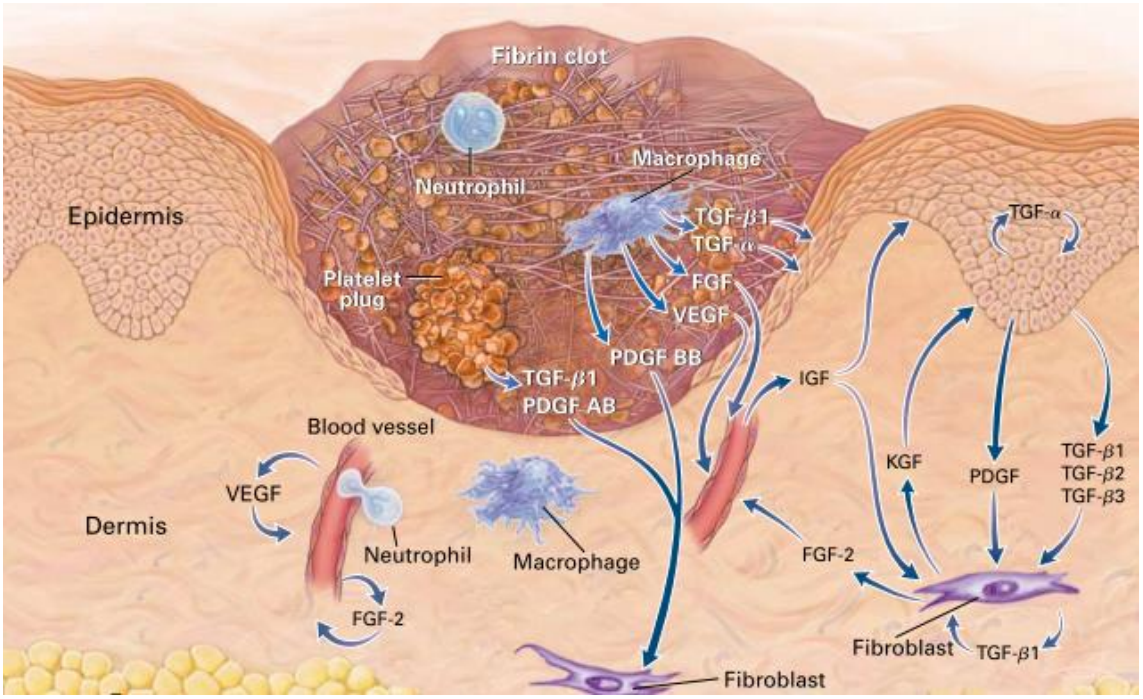


Figure I. 3. Inflammatory phase. Adapted from [47]. TGF: transforming growth factor; FGF: fibroblast growth factor; VEGF: vascular endothelial growth factor; PDGF: platelet-derived growth factor; IGF: insulin-like growth factor; and KGF: keratinocyte growth factor.

Platelets activation initiates cellular and molecular events, such as complement cascade [38], that lead to the migration of inflammatory cells to the wound site, being the neutrophils the first leukocytes to arrive on site [27].The chemoattractive agents that signal this initial migration include, not only the platelets' degranulation molecules (*e.g.* TGF-β) and complement components (*e.g.* C3a, C5a), but also bacterial products (like, formyl-methionyl peptides and lipopolysaccharide) and proteolysed fragments of extracellular matrix (ECM) proteins [28,38,44,46].

The migration of chemoattracted polymorphonuclear leukocytes (PMNs) from the circulating blood into the wound site comprises two actions: adhesion to the endothelial cells of the capillaries adjacent to the wound (margination) and penetration through the capillary walls into extravascular space at the wound site (diapedesis) [3,38,46]. These mechanisms are essentially mediated by interactions between selectin and integrins of the β2 subfamily [48,49].

Once at the wound site, neutrophils begin to phagocytise debris of wounded tissue and infectious agents [28]. Phagocytosis involves first a recognition of phagocytic Fc receptors (FcγRIIA and FcγRIIIA) and complement receptors (CR1 and CR3) [49], and then, digestion by releasing several proteolytic enzymes, such as elastase (HNE), cathepsin G, proteinase 3, urokinase-type

plasminogen activator (u-PA), and collagenases (matrix metalloproteinase-1 (MMP-1), MMP-8 and MMP-13), and reactive oxygen species (ROS) [28]. Neutrophils have a relatively short lifespan (only survive for 1-2 days after their activation) [29], and unless the wound is infected, their activity should gradually decrease and cease within a few days of injury [46].

Other leukocytes present at the wound site are the mast cells, also known as mastocytes [28]. Their action is crucial for proper wound healing, since they are a major source of proinflammatory mediators and cytokines [28]. Specifically, granules content of mast cells includes several digestive enzymes (*e.g.* chymase, tryptase), histamine, fibroblast growth factor (FGF), tumour necrosis factor (TNF), interleukins and other active amines [28,50]. Mast cells degranulation promotes vasodilation and the leakage of plasma proteins into the extracellular space, allowing the further efflux of other inflammatory cells (mainly through histamine release) [50], being also involved in fibroblast recruitment to the wound site (through FGF release) [45]. Since mast cells cause the accumulation of fluid at the injury, they are the main cause for the characteristic signs of inflammation: *rubor* (redness), *calor* (heat), *tumor* (swelling/oedema), *dolor* (pain) and *functio laesa* (loss of function) [9,50]. Similarly to neutrophils, 48 hours after the wound, the mast cells levels at the wound site decrease; thus as the healing progresses, these symptoms should also fade [28].

At a later phase (within 48-72 hours), macrophages, differentiated from monocytes, follow the neutrophils action [38], being those cells considered as the most essential inflammatory cells [50]. Besides their involvement in further tissue debridement and phagocytosis of remaining pathogenic organisms (including bacteria-filled neutrophils) [50], they also play a central regulatory function in tissue proliferation through release of several growth factors, such as TGF-β, platelet-derived growth factor (PDGF), transforming growth factor α (TGF-α), IGF, interleukin-1, basic fibroblast growth factor (bFGF), heparin-binding epidermal growth factor and vascular endothelial growth factor (VEGF) [28,38,47,50]. Moreover, lymphocytes, the last inflammatory cells to reach the wound site (after 72 hours) [3], also appear to modulate and regulate the healing process through the secretion of cytokines [29], however their role in wound healing is still unclear [50].

During the late inflammatory phase, the mitotic activity of basal cells at the damaged epidermis increases. Along with the migration of epithelial cells and their deposition of components of basement membrane, early reepithelialisation and proliferation begins [38].

Proliferation – Reepithelialisation, formation of granulation tissue and angiogenesis

The proliferative phase (schematised in figure I.2 and figure I.4) progresses from the 3rd day until the 2nd week of injury [3], nearly overlapping the migration phase and basal cell proliferation [11]. It comprises events of reepithelialisation, angiogenesis, granulation tissue formation and deposition of the extracellular matrix [38,45].

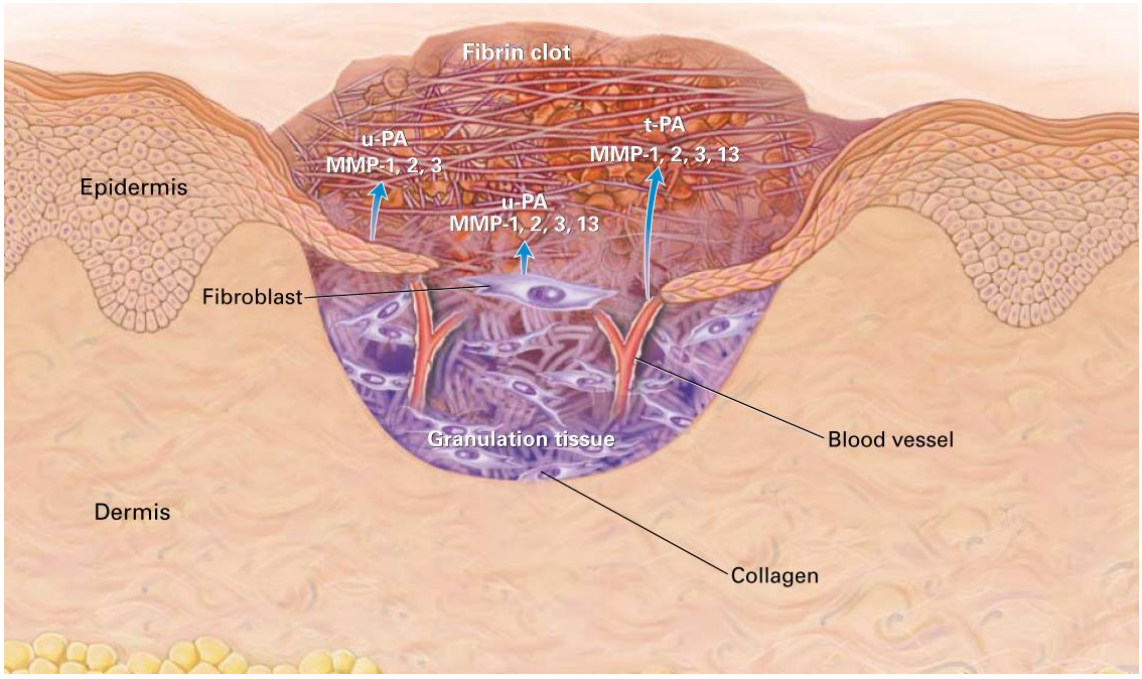


Figure I. 4. Proliferation phase. Adapted from [47]. MMP: matrix metalloproteinase; u-PA: urokinase-type plasminogen activator; and t-PA: tissue plasminogen activator.

The epidermal response in wound healing is mainly comprised by keratinocytes of the basal layer, since these cells compose almost 95% of the epidermis [27]. During reepithelialisation, keratinocytes, induced by epidermal growth factor (EGF) and keratinocyte growth factor (KGF) [46], proliferate and migrate over the wound to fill in the matrix defect [27]. Furthermore, epidermal cells from the wound edges, including from dermal appendages of hair follicles, sweat and sebaceous glands [45], dedifferentiate into keratinocytes [30,45].

To allow their migration between the dermis ECM and the fibrin clot, keratinocytes use proteases, such as MMPs and tissue and urokinase plasminogen activators (t-PA and u-PA), to dissolve the fibrin barrier [27,46], and also, to dissect the wound separating devitalised (eschar) from viable tissue [47].

Upon contact with the defected ECM, keratinocytes' hemidesmosomes attach to the lamina's integrin, and begin to spread a new basement membrane [27,46]. Keratinocytes migration is controlled by contact inhibition [46], since their physical connection with the lamina prevents further movement, allowing epiboly to occur inwardly over the wound [30,38].

As the proliferation progresses, fibroblasts become predominant at the wound site [50]. Their chemotaxis and activation is owed to the preceding release of several growth factors, such as PDGF and TGF-β [3]. Once at the wound, fibroblasts proliferate and begin to produce and repair the ECM of the injured tissue [3,29]. Fibroblast function, namely their production of ECM proteins, is highly regulated by TGF-β [50]. This secreted growth factor induces fibronectin, proteoglycans and collagen gene transcription, increasing their production by fibroblasts [50]. Fibroblasts begin to complement the initial wound matrix (constituted of fibrin and fibronectin) through secretion of several ECM, though their deposition occurs in a disorganised manner [30,41]. Moreover, as result of exposure to growth factors at the wound site, some fibroblasts differentiate into myofibroblasts, which are contractile cells [40]. The combined action of myofibroblasts with the deposition of ECM components produces an organised matrix, their contraction action brings the edges of a wound together and aligns the matrix [30,40].

At the same time, numerous new capillaries and lymphatic vessels begin to invade the wound neodermis from pre-existing vessels [46], forming the often called granulation tissue due to its pink, soft and granular appearance [46,47]. This neovascularisation (termed as angiogenesis process) arises to sustain the newly formed ECM of nutrients and oxygen [47,50]. The release of VEGF, bFGF and TGF-β growth factors by epithelial cells, keratinocytes and macrophages promotes the angiogenesis events [44,46,50]. First, capillary sprouts invade the fibrin wound clot [38], then within five days, maximum formation of blood vessels occurs, and angiogenesis ceases [11,47]. At this point, the wound is filled with a microvascular network, however these new vessels are oedematous due to their incomplete formation [38]. Further epithelisation and collagen deposition continues to occur, for almost two weeks [11,38]. As the wound heals and closes, the oedema recedes, due to the collagen accumulation in the granulation tissue that diminished the density of the blood vessels [11,38], and the redundant fibroblasts and macrophages are eliminated by apoptosis [3].

Maturation and remodelling – Wound closure and scar tissue formation

The final phase of wound healing (Figure I.2) culminates the previous three stages [30], and occurs within the 1st week after wounding for up to several weeks [38]; for some difficult wounds, it can last up to one year or more [41]. Upon wound closure, the resulting scar undergoes through a maturation and remodelling process [24], characterised by the reorganisation and strengthening of the newly formed epithelium [11].

At this stage, the synthesis and remodelling of ECM continues, mainly through replacement of collagen type III to type I, and reorganisation of the matrix by collagen breakdown and by local contraction [29,38]. The wound remodelling requires a tight control between degradation and synthesis events [3]. For example, the breakdown of collagen, catalysed by proteolytic enzymes released by PMN cells , is balanced with inhibitory factors for these enzymes [3]. The tensile strength of the wound increases over time, being this dependent on the formation of larger collagen bundles with increased number of intermolecular crosslinks [47]. However, in general, healed skin never gains its original strength [47].

As the wound heals, the cellular granulation tissue changes to an acellular mass [11] due to the apoptosis or exit of the remaining cell types from the wound [3,30,40,44]. The excess blood vessels retract [27] and the blood flow and metabolic activity at the wound site decreases [3]. Finally, the healing wound results in a fully matured scar [3].

The knowledge in wound healing process has extensively progressed over the years, however much is yet unknown [46,51]. The complexity and dynamic of the wound healing process limits our understanding, and consequently affects our ability to treat wounds. Part of the difficulty in unravelling the healing process is its continuum interconnectivity at a cellular but also at a molecular level [11,30]. Indeed, early events overlap and affect the later phases, but also these later processes influence the resolution of the earlier phases [30]. For example, inflammation stage directly affects the quality of tissue repair, but the constitution of tissue repair is only possible through expression of anti-inflammatory mediators [28]. Still, for a proper healing, these stages and events must progress at this specific order, for a specific time and with an optimal magnitude [26].

I.4. Clinical assessment and its implications

Currently, there is not a standard classification for wounds [52,53], however clinicians can follow a set of guidelines to classify a wound and assess its treatment and prognostic, making the healing as fast as possible [37]. The definition of a healed wound stands as a key concept for wound assessment. A wound is considered healed when the anatomical structure and function of the injured tissue is sustainably restored [38]. Another important concept for clinical assessment is the categorization of the healing process [3].

I. 4.1. Acute and Chronic wounds

Typically, wounds are classified according to their healing time frame, into *acute* (healing) or *chronic* (non-healing) wounds [3,54]. When a wound heals at a predictable and expected rate, and follows the normal phases of healing, is considered as *acute* [3,37]. Whereas, if a wound fails to follow the timely and orderly healing process, or if the tissue does not regain its initial structural integrity, the wound is termed as *chronic* [29,37].

The expected time line for an acute wound to heal (or at least to show signs of healing) usually goes from 5 days to 4 weeks [3] (Figure I.1), whereas a chronic wound is defined as one that does not improve after 4 weeks, or does not heal within 8 weeks [54]. The healing time frame depends on many factors [37], including type and nature of the injury, but also the overall medical condition of the patient [37,38,52]. Therefore, ideal wound assessment must take into account any factor that might influence the wound status and have an impact on optimum wound management [10,37,38,52].

The type and nature of the injury greatly defines on how the healing will progress [52,54]. Acute wounds often result of traumatic loss of tissue caused by mechanical injuries or burns [3,11]. Mechanical injuries include abrasions and tears of the skin (due to frictional contact between the skin and hard surfaces) and penetrating wounds (caused by sharp objects and gun shots) [11]. In these type of injuries, one of the most important factors to consider is the depth and extent (size) of the damage [3,52]; for example if it only affected the surrounding soft tissue, or caused significant cell and damage to underlying blood supply [52]. In the case of burns and chemical injuries, besides the general evaluation of size and extent of tissue damage [52], it is very important to assess the degree of thermal burning (which is defined by nature and temperature of the source and exposure time) [11].

When injuries slowly heal and/or constantly reoccur, they develop into a chronic wound (Figure I.2) [11,54]. Anomalies in certain phases of the healing process can also result in excessive healing, leading

hypertrophic scars (stay within the boundaries of the original wounds) and keloids (extend beyond those limits) to occur [27,38,55]. These entities are a result of overabundant collagen production and decrease collagen breakdown, during an enhanced proliferative and remodelling phase [38]. Even though, their underlining mechanism are not fully understood, abnormal scaring has also been shown to be affected by an altered inflammatory phase [28,29]. For example, the secretion of histamine by mast cells (that were kept it abnormally large numbers due to a prolonged inflammation phase) may contribute to the formation of excessive wound collagen [29]. Additionally, clinical evidence also showed that variances in cytokines and growth factors profile determine the scar outcome [28,56].

Even though the majority of wounds (80%) result of surgery or traumatic injuries, the most challenging non-healing wounds are those caused by other underlying diseases [57]. To these branch belong the ulcers which are lesions not caused by physical means but, instead, by an internal aetiology that causes consequences to the skin integrity [58]. Considering the aetiologies for their occurrence, the Wound Healing Society classifies them into four major categories: diabetic ulcers, arterial ulcers, venous ulcers and pressure ulcers [5] (Figure I.5).

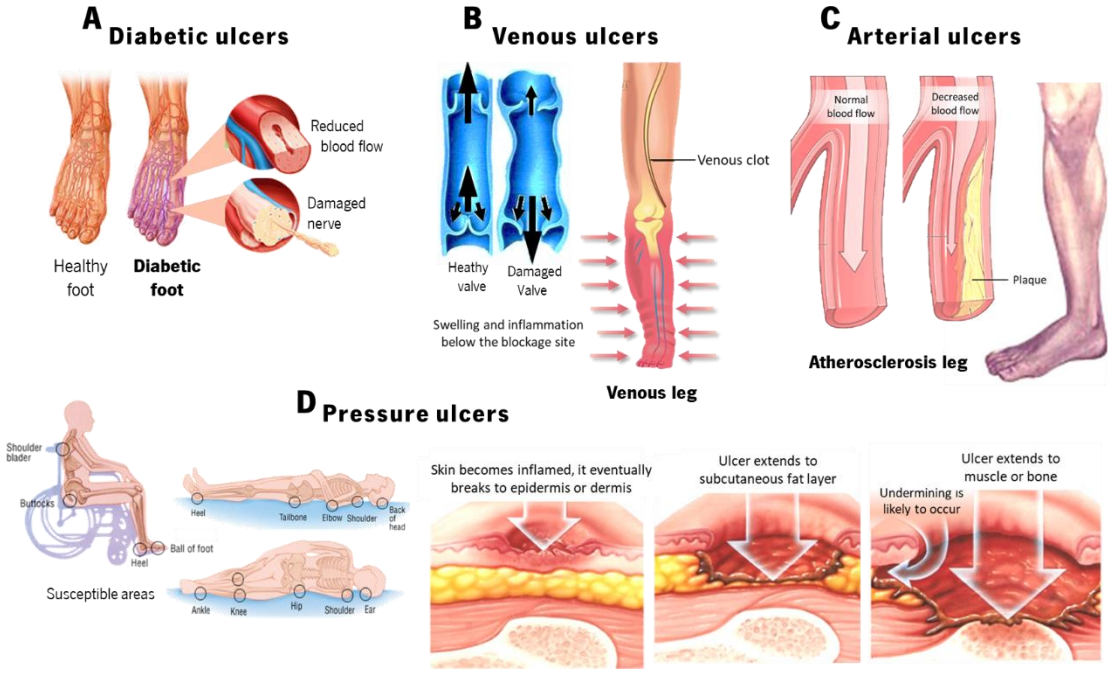


Figure I. 5. Classification of ulcers according to the Wound Healing Society. (A) Diabetic foot ulcer. (B) Venous ulcer. (C) Arterial ulcer. (D) Pressure ulcer. Adapted from digital images on public domains [59–65].

Diabetic ulcers are typically associated to feet or toes, as a result of vascular and neurological complications of diabetes (Figure I.5A) [66]. Diabetes mellitus affects hundreds of millions of people worldwide, with predictions of doubling for 2030, reaching values as high as 366 million people [26,42,67]. In addition to other cardio-, retino- and nephropathies, patients with diabetes are greatly prone to develop chronic non-healing wounds [26,45]. Wound healing is impaired by numerous of physiologic factors associated to the disease, including decreased growth factor production and cytokines release, impaired macrophage function, decreased collagen accumulation and imbalance between proteolytic action of MMPs for ECM remodelling [42,68,69]. In addition, these patients often have microvascular and/or macrovascular disease [45], where the resulting deficiencies in blood supply further hinders the healing [58]. Diabetic ulcers are always accompanied by hypoxia, prolonging the inflammatory response, and hyperglycaemia, that alters the permeability and delivery of nutrients to the wound site [26,45]. Frequently, these wounds evolve with extensive necrosis and infection [67], resulting in amputation of the foot or even the lower leg [9]. Indeed, diabetic ulcers are the main cause for all lower limb amputations (70%) [5]. Worldwide it is estimated that there is an amputation every 30 seconds as a result of a non-healing diabetic ulcer [5].

Venous and arterial ulcers occur typically in legs, being associated to venous or arterial insufficiency in the lower extremities of the body (Figure I.5B and Figure I.5C) [58]. Both diseases commonly exist in the same patient, resulting in wounds of mixed aetiology, broadly termed vascular ulcers [58,70]. However, misdiagnosis and failure to identify the major contributing factors for the non-healing ulcer impacts their management [58]. Venous ulcers occur when deep and/or superficial veins become incompetent due to damaged valves or blockages (*e.g.* deep-vein thrombosis), leading to pressure build-up in the veins (sustained hypertension) [54,66]. It can also be caused by insufficiency of calf muscle pumps, (venostasis) limiting the blood return to the heart [54,71]. Most leg ulcers (60-80%) are caused by venous disease [58], being the major cause of morbidity with prevalence range of 1.9-13.1% in the community [54]. These ulcers are characterized by local inflammation, swelling, itching, hardened skin and irregular and sloping edges extremely moist (high exudate level) [71]. On the other hand, arterial ulcers result of failure or reduction in the blood supply to a body area, commonly due to atherosclerosis disease [66], or to other underlying diseases including diabetes, thromboangiitis obliterans, vasculitis, thalassaemia, etc. [71]. The lack of blood flow to tissue causes tissue hypoxia, resulting in a very painful deep wound with “punched out” edges, often covered with necrotic tissue [71].

Pressure injuries occur as a result of intense and/or prolonged pressure or pressure in combination with shear and/or friction (Figure I.5D) which instigates cellular deformation, ischemia, cell death and tissue necrosis [58]. Disposition for these tissue injuries is also related to microclimate, nutrition,

perfusion, comorbidities, and other skin-related and underlying soft tissue conditions [58]. Risk factors to develop these wounds comprise immobility, advanced age, low body mass index, musculoskeletal disorders and fractures and occurrence of other medical conditions (*e.g.* renal disease, gastrointestinal diseases, chronic obstructive pulmonary disease, dementia) [1,2,66]. For this reason, pressure ulcers are particularly common in vulnerable patients including elderly people, stroke victims or those in wheelchairs and incapacitated [2,66]. As a major cause of infection, these ulcers can lead to severe complications, septicaemia, osteomyelitis and ultimately death [2].

Even though they are less common, wounds caused by trauma and surgery can become chronic, being infection the main cause of their derange. Contaminated or dirty trauma wounds, with delayed healing or with extensive damage, have higher risk of becoming infected [11,54]. Most heath care associated infections (previously described as hospital-acquired infection, HAIs) occur in surgical patients [19]. Surgical wound infections (also known as surgical site infection) are estimated to affect between 30-40 surgical patients per 1000 operations, with a mortality incidence of 1.5% [16,19,72]. Presence of foreign body (*e.g.* retained gauze, drains, sutures, environmental debris), prolonged hospitalization and obesity are major contributing factors for infection [10,16,73]. Other complications can arise from surgical incisions [10,58]. Wounds can break open along the surgical incision (dehiscence), exposing the underlying tissue and organs that can even protrude through the wound opening [58]. Major contributing factors for dehisced surgical wounds includes subacute infection, excessive tension on wound edges, poor surgical technique and poor perfused wound edges [58].

The repair of damaged tissues can be impaired by a wide range of local and systemic factors (Table I.I), which ultimately might lead to non-healing chronic wounds [10,38]. Local factors, such as infection, poor oxygenation and venous drainage, increased skin tension, excess local mobility, deficient debridement, oedema, presence of foreign body, and others, directly affect the wound characteristics and limit the progression of the healing process [10,26,38]. Systemic factors are related to the patient's medical condition and consequently to its ability to heal [26]. Example of systemic factors are increased age, malnutrition, obesity, stress, alcoholism and smoking, interference of medications and concurrent illness, pre-existing diseases (*e.g.* diabetes mellitus, vasculitis, rheumatoid arthritis, ischaemia, fibrosis, uraemia and jaundice), and immunocompromised disorders (like, leukocyte adhesion deficiency) or conditions (such as, cancer, radiation therapy and AIDS) [10,26,38,54]. Many of these factors are related to each other, and mainly, a wound fails to heal due to a combination of several of these factors [26]. Failure to recognise the factors that might impede the healing of a chronic wound affects its management and prognostic, and consequently can lead to a negative outcome for the patient [10,54].

Table I. I. Factors that might influence wound healing ability.

Local factors		Systemic factors		
Wound-related microenvironment	**Overall patient-related factors**	**Patient comorbidities**	**Medications**	**Healthcare professional factors**
Type, size and site	Age and gender	Obesity	Radiation	Skill, knowledge and experience of clinicians
Duration	Alcohol	Diabetes mellitus	Chemotherapy	
Infection	Smoking	Chronic pulmonary disease	Steroids	
Presence of foreign bodies	Poor hygiene	Chronic cardiac disease	Anticoagulants	
Insufficient oxygenation or perfusion (hypoxemia, hypoxia, anaemia, hypovolemia)	Psychophysiological (pain, anxiety, stress, depression)	Peripheral vascular disease	Pennicillamine	
Nutritional deficiency (protein-calorie, vitamins, minerals)	Psychosocial (motivation, social and family support, culture and traditions, compliance with prescribed treatments, behavioural conditions affecting self-care ability)	Neuromuscular disease and deformities	Cyclosporine	
Temperature and pH		Renal disease	Methotrexate	
Moisture		Autoimmune disease	Hydroxyurea	
Tissue maceration		Immunocompromised conditions (Cancer, AIDS)		
Pressure and/or shear	Malnutrition	Substance-related disorder		
Trauma and oedema	Malabsorption			
Necrosis				
Biochemical imbalances (abnormal levels or dysfunction of cytokines, enzymes and substrates, nitric oxide (NO), reactive oxygen species (ROS), growth factors and receptor sites)				

Information compiled from [10,13,24,26,27,33,52,74–76].

I. 4.2. Primary and secondary healing

A wound successfully heals through a timely and orderly progression of several healing events and processes, but its healing can occur by primary or secondary intention [3]. Simple wounds follow primary healing processes and close within 12-24 hours of wounding [3,38], whereas secondary healing takes longer time and occurs upon any disruption of the healing process [3,27,66].

Non-infected wounds without significant loss of tissue that were cleaned and well-closed within six hours upon injury, normally heal by primary intention (Figure I.6A) [27,52]. These comprise surgical wounds with cleaned incisions, cleared lacerations and edges well-approximated using sutures, staples or glue [52]. However, if the wound was not surgically closed within that time, and instead followed closure only through contraction and reepithelialisation of the final healing stages, it heals by secondary intention (Figure I.6B) [52].

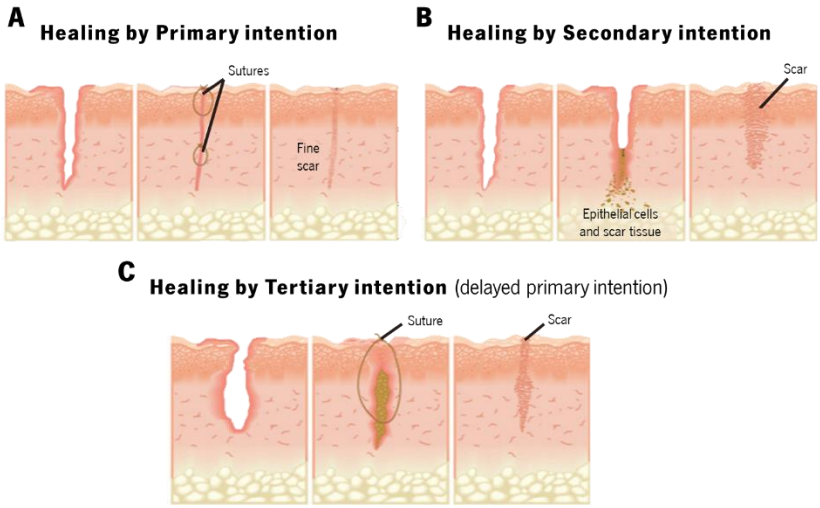


Figure I. 6. Classification of the healing process, by (A) primary intention, (B) secondary intention and (C) tertiary intention. Adapted from [77].

Secondary healing mostly occurs in wounds with extensive loss of tissue, caused by major traumas, severe burns and difficult surgical procedures, as the wound edges cannot be approximated [38]. In secondary intention, the wound heals from the bottom, being mainly characterised by larger granulation tissue formation and epithelisation to fill the large tissue defect [3] and presence of high number of myofibroblasts for smooth muscle contraction [38]. By secondary intention, wounds take longer time to heal and require a more complicated reparative

process [3]. Consequently they are more susceptible to infection and unordered healing [27]. In addition, secondary healing also occurs when the healing process is disrupted or impeded by dehiscence, hypoxia, fibrosis and others local and systemic factors (mentioned above) [27]. If these healing impairments/complications are not detected in time and managed accordingly, a chronic wound might arise [27].

Occasionally, wounds are closed by delayed primary healing, also denominated by tertiary intention (Figure I.6C) [78]. This is a combination of primary and secondary healing [78]. When wounds are contaminated, unwell drained or poorly delineated, they are cleaned and left open for a few days to prevent infection [38,78]. These wounds, typically resulting from bites or lacerations, are then closed after debridement by host defences of all nonviable tissue [38,78].

I. 4.3. Clinical indicators of impaired wound healing

The challenging nature of wound healing compels the clinical practitioners worldwide to adopt a comprehensive and fundamental approach for the management and treatment of the wounds [79]. Even though there is not a standard care guideline for clinicians to follow when managing a chronic wound [79], the following criteria have been established to address the complexity of the problem: (1) extensive loss of integumentary system (natural covering comprising the skin and its appendages) which can delay or hinder the proper closure of the wound; (2) infection; (3) compromised viability of surrounding tissue (significant cell damage, necrosis or impaired blood supply); and/or (4) presence of pathologies (systemic factors related to patient's medical condition; see table I.I) [11,54,67].

Considering these criteria and the factors that might influence wound ability to heal (healability), a set of key points for management and treatment of the wound can be followed (Figure I.7). First steps comprise a complete evaluation of the patient and the wound [70,79]. When assessing the wound environment, the acronym TIME has been universally accepted to assist with implementation of the basic healing principles of wound bed preparation: **T**issue management, **I**nfection/inflammation control, **M**oisture balance and control of the **E**dge of the wound [13,80,81]. Then, the wound care practitioners have to define what treatment would be the most effective, and what type of intervention, technology or dressing material would the best option for the patient [1,55]. For a successful healing, reassessment of these key points have to be made continuously, during the complete course of the wound management [70,79].

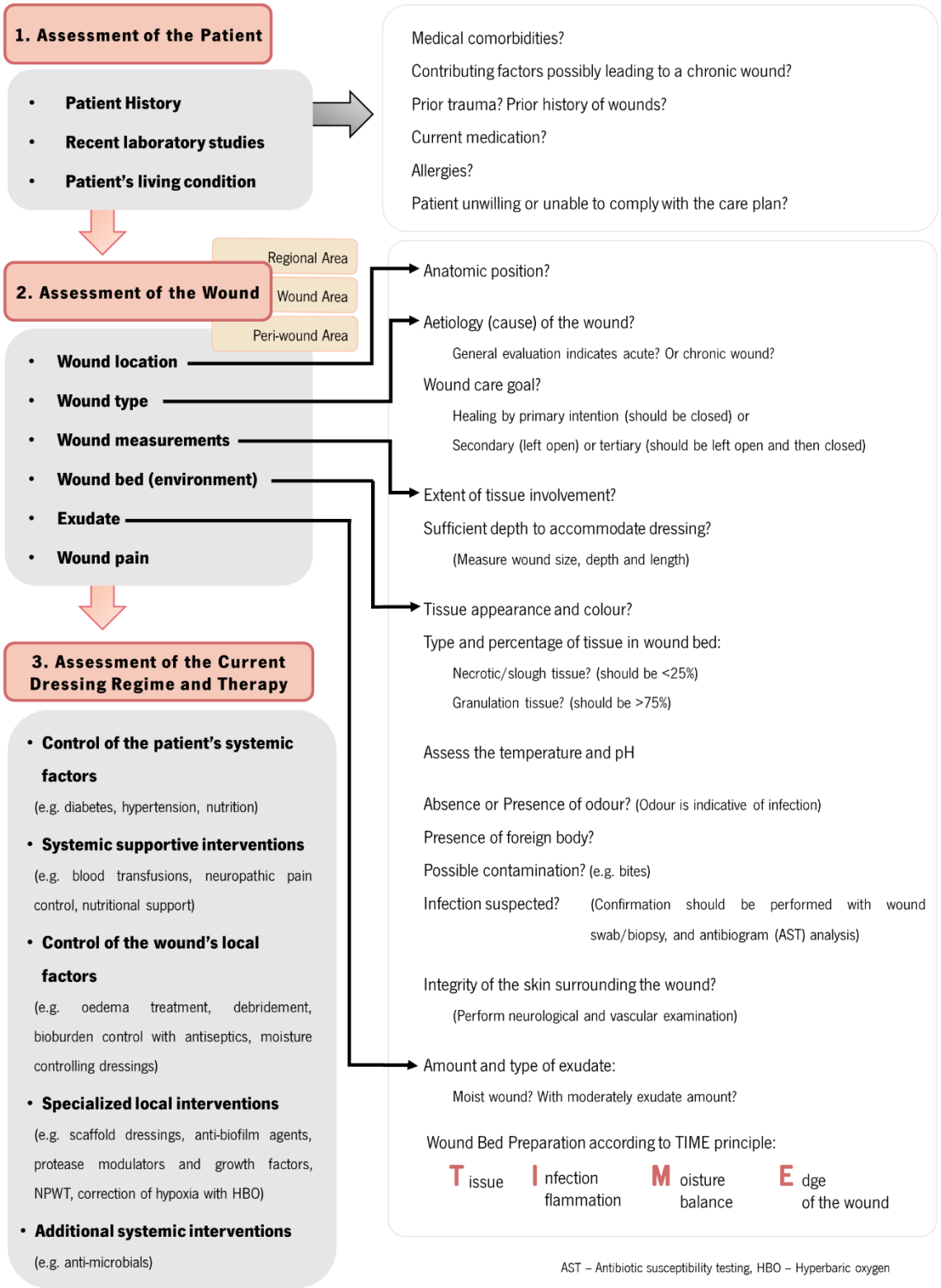


Figure I. 7. Sequence of key-points and interventions for the assessment and management of wounds [70,79–84].

Abnormal wound healing can occur during any phase of the healing phase in which the wound slowly returns to the inflammatory phase [28] (Figure I.2). The transition from the inflammatory to proliferation phase is a critical step for a successful healing [85]. One requisite to disrupt the cycle of excessive inflammation, and consequently achieve a successful healing, is the understanding of the reasons for the persistent inflammation [28,85]. It is extremely important to recognize what are those major factors that imped the resolution of inflammation, and consequently impair the healing process. In other words, it is important to identify which markers can be used to evaluate the wound healing process, namely during the inflammation phase.

I. 4.3.1. Biological markers in the wound

Identification of biomarkers and study of their implications in wound healing not only helps us to understand the mechanisms involved in healing, but more importantly allow us to associate them into the management process of a wound [51]. By definition, a biomarker is a biological characteristic that is objectively measured and evaluated as an indicator of normal biological or pathogenic processes, or pharmacologic responses to a therapeutic intervention [1,44,51]. As medical signs, they allow a better and accurate assessment of a certain disease or disorder, as opposed to medical symptoms [51]. They can be used to assess a wide range of diseases [86–90]. According to their application, biomarkers can be diagnostic (to identify what is wrong), prognostic (to predict disease course and/or severity) or therapeutic monitor (to predict whether a therapy will or is working) [44]. Biomarkers can be either produced directly by the disease, or by the body as a response to the disease [44]. They can be physiological (*i.e.* the normal functions present in the wound site), histological (tissue-related) or biochemical (biochemistry processes and its intermediates) [1]. Currently, biomarkers for assessment of chronic wounds are not well defined [51]. However, progress has been made in identifying them and in their validation in the wound healing progress [44,51]. In the following pages is an overview of the markers that have been identified and characterized regarding their function in the wound healing process [44].

a) Physiological biomarkers

General information about the wound healing can be collected through measurement and assessment of the basic physiology at the wound site, it includes blood flow, oxygen supply, pH, temperature and surface moisture [1]. These measurements provide insight about the viability of the tissue and its ability to heal (healability) [34].

Blood supply

The healing process requires a lot of energy and nutrients (specifically, carbohydrates and oxygen), as it also produces several waste products that must be removed from the wound site [34]. Blood vessels provide the network for these energy demand and exchanges, being a major importance in all wound healing phases, specifically for angiogenesis [34]. Inadequate blood supply leads to ischemia and hypoxia in the wound [58], causing intense pain, and if not treated, can lead to amputation [70]. The wound site in the body significantly affects the body supply, as well as systemic factors related to the patient. Majority of hard-to-heal wounds are seen in the lower part of the body, specifically in the extremities (*e.g.* leg and foot ulcers) [1], and in patients with advanced age and/or diagnosed with medical conditions (76% of patients with chronic wounds have 3 or more comorbid conditions including hypertension, vascular disease, arthritis, obesity or diabetes) [13]. Typical treatment comprises topical negative pressure therapy, applied after debridement; the applied force causes the tissue to open up the capillaries, consequently increasing the flow [70,91]. Another therapy involving ultrasounds has also been proposed, the thermal effect produced by the ultrasound waves, enhances neovascularization, also accelerating the wound healing [10,92].

Carbohydrates provide the necessary energy, being a key factor for collagen synthesis, configuration, deposition, and remodelling [44]. It has been estimated that each gram of collagen synthesis requires nearly 900 calories [44]. Carbohydrates are also involved in other processes in wound healing, namely structural lubrication, transportation, immunologic and enzymatic functions [44]. These key source of energy can be used as a marker, typically through glucose concentration, to assess if the wound is healing at an optimal rate, where its levels should decrease with the necessary calorie intake [44].This is an especially important factor for diabetic patients [93].

Oxygen

Oxygen plays an important role during the wound healing process, namely in inflammation (to interact with numerous cytokines and as an effector for the neutrophils burst), in angiogenesis and epithelization (to supply the actively proliferating cells), and during collagen deposition [27,42]. Wound requires at least a tissue oxygen tension of 20 mmHg to heal, being shown that non-healing wounds measure oxygen tensions lower than 5 mmHg [42]. Any alteration in the oxygen delivery compromises the immune system and can slow down healing, as more necrotic debris facilitates bacterial growth [27,42]. Several factors can impend oxygen delivery, including smoking (as a potent vasoconstrictor, nicotine reduces subcutaneous tissues oxygen tension) [10]. Oxygen is directly linked to the blood supply, so therapies enhancing the blood supply at the wound site also increase the inflow of oxygen [55]. Specific topical oxygen treatment can be achieved through hyperbaric oxygen therapy that subjects the body to 100% oxygen at increased atmospheric pressure in a pressurized chamber [70,94]. It imposes the wound into hyperoxia, stimulating neovascularization and assisting the healing as a oxidative bactericidal and in wound matrix repair [94].

Temperature and pH

Temperature and pH play an important role in allowing a wound to heal [95]. Skin temperature is influenced by physiological and environment factors, being a good indicative for the healing assessment [96]. Normal tissue temperature improves the blood flow to the wound bed and enhances epidermal migration [11]. Healing has been described to be most effective at temperature ranging 33-35˚C [97]. Decrease in temperature below that of the core body is indicative of a healing wound, whereas temperature increase is associated to delayed healing [96,97]. On the other hand, higher temperatures are a sign of bacterial colonisation or excessive mechanical loading, causing inflammation. They can also cause the release of nitric oxide due to cell deformation, leading to vasodilatation [97]. Even so, temperature measurement is related to a few inconsistencies, being difficult to accurately access the wound status according to its values. Indeed, studies have also reported that lower temperatures are indicative of inadequate collagen deposition and decreased activity of neutrophils, fibroblast and epithelial cells [97]. For this reason, measurements of wound temperature coupled with information regarding other factors offers more value in predicting the wound status [97]. Combination with infrared camera can assist wound management, as it allows a more sensitive and specific analysis of the wounds [96,97].

Intact skin has a naturally acidic pH in the surface, ranging from 4 to 6 [97]. It has been an ideal parameter to follow the wound healing process since fluctuation on pH can indicate certain events in healing [93]. In the course of normal healing, pH increases during granulation (proliferation phase) and decreases afterwards, reaching the typical values of surface (pH 4-6) [93]. An acidic environment is considered favourable for fibroblast proliferation, epithelisation and angiogenesis. In addition, low pH not only enhances oxygen supply but also helps controlling bacterial colonisation, preventing infection [97]. Indeed, when pH levels decrease from alkaline towards neutral, is a sign that the wound is healing [97], whereas pH in non-healing wounds tend to oscillate between pH 7-8 [93]. Alkaline environment deprives the wounds from oxygen, providing a favourable environment for bacterial growth [97]. In fact, wounds developing infection typically possess high alkaline pH levels [97].

Wound moisture (Exudate)

For an effective wound assessment and management, besides the need of a thorough observation of the wound itself, the wound fluid, also known as exudate or wound drainage, requires characterisation [6,51]. By definition, exudate is the fluid, cells or other substances leaked from a wound, once the haemostasis stage ends and inflammation begins [11,98]. The wound fluid plays a crucial role in the healing process, mainly by providing the ideal environment for healing through its continuous irrigation and moisture [11]. It also supplies the wound with nutrients for cell metabolism, promotes cell proliferation and facilitates the diffusion of healing factors and the migration of inflammatory cells [11,98,99]. The exudate is mainly composed of water and blood, but also comprises several cell types, inflammatory mediators, growth factors, proteolytic enzymes, electrolytes, nutrients, and even microorganisms (which are not necessarily an indicative of infection) [98].

Nowadays, the scientific and medical community analyses the wound exudate to better understand the process of the wound healing since it provides an insight into the local environment of a wound [6]. The exudate's composition, appearance and consistency are significantly different in acute and chronic wounds [98–100]. The healing wound fluid usually has a clear, pale amber colour with a watery consistency and is odourless (serous exudate) [99]. However, when infected, the wound exudate presents a murky, yellow, green or creamy-coffee colour, its consistency thickens and appears as creamy or cloudy and begins to present a foul odour [98,99]. Depending on the severity of the infection, the exudate can be classified from seropurulent and purulent

(pyogenic infection, commonly referred as pus) to haemopurulent (established infection, which causes damage to dermal capillaries and has a viscous and sticky dark blood-stained appearance) and haemorrhagic (severe infection and trauma, that causes spontaneous bleeding) [99].

An excessive healing response and overabundance of inflammatory components at the wound site, such as neutrophils, fibrinogen, fibrin and proteolytic enzymes, can also affect the wound fluid appearance and consistency [98,99]. For example, fibrinous exudate presents a yellow and cloudy, milky or creamy consistency due to the presence of fibrinogen and ultimately fibrin protein strands, which in excess can lead to fibrosis and to the arise of a chronic wound [50,99]. Another example is the exudate from a necrotic wound which presents a grey opaque appearance that progressively darkens as a result of intense autolysis and debridement through phagocytosis and elevated action of proteolytic enzymes [98].

b) Histological markers

Histological examination of wounds is one of the most important steps in wound assessment [1]. A variety of parameters are examined, ranging from the type of injury, size and depth (extent) of the wound, location of wound appearance and even odour [1].

Wound closure and dimensions

Wound closure is defined as "full epithelialisation and no drainage, without need for additional dressing" [1]. This parameter is considered as a clinically meaningful endpoint in the assessment of wounds, being a clear indicative of a healed or healing wound [1]. Several clinical trials have defined reduction of wound site as a strong sign of healing, being associated to epithelization processes [1]. However, chronic wounds do not typically heal in a linear fashion, making parameters like wound area and volume unreliable indicators [1].

ECM composition

Tissue biopsy of wounds provides insights regarding the composition of the wound. This examination helps evaluate a few processes of wound healing, including dermal collagen, elastin content, epithelisation [1]. It also provides knowledge on underlying cellular pathology involved in the non-healing, including the wound microflora [1]. Current management of the wound includes colour examination, namely epithelial tissue has a typical pearly pink colour, granulating tissue has

a beefy red colour, sloughy tissue has a stringy yellow colour, necrotic tissue has a hard black colour and infected tissue has a pus green colour [11]. Wounds with necrotic, sloughy and infected tissue have larger risk for turning chronic [34]. Wounds possessing this appearance should be clean and debrided, so that the wound may progress beyond the inflammatory stage towards healing [58].

Bioburden and Infection

The presence of microorganisms poses a constant threat in wound healing [97]. Bioburden corresponds to the number of microorganisms living on wound surface, accounting not only the microbial load and diversity but also their pathogenicity [34]. Since the threshold between contamination and mild colonialization to infection can quickly change, it is extremely important to identify these changes at an early stage [34]. Additionally, identification of the microorganisms involved in the wound also provides an effective measure of action, as well as their pathogenicity evaluation [34].

Microbial contamination and mild colonisation tends to be normal in healing wounds, however abnormal and critical bioburden can potentially disrupt the orderly healing sequence [34]. Microorganisms degrade and damage the host underlying tissue at the wound site [34]. For example, ammonia, a bacterial by-product, is extremely toxic to wound tissue [76,97]. Additionally, it raises tissue pH, resulting in an ideal environment for further bacterial colonisation [76,97]. In response, abundant neutrophils and macrophages infiltrate to the wound attempting to destroy them, secreting high levels of reactive oxygen species (ROS), proteases and other destructive enzymes,. With this scenario the wound remains in the inflammation step and do not progress [21].

Furthermore, biofilms are a precursor to apparent infection, being a sign of tolerance to antimicrobial agents (including host antibodies and inflammatory cells, antibiotics and disinfectants) [21,101]. Biofilms are complex communities of microorganisms, often composed of multiple species [102]. Biofilms offer a multi-layered defence for the pathogens, possibly due to poor antibiotic penetration, adaptive stress responses and formation of persister cells [102]. The presence of biofilm causes the wound to remain in the inflammatory phase and inhibits tissue granulation and epithelialisation, thus delaying healing [21]. Indeed, majority of chronic wounds (about 60%) have bacterial biofilms [21].

Tissue bacteria levels can be used to anticipate healing in both acute and chronic wounds [44]. A common approach to detect infection is through odour assessment [103]. As bacteria degrade wound tissue, several malodorous volatile molecules are released as by-products, for example putrescine, cadaverine, sulfur and short-chain fatty acids including *n*-butyric, *n*-haptonic, *n*-valeric, and others [103]. In some cases, depending on the smell, it is possible to identify the bacteria involved; for example *Pseudomonas aeruginosa* smells like sulfur (similar to almonds) due to the release of dimethyl trisulfide [103]. Other methods of infection detection may include measurements of the bacteria by-products at the wound site, or even by the bacteria consumption of certain substrates [103]. For example, infected wounds revealed significant depletion of arginine when infected with *P. aeruginosa* [103].

c) Biochemical markers

Wound healing comprises a range of biochemical events, being them considerably affected in non-healing wounds [1]. Molecules involved in those events (cytokines, growth factors, proteases and other enzymes) are significantly different in wound fluids from chronic or acute wounds, making them potential biochemical markers for healing.

Cellular and function activities that take place in the wound healing process are mediated through the action of chemical signals, cytokines and growth factors [50]. These molecules play a critical role in cell migration and differentiation, matrix production and enzyme expression [50].

Depletion of these molecules negatively impacts the healing process, as they can no longer modulate the cell-signalling cascade involved in healing [50]. Moreover, the receptors expressed on target cells, that interact with these chemical signals, are obviously required for these processes [50].

Growth factors and cytokines

It was thought that non-healing wounds had reduced response to, or lack of, growth factors and cytokines [104]. Due to their importance in the healing progress, a common therapy for chronic wounds comprises topical supplementation of cytokines and growth factors. However, clinical trials attempting this treatment had limiting results, being ineffective in most cases [104]. Instead of underproduction, it was found that the problem resides in their rapid destruction by proteases and other destructive enzymes [104]. Interference with the availability of growth factors undermines

the wound healing trajectory, as it slows down or prevents cell proliferation [21]. For instance, human neutrophil elastase destroys PDGF and TGF-β (which, besides other functions, regulate fibroblasts during proliferation phase) [50].

Even so, elevated levels of pro-inflammatory cytokines can also implicate the wound healing process, as these molecules further induce wound to remain in inflammation phase [21]. Namely, the levels of pro-inflammatory cytokines IL-1, IL-8, IL-6 and TNF-α are elevated in non-healing wounds [21,44]. However, their levels are very inconsistent, which makes them difficult to use as valid biomarkers of the wound process [44].

Proteases and other enzymes

Polymorphonuclear (PMN) cells (also known as granulocytes) are the primary line of defence against the invasion of a microorganism or in tissue inflammation [49,105]. PMN cells often refer to neutrophils as they are the most abundant granulocytes, however they also include eosinophils, basophils and mast cells [106]. At the wound site, pathogens are chiefly eliminated by neutrophils, through both intra- and extracellular mechanisms [107]. When neutrophils encounter microorganisms, they eliminate them by phagocytosis (intracellular mechanism), releasing soluble antimicrobials (extracellular mechanism) or through formation of neutrophil extracellular traps (NETs) (Figure I.8) [107]. Granules are essential for the neutrophils' role in the immune response [106]. Upon cell activation, specific proteins are released from the neutrophils' granules, like MMPs, myeloperoxidase, elastase, cathepsin G, defensins (also known as HNPs – human neutrophil peptides), azurocidin (also termed CAP37 - cationic antimicrobial protein of 37kDa), proteinase 3, u-PA and t-PA, bactericidal permeability-increasing protein (BPI), phospholipase A2, NADPH oxidases, lactoferrin, histaminase (diamine oxidases), lysozyme and others [49,104,106,108–110]. Non-protein active molecules are also released by neutrophils, including inflammatory mediators, reactive oxygen species (ROS) and eicosanoids [28,49,110].

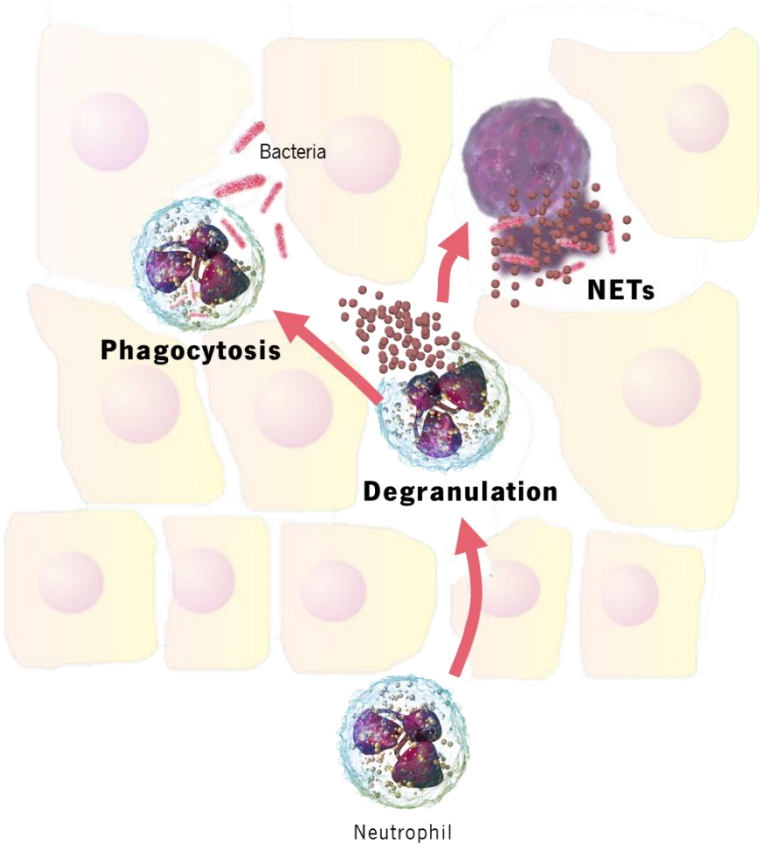


Figure I. 8. Mechanisms used by neutrophils to control infection: phagocytosis, degranulation and release of neutrophil extracellular traps (NETs). Adapted from digital images on public domains [111,112].

The oxidative and proteolytic potential of neutrophils enables extracellular matrix (ECM) degradation [113], allowing those cells to rapidly migrate between tissues, but also to participate in tissue remodelling/repair, wound healing, coagulation and fibrinolysis [108,114]. Proteases not only contribute directly to anti-microbial activity but they are also involved in the proteolytic processing of chemokines, cytokines and receptors [115] (table I.II). Besides this, neutrophil secretions stimulate other cells, like monocytes and macrophages, acting as pro-inflammatory mediators [116].

Table I. II. Biological functions of several enzymes released by neutrophils.

Enzyme	Biological functions	References
Cathepsin G (CG)	Degradation of ECM components Degradation of plasma proteins Bactericidal properties Cleavage of inflammatory mediators Cleavage of receptors Platelet activation	[117–128]
Elastase (HNE)	Degradation of ECM components Degradation of plasma proteins Bactericidal properties Cleavage of inflammatory mediators Cleavage of receptors Activation of lymphocytes and platelets Activation of proteases Inactivation of endogenous inhibitors Cytokines and chemokines induction	[121–125,127,129–141]
Lysozyme	Bactericidal properties Phagocyte activation Inflammatory mediator	[142–148]
Matrix metalloproteinases (MMPs)	Degradation of ECM components Degradation of plasma proteins Cleavage of receptors Cytokines and chemokines inactivation Regulation of cell proliferation, adhesion and migration Platelet aggregation Promotion of angiogenesis Pro-inflammatory and anti-inflammatory mediator	[149–162]
Myeloperoxidase (MPO)	Bactericidal properties Inhibition of apoptosis and inflammation Pro-inflammatory mediator Induction of endothelial cells apoptosis Platelets activation and aggregation	[163–168]
Proteinase 3 (PR3)	Degradation of ECM components Bactericidal properties Cleavage of inflammatory mediators Platelet activation Induction of endothelial cells apoptosis	[123–127,169–175]

Proteases play a number of roles in the wound healing process, being active in all phases of wound healing (from haemostasis to the last phase of remodelling) [51]. Normal wound healing requires the release of these specific proteases at precise time periods, at specific places and at controlled levels [97]. In the beginning of an acute wound healing there is a burst on protease concentration in the first few days, which should decline after one week as the healing progresses [51]. However, in non-healing wounds protease levels remain high, due to the abundant infiltration of PMNs in the wound (the wound remains or returns to the inflammation phase) and/or as a response to bacteria in the wound (infection) [50,51].

Proteases has been consensually endorsed as a marker of inflammation [74]. Prolonged high levels of proteases impairs the healing progress on the wound [97], and for these reason their levels can be used to measure the healing process. However, they do not constitute a specific diagnosis of the cause of wound healing failure or delay [74]. Instead, they are a response to an underlying stimulus that must be specifically identified [74]. The answer relies on the measurement of more than one protease, hence a allowing a better and more accurately overview of the healing process [74].

The principal proteases involved in wound healing are MMPs and serine proteases (including, cathepsin G, HNE and proteinase 3) [21,51].

MMPs can influence central physiological events towards healing, but they can also lead to pathological events [97]. Elevated levels of MMPs are indicative of abnormal healing, specifically levels of MMP-2 and MMP-7 and MMP-9 [21,44,97]. Another possible marker is the tissue inhibitors of metalloproteases (TIMPs), where their levels tend to be lower in chronic wounds [44,97]. In fact, a good prognostic of wound healing is when MMP-9/TIMP ratios are lower, being this a sign of proper deposition of matrix proteins [44,97].

Together with proteases, other neutrophils-released enzymes y can prevent completion of healing if unregulated [51,176]. Examples of this are myeloperoxidase (MPO) and lysozyme that are both involved in bacteria degradation [51,176]. However, their levels have been associated to infected or non-healing wounds [44,176].

Various reactive oxygen species (ROS), which include superoxide anion, hydroxyl radicals, singlet oxygen and hydrogen peroxide, are released into the wound environment by neutrophils and also endothelial cells and fibroblasts [28]. These molecules in combination with proteases and other destructive enzymes prevent bacterial contamination and cleanse the wound cellular debris

(debridement) [70]. However, excessive ROS directly damages cell membranes and structural proteins of ECM, and also affects signalling pathways essential to healing [28]. Oxidant/antioxidant imbalance within the chronic wound environment is a major contributor to impaired healing, as it escalates the unrestrained and persistent inflammatory state of chronic wounds [28].

I.4.3.2. Human Neutrophil Elastase (HNE)

HNE, a serine proteinase of the chymotrypsin family, is found in PMN cells (neutrophils, mast cells and eosinophils) and also in monocytes, keratinocytes and fibroblasts, being one of the most abundant proteinases in chronic wounds [114]. HNE (also known as HLE – Human Leukocyte Elastase) is encoded by *ELANE* gene (also known as *ELA2*), located within a 50kb segment in the terminal short arm of chromosome 19 p13.3 [114]. Mutation in this gene is associated to severe congenital neutropenia (SCN), an inborn immunodeficiency, and another related disorder, cyclic neutropenia (CN) [114,124,177,178]. SCN is a rare haematological disease characterized by impaired maturation of neutrophil granulocytes [177]. It leads to low or periodic oscillating levels in the production of PMN's (and other peripheral blood cells) [124,178], making patients prone to recurrent, and often life-threatening infections, and even to develop leukaemia and myelodysplasia [177,178].

HNE is an extremely cationic protein with a basic isoelectric point (pI) ≈10.5 and an optimal activity at pH close to neutral (pH 8 - 8.5) [114,124].Structurally, HNE (EC 3.4.21.37) is a glycoprotein composed by 218 a.a. in a single polypeptide chain, comprising four intra-chain disulphide bonds and two asparagine-linked carbohydrate side chains at Asn109 and Asn159, making up a molecular mass of 29.5 kDa (Figure I.9A) [114,124,179]. The HNE's active-site is formed by the catalytic triad His57, Asp102 and Ser195 residues [108,114], that are separated in the primary structure but when folded are placed in the cleft between the two β-barrels [124,180].

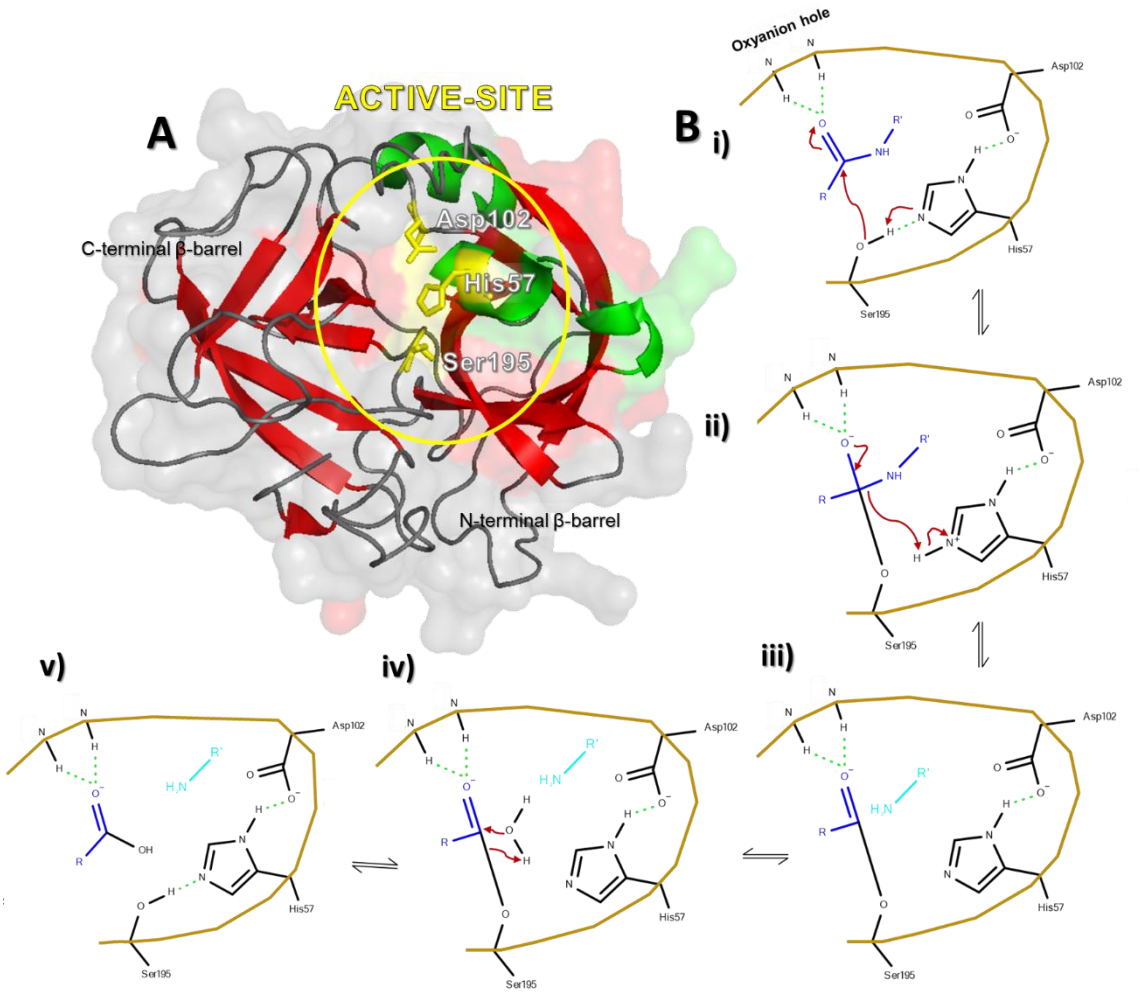


Figure I. 9. (A) Secondary structure of Human Neutrophil Elastase (HNE) protein. β-sheets and α-helixes are presented in red and green, respectively. Catalytic active-site comprising residues His57, Asp102 and Ser195 are depicted in yellow. Structure was designed with Pymol software (PDB 3q77). **(B)** Generally accepted mechanism of action for serine proteases. Hydrogen bonds are presented in green.

As a serine protease, the catalysis starts with the nucleophilic attack of the essential serine of the active-site (Ser195) to the substrate's carbonyl group of the cleavable amide group, and the transfer of the hydroxyl hydrogen of the serine to the sided histidine (His57) (Figure I.9B i) [124,125,180]. In the pocket of the active-site is the oxyanion hole, consisted of the backbone amides of Gly193 and Ser195. Oxyanion hole stabilizes the negatively charged transition state of the so-called intermediate state complex with a tetrahedral coordination of the carbon atom (Figure I.9B ii) [180–182]. This stabilization lowers the activation energy, being responsible for much of the catalytic efficiency of serine proteases [182]. The transfer of the hydrogen to the resulting N-H

bond on His57 is also stabilized by a hydrogen bond to Asp102 [180]. This acylation step leads to the breakage of the substrate's C=O bond from amide group, and an acyl-enzyme covalent intermediate between the enzyme and the remaining piece of the substrate is formed (Figure I.9B iii)[124,125,182]. Then, deacylation occurs through the nucleophilic attack of a water molecule on the substrate's carbonyl group (Figure I.9B iv), resulting in the cleavage and release of the N-terminal part of the substrate when the catalytic triad is regenerated (Figure I.9B v) [124,125].

HNE has been described as a biomarker for several health problems. In wounds, it plays an important role as regulator of inflammatory response [183]. Neutrophil elastase with the ability to virtually degrade all of the connective components in the body, is known as one of the most destructive enzymes [184]. Breakdown of ECM components at inflammatory sites allows the migration of the cells to the target site. HNE also has bactericidal properties, acting in the cleavage of virulence factors and outer membrane proteins of Gram-negative bacteria [124]. This protease is also involved in the caspase-independent activation of IL-1β and IL-18, conversion of anti-inflammatory progranulin to pro-inflammatory granulin, and in the coagulation pathway by cleaving the tissue factor pathway inhibitor on NETs [115]. NETs are composed of a sticky meshwork of chromatin and antimicrobial peptides and enzymes released from neutrophils [107,110]. This structures provide the perfect environment to not only immobilize the pathogens, preventing them from spreading, but also to facilitate phagocytosis [107,110]. They are formed by a process of cell death called NETosis, where the dominant activity has been attributed to HNE [115]. In addition, HNE was found to be tightly bound to DNA, possibly due to high affinity for the negative charged DNA, as HNE is a positive charged protein [115].

In spite of its protective role, HNE's non-specific action can cause extensive cell damage [124], being greatly involved in numerous disorders, including photoaging, delayed wound healing, chronic obstructive pulmonary disease (COPD), acute respiratory distress syndrome (ARDS), asthma, acute lung injury, cystic fibrosis [114,184], lung and breast cancer [185], joint diseases, rheumatoid arthritis [186], spontaneous preterm delivery [187], male adnexal affections [188] and other inflammation-related diseases. Moreover, it is evident that HNE plays a key role in several pathways, that when unregulated can also intensify tissue damage and inflammation [115]. Targeting HNE could minimize those adverse effects of unregulated proteolysis [114,115]. Hence, monitoring HNE in wounds could allow the regulation of its activity, being thought to represent a promising therapeutic approach to not only assist the healing of chronic wounds but also to treat other HNE-related diseases [114].

I. 4.3.3.Current methods for biomarkers sensors

Biomarkers should be (1) safe and easy to measure, (2) imply low budget techniques to measure, (3) should not vary with gender and ethnic group, and (4) should allow an effective, sensitive and specific relation to an abnormal event, disorder or disease [44]. Validation is the most important requirement for a biomarker [44]. Even though, currently most biomarkers do not satisfy these requirements, research has been progressively giving answers for these limitations [44].

To overcome unnecessary removal of the dressing or even to access whether the current method of treatment is being effective, novel non-invasive monitoring systems have been developed [93]. The wound environment offers multiple ways to monitor the healing process as it undergoes several molecular and physiological process over its course, until it reaches complete recovery [93]. Monitoring of this process can be achieved through the use of sensors.

Most sensors are meant for external use, where a sample of exudate is taken from the wound for analysis, and/or require other devices for readout [93]. Only a few sensors have been design to give a visible sign directly in the wound dressing [93]. Nowadays, research is trending towards wearable sensor devices for continuous or semi-continuous measurements, *in situ* and in real-time [93]. The deployment of a smart system coupled to a dressing, "smart dressing" can provide detailed information of the wound status, and proactively alert the patient and practitioners when the wound is becoming impaired, either due to infection, excess of inflammation, or any other impairing factors [189] (Table I.I). "Smart dressings" use biochemical cues to generate readable output of diagnostic or theranostic value [190]. Depending on the degree to which they indicate an appropriate intervention, these systems can be classified in three distinct categories: nonspecific, diagnostic or theranostic [189].

General/nonspecific tests do not necessarily provide a particular diagnostic, as they may not be specific to the wound environment [189]. Examples of these tests include measurements of pH, temperature, moisture, blood pressure, etc. [189].

Recently, a flexible and wearable sensor has been developed for the local monitoring of skin pressure, relative humidity and temperature [191]. It is composed of a flexible polyamide printed circuit placed on an adhesive film [191]. Other systems have also been developed for measuring temperature [192,193,193–197], however most of them are only applicable to perilesional skin and yet are not suitable for wound bed [198]. Salvo *et al.* successfully developed sensors for pH and temperature using reduced graphene oxide and graphene oxide boarded onto a flexible

polyethylene terephthalate matrix, being applied to measurements in human serum and plasma [199–201]. Even though, nonspecific sensors are helpful to the clinician, they require further interpretation, wherein other parameters have to be taken into account [189].

Diagnostic tests are more specific and provide an accurate and non-subjective decision-making output [189]. Even though these tests provide unambiguous answers relative to a specific physiological or biochemical condition, they require little interpretation from the practitioner to analyse the extent of that specific phenomenon. These include assessment of microbial load, biofilm, cell count and proteolytic activity [189].

A number of sensors have been developed to detect bacterial by-products (autoinducers and toxins) [202]. Sharp *et al.* was able to detect pyocyanin toxin and the consumption of uric acid at the wound site by the pathogens. They used an electrochemical sensing matrix composed of carbon fibre and measured oxidation/reduction of the analytes by square wave voltammetry [203,204]. Even though it is promising, the signal efficiency decreased over time due to electrode fouling [203,204]. Zhou *et al.* provided another alternative using trojan-like phospholipid vesicles loaded with a fluorophore indicator [205,206]. These molecules were immobilized onto/within the fibers of a dressing, that when in contact with bacterial toxins would rupture and release a fluorescent dye cargo, easily detected by low intensity UV light [205,206].

The most sensitive detector of early infection is the host's immune response, namely through protease activity [202]. New information about the healing process has allowed identification of several biomarkers for impaired healing, being evident the major role that HNE plays in it. HNE activity is elevated in fluids from chronic wounds and reduced in healing wounds, making it possible to be used as a marker of inflammation in impaired wound healing [100,207–209]. It is also suited as a target for detection of wound infection, since elevated HNE levels are described at the very beginning of an infection [208].

Better strategies for wound assessment are in demand, as it becomes clear that early detection is the most important factor for the properly treatment of a chronic wound. Common methods for HNE detection include *in vitro* analysis through enzyme-substrate activity assays [68,210–213], immunoassays (including enzyme-linked immunosorbent assay – ELISA and radioimmunoassay's) [214,215], aptamer-based assays [216], or others. HNE measurements are typically performed using specific peptide sequences linked to a chromophore (most commercially available peptides use *p*-nitroaniline *p*Na), or to a fluorophore (*e.g.* 7-amino-4-ethylcoumarin, AMC or 7-amino-4-

trimethylcoumarin, AFC) or within a Förster resonance energy transfer (FRET) system [217–219]. New strategies have been developed for a real-time and *in sit*u analysis at the wound site, not only for HNE but also for the detection of other biomarkers [190,198,202,220–223]. The following table I.III presents some approached developed to monitor HNE in the wound environment.

Even though advances are yet to be made for protease-detection "smart dressings", a point-of-care (POC) device is being developed for evaluating elevated protease activity at the wound site, termed as WoundChek™ Protease Status diagnostic [190,224,225]. The clinical trials regarding this technology are currently ongoing, paving a way for guided assessment and management of wounds [190,224,226].

Theranostic systems provide specific information and help guide treatment by confirming the need for a specific intervention [189]. These could be, for example, the identification of a specific bacteria in the wound, allowing the medical staff to prescribe specific antibiotic; or the identification of a specific MMP that is impairing the wound; or the depletion of a specific growth factor that needs to be balanced; etc. [189,190]. The ability to monitor wound healing as well as to predict possible debilitating markers in real-time and *in situ* will revolutionize the way that wounds are managed [190]. These new-age approaches, either through nonspecific, diagnostic or theranostic systems, will make sure the proper management of potentially problematic wounds, helping them to receive the appropriate attention at an early stage [190]. They will help the clinicians to adopt the most suitable management and treatment strategy, at the right time, to faster achieve proper healing [190].

Table I. III. Summary of approaches developed to monitor HNE in the wound environment.

Technology presentation	Method	Sample analysed	Limitations	References
Dip-stick	Chromogenic peptides immobilized in a cross-linked ethoxylate acrylate resin	Enzyme solution *(in vitro)*	Faint colour change (light yellow) based on pNa	[227]
Drop-and-sip	Fluorogenic peptides immobilized in a capillary-assembled microchip using reagent-release capillaries	Enzyme solution *(in vitro)*	Requires off-line fluorescent image analysis	[228]
Microdialysis sampling probe	Chromogenic and fluorogenic peptides infusion in a microdialysis sampling probe	Enzyme solution *(in vitro)*	Requires off-line detection by liquid chromatography-mass spectrometry (LC-MS) with electrospray ionization (ESI)	[229]
Dressing	Specific-HNE peptides immobilized in hydrogel films	Enzyme solution *(in vitro)*	Requires off-line measurements of the film degradation by quartz crystal microbalance	[230]
Dip-stick and Dressing	Chromogenic peptides in several solid-supports and dressings (including polyethyleneterephthalate, polyamide, silica gel, collagenous matrices)	Exudate *(ex vivo)*	Faint colour change (light yellow) based on pNa	[208,231]
Dressing	Chromogenic and fluorogenic peptides conjugated in a cotton cellulose nanocrystals and nanocellulosic aerogels	Enzyme solution *(in vitro)*	Faint colour change (light yellow) based on pNa Requires off-line fluorescence detection in a spectrofluorometer	[232–234]
Dressing	Fluorogenic peptides immobilized in several cellulosic and nannocellulosic materials (including, filter paper, print cloth, cellulose nanocrystals, nanocellulosic composites and nanocellulosic aerogels)	Enzyme solution *(in vitro)*	Requires off-line fluorescence detection in a spectrofluorometer	[235,236]
Dip-stick	FRET sensor based on two fluorescent proteins (cyan (CFP) and yellow (YFP) fluorescent proteins) connected via a short HNE-specific peptide	Enzyme solution *(in vitro)*	Immobilized in nickel-coated surface, to be used as strip or electrodes, and not as a dressing.	[237,238]

CHAPTER II.

HNE-specific chromogenic sensors

II. HNE-specific chromogenic sensors

Subchapter II. (a)

Design of a chromogenic HNE protease sensor based on split-GFP system

Subchapter II. (b)

Model substrates based on ultramarine GFP-like chromoprotein for elastase sensors

---

This chapter is based on the following scientific papers:

Ferreira, A. V., Cunha, J., Antunes, E., Ribeiro, A., Matama, T., Azoia, N., Cavaco-Paulo, A., Design of a chromogenic HNE protease sensor based on split-GFP system, *Applied Microbiology and Biotechnology*, to be submitted.

Ferreira, A. V., Cunha, J., Antunes, E., Ribeiro, A., Cavaco-Paulo, A., Model substrates based on ultramarine GFP-like chromoprotein for elastase sensors, *Biomacromolecules*, submitted.

II. (a) 1. Design of a chromogenic HNE protease sensor based on split-GFP system

Abstract

Chronic wounds are a heavy burden for the health care system, accounting for almost 4% of its total budget, and currently increasing. Recent studies have demonstrated that chronic wounds fluids have elevated concentration of human neutrophil elastase (HNE) that can be used as inflammation/infection marker for this type of wound. In this work, we aim to develop a chromogenic sensor activated specifically by HNE. The sensor was designed based on the GFP-like non-fluorescent ultramarine (UM) chromoprotein, following the previously reported strategy of split-GFP. The best peptide cleavage sequence for HNE optimized by an *in silico* studies was incorporated in the signalling protein, turning it into a chromogenic sensor. Our findings explore the possible application of GFP-like chromogenic sensor in a point-of-care device for wounds status evaluation. This work is a major step towards the development of a medical device for chronic wound control, being estimated to have a great positive impact on patient's wellbeing and life quality.

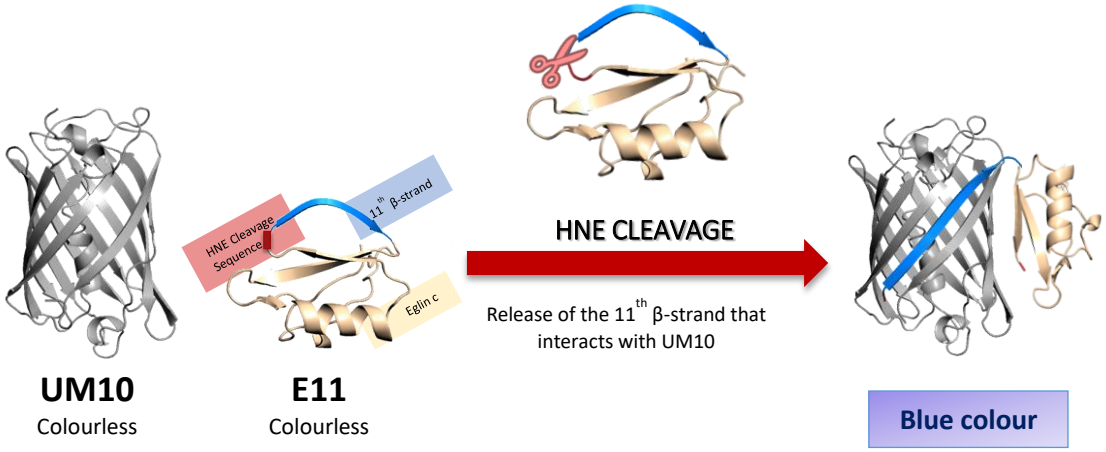


Figure II. (a) 1. Graphical abstract of the subchapter. Schematic representation of the split-UM strategy developed as sensor substrate for HNE. The chromogenic GFP-like ultramarine protein (UM) was engineered with the last 11th β-strand dislocated from the 10 β-sheet-barrel, creating a colourless protein (UM10). After HNE proteolysis at the cleavage site inserted on E11 portion, the 11th β-strand is released and its proximity to the UM10 β-barrel should regenerate UM's blue colour. Structures were created with PyMol software (UM PDB 3vk1 and eglin c PDB 1egl). Incomplete β-barrel is presented in grey, eglin c moiety is coloured golden, 11th β-strand is coloured blue and the cleavage sequence for HNE is represented as a red box.

II. (a) 1. Introduction

The inflammatory response is an important step on wound healing. However, if there is an imbalance between the immune response and tissue regeneration, the healing process will be delayed, resulting in a chronic wound [27]. As one of the most billed service in health care, chronic wounds are a costly burden on society, being considered as a silent epidemic [1,2,6]. Early detection of incipient wound infection and chronic inflammation reduces the severity of the lesion and decreases health care expenses [239]. It is difficult, expensive and time consuming to accurately assess the wound status, hence, there is an urgent need for a new diagnostic tool [2].

Human Neutrophil Elastase (HNE) plays a critical role during inflammation. In spite of its protective role, HNE is also implicated in numerous disorders, including delayed chronic wound healing [208,240–242]. The progress of wound healing and the assessment of wound status can be achieved through monitoring and detecting HNE in wounds. Even though several approaches have been developed to monitor HNE in the wound environment [208,227–238], alternative strategies are in demand as these present striking limitations. Most of them are based on fluorogenic approaches, requiring always an off-line detection system. And the ones based on a chromogenic approach use *p*-nitroaniline (*p*Na) as a chromophore, being difficult its visualization and discrimination from the wound fluids.

Green fluorescent protein (GFP) is one of the most used system as a tagging and detection method in several biological and molecular studies, in some of them due to its inherent ability for self-reassembling of the β-chains [243]. Cabantous *et al.* 2005 engineered a split GFP system involving two non-fluorescent portions of GFP that when mixed together restored the green fluorescent signal: one portion corresponds to GFP 1-10 fragment (amino acids 1-214, 10 β-sheets) and another portion corresponds to GFP11 (amino acids 215-231, 11th β-sheet). In following works, this split GFP system has been extensively adapted to integrate a protease-based switch-on system for HIV protease, caspase-3, factor Xa, enteropeptidase and thrombin [245].

In our work, we used the same described rationale to develop a HNE switch-on colour system using a GFP-like chromogenic protein. The colour change upon HNE proteolytic activity must include the following two criteria to meet its intended application: (1) easy discrimination by the human eye in the wound dressing, and (2) direct correlation between colour intensity/development time vs the amount of HNE in the wound. Considering the reddish to brownish colour of the wound environment (due to blood and pus) [246], we determined that the colour of choice for the sensor

should be dark blue, dark green or deep purple [247,248], to avoid misleading interpretations. Taking this into consideration, we selected ultramarine (UM), a chromogenic blue protein derived from Rtms5 (a naturally occurring GFP-like fluorescent protein) [249,250], as subject of our work. The genetic modifications introduced by Pettikiriarachchi *et al.* (Val40Ala, Ser121Arg, Leu123Thr, His142Asn and Phe158Arg) converted Rtms5 into a monomeric and non-fluorescent chromogenic protein of an intense dark blue colour [249,250].

Our strategy, inspired by the method described in Callahan *et al.* 2010, converted UM into a protease switch for elastase (Figure II. (a) 1) [245]. Briefly, we genetically modified UM to delete its last 11th β-sheet, leading to a colourless protein composed of a barrel with 10 β-sheets (UM10 protein). The 11th β-sheet was produced hybridized with the stable surface-exposed α-helix from eglin c containing the HNE-cleavage sequence (E11 portion). As observed by Callahan *et al.* 2010, we expected to restore the chromophore group when both polypeptides are mixed together in the presence of the HNE protease. Similarly to GFP, the released 11th β-strand will interact with the incomplete UM10 β-barrel leading to the appearance of a blue colour.

The design of a chromogenic recombinant protein sensor for the monitoring of HNE is not only a major step in the wound care field, but it can also revolutionize the diagnostics and medical sensors field since colour-based switch-on approaches with non-fluorescent GFP-like proteins were never reported before.

II. (a) 2. Materials and Methods

Materials and Reagents

All reagents were analytical grade, purchased from commercial suppliers and used as received. Standard molecular biology procedures were used for the gene cloning and protein recombinant expression in Escherichia coli TOP10 (Invitrogen) and E. coli BL21 DE3 (Novagen), respectively. DNA restriction enzymes *Not*I and *Nde*I and kanamycin antibiotic were purchased from ThermoFisher. Gold View for DNA staining was from UVAT Bio (Valencia, Spain). Culture media LB Broth and Terrific Broth (TB) (Auto induction medium) were purchased from Grisp (Porto, Portugal). Isopropyl-β-D-thiogalactopyranoside (IPTG) inductor was purchased from Acros Organics (Geel, Belgium). Nickel magnetic beads for His6 tag protein purification and respective magnetic separator were purchased from Bimake (Houston, USA). Protein molecular weight markers, Precision Plus Protein All Blue or Precision Plus Protein Dual Xtra Standards, were purchased from Biorad (Portugal). Chaotropic agent urea was purchased from labkem (Spain). All other chemicals were purchased from Sigma-Aldrich (Spain), including the enzyme elastase from human leukocytes, synthetic elastase substrate *N*-methoxysuccinyl-Alanine-Alanine-Proline-Valine-*p*-nitroanilide (MeOSuc-AAPV-*p*NA), imidazole and N-Laurylsarcosine sodium salt (sarkosyl) detergent. The dialysis tubing cellulose membranes (MWCO, 1-2 KDa and 12-14 KDa) and GenEluteTM Plasmid Miniprep Kit were also obtained from Sigma-Aldrich. The ultramarine's 11th β-strand peptide (pep11) was synthetized by JPT Peptide Technologies GmbH (Germany).

Instrumentation

All absorbance and fluorescence measurements were carried out in 96-well microplates of 300 µL capacity/well using a Synergy Mx spectrometer with the Gen5™ Data Analysis Software (Bio-Tek Instruments, Inc., USA). DNA and total protein were performed quantified in Nanodrop 1000 (ThermoScientific). Bacterial cell lysis was accomplished with an Ultrasonic Processor VCX-500 watt (Sonics & Materials, Inc., Connecticut, USA). Purified recombinant proteins were lyophilized in a FreeZone 2.5 Freeze Dry System (Labconco, Missouri, USA).

Methods

1. Protein expression and purification

All the genes inserted in a pET28a(+) plasmid were ordered from Genscript (New Jersey, USA). Gene size confirmation was performed with GenEluteTM Plasmid Miniprep Kit and double digested with the restriction enzymes *Not*I and *Nde*I; the molecular weight of the resultant DNA fragments was confirmed in a 1% agarose gel stained with Gold View. All plasmids were first established in *E. coli* TOP10 and then expressed in *E. coli* BL21 (DE3). The TSS method was used for transformations as previously described [251]. Optimized protein expression was accomplished in 24 hours using LB medium supplemented with kanamycin (50 µg/mL) and 180rpm after induction with 0.25 µM IPTG at a culture OD of 0.5. All proteins demanded a culture/flask ratio of 1:10 and aeration *via* gauze sheets. UM and E11 were incubated at 30˚C, whereas UM10 required a low incubation temperature (16˚C) to increase solubility. See also II. (a) 5.Supplementary Information, Table II. (a). S I, II and III, and supplementary Figure II. (a) S 1 and S 2 for details on parameters optimized. After expression, cultures were placed at 4°C for at least 2 hours to enhance chromophore folding. Then, the cells were harvested by centrifugation at 8,000*g* at 4°C for 10 minutes, cell pellets were resuspended in lysis buffer (20mM NaH_2PO_4, 500mM NaCl, pH 7.4) and subsequently lysed by ultrasounds. The ultrasonic disruption of the bacterial cells was accomplished on ice with a 3-mm probe (small-scale production) or 13-mm probe (medium-scale production). The lysate was centrifuged at 10,000*g* at 4°C for 30 minutes. Imidazole was added to a final concentration of 10mM, and protein purification was done using nickel magnetic beads using an imidazole gradient of 10mM to 500mM. At every step, the fractions obtained were monitored by SDS-PAGE with Coomassie blue staining. Removal of imidazole from the eluted fractions was performed through dialysis against ultrapure water using a cellulose membrane with a MWCO of 1-2 KDa for E11 protein and 12-14 KDa for the other proteins. The pure protein fractions were then frozen at -80°C and lyophilized. The molecular weight of all proteins obtained by SDS-PAGE was in accordance with the theoretical size expected from the polypeptide sequences including the amino acids encoded by pET28a(+) vector.

2. Molecular docking simulation

Molecular docking simulations were performed to evaluate the binding affinity between elastase enzyme and 11 small oligopeptides (tetra, penta and hexapeptides). The 3Q77 entry on RCSB protein databank [179], corresponding to HNE structure obtained by X-ray diffraction, was used as computational model receptor on docking simulations. The PyMOL software [252] was used to create all the peptide models on PDB (Protein Data Bank) format. The models of the receptor and each peptide were pre-processed with Autodock tools [253] to correct the charges, the hydrogens and the bonds flexibility when needed. Later, Autodock Vina [254] was used to perform the docking simulations between elastase and each peptide (10 replicas for each system). All docking calculations were performed with one box of 4x2.4x3.6nm centred on the enzyme's active site and the exhaustiveness value applied was always 80. The resulting three best models (lowest free energy ΔG) of each peptide were chosen to calculate the mean average binding affinity for each peptide.

3. Assessment of the UM-based split proteins as HNE protease sensor

HNE activity was first evaluated for the batches used in the experiments with a control assay with the synthetic substrate MeOSuc-AAPV-*p*NA following the protocol supplied by Sigma-Aldrich. Briefly, the enzyme (0.5 U/mL) was mixed with 25-1500 µM of substrate, to a final volume of 300 µL of reaction buffer (100 mM HEPES with 500 mM NaCl, pH 8). A blank consisting only in buffer and substrate was also included. The kinetic constants were determined from the initial rates of hydrolysis by Michaelis-Menten method. All enzymatic assays were conducted at 37°C for 10 minutes in triplicate and the absorbance was measured at 405 nm by UV-Vis spectrophotometry.

The lyophilized proteins were resuspended immediately prior to the assay in 100 mM Tris-HCl at pH 8. The absorbance spectra of the UM-based split proteins prior and after addition of HNE were recorded in a spectrometer for colour change assessment. The split UM system was prepared by mixing UM10 (fixed at 1.5 mg/mL or 3.4 mg/mL) and protein E11 in a final molar ratio of 167:1 or 167:5 (UM10:E11), or by mixing in the same ratios UM10 and pep11 (the synthetic peptide equivalent to free 11th β-sheet). In addition, to improve the sensibility of the assay, the same assays were performed in a 96-well microplate firstly blocked with a solution of 0.5% bovine serum albumin (BSA), as described in Cabantous *et al.* [255].

II. (a) 3. Results

AAPV is the preferred peptide substrate for HNE by molecular docking analysis

Several small peptide sequences were designed as potential specific substrates for HNE according to residues' affinity to the enzyme described in literature [124,125,175,180,240–242,256] (Supplementary Figure II. (a) S 3). Tetra, penta or hexapeptides were assessed by molecular docking regarding their interaction and affinity to the HNE's active site (Table II (a) I). In this evaluation, the lowest binding free energy (ΔG) indicates the higher affinity to the enzyme.

Table II. (a) I. Summary of the binding free energies (ΔG) involved in the interaction of the peptides with HNE's active site. Values presented are means and standard deviation of the best three replicas out of ten. Theoretical molecular weight (MW) was calculated by Compute pI/Mw tool in ExPASy Bioinformatics Recourse Portal.

Peptide Sequence ... P4-P3-P2-P1	ΔG (kcal/mol)	**Number of residues**	**MW** (Da)
AAPA	-5,87 ± 0.12	4	328.37
AAPV	-6.40 ± 0.00	4	356.42
AAPI	-6,07 ± 0.35	4	370.45
SSPA	-5,83 ± 0.35	4	360.37
SSPV	-5,73 ± 0.40	4	388.42
SSAPV	-5.17 ± 0.50	5	459.50
ASAPV	-6,13 ± 0.15	5	443.50
ASASPA	-5,93 ± 0.12	6	502.52
SASAPA	-5.63 ± 0.15	6	502.52
ASASPV	-5.36 ± 0.25	6	530.58
SASAPV	-5.67 ± 0.29	6	530.58

The lowest binding free energy (ΔG) was observed for the peptide AAPV, meaning that it is the peptide most specific as HNE's cleavage sequence. Its higher affinity for the enzyme and strong interaction with its active site was evident in docking simulations (Figure II. (a) 2A).

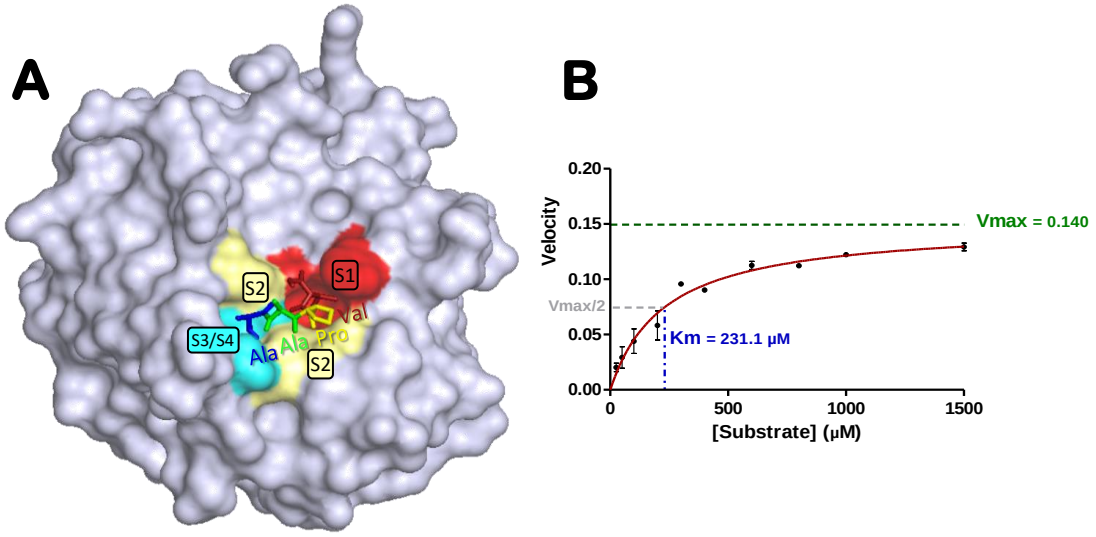


Figure II. (a) 2. Affinity of AAPV peptide to HNE. (A) Docking images of the interaction between HNE (in grey) and peptide AAPV (P1 Ala in blue, P2 Ala in green, P3 Pro in yellow and P4 Val in red). Enzyme's subsites are labelled according to the nomenclature of Schechter and Berger [257], and pockets are coloured as its interacting residue from substrate (S1 is red, S2 is yellow and S3/S4 is cyan). Structures were visualized with PyMol Software. (B) Reaction velocity plot of HNE (0.5 units/mL) as function of substrate's concentration for the synthetic peptide MeOSuc-AAPV-*p*NA. Kinetic parameters were determined by nonlinear regression Michaelis-Menten plot, using Graph Pad Prim 5. Values plotted are the means of triplicates.

The interaction sites between HNE's pockets (Sn, ... S1, S1', ... Sn') and the corresponding peptide residues (Pn, ... P1, P1', ... Pn') are named using the Schechter and Berger nomenclature, where P1-P1' is the cleavable peptide bond [125,257] (Supplementary Figure II. (a) S 3). Valine residue at position P1 accommodates in the deep pocket S1, proline at position P2 interacts with subsite S2, and alanine residues at positions P3 and P4 are well-established in the S3 and S4 cleft (Figure II. (a) 2).

To validate AAPV as a good substrate for HNE, we performed kinetic studies with the enzyme and commercially available synthetic HNE substrates using UV-Vis spectrometry (Figure 2B). The obtained kinetic parameters are within the range found in literature, under similar conditions [68,180,256,258–260].Therefore, the peptide sequence AAPV was selected for the consequent gene design for the development of HNE sensor.

Production of the split-UM sensor for HNE detection

The incomplete version of ultramarine made of 10 β-sheets (UM10 protein) and the sensing substrate composed by the peptide AAPV+11th β-sheet incorporated in eglin c moiety (E11) were firstly expressed in the optimal conditions previously established for UM (Supplementary Tables II (a) S I, II and III). UM and E11 were obtained soluble using LB medium with 0.25 μM of IPTG for 24 hours at 30°C and 180 rpm agitation (Supplementary Table II (a) S I and II). Aeration was determined to be a crucial factor for colour generation, so no more than 1:10 of culture/flask volume ratio can be grown in Erlenmeyers and these must be covered with gauze sheets instead of cotton plugs (Supplementary Table II (a) S III). In addition, after the incubation time, cultures are allowed to rest at 4 °C for 2 hours for stabilization of the chromophore. After verifying the low initial protein expression yield for UM10, we undertook an optimization of the conditions for controlled culture growth and proper protein expression. Culture's growth rate was slowed-down by reducing the incubation temperature to 16 °C to improve the chances of correct folding of the protein being expressed (Supplementary Figure II (a) S 1A) and colonies' selection was implemented to choose the best soluble/insoluble ratio, even if the overall production yield had to be compromised (Supplementary Figure II (a) S 1B). In addition, after cell lysis, several ice-vortex cycles were performed to aid the solubilisation of UM10 protein, thus enhancing its correct folding. The optimal experimental set-up for UM10 is schematized in Supplementary Figure II (a) S 2. Under these conditions, UM10 was expressed ≈50% soluble (Supplementary Figure II (a) S 1B). Other strategies for improving protein solubility of this protein were also tested, although no further gains were obtained (Supplementary Figure II (a) S 1D and 1E).

Under the optimal conditions for expression, the original UM presented a dark blue colour and the engineered proteins UM10 and E11 were non-coloured, as expected (Figure II (a) 3).

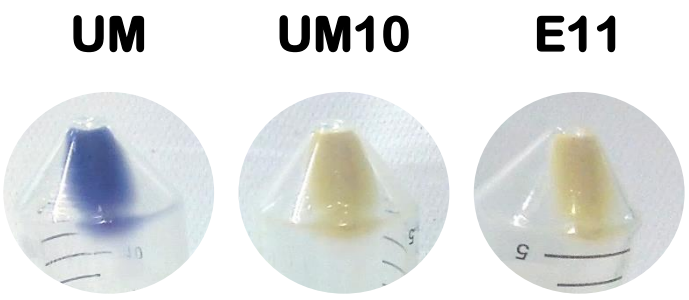


Figure II. (a) 3. Bacterial pellets after expression of UM, UM10 and E11 under the optimized laboratorial set-up.

Effect of HNE on split-UM strategy

Prior to the assessment of the absorbance changes on UM-split sensor in the presence of HNE, we evaluated the protease effect in the original UM as a measure of specificity analysis. Foremost, loss of colour was not observed in ultramarine after incubation with HNE, even over 24 hours of incubation, indicating no significant proteolytic effect of elastase on this protein. However, a slight and transient increase in absorbance was registered upon HNE addition (≈ 0.18 a.u. corresponding to ≈11% increase) (Supplementary Figure II (a) S 4A). Somehow, in the first moments, the interaction of the protein with HNE led to a potentiation of the absorbance, but since it returned to baseline afterwards, this effect was disregarded. However, by SDS-PAGE we detected a small molecular weight decrease of approximately 1kDa in ultramarine after incubation with HNE (Supplementary Figure II (a) S 4B). After analysis using ExPASy Peptide Cutter software (SIB ExPASy Bioformatics Resources Portal, available online tool) [261], we inferred, by the corresponding fragment's size, that it probably resulted from a small cleavage right after the His^6 tag at protein's N-terminal (Supplementary II (a) Figure S 5). Still, we can conclude that this cleavage does not affect the protein conformation nor chromophore's arrangement since the colour remained blue even after several days of incubation with the enzyme (Supplementary II (a) Figure S 4 and data not shown). Hence, we were confident that any colour change in the split-UM and split-fused UM would be specific to HNE proteolysis at the cleavage site.

The efficiency of the system was assayed by adding HNE to purified UM10 (fixed at 3.4 mg/mL) previously mixed with E11 in the molar ratios 167:1 and 167:5 of UM10:E11. The synthetic 11^{th} β-strand peptide (pep11) was also included in this assay and mixed with UM10 at the same ratios as E11. Evaluation of the interaction of the 11^{th} β-strand and the incomplete β-barrel was made by measurement of the absorbance over time (Figure II (a) 4).

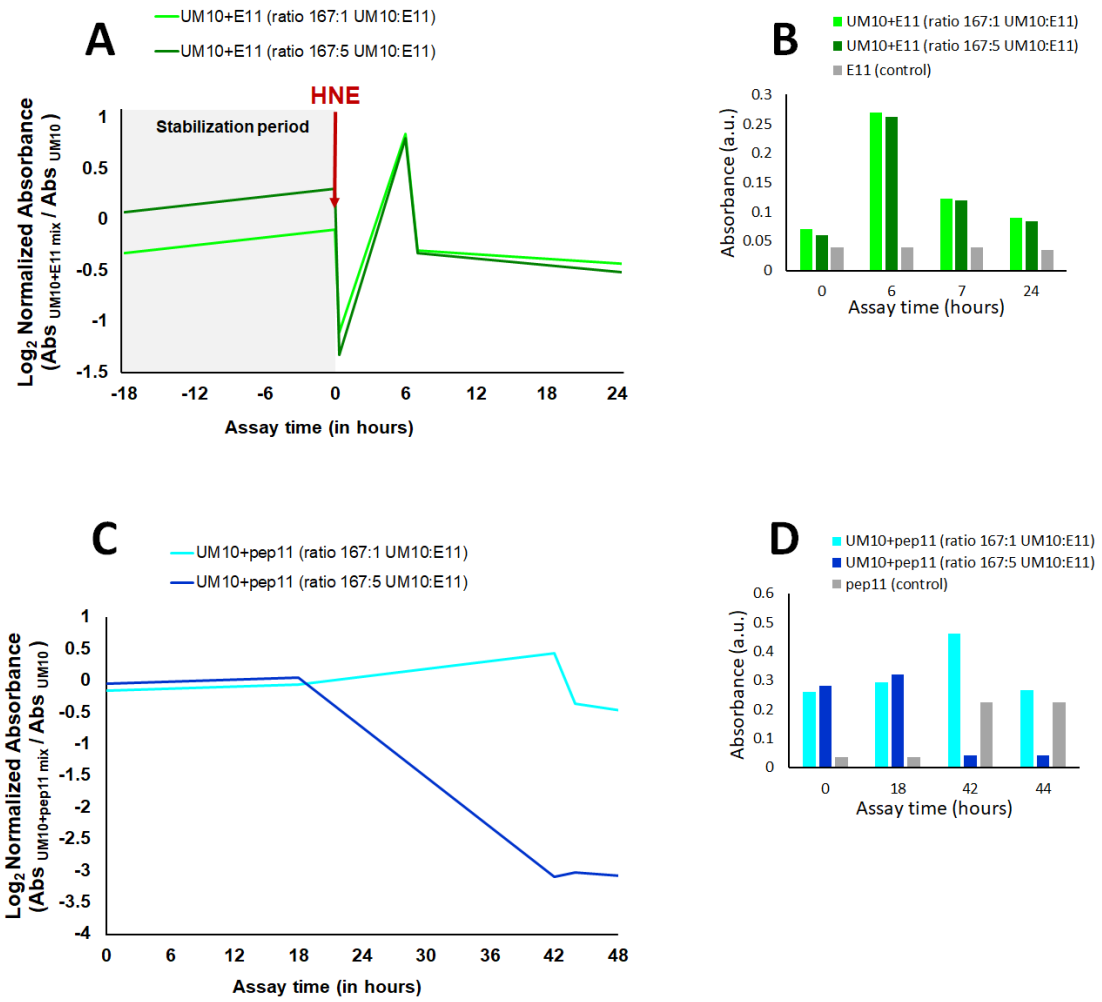


Figure II. (a) 4. Efficiency of the **(A-B)** split-UM system in detecting HNE and comparison with the mixture of **(C-D)** UM10 with the synthetic peptide pep11, in molar ratios of 167:1 or 167:5. Absorbance was measured at 585 nm for 24 and 48 hours, respectively. **(A-B)** Effect of HNE on mixture UM10+E11. Split UM system was first allowed to stabilize overnight before the addition of HNE, as done by Callahan *et al.,* 2010 [245]. The absorbance values at time points that registered abrupt changes are presented in **B**, namely at 0, 6, 7 and 24 hours. **(C-D)** Effect of HNE on mixture UM10+pep11. Absorbance values at stipe changes are presented in **D**, namely at 0, 18, 42 and 44 hours. Absorbance values were normalized against the absorbance of UM10 in **A** and **C**. The legend shows the categorization of the absorbance value in arbitrary units (a.u.) in **B** and **D**. All assays were performed at room temperature.

For split-UM system, a measurable increase in absorbance was observed for a period of 6 hours after the addition of HNE (≈ 0.2 a.u of absorbance in UM10+E11+HNE mixture, corresponding to ≈75% increase) (Figure II. (a) 4A and 4B). This effect is possibly due to the association of the split protein UM10 and cleaved E11, as we intended. After this time, the absorbance steeply decreased and then stabilized at the 7th hour of incubation, continuing with a steady and very slow decrease in the absorbance verified until the end of the assay. The interaction of UM10 with a free and readily available 11th β-sheet was evaluated using pep11instead of E11 protein that needs be cleaved to correctly interact with the β-barrel (Figure II. (a) 4B). This system followed almost the same trend as the described for UM10+E11+HNE, although contrarily to the observed with E11, the interaction of UM10+pep11 differed in each tested ratio. When mixing UM10+pep11 in 167:1 ratio, the absorbance of the complex slowly increased during 42 hours. Then, in 30 minutes, it rapidly recovered the initial values and continued to drop. However, increasing the number of pep11 molecules, the decrease in absorbance occurred in only 18 hours, then it continued to drop for 24 hours to much lower values than those initially recorded, and finally it stabilized in the last hours of the assay.

II. (a) 4. Discussion

Selection of the sensing substrate to incorporate in HNE sensor

Human neutrophil elastase (HNE) is a glycoprotein composed by 218 a.a. in a single polypeptide chain, comprising two asparagine-linked carbohydrate side chains and four intra-chain disulphide bonds that drive the folding of the protein in two β-barrels [124,179]. Its active-site is formed by the catalytic triad His57, Asp102 and Ser195 [108] that are joined in the tertiary structure in a cleft between the two β-barrels [124]. The enzyme recognition site is located in that cleft, where the catalytic triad and other surrounding amino acids form binding pockets (Sn, ... S1, S1', ... Sn') that interact with the substrate peptide (Pn, ... P1, P1', ... Pn') (Supplementary Figure II. (a) S 3).

In silico studies allowed us to analyse the interaction and affinity of several peptide sequences to the HNE's active site. The advantage of using molecular simulations was aiding in the prediction of peptides' behaviour in face of HNE, making it more cost and time effective [262]. Docking analysis gives a theoretical quantitative assessment of the binding efficiencies of the HNE enzyme with the designed peptides [262,263]. The interaction between the receptor (in our case, the HNE

enzyme) and the ligand (the peptide cleavage sequence) is calculated through the total Gibbs binding free energy (ΔG) [263]. In order for the binding between receptor and ligand to occur spontaneously, the value of ΔG must be negative, where its magnitude determines the stability of the formed complex [262]. In other words, the more negative the free binding energy is, the stronger is the binding [262].

There are a number of elements to consider when selecting the cleavage sequence for HNE, more specifically the amino acid composition and the sequence length. Firstly, the designed sequence must allow binding and interaction with enzyme's active-site and pockets, but also it can't interfere with the conformation of the anchor polypeptide (eglin c) where the cleavage sequence will be embedded. The mechanism and specificity of HNE enzyme has been extensively described [124,125,175,180,256]. Information retrieved from these studies, combined to the known sequences of HNE substrates and/or inhibitors [240–242] was taken into consideration in defining the cleavage sequence for HNE.

Currently, interactions of S' sites are not completely understood and P' side chains have either not been completely defined for HNE [180]. Yet, it is known that S' sites have a distinctive preference for Gly, Ala, Val, Leu and Ile residues in the P' positions. For this reason, peptide positions of P' were not explored.

S1 pocket of the active site of HNE is deeply buried within the enzyme's structure, containing a negatively charged residue (Asp226) and several hemispherical and hydrophobic residues in the vicinity (Val190, Phe192, Ala213, Phe228 and the disulphide bridge Cys191-Cys220) [124]. Specific HNE peptides should be composed in P1 of small hydrophobic residues, for example Ala, Val, Ile or Leu. Our results revealed a distinct preference in the P1 position for Val, presenting the lowest free energy when comparing Ala, Val or Ile at P1 (Table II. (a) I). However, this preference was affected by the interactions in other positions. When a Ser residue was placed at position P3, instead of Ala, a slight preference for Ala in position P1 was observed. The peptide length showed to impact this preference, since in a tetrapeptide preference for Ala differed only in ≈0.10 kcal/mol (SSPA and SSPV) while in a hexapeptide, this difference increased to ≈0.57 kcal/mol (ASASPA and ASASPV) when a Ser was replaced by an Ala in P3 (Table II. (a) I).

The bowled-shaped subsite S2, bounded by Phe215, Leu99 and His57 [124,180], the latter being a component of the catalytic triad, is the most specific subsite. Its specificity correlates to the hydrophobicity of P2 [180] and, hence S2 does not accept charged residues, like Lys, Arg or

Asp [124]. Instead, P2 residue should be an amino acid with medium-sized hydrophobic chain, or less bulky aromatic derivatives, such as Pro [124,256]. The pentameric pyrrolidine ring of the Pro residue completely fills the S2 pocket, being systematically described as the best residue for P2 position [175,256]. For this reason, we fixed P2 as Pro in all simulations.

The same applies for the subsites S3 and S4, that also preferably accommodate hydrophobic residues, like Ala, but have low tolerance for positively charged residues, like Lys [124,256]. Still, the S3 site is less restricted than S4, being able to accommodate even bulkier residues, as long as they are hydrophobic [180,256]. Negatively charged residues, like Glu, and even residues with polar uncharged side chains, like Gln, have been reported to significantly enrich HNE activity [115]. We decided to further evaluate this preference, comparing Ser, with a polar uncharged side chain, and Ala, a small hydrophobic residue. Indeed, the substrate's affinity was higher with Ala residues in positions P3 and P4. As before, interactions in other positions affected this preference as when P1 was a Val, the preference for Ala on P3 and P4 *versus* Ser increased (difference of ≈0.67 kcal/mol) (Table II. (a) I).

The side chain from P3 residue tends to protrude out of the active-site cleft, but additional Pn residues can strongly influence the substrate specificity [180]. Besides the impact of the peptide length on the interaction with other enzyme's subsites, we did not recognize a preference for hexa- or tetrapeptides. With all the information retrieved from molecular docking analysis, we selected the shorter peptide that presented the lowest free energy, AAPV, as HNE-specific cleavage site to insert in ultramarine's sensor.

Evaluation of the split-UM sensor for HNE detection

The rationale developed years ago by Callahan *et al.* [245] to adapt the split-GFP technology developed by Cabantous *et al.* [244] into a protease switch, and the need of a naked-eye detection system served to us as motive to engineer a switch-on sensor for HNE based on the chromogenic GFP-like ultramarine. We inserted the last 11th β-strand into the exposed loop of eglin c and added the selected AAPV peptide as HNE cleavage site upstream the sequence of the11th β-strand.

In order to obtain a switch-on strategy, the absorbance should increase upon HNE addition. When HNE was added to the mixture of UM10+E11, we detected a ≈75 % increase in the absorbance in the first 6 hours. However, this effect was lost afterwards and, from this point on,

the absorbance decreased (Figure II. (a) 4A and 4B). HNE cleavage on E11 released the 11th β-strand from the eglin c assembly, and once released, the 11th β-strand could interact with the split protein UM10, allowing the chromophore environment to be re-established. However, our interpretation is that the interaction of UM10 with β11th was not stable and the chromogenic chromophore was not maintained for long. The registered decrease in absorbance is the result of instability of the established interaction between the 11th β-strand and UM10; the 11th β-strand might have drifted to the solution and no longer interacted with UM10 protein. The interaction was not dependent of number of E11 molecules, but it appears to be affected solely on the UM10 molecules, since the same absorbance changes were observed for both tested ratios of UM10:E11. The same was observed in Callahan *et al.* work, as the fluorescence changes were mainly influenced by the GFP1-10 molecules rather than GPF11 [245].

To exclude the eventual entropy caused by the presence of HNE or the inefficacy of the enzyme in releasing the 11th β-strand as cause for transient increase in absorbance, we added the 11th β-strand readily available (pep11) to UM10. Contrarily to the observed for UM10+E11, system's behaviour seemed to be dependent of the number of molecules of pep11 present (Figure II. (a) 4C and D). The interaction was faster and steeper when more molecules of pep11 were added to UM10. In addition, we observed that the peptide in the control assay precipitated after 18 hours (data not shown). It coincided with an absorbance increase from 18 to 42 hours (Figure II. (a) 4D). The same happened for the mixture UM10 + pep11, being the rate of the peptides' precipitation higher and faster when more peptide molecules were involved.

The observed results at this stage, though promising, were still inconclusive since the mechanism of interaction here presented is not yet fully understood.

Considering that the established interaction between UM10 and E11/pep11 was not stable, and since the split-UM strategy requires the production of two proteins, we went forward and engineered a split-fused UM system which is made of the same genetic modifications as the first one, but it's an *all-in-one* approach with the two portions fused in a single protein (UM10E11) (Supplementary Figure II. (a) S 1 and Supplementary Figure II. (a) S 6A).

It was extremely challenging to obtain UM10E11 in the soluble fraction and, like UM10, only ≈50% of the protein was soluble when expressed in optimized conditions (Supplementary Figure II. (a) S 6B). Other strategies for improving UM10E11 solubility were also explored (Supplementary Figure II. (a) S 1). As expected, UM10E11 was expressed non-coloured (Supplementary Figure II.

(a) S 6B). We encountered more problems assessing the effect of HNE on this protein. UM10E11 precipitated upon addition of elastase, making difficult to accurately measure the absorbance changes (Supplementary Figure II. (a) S 6C).

The work here presented proves the difficult process on achieving a stable chromophore after cleavage in chromoproteins. Nowadays, methods using fluorescence-based switch-on approaches with GFP-like proteins are widely used [244,245,255,264–267], however GFP-like colour-based approaches are still a long way to be achieved. We made an effort to conquer this challenge, and even though we could not obtain a stable colour change on our split-UM system, we were able to register an interaction between the incomplete β-barrel and the 11th βstrand (in both strategies) upon HNE cleavage.

Field of application

This work serves as a proof-of-concept that a recombinant protein based in a split chromogenic approach may be used as a detection sensor. The embedding of a chromogenic HNE-specific recombinant protein, either based in a GFP-split or split-fused strategy, into a wound dressing material could allow *in situ* and real-time assessment of the status of a wound at an early stage of inflammation and/or infection. HNE enzyme present in the chronic wound fluid would recognize and cleave the sensor leading to a colour change on the dressing. By simple visualization of the dressing colour, the medical staff could monitor the activity levels of HNE in the wound, and consequently recognize whether the current treatment is being effective for the wound healing. Monitoring of a wound status can be further explored through a combination of other markers of inflammation/infection aside from HNE enzyme, for example matrix metalloproteinases (MMPs), proteinase 3, collagenase, reactive oxygen species (ROS) or even pH.

II. (a) 5. Supplementary Information

Otherwise stated, all the materials and methods used to produce these data are the same as described in II. (a) 2. Materials and Methods section.

Experimental set-up and optimization of the expression of ultramarine (UM)

UM protein expression in the soluble protein fraction, assessed by a more or less intense blue purple colour, was successively optimized regarding culture medium, expression time (Supplementary Table II. (a) S I), expression temperature (Supplementary Table II. (a) S II) and oxygen aeration conditions (Supplementary Table II. (a) S III). Protein amount in the soluble extract was verified by SDS-PAGE and quantified in Nanodrop and the assessment of the characteristic blue colour was used as means of evaluation of correct folding.

Table II (a) S I. Optimization of culture medium, type and time of induction at 37°C. Colour intensity of cell pellet is presented in a qualitative ordinal scale: (-) for non-coloured, (+) to (+ + +) for blue-coloured pellet.

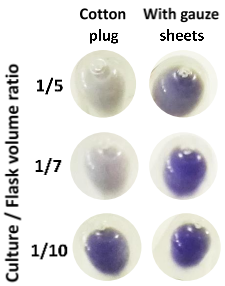
Culture medium	Expression time /hours	Protein present in cell lysate fraction	Colour
LB-IPTG	2	Soluble	-
	4	Soluble	-
	6	Soluble and Insoluble	-
	10	Soluble and Insoluble	+
	24	Soluble	+ +
Auto-induction medium (TB)	16	Soluble and Insoluble	+
	24	Insoluble	+

Table II (a) S II. Optimization of incubation temperature and evaluation of the effect of oxygen renewal on ultramarine expression in LB medium with 0.25 µM IPTG for 24h. Aeration was evaluated using culture flasks covered with gauze sheets (Yes) or with a common cotton plug (No).

Expression temperature	Oxygen renewal	Protein present in cell lysate fraction	Colour Intensity
16 ºC	No	Soluble and Insoluble	-
	Yes	Soluble	+
23ºC	No	Soluble and Insoluble	+
	Yes	Soluble and Insoluble	+ +
30ºC	No	Soluble and Insoluble	+
	Yes	Soluble and Insoluble	+ + +
37ºC	No	Soluble and Insoluble	+
	Yes	Soluble and Insoluble	+ +

Table II (a) S III. Selection of the culture/flask volume ratio and aeration conditions for the production of dark blue-coloured UM protein using LB medium with 0.25 µM IPTG for 24h at 30°C.

Aeration condition	Culture/Flask volume ratio	Protein present in cell lysate fraction	Colour Intensity
Flask covered with cotton plug	1/5	Soluble and Insoluble	-
	1/7	Soluble	+
	1/10	Soluble	+ +
Flask covered with gauze sheets	1/5	Soluble	+ +
	1/7	Soluble	+ +
	1/10	Soluble	+ + +



Brief overview on strategies for improving protein solubility applied to UM10 and UM10E11 proteins

Expression of the split(-fused) proteins used in this work (UM10 and UM10E11 – see Supplementary Figure II. (a) S 6) were challenging, as they were mainly obtained in the insoluble fraction. Several strategies for improving their solubility were explored and the most effective were implemented afterwards.

Proteins correctly folded are typically produced in the soluble fraction, while if misfolded, they aggregate and form inclusion bodies (IBs) that are part of the insoluble fraction. IBs are dynamic structures formed due to an unbalanced equilibrium between protein aggregation and solubilisation [268]. The hydrophobic regions exposed in misfolded or partially-folded proteins interact with other similar proteins, or even with correctly folded ones, through non-covalent hydrophobic and/or ionic interactions, leading to the formation of protein aggregates [268]. This is aggravated for large scale expression, being associated to molecular crowding and saturation of the cellular folding machinery [269].

Several strategies are described to overcome IBs' formation. Slowing-down the protein expression, for example by lowering the growth temperature [270] or reducing the inducer's concentration and time of expression [271], prevents and/or reduces IBs' formation [269,272]. We performed adjustments in these parameters for the successful optimization of UM10 and UM10E11 expression (Supplementary Figure II. (a) S 1A and 1B). The use of N-terminal or C-terminal tags has also been described to enhance protein expression in the soluble fraction

[269,273–275]. We observed that fusing the N-terminal of UM10E11 with SUMO or TSF tags effectively improved its solubility (Supplementary Figure II. (a) S 1C).

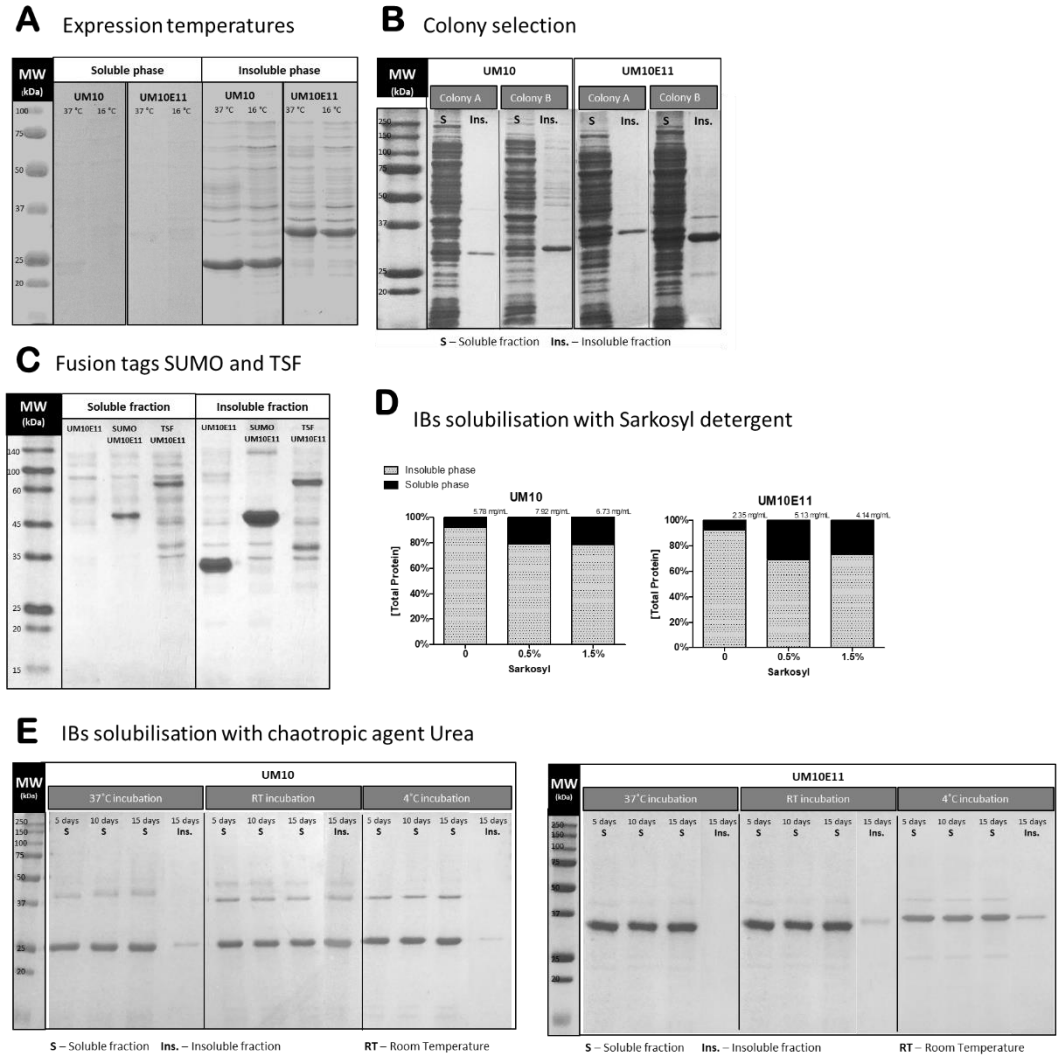


Figure II (a) S 1. Methods used to enhance the solubility of UM10 and UM10E11: (A) lower expression temperatures; (B) colony selection for lower production yield and better soluble/insoluble ratio, (C) inclusion of N-terminal fusion tags (SUMO or TSF); (D) solubilisation of inclusion bodies (IBs) with *N*-Laurylsarcosine sodium salt (sarkosyl) detergent (Sigma-Aldrich) or (E) with the chaotropic agent urea 8M (Labkem). SDS-PAGE gels were stained with Coomassie Brilliant Blue, and first lanes show protein molecular weight markers (Precision Plus Biorad All Blue for Figures A, B and E, or Dual Xtra for Figure C). Theoretical molecular weights are: 24.871 kDa for UM10, 34.829 kDa for UM10E11, 46.408 kDa for SUMO-UM10E11 and 66.314 kDa for TSF-UM10E11.

Other possibilities for obtaining soluble protein may comprise downstream (post-expression) methods, which mainly consist in solubilisation of the protein of interest from IBs [276,277]. First, IBs are thoroughly cleaned from adsorbed unwanted material, then proteins are extracted (solubilized) from IBs in strong denaturant environments, and finally they are renatured aiming the correct folding.

Denaturation can be achieved either exposing IBs to denaturation conditions or by using denaturation reagents. Examples of denaturant solubilizing methods are: ionization changes through acidic or basic pH; temperature variations; detergents including SDS, CTAB or sarkosyl; organic solvents such as ethanol and propanol; organic solutes like guanidinium-HCl and urea; or use of inorganic salts at higher concentrations [277,278]. We tested two methods of solubilisation, one with mild denaturant conditions, using the anionic detergent sarkosyl, and another implying harsher denaturation, the most commonly used urea. Denaturation with sarkosyl allowed us to recover 1/5 of the proteins onto the soluble fraction (Supplementary Figure II. (a) S 1D), even using lower percentages than the described in literature [279]. Still, solubilisation with urea was more effective, since proteins were completely extracted onto the soluble fraction (Supplementary Figure II. (a) S 1E). The temperature influence on solubilisation with urea was also evaluated. Even though extraction of the proteins onto the soluble fraction was higher at 37°C of incubation, incubation at 4 °C showed a better performance afterwards in the refolding of the protein. In fact, the main difficulty associated to these downstream solubilizing methods is the afterwards removal of the denaturation agent, and the refolding of the extracted protein.

Different methods for the last steps – cleaning and refolding – have been described: dialysis, dilution, renaturation or chromatography [268,276–278]. Removal of the denaturants and refolding was challenging for our proteins, either using sarkosyl or urea denaturants. At this stage, we had to compromise between total amount of folded soluble protein and time to obtain it to have our functional products in a reasonable working-time. Hence we assembled the experimental set-up for protein expression as schematized in Supplementary Figure II. (a) S 2.

Optimized protocol for the expression of UM, UM10, E11 and UM10E11 proteins

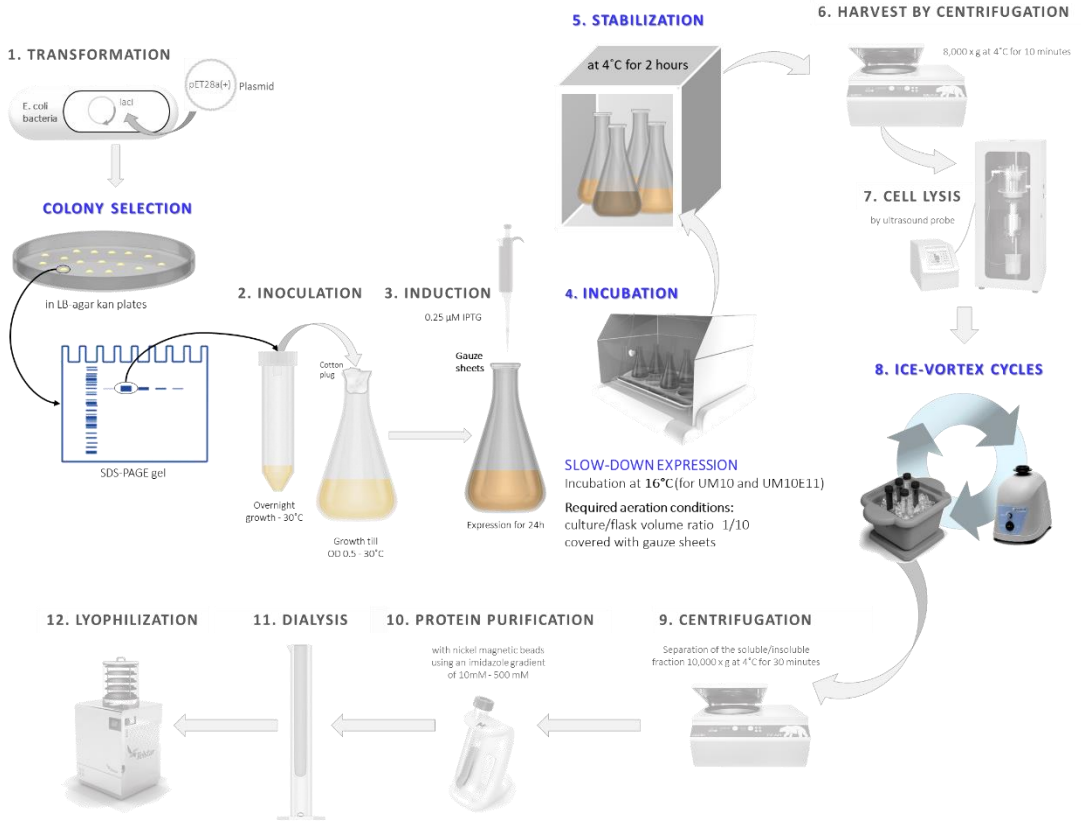


Figure II (a) S 2. Optimized experimental set-up for the expression of split UM-based protein: (1) Transformation of *E. coli* bacteria with plasmids and colony selection compromising between amount of total protein and soluble/insoluble ratio; (2) Inoculation of the colony with best soluble/insoluble fraction ratio in LB-kan medium and incubation overnight at 37°C, followed by regrowth in a larger volume (re-inoculation) at 30°C until O.D. 0.5 is reached; (3) Induction with IPTG and change of the aeration conditions to allow better oxygen exchange during incubation (culture/flask volume ratio 1/10 covered with gauze sheets); (4) Expression during 24 hours of incubation at 16˚C (slowed-down expression); (5) Stabilization in cold environment for 2 hours to enhance chromophore folding; (6) Recover of the bacterial pellet by centrifugation; (7) Resuspension of the harvested cells in lysis buffer followed by disruption by ultrasounds; (8) Cycles of slow-vortex and ice stabilization of the lysate to enhance solubilisation and improve protein folding; (9) Recover of the soluble fraction by centrifugation; (10) Purification of target proteins by affinity of the His 6x tag to nickel magnetic beads in a imidazole gradient 10-500 mM; (11) Dialysis of the resulting pure fractions for imidazole removal; (12) Lyophilisation of the pure dialysed fractions, thus obtaining the solid pure sample of the target protein.

Overview of the HNE recognition sites and active-site

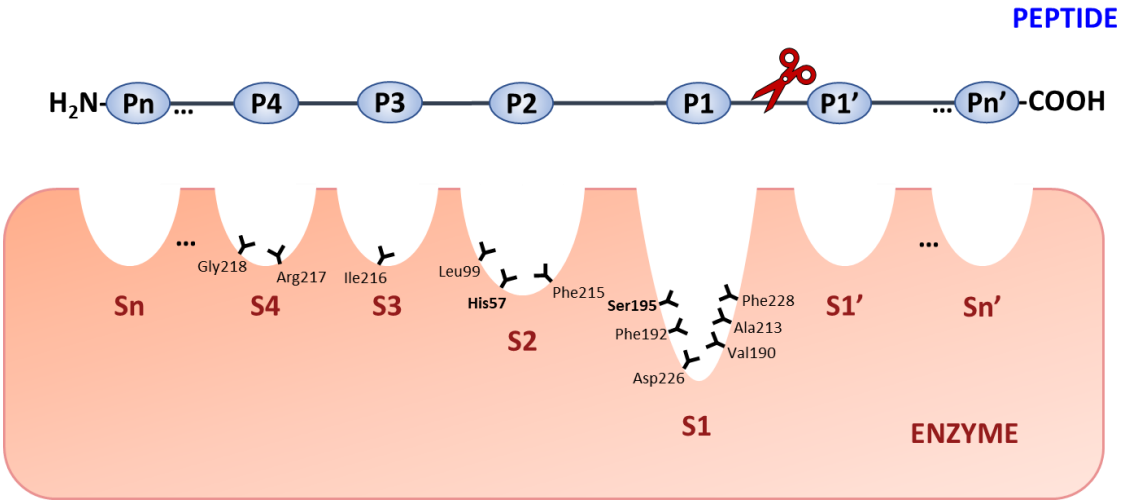


Figure II (a) S 3. Map of the binding sites of HNE, presenting the key amino acids on recognition subsites. Schechter and Berger convention was used for the numbering of enzyme-ligand binding sites, where P1-P1' is the cleavable peptide bond and the subsites of enzyme and corresponding peptide represented as Sn, ... S1, S1', ... Sn' and Pn, ... P1, P1', ... Pn', respectively [125,257].

Control assay of UM protein with HNE enzyme

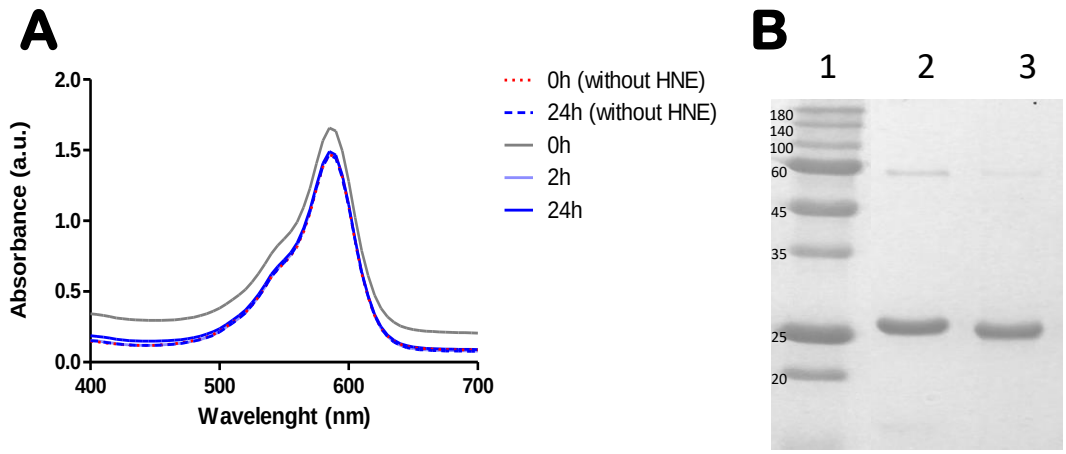


Figure II (a) S 4. (A) Absorbance spectrum for ultramarine before (dashed lines) and after (filled lines) addition of HNE (150mU) and incubation at room temperature (RT) for 24 hours. Absorbance spectra were measured at 0, 2 and 24 hours. **(B)** SDS-PAGE image of ultramarine (27.090 kDa) before (lane 2) and after incubation with HNE (lane 3). Protein molecular weight marker (Precision Plus Protein Dual Xtra) is shown in lane 1. Gel was stained using Coomassie Brilliant Blue.

Investigation of the possible cleavage of UM protein by HNE enzyme, using ExPASy Peptide Cutter software

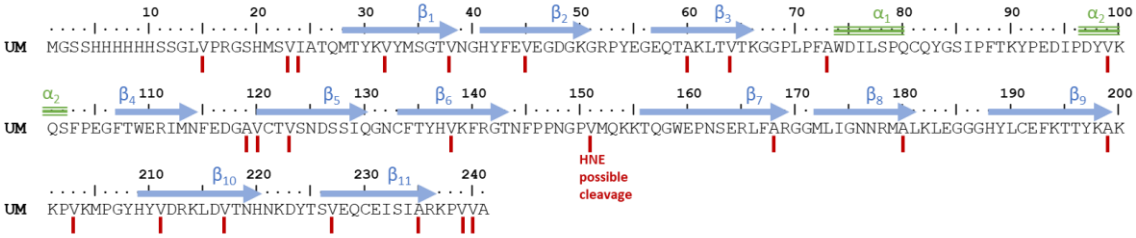


Figure II (a) S 5. Analysis using ExPASy Peptide Cutter software (SIB ExPASy Bioformatics Resources Portal, available online toll) (Artimo *et al.* 2012), presenting the positions of possible cleavage by HNE enzyme (as red lines). Secondary structure elements are also depicted above the sequence of UM, β-sheets 1-11 and α-helix 1 and 2 are presented as blue arrows and green boxes, respectively.

Development of a split-fused UM strategy, based on the UM10E11 recombinant protein

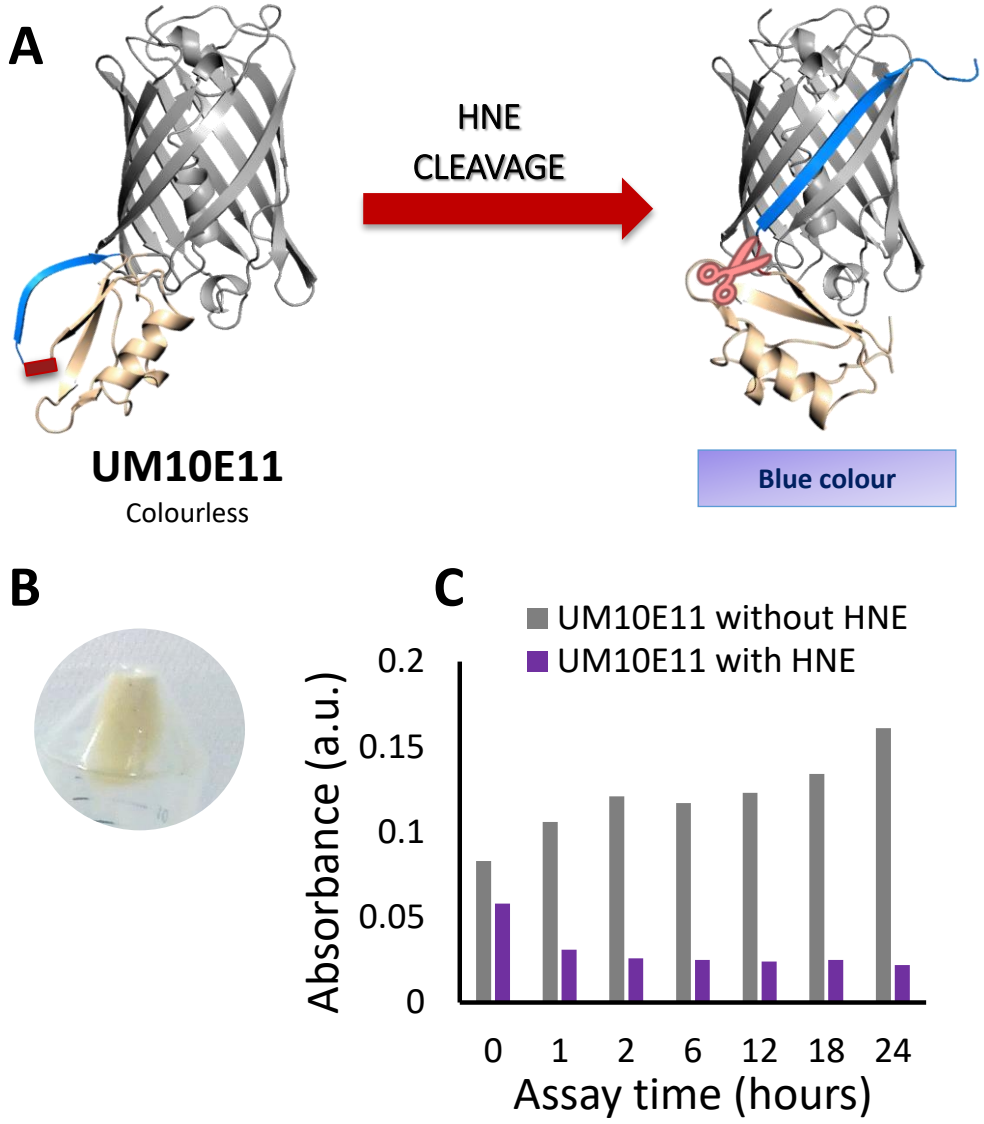


Figure II (a) S 6. Split-fused strategy for HNE sensor **(A)** Schematic representation of the split-fused UM strategy. Structures were created with PyMol software. Incomplete β-barrel is presented in grey, eglin c moiety is coloured golden, 11th β-strand is coloured blue and the cleavage sequence for HNE is represented as a red box. **(B)** Bacterial pellet after expression of UM10E11. **(C)** Elastase activity on split-fused UM system using UM10E11 protein at 1.5 mg/mL. The assay was performed at room temperature (RT) during 24 hours. Absorbance before and after the addition of HNE (150mU) was measured at 585 nm. The legend shows the categorization of the absorbance value in arbitrary units (a.u.).

II. (b) 2. Model substrates based on ultramarine GFP-like chromoprotein for elastase sensors

Abstract

Green fluorescent protein (GFP) has been extensively used as a tag and reporter of target proteins. However, for certain applications, a chromogenic reporter may be more desirable than a fluorescent one. The recent development of ultramarine, a GFP-like non-fluorescent chromoprotein, could represent a starting point for the development of sensors based on colour changes. Here we exploit the natural tendency of ultramarine to undergo a reversible self-assembly that is accompanied by the appearance of colour that is visible in the UV-Vis spectra range. Seven mutants were designed to produce switch-on or switch-off signals upon proteolytic cleavage by HNE, due to a dealignment of β-sheets and rearrangement of the chromophore environment. The impact of mutations on ultramarine conformation was evaluated *in silico* and by *in vitro* confirmation of colour appearance (expression) or diming after HNE addition.

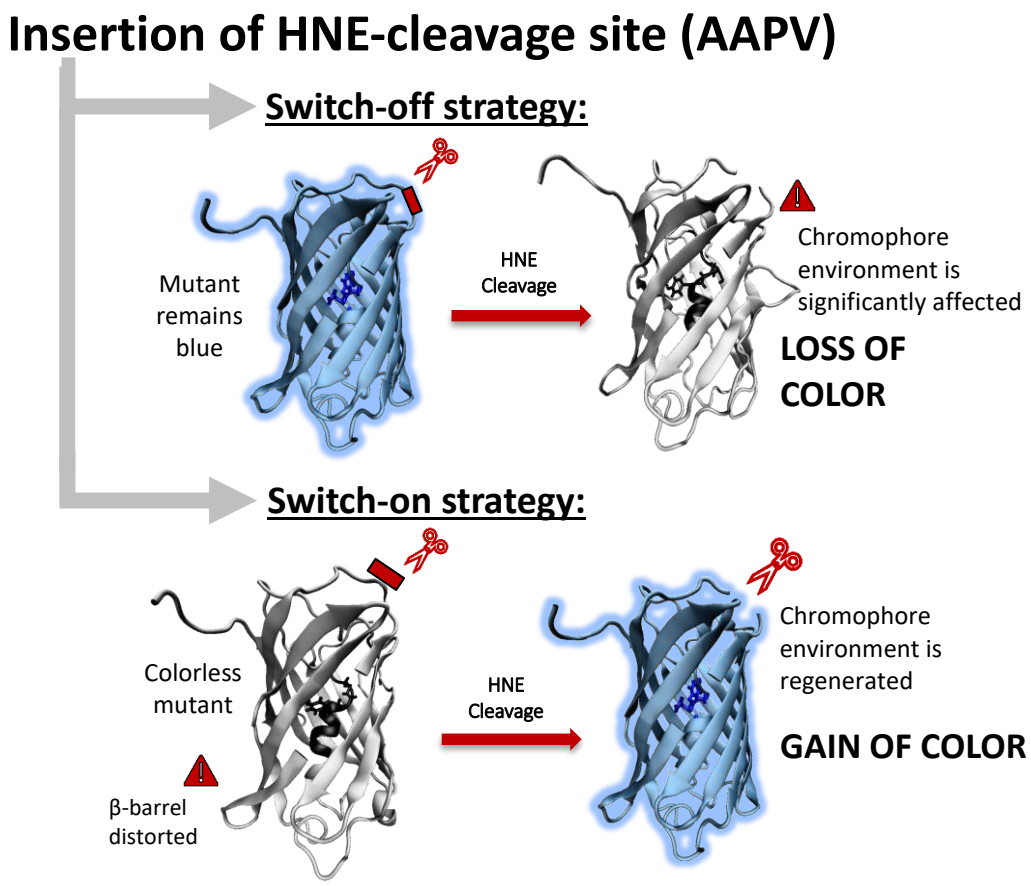


Figure II (b) 1. Graphical abstract of the subchapter. Schematic representation of the two strategies of HNE-specific recombinant substrates acting as switch-off or switch-on sensors, through the insertion of HNE-specific cleavage sequence (AAPV) in the ultramarine chromogenic GFP-like protein. Examples of mutated proteins are represented for insertions of HNE cleavage site (red box) in loop region between sheets β9 and β10. Structures were designed with VMD software.

II. (b) 1. Introduction

Green fluorescent protein (GFP) has been extensively used as a tagging and detection method due to its self-reassembling behaviour [243]. The unique ability of GFP to spontaneously reassemble is associated with well-established forces of intramolecular interaction that occur within its β-barrel structure and chromophore regions [243]. In fact, folding in GFP is characterized by hysteresis mainly due to the decreased flexibility of the chromophore and the compact structure of the β-barrel upon its formation [243,280].

Fluorescence-based switch-on approaches have been widely described [244,245,255,264–267,281–283]. To our knowledge, colour-based switch-on approaches with non-fluorescent GFP-like proteins have not been reported, possibly as on account of difficulties in achieving a stable chromogenic environment after cleavage. The mechanisms underlying the properties of GFP-like proteins (fluorescent and non-fluorescent) are not yet fully understood [266], making the development of this type of sensor substrate even more challenging. Previously, when setting out to use the reassembly properties of a GFP-like chromoprotein for the detection of Human Neutrophil Elastase (HNE), we selected ultramarine (UM), an engineered chromoprotein derived from Rtms5 (a naturally occurring GFP-like fluorescent protein) [249,250]. Genetic modifications previously reported by Pettikiriarachchi *et al.,* 2012, Val40Ala, Ser121Arg, Leu123Thr, His142Asn, and Phe158Arg, were shown to convert Rtms5 into a monomeric and non-fluorescent chromogenic protein that was named ultramarine on account of it producing an intense dark blue colour [249,250].

Like all GFP-like proteins, ultramarine folds into a distinctive β-barrel composed of 11 β-sheets surrounding an α-helix core that restrains a chromophore group [249,280,284]. After folding of the β-barrel, the chromophore in GFP-like proteins undergoes a spontaneous 3-step autocatalytic maturation of cyclization, oxidation, and dehydration in the Gln62-Tyr63-Gly64 tripeptide While not needing a contribution from another enzyme or substrate [243] the manifestation of colour or fluorescence does however require a network of polar interactions involving the chromophore group and several closely-apposed amino acids: Tyr10, Gln38, Ala40, Pro59, Gln60, Ser65, Ile66, Trp89, Arg91, Asn142, Glu144, Asn157, Met159, Thr175, Arg199, Gln215 and Glu217 (Supplementary Table II (b) SI) [250].

In the mature form, the cyclized chromophore leads to a tighter folding of the β-barrel [285]. It is theorized that this tensing of the β-barrel is the reason for the hysteresis observed in the folding

of GFP and GFP-related proteins. Indeed, the chromophore formation and maturation does play a critical role in maintaining the protein stability as it was shown that immature forms of the chromophore (non-cyclized tripeptide) are much more flexible in the tripeptide region than mature chromophore forms [280].

According to recent studies, GFP sheets β1–3 (N-terminus sheets), β4–6 (central sheets) and β7–11 (C-terminus sheets) move as groups, and their interaction with each other is stronger inside the same group [280]. Since GFP starts to unfold from β7–11 [280], targeted mutagenesis aimed at impacting self-reassembly have been mainly directed towards the C-terminal sheets (β7–11) [280].

Here, we report the development of seven UM mutant variants towards their use as switch-on or switch-off sensors for HNE activity by the insertion of the specific cleavage sequence (Ala-Ala-Pro-Val) of this enzyme (Figure II (b) 1). The rationale of the introduced mutations was to alter the alignment of the β-sheets either before or after HNE cleavage (Table 1). Sites with an already existing Pro and/or Val were modified by point mutations, and distortions on the secondary structure were made by insertion and/or deletion of adjacent residues. In switch-off mutants interactions within the chromophore environment would be disrupted after cleavage, whereas in switch-on mutants they would be restored as observed in UM.

II. (b) 2. Materials and Methods

Materials and Reagents

All reagents were analytical grade, purchased from commercial suppliers and used as received. Standard molecular biology procedures were used for expression of the interest in Escherichia coli TOP10 (Invitrogen) and E. coli BL21 DE3 (Novagen). DNA restriction enzymes *Not*I and *Nde*I and kanamycin antibiotic were purchased from ThermoFisher. Gold View for DNA staining was obtained from UVAT Bio (Valencia, Spain). Culture media LB Broth was purchased from Grisp (Porto, Portugal). Isopropyl-β-D-thiogalactopyranoside (IPTG) inductor was purchased from Acros Organics (Geel, Belgium). Nickel Magnetic Beads for His Tag Protein Purification and respective magnetic separator were obtained from Bimake (Houston, USA). Molecular weight marker Precision Plus Protein Dual Xtra Standards was purchased from Biorad (Portugal). All other chemicals were purchased from Sigma-Aldrich (Spain), including the enzyme elastase from human leukocytes, synthetic elastase substrate *N*-methoxysuccinyl-Ala-Ala-Pro-Val-*p*-nitroanilide (MeOSuc-AAPV-*p*NA), and imidazole. The dialysis tubing cellulose membranes (MWCO, 1-2 KDa and 12-14 KDa) and GenEluteTM Plasmid Miniprep Kit were also obtained from Sigma-Aldrich.

Instrumentation

All absorbance and fluorescence measurements were carried in microplates of 300 µL using a Synergy Mx reader spectrometer and Gen5™ Data Analysis Software (Bio-Tek Instruments, Inc., USA). DNA and protein quantification was carried using a Nanodrop 1000 (ThermoScientific). Bacterial cell lysis was accomplished by sonication (Ultrasonic Processor VCX-500 watt, Sonics & Materials, Inc., Connecticut, USA). Lyophilisation of protein was performed using a FreeZone 2.5 Freeze Dry System (Labconco, Missouri, USA).

Methods

1. Gene design

The amino acid sequence of Ultramarine [249,250] was modified to create seven variants as described in Table I. The gene constructs encoding ultramarine (UM) and UM-derived mutants (A-G) ware cloned in the expression plasmid vector pET28a(+) (Genscript, New Jersey, USA).

Table II (b) I. Rational for the design of the seven variants of UM with inserted HNE cleavage sequences.

Mutants ID	Mutations	Rationale
Mutant A	G47A; G48A; L50V; K70A; Y71A; E73V	Strategy: non-predictable Insertion of two HNE cleavage sequences, flanking the chromogenic tripeptide to study the cleavage effect at this site of the chromophore region and to retrieve information regarding the enzyme's accessibility to the β-barrel core.
Mutant B	N128A; G129A	Strategy: switch-off Insertion of one HNE cleavage sequence to evaluate the higher susceptibility to HNE cleavage at the longest loop (β6-β7) with higher tolerance to mutations [286].
Mutant C	K180A; K181A	Strategy: switch-off Insertion of one HNE cleavage sequence in loop β9-β10. Maintenance of the length of the loop avoids disarrangement of the chromophore, which was postulated to occur upon HNE cleavage.
Mutant D	K180A; K181A; K184_Y188del	Strategy: switch-on Insertion of one HNE cleavage sequence in loop β9-β10. Decrease of the loop length was postulated to create tension in the structure possibly disrupting the chromophore environment prior to HNE cleavage. Upon cleavage at the inserted cleavage site, the tensile strengths may be diminished allowing the chromophore interaction with β-sheet to occur.
Mutant E	K180A; K181A; Y188_H195insAAAAPV	Strategy: switch-on Insertion of two HNE cleavage sequences in loop β9-β10, increasing the size of the loop. May form a more flexible structure affecting the chromophore environment. Upon cleavage, the necessary interaction between chromophore and β-sheet might be restored.
Mutant F	Y210A; T211A; S212P; N205_N207del	Strategy: switch-on Insertion of one HNE cleavage sequence and shortening of protein's last loop (β10-β11). The created tension may disrupt the chromophore environment only to be re-established upon HNE cleavage.
Mutant G	Y210A; T211A; S212P	Strategy: switch-off Insertion of one HNE cleavage sequence in the last loop (β10-β11) of the protein, which maintains the length of the loop. Disarrangement of chromophore environment might occur upon HNE cleavage.

2. Protein expression and purification

Standard techniques were used for all DNA manipulations. Plasmid purifications were performed using the GenEluteTM Plasmid Miniprep Kit. Size of gene inserts was confirmed by double-digestion with the restriction enzymes *Not*I and *Nde*I. The resultant DNA fragments was analysed by 1% agarose gel stained with Gold View (UVAT Bio). All plasmids were first established in E. coli TOP10 before transforming into E. coli BL21 (DE3) in order to express recombinant protein (TSS method was used for transformations, described in Chung *et al.,* 1989 [251]). Bacterial cultures were grown in LB medium (supplemented with kanamycin, 50 µg/mL) till an OD 0.5, and the protein's expression was induced by the addition of IPTG (0.25 µM). The cultures were then incubated for several time periods (2h – 24h) and at different temperatures (16°C – 37°C) with agitation at 180 rpm. After expression, cells were placed at 4°C for at least 2 hours to enhance chromophore folding. The cultures were then harvested by centrifugation at 8,000*g* at 4°C for 10 minutes, resuspended in lysis buffer (20mM NaH2PO4, 500mM NaCl, pH 7.4) and subsequently lysed by sonication on ice with a 3-mm probe (small-scale production) or 13-mm probe (medium-scale production). The lysate was centrifuged at 10,000*g* at 4°C for 30 minutes for the collection of the protein in the soluble fraction. Imidazole was added (10mM) and protein purification was performed using nickel magnetic beads using an imidazole gradient of 10mM - 500mM. Recovered fractions were analysed by SDS-PAGE. Removal of imidazole from selected fractions was performed by dialysis against ultrapure water using a cellulose membrane with a MWCO of 12-14 KDa. Ultrapure water was used to better control salt and pH levels in subsequent proteolytic HNE assays (pH 8 is optimal). The purified UM and the UM mutants fractions were then frozen at -80°C and lyophilized. All proteins were observed to match their theoretical size (including the N-terminal hexahistidine tag) when analysed by SDS-PAGE.

3. Assessment of UM mutants as HNE protease sensor

HNE activity was first evaluated in control assays using the synthetic substrate MeOSuc-AAPV-*p*NA as recommended by the manufacturers (Sigma-Aldrich). Briefly, the HNE enzyme (0.5 U/mL) was mixed with 25-1500 µM of substrate, in a final volume of 300 µL of reaction buffer (100 mM HEPES + 500 mM NaCl, pH 7.5). A blank consisting only substrate in buffer was also included. The kinetic constants were determined from the initial rates of hydrolysis using the Lineweaver-

Burk method. All enzymatic assays were conducted at 37°C for 10 minutes with triplicates and the absorbance was measured at 405 nm by UV-Vis spectrophotometry.

For the HNE activity testing, lyophilized proteins (UM and UM mutants) were resuspended in 100 mM Tris-HCl at pH 8 immediately prior to the assay, and the absorbance spectra was measured prior to and after the addition of HNE using a spectrometer for colour variation assessment. In addition, the same assays were performed in a 96-well microplates that was first blocked with 0.5% bovine serum albumin (BSA) solution, as described in Cabantous *et al.,* 2006 [255].

4. Structural Bioinformatics

4.1. Homology modelling

Molecular models for all the proteins were obtained by homology modelling using the PDB X-ray model 3vk1 as template, available at the SWISS-MODEL web service (https://swissmodel.expasy.org). To obtain the models for cleaved mutants, computational models were manually cutting the amino acid sequence. The software VMD (Visual Molecular Dynamics) [287] was used to picture all the structures analysed.

4.2. Molecular dynamics (MD)

All molecular dynamics simulations were performed with the Gromacs 4.0.7 package using the GROMOS 54A7 united-atom force-field [288–292], with periodic boundary conditions, and applying the LINCS [293] and SETTLE [294] algorithms to constrain the peptide and water bonds respectively. The simulations ran with a time step of integration of 2fs and the single point charge (SPC) model [295] was used to represent water. The temperature was maintained at 300K with the V-rescale thermostat [296,297] whereas the Parrinello-Rahman barostat [298,299] (with isotropic coupling) was used to maintain the pressure at 1atm. Van der Walls and electrostatic interactions were treated using a twin-range method, with short and long range cut-offs (0.8 and 1.4 nm, respectively), and a reaction field correction for electrostatics using a dielectric constant of 54 [300], and the neighbour list was updated every 10 steps.

Each simulated system consisted of the protein computational model in a water box. In total 15 different systems were simulated, one each for UM, the 7 mutants and the 7 cleaved mutants. All simulated systems were initially energy minimized for around 2000 steps using the steepest

descent method. Afterwards the systems were initiated to a series of three short equilibration simulations (500ps each simulation), with position restraints allowing the slow relaxation of the structures for the final production run (the atoms were restrained with a harmonic force of 103kJ/mol.nm2). The first was performed in the NVT ensemble (number of particles, volume and temperature constant) applying position restraints to all heavy atoms. The second simulation was done in the NPT ensemble (number of particles, pressure and temperature constant) with position restraints to the same atoms. Finally, the third simulation ran also in NPT ensemble but with position restraints only on alpha-carbons atoms in all the amino-acids. After the systems' preparatory simulations, the production runs were performed in duplicated, in NPT ensemble and without any positions restraints by at least 50ns.

Equilibration of the systems was verified by the evaluation of pressure, temperature, potential energy and root-mean-square deviation (RMSD) that did not significantly vary on the last 10ns of the simulation time. The GROMACS tool "g_cluster" was applied to each system type to determine the spatial conformation of the simulated proteins that most frequently occurs in the analysed period of time. The tool was applied to 20ns of simulation for each system type (corresponding to the last 10ns of simulation for both replicas) and 0.1nm of root mean square cut-off was used for the calculations. The resulting spatial conformations were visually inspected and used in structural alignments to easily perceive the possible significant structural differences between the spatial conformations of proteins. These alignments were made between UM and each mutant, between the UM and each cleaved mutant, and between each mutant and its cleaved form. The RMSF (root mean square fluctuation) per residue was also calculated with the corresponding GROMACS tool, to the final 10ns of each simulation and taking as reference the structure resulting of the previous cluster analysis. This measure calculates the standard deviation of the positions of each residue after fitting to the reference structure, providing information about which residues have displayed more or less structural variation during the analysed time.

II. (b) 3. Results and Discussion

Overview of ultramarine's structure and site-directed mutagenesis

In the present study, we combined structural bioinformatics and site-directed mutagenesis to construct a protease-sensitive colour-based switch system for human neutrophil elastase (HNE) using ultramarine, a chromogenic protein derived from the fluorescent GFP-like Rtms5, as model. The mutants were designed to change the chromophore environment resulting in gain of colour or loss of colour upon HNE proteolysis at the strategically introduced HNE-specific cleavage sequence into the original ultramarine's structure.

Overviews of the structure of Rtms5 protein, including the chromophore environment with its interacting residues and the conserved residues, have been extensively reported in previous studies [249,250,301]. Information retrieved from these studies is compiled in Supplementary Table II (b) SI and was taken into consideration when defining the strategy for mutagenesis.

The chromophore environment given by the chromophore triad Gln62-Tyr63-Gly64 and 17 surrounding residues (Supplementary Table II (b) SI) is extremely sensitive to colour generation [250]. In fact, chromophore maturation is effectively linked to the hysteresis behaviour in the folding of the β-barrel [302], reinforcing the critical process of defining the mutagenesis design. For this reason, mutagenesis directly affecting the chromophore environment was avoided. To allow enzyme's accessibility, mutations to construct the HNE cleavage sequence were introduced into the loop regions, since they are externally located on the β-barrel lids [243]. Three variants were mutated on the top-lid in β9-β10 loop (mutants C, D, and E), and another three variants on the bottom-lid in β6-β7 loop (mutant B) and β10-11 loop (mutants F and G). In opposition, we created mutant A with two mutations in the core region between β3 and β4, to examine whether variations near the chromophore region are tolerated. The rationale for the design of the seven variants is detailed in Table II (b) I and schematized in Figure II (b) 2.

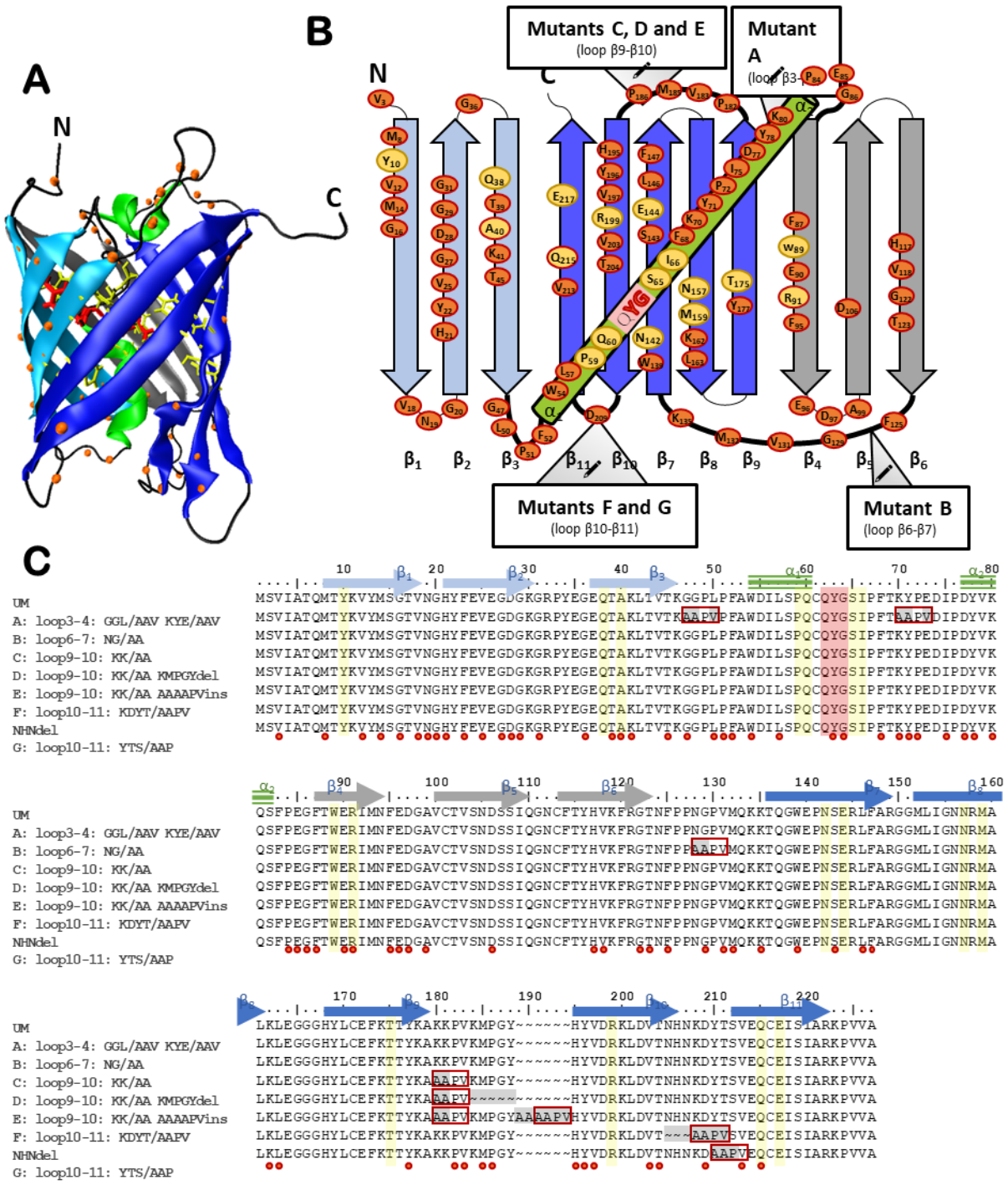


Figure II (b) 2. (A) Secondary structure of ultramarine (UM) protein and **(B)** its splay representation. N-terminus (β1–3), centre (β4–6) and C-terminus β-sheets (β6–11) are grouped and represented in light blue, grey and dark blue, respectively. Core α-helices are presented in green, chromophore region QYG is shaded in red, chromophore interacting amino acids are presented as yellow circles, and conserved residues are presented as orange circles. Targets of mutagenesis are also pointed in grey. **(C)** Alignment of amino acid sequences for ultramarine (UM) and the seven designed mutants with cleavage sequences for HNE highlighted in red boxes with

mutations shaded in grey. Secondary structure elements are also depicted above the alignment. Chromophore tripeptide is shaded in red, chromophore interacting residues are presented in yellow, and conserved residues (Supplementary Table II (b) SI) are indicated below the alignment by orange circles. Residues are numbered relative to mutant E and adapted from Prescott *et al.*, 2003 [250] and Ong *et al.*, 2011 [284].

Structure prediction of UM mutants

Structures of UM and UM variants were predicted by homology modelling. The majority of available PDB structures of GFP-like proteins resulted from a mature protein (*i.e.* with cyclized chromophore) [280,285,303,304]. In order to analyse immature proteins, the chromophore could be computationally edited using quantum mechanics/molecular mechanics (QM/MM) tools [303,304], which were out of scope of our work.

Chromophore maturation occurs only after the complete folding the β-barrel. And despite maturation is a critical step to achieve colour (or fluorescence), the favourable conditions are only completed after the establishment of interactions between the chromophore triad and its interacting residues (multiple van der Walls interactions, 9 hydrogen bonds and 2 water-mediated hydrogen bonds [305]). Hence, the possible bias associated with the use of mature templates for homology studies is diminished due to the inherited hysteresis observed in all GFP-like proteins. β-barrel formation promotes chromophore cyclization which, in turn, increases the stability of the barrel, therefore allowing the establishment of the favourable environment for colour generation [306]. All our designed structures were generated in the typical β-barrel configuration (Supplementary Figure II (b) S1), so we can assume that favourable tensile forces may be established for chromophore maturation.

Molecular dynamics studies were then conducted to compare the structures of ultramarine and the designed mutants. As a quantifying measure, we used the root-mean-square fluctuation (RMSF) during the simulation time as it can provide physical information regarding residues' motion throughout the time of analysis. RMSF values (Figure II (b) 3) describe the flexibility differences of targets, being helpful to determine whether the mutations affect the dynamic behaviour of the protein. A higher RMSF value is related to more flexible movements whereas a low RMSF value indicates limited movements during the simulation time in relation to its average position.

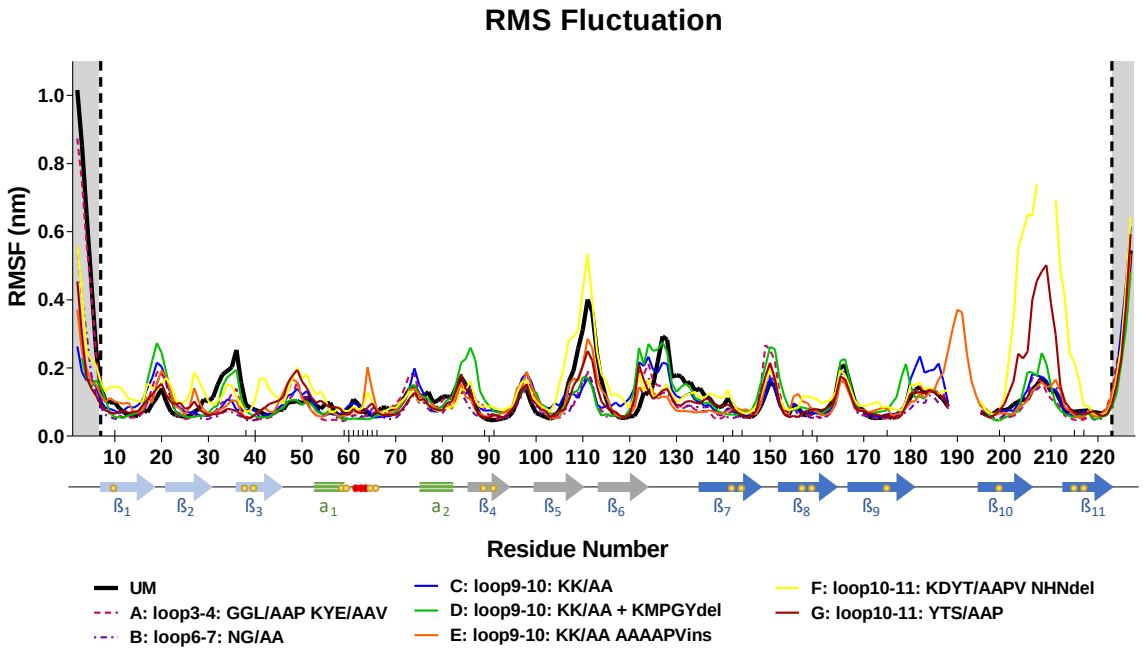


Figure II (b) 3. Root-mean-square fluctuation (RMSF) analysis of ultramarine protein (UM) and the seven designed mutants (A-G). Secondary structure elements are depicted below the x axis, and chromophore region and interacting residues are indicated with red (●) and yellow (○) circles, respectively (their location is also pointed on the axis). Terminal residues that will not be considered in the following analysis are shaded in grey (residues 1-7 and 223-227).

An overall analysis of the RMSF values (Figure II (b) 3) showed that fluctuation of ultramarine and the mutants follows a specific trend, with higher fluctuation observed in loop regions and lower fluctuation in β-sheets, as anticipated [280]. Despite this, we were expecting differences in the fluctuation to mainly occur in the residues near the mutation sites, which did not occur for all variants, namely variant A. Terminal residues have free movement due to the absence of a constraining force at one end. To limit a biased interpretation due to this inherited freedom, in the following RMSF analysis the terminal residues 1-7 and 217-221 were not considered for comparison.

We considered the basal level of fluctuation for ultramarine to be 0.1 nm (1 Å), based on its average RMSF value (0.105 nm), although the RMSF range varied between 0.0471 nm (Arg91) and 0.4009 nm (Thr111). In ultramarine, 41.6% of the residues had RMSF values higher than 0.1 nm. The majority of residues presenting high values of RMSF are located in the vicinity of bends, acting as a transition between the loop regions and subsequent or precedent β-strands or α-helices. Available data [280,307] corroborate these findings showing that residues located in transitions of

secondary structures contribute to the folding pattern and stability of GFP and GFP-like protein and present distinctive high fluctuation. Gly36, Glu85 and Asp209 are examples of residues located in transitions and higher importance can be given to them considering they are conserved among GFP-like proteins (Figure II (b) 2) and Supplementary Table II (b) SI).

All UM variants, except mutant F, presented a higher percentage of residues with fluctuations lower than 0.1 nm (Figure II (b) 3 and Figure II (b) 4). As a whole, these mutants were characterized by a decrease of the protein flexibility.

For a deeper analysis, deviation from ultramarine's fluctuation was calculated and relative values are presented in Figure II (b) 4. In our analysis, we focused on deviations 2-fold lower (Log_2 relative fluctuation < -1) or higher (Log_2 relative fluctuation > 1) than ultramarine to infer about the similarities between the overall structure of the mutants and UM, and to speculate about possible implications with mutants' chromophore environment. Deviation from ultramarine was larger in residues 10-28, 30-38, 43-54, 107-114, 120-125 and 127-141 in all variants (Figure II (b) 3 and Figure II (b) 4A). In addition, for mutants F and G deviation was also higher in residues 201-216, probably since they are in the vicinity of the mutated residues (Figure II (b) 2 and Figure II (b) 4A).

Low relative fluctuations may indicate an increase in protein stability, and, thus, be the result of a more rigid structure. Consequently, interaction of the residues with the chromophore region may be affected, altering the chromophore environment, critical for colour generation. On the other hand, if well positioned, higher rigidity of critical residues may be favourable for the stabilization of the chromophore [308,309]. By contrast, high relative fluctuation can indicate the diminishing of protein rigidity with an increase of residues' interaction with the surrounding environment and, particularly, with the chromophore region [308,309]. To better understand the importance of those deviations in fluctuation, we further analysed the RMSF values in residues specifically involved in the chromophore region (Figure II (b) 4B) and in residues conserved in GFP-like proteins (Figure II (b) 4C).

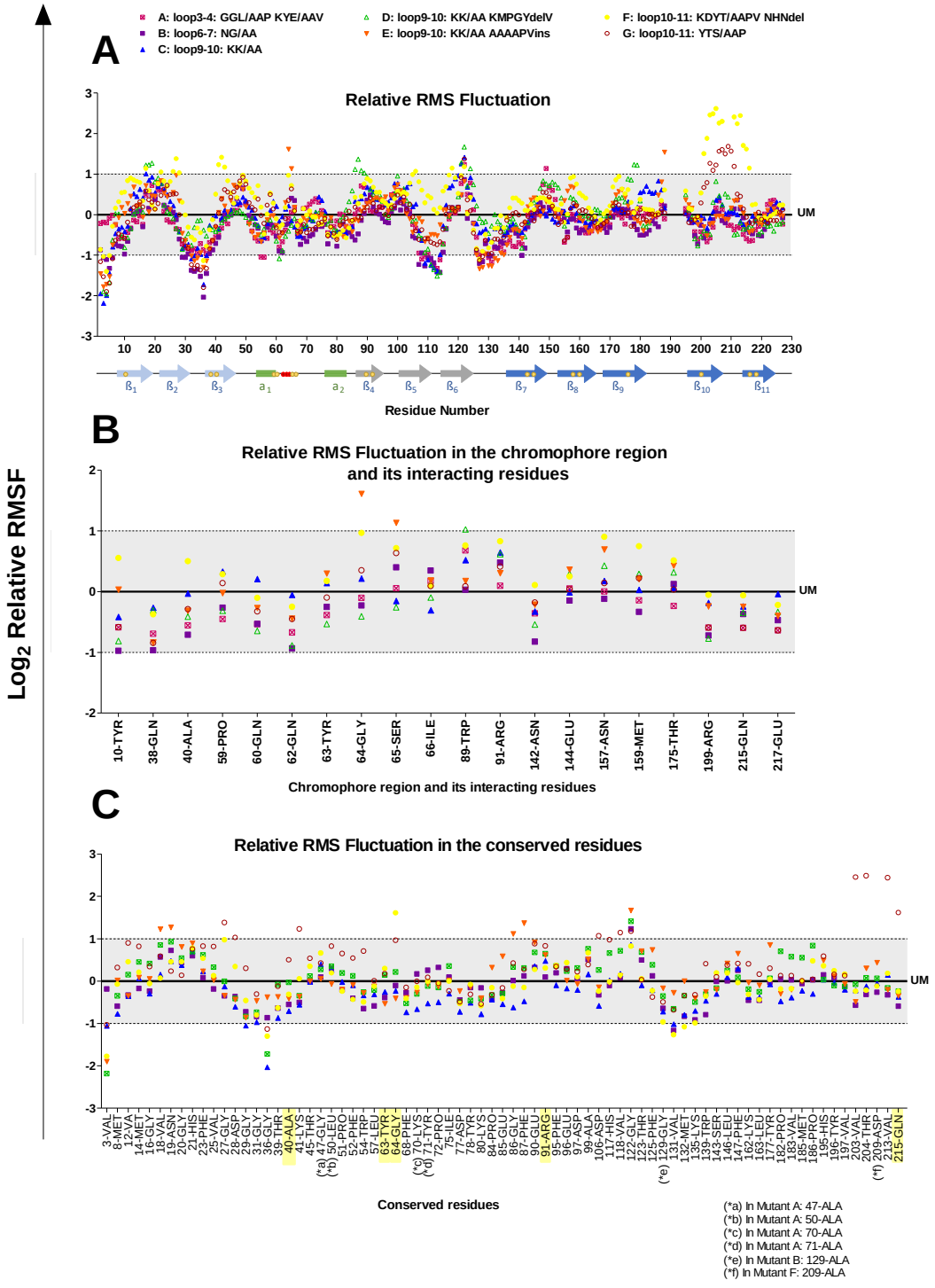


Figure II (b) 4. Relative RMSF analysis of seven designed mutants (A-G), in relation to ultramarine protein, considering **(A)** all residues, **(B)** residues involved in the chromophore environment, or **(C)** conserved residues (Supplementary Table II (b) SI). Shadowed region highlights 2-fold variation in relation to UM. In Figure A, elements of the secondary structure are depicted below the x axis, and chromophore region and its interacting residues are represented by red (●) and yellow (●) circles, respectively.

Colour prediction of UM mutants

In general, mutations did not affect the fluctuation of the residues forming the chromophore group (Gln62, Tyr63, Gly64) as the relative fluctuation in variants A, B, C, D and G was near 1 ($Log_2 \approx 0$ in Figure II (b) 4B). There was a slight decrease in the relative fluctuation in residue Gln62 but it was within the 2-fold range ($-1<Log_2<01$). However, significant differences were seen in Gly64 of variants F and E, being its fluctuation twice and thrice larger than in ultramarine, respectively (Figure II (b) 4B).

In relation to the residues directly involved in the establishment of the chromophore environment, most of the mutants showed a similar fluctuation behaviour, regardless of the mutation site (Figure II (b) 4B). However, relative fluctuation of Tyr10, Gln38 and Gln62 of mutant B is significantly decreased and the opposite was observed for Ser65 of mutant E, which is 2 times higher compared to UM. Interestingly, these residues locate in opposing locations in relation to mutation sites: mutation in B is located in the bottom lid and the affected residues are part of the top lid or chromophore group; mutation in E is located in the top-lid and the affected residue is in the core, next to the chromophore. This behaviour was not predictable.

Mutant A, modified in the loops that hold the core α-helices which restrain the chromophore group, presented relative fluctuation mainly unaltered in all the residues involved in creating the chromophore environment. This can be an indication that mutant A should maintain the original blue colour and might work as a switch-off sensor for HNE. When we started the work, we could not estimate the influence of mutations in the colour of this mutant.

The most important property linked to biomolecular function, activity and regulation of any protein is its stability [309,310]. The conservation of residues across species is strongly linked to the protein function and structural stability. Throughout evolution, mutations in residues that positively affect the protein function and stability were prone to the host survival, consequently leading to their prevalence across that species.

Previous comparative studies of the structure of Rtms5 over numerous GFP-like proteins identified 75 highly conserved amino acids [250,284], 73 of which are present in ultramarine (Supplementary Table II (b) SI). The two absent conserved residues are Val40 and Leu123 of Rtms5, that were substituted by Ala40 and Thr123 to engineer ultramarine [249].

We can speculate if the introduced mutations affect the protein stability by analysing the deviation on these conserved residues compared to ultramarine (Figure II (b) 4C). Overall, the fluctuation of the conserved residues in mutants was similar to the ultramarine's and variations in relative fluctuation were in accordance in all the variants, regardless of the mutation site. From the 75 conserved residues analysed, only seven presented higher relative fluctuation and nine showed lower relative fluctuation in all the mutants, plus 4 other residues that decreased the relative fluctuation in all the mutants but in one where the opposite deviation was verified (namely Pro84 and Glu85 in mutant E and Trp139 and Gln215 in mutant G increased relative fluctuation values). Interestingly, Pro84 and Glu85 are closely positioned in the top-lid of the barrel where is located the mutation site in variant E, in which the length of β9-β10 loop was also increased. However, mutants C and D also have the HNE cleavage site inserted at the same location, though loop length was either not modified or decreased. Higher flexibility of Pro84 and Glu85 verified in mutant E is probably associated with the increased disturbance that the longer β9-β10 loop creates all over the top lid (Supplementary Figure II (b) S1). Concerning residues Trp137 and Gln215, they are located within β-sheet 7 and β-sheet 11, respectively, and Gln215 is in the immediate region of mutation of variant G (β10-β11 loop). Besides belonging to the same C-terminal β-sheets group, β7 and β11 do not directly interact. Nevertheless, the majority of these variations are within the range $0<Log_2<1$.

The most prominent variations were verified for mutant G with 11 residues presenting relative fluctuation over 2-fold higher, including Gly64 from chromophore triad and the chromophore interacting residue Gln215. In fact, mutant G presented much higher flexibility (3 to 5 times) in all the conserved residues in the vicinity of the mutation site (Val203, Thr204, Val213, Gln215), with the exception of the immediately precedent residue, the conserved Asp209, that remained surprisingly similar to UM. Mutant F also increased relative fluctuation to values > 2 times higher than UM in residue Gly64 from chromophore group and the unrelated residue Gly27. In mutant E five conserved residues (Val18, Asn19, Gly86, Phe87 and Gly122) showed increased flexibility with relative fluctuation values > 2-fold higher, though none is directly implicated in chromophore environment.

Worth mentioning is the very much increased relative fluctuation of residue Gly122 in all the mutants, with values > 2-fold higher than UM for all variants except for mutants C and F that show the increased relative fluctuation within the 2-fold range. Gly122 is not known to influence the chromophore environment, so the increased flexibility measured should not affect the colour of the

mutants. In opposition, Val3 and Gly36 presented much lower relative fluctuation in all the variants, but particularly in mutants D, E and F and mutants C and D, respectively, reaching 3 to 4 times lower flexibility than in UM. Mutants C, D and E were mutated in β9-β10 loop which shares the top lid neighbouring with the N-terminal and β2-β3 loop where those residues locate. Apparently, the amino acid substitution played a greater impact on the flexibility of this region than the modification of the length in β9-β10 loop. Despite this, no critical function is known for these residues.

In sum, *in silico* studies gave us an indication about the phenotype of mutant A which we could not predict before these studies – it should remain blue as ultramarine. Loss of colour directly related to instability in the chromophore environment is only estimated to occur in mutant F (increased flexibility in the chromophore residue Gly64). However, the complexity of the interactions between adjacent residues (either side by side in the amino acid chain or brought closely together by the β-barrel folding) makes colour prediction a challenging goal with an uncertain result. Nevertheless, the β-barrel structure was achieved for all the mutants (Supplementary Figure II (b) S2), allowing chromophore cyclisation.

Expression of the designed HNE sensors

The seven UM-derived mutants were successfully expressed in *E. coli* BL21 (DE3), and were briefly characterized according to their colour and expression profile. Bacterial pellets and consequent total extracts of ultramarine protein and variants B and C presented a deep purplish-blue colour, whereas the other mutants D, E, F and G were expressed colourless (Figure II (b) 5). We were expecting protein A to maintain its original blue colour, since molecular dynamics simulations showed its RMSF to be very similar to ultramarine's. However, bacterial pellets were grey.

Ultramarine and the seven mutants were obtained in both soluble and insoluble phases of the protein extract. As described in the work of Beddoe *et al.,* 2003 [301], the majority of ultramarine was collected in the soluble phase, giving a blue-coloured supernatant. However, a small amount was also produced in inclusion bodies, corresponding to misfolded forms which are always colourless [278,301]. Similar expression profiles were obtained for the coloured variants despite soluble/insoluble ratios varied (Figure II (b) 5). Mutant A was mainly expressed in the insoluble phase, an indication of protein misfolding. Low amounts of soluble protein in conjunction with

possible immature forms of the chromophore justify the absence of an undoubted blue coloured pellet. Expression yields in the soluble phase were higher for variants C and F, whereas a great amount of insoluble protein was found for mutants A, B, D, E and F.

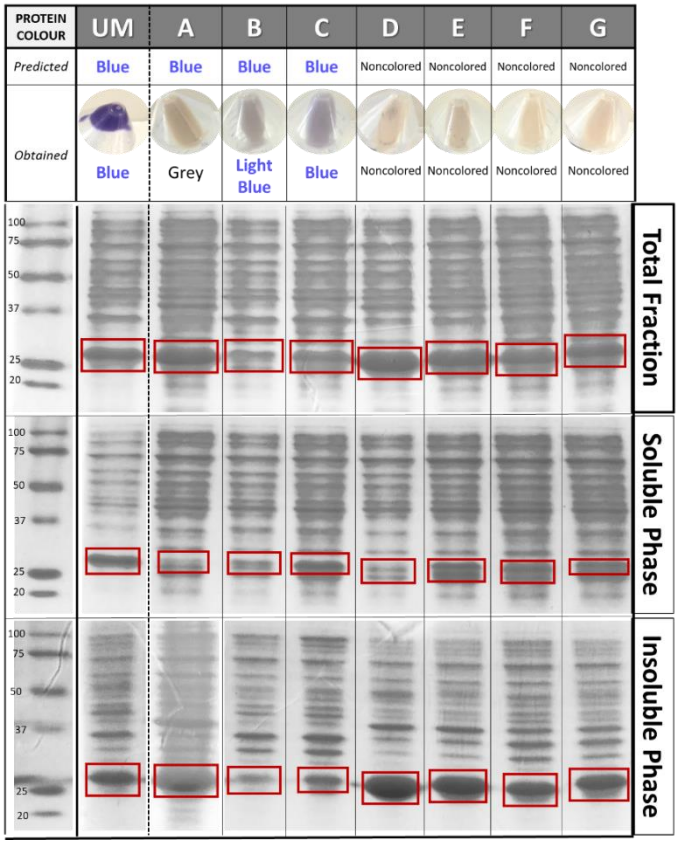


Figure II (b) 5. Expression profiles for ultramarine and the seven UM mutants. Predicted by molecular dynamics simulations and obtained colours (bacterial pellets) are indicated for each protein. Images of SDS-PAGE show the expression of each protein in the total extract, in the soluble phase and in the insoluble phase. Protein molecular weight marker is shown in the first lane (molecular weight in kDa). Theoretical molecular weights for all the proteins are the following (in kDa): UM 27.090, A: 26.925, B: 27.061, C: 26.975, D: 26.399, E: 27.456, F: 26.555 and G: 26.978. Gels were stained using Coomassie Brilliant Blue.

A preliminary analysis of proteolysis on mutants A-G was conducted adding HNE to all the proteins and recording absorbance values over time (Figure II (b) 6). The registered absorbance values were near the limit of detection of the assay, so no significant variations were observed after the addition of the enzyme.

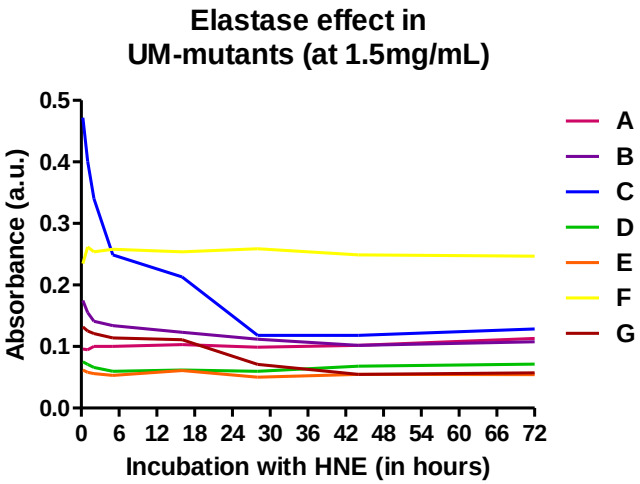


Figure II (b) 6. Absorbance profile of UM mutants (concentration of 1.5 mg/mL) after incubation with HNE (150 mU) at room temperature over 72 hours. Absorbance (arbitrary units, a.u.) was measured at 585 nm.

Due to the low amount of soluble protein obtained for mutants (even with the expression conditions previously optimized – data not shown), we decided to focus our efforts in upscaling the production of two of the most promising mutated proteins. We selected one mutant for each HNE sensor strategy: for the switch-off approach we were looking for a blue protein that could lose its colour after cleavage by HNE due to interference with the chromophore environment; for the switch-on approach we needed a non-coloured protein that could turn blue after establishment of the correct chromophore environment allowed by reorganization of the β-sheets promoted by HNE proteolysis.

Considering the switch-off strategy, mutants B and C showed some absorbance decrease after HNE addition (Figure II (b) 6), however expression yield of protein C was higher than protein B (Figure II (b) 5) which led us to select protein C ($C^{on\text{-}off}$). Regarding the switch-on strategy, mutant F ($F^{off\text{-}on}$) was selected because it was the only non-coloured variant that showed a slight increase on the absorbance spectrum after HNE addition (Figure II (b) 6) and its soluble/insoluble ratio was better than for mutants D, E and G (Figure II (b) 5).

Proteins $C^{on\text{-}off}$ and $F^{off\text{-}on}$ were upscale from 50 mL to 1 litter of culture (Figure II (b) 7A). However, the production yield felt short than the desired amount, mostly due to insolubility problems but also due to precipitation during dialysis. This latter problem occurred mainly for protein $F^{off\text{-}on}$ with more than half of the protein precipitating in the dialysis tube, even when performing dialysis against

different buffers (20mM NaH_2PO4, 500mM NaCl, pH 7.4; 20mM NaH_2PO4, pH 7.4; and 100 mM Tris HCl, pH 8). Control of pH (pH 8) in the assay was of extreme importance since ultramarine has been described to change its colour from yellow (pH 3.5), to red (pH 4.5) and to purplish blue (pH 8) depending on proton availability [301]. In addition, the variations of ultramarine's absorption spectrum at different pH relates with neutral and anionic forms of the chromophore that translate into absorption peaks at ~450 nm and ~590 nm, respectively [249]. The maximum absorbance peaks were registered at 585 nm and 530 nm without any other peak observed at ~450nm. This shows that the chromophore remained in its anionic form (Figure II (b) 7C and D).

Switch-off and switch-on sensors in action

With increased amounts of mutants $C^{on\text{-}off}$ and $F^{off\text{-}on}$ obtained, we repeated the analysis of the proteolytic effect of HNE on colour variation of these proteins (Figure II (b) 7).

For protein $C^{on\text{-}off}$, the switch-off strategy, after a transient increase in spectrum's intensity immediately after the addition of the protease, a consistent decrease in absorbance was registered over the incubation time with HNE (Figure II (b) 7B and C). Spectra were registered with a maximum peak at 585 nm and a secondary maximum of absorbance at 530 nm, and the absorbance decrease over 72 hours was calculated to be 80.8% and 74.2% at each wavelength. Most evident effect was observed in the first 2 hours of the assay and from 48 to 72 hours of incubation with HNE.

Regarding the switch-on strategy, mutant $F^{off\text{-}on}$ was expected to increase its absorbance after the addition of HNE. However, this behaviour was not observed and, instead, no significant differences were registered over time of incubation with the protease (Figure II (b) 7B and D). We observed a very small increase of 0.05 a.u. of absorbance on the calculated total area under the curve (AUC) associated to peak at 585nm after incubation with HNE. As in mutant $C^{on\text{-}off}$, immediately after the addition of HNE we registered an absorbance increase. Somehow, in the first moments, the interaction of HNE with ultramarine (Supplementary Figure II (b) S2) and the mutants (Figure II (b) 7C and 7D) leads to a potentiation of the absorption which is lost afterwards. We disregarded this phenomenon since it seems not to be dependent on the mutant itself.

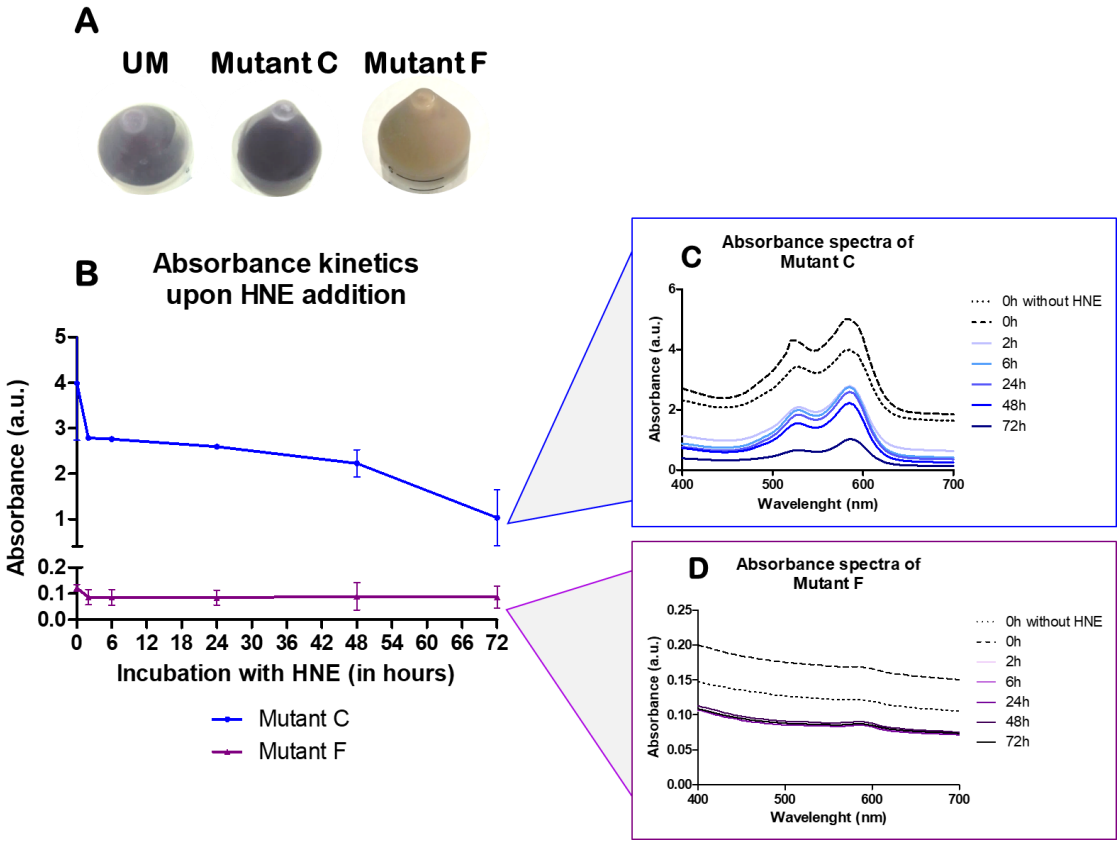


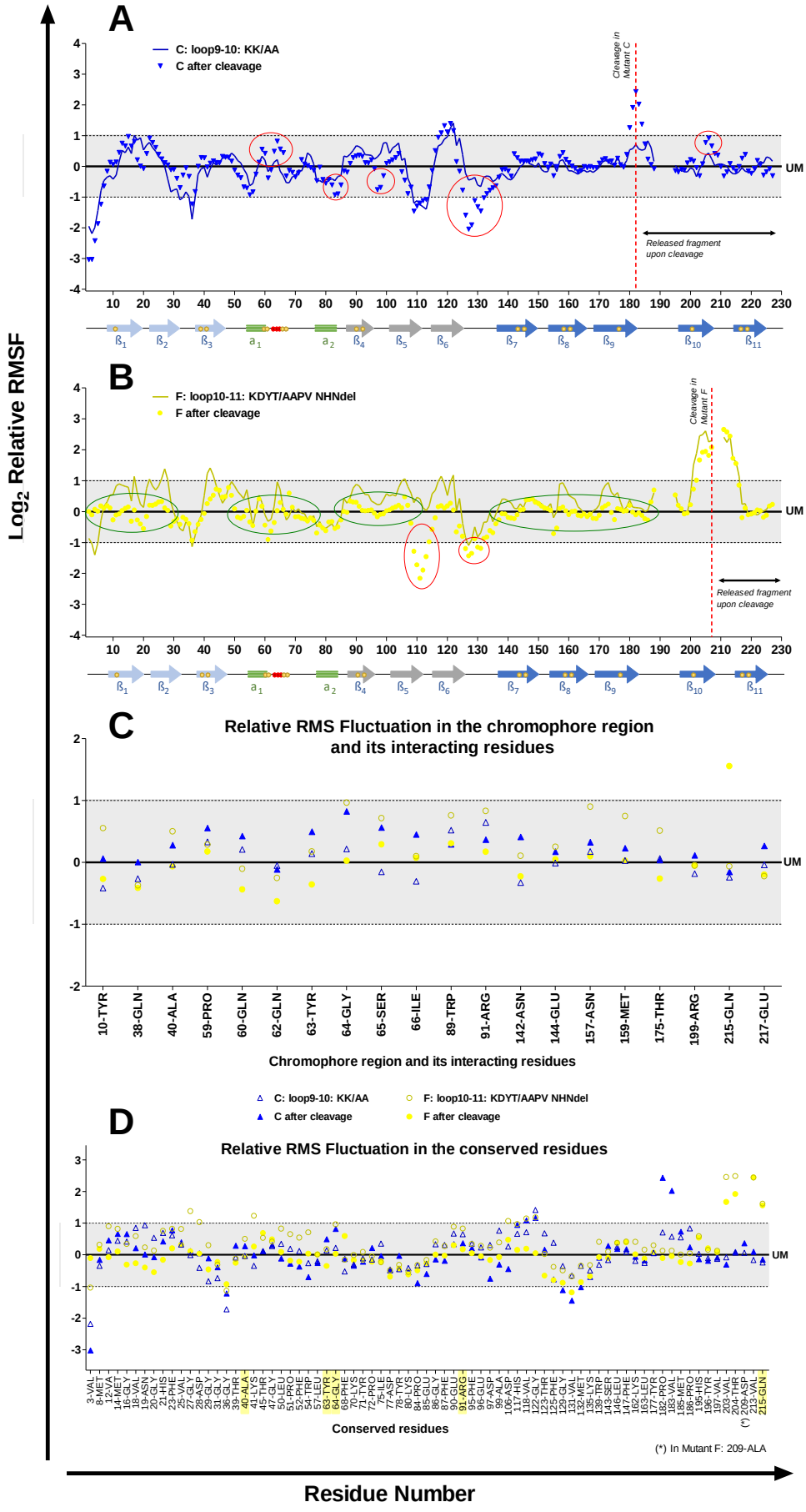
Figure II (b) 7. HNE effect on switch-off and switch-on mutants **(A)** Bacterial pellets after large scale expression of the blue proteins ultramarine and mutant C, and non-coloured protein mutant F. **(B-D)** Absorbance at 585nm was recorded over 72h of incubation at room temperature (RT) for mutant C (12 mg/mL) and mutant F (3mg/mL) before (dashed line) and after (filled lines) addition of HNE (150mU). Extinction coefficients at 585nm registered mutants C and F were 6057 $M^{-1}cm^{-1}$ and 666 $M^{-1}cm^{-1}$. UM's extinction coefficient is 64,000 $M^{-1}cm^{-1}$, as described in Pettikiriaracchchi *et al.*, 2012 [249].

Understanding disarrangement or establishment of chromophore environment with molecular dynamics

Mutants $C^{on\text{-}off}$ and $F^{off\text{-}on}$ were computationally cleaved and subjected to molecular dynamics simulations to evaluate residues' fluctuation as a measure of protein stability. Variants with well-established chromophore environment should be as stable as ultramarine and express the blue colour. For the switch-on strategy, we expected the deviation of fluctuation after cleavage to be near 0, meaning that the RMSF values were very similar to the ultramarine's. By contrast, for the switch-off strategy, RMSF values after cleavage should significantly differ from ultramarine's. The deviation of fluctuation of the variants from ultramarine, before and after cleavage, was calculated and is presented Figure II (b) 8.

As before, we focused our analysis in values of fluctuation 2-fold lower or higher in comparison with ultramarine's RMSF values. Unsurprisingly, residues in the cleavage sites suffered a great increase in fluctuation when cut, as a result of becoming end-terminals. This was taken into account in our analysis (and was not considered) not to bias interpretations.

Figure II (b) 8. Relative RMSF analysis of **(A)** mutant $C^{on\text{-}off}$ and **(B)** mutant $F^{off\text{-}on}$ before (filled line) and after (dots) cleavage, in relation to ultramarine, considering all residues. Elements of the secondary structure are depicted below the x axis, and chromophore region and its interacting residues are presented by red (●) and yellow (●) circles, respectively. Cleavage sites are indicated by vertical red lines. Shadowed region highlights 2-fold variation in relation to UM. Red or green ellipses indicate areas of divergence or convergence after cleavage, respectively, to RMSF values registered for UM. **(C)** Residues involved in the chromophore environment and **(D)** the conserved residues (Supplementary Table II (b) SI) were analysed separately.


A
C: loop9-10: KK/AA
C after cleavage
Cleavage in Mutant C
UM
Released fragment upon cleavage
B
F: loop10-11: KDYT/AAPV NHNdel
F after cleavage
Cleavage in Mutant F
UM
Released fragment upon cleavage
Log2 Relative RMSF
C
Relative RMS Fluctuation in the chromophore region and its interacting residues
10-TYR
38-GLN
40-ALA
59-PRO
60-GLN
62-GLN
63-TYR
64-GLY
65-SER
66-ILE
89-TRP
91-ARG
142-ASN
144-GLU
157-ASN
159-MET
175-THR
199-ARG
215-GLN
217-GLU
Chromophore region and its interacting residues
C: loop9-10: KK/AA
C after cleavage
F: loop10-11: KDYT/AAPV NHNdel
F after cleavage
D
Relative RMS Fluctuation in the conserved residues
Conserved residues
(*) In Mutant F: 209-ALA
Residue Number

Changes in the fluctuation after cleavage were greater in residues further located from the cleavage site. In particular, the main differences on fluctuation registered before or after cleavage for these variants $C^{on\text{-}off}$ and $F^{off\text{-}on}$ (both mutated in C-terminal loop regions) were mainly on the internal loop and N-terminal loop regions.

An overall analysis of variant $C^{on\text{-}off}$ shows that cleavage rendered increased flexibility in at least five regions compared to the non-cleaved form, diverging even more from ultramarine's RMSF (Figure II (b) 8A). However, fluctuation of only few residues was significantly affected after cleavage, namely in the internal loops region, in the β6-β7 loop and in the β10-β11 loop.

As residues Pro59, Gln60, Gln62, Tyr63, Gly64, Ser65 and Ile66 are critical for the chromogenic environment (Figure II (b) 8C), increased flexibility of these residues might impair the establishment of the necessary and stable interactions for colour generation. In addition, protein conformation was evidently altered on β6 region which escapes out of the barrel in an amorphous conformation (Figure II (b) 9). This might be explained by the 2- and 3-fold decrease in the values of relative fluctuation of conserved residues Gly129, Val131 and Met132, in relation to UM (Figure II (b) 8D), accompanied by the 3- to 5- fold decrease in neighbouring residues Pro126, Pro127 and Asn128 (Figure II (b) 8A). These results obtained by molecular dynamics simulation are in agreement with *in vitro* experiments, where blue protein C decreased its absorbance after incubation with HNE (Figure II (b) 6 and Figure II (b) 7).

In mutant $F^{off\text{-}on}$, deviation of fluctuation decreased in most of the residues, compared to the non-cleaved variant (Figure II (b) 8B), with at least 5 well-defined regions approaching UM's behaviour (~76.5% of residues present deviation of fluctuation within $-1<Log_2<1$ range). Nevertheless, β5-β6 and β6-β7 loops showed an extreme decrease of fluctuation after cleavage. The increase in rigidity of these regions compared to ultramarine, including in the conserved residue Val131 (Figure II (b) 8D), could constrict the structure, impeding the establishment of the chromogenic chromophore environment. In addition, β10 and β11 that were displaced by the mutations introduced in this variant could not relocate in the proper alignment after released by the cleavage (Figure II (b) 9). These limitations, in sum with the decreased flexibility of the chromophore residue Gly62 and its sided residue Cys61 can contribute to the inability to restore ultramarine's blue colour after cleavage by HNE, as verified in *in vitro* experiments (Figure II (b) 7).

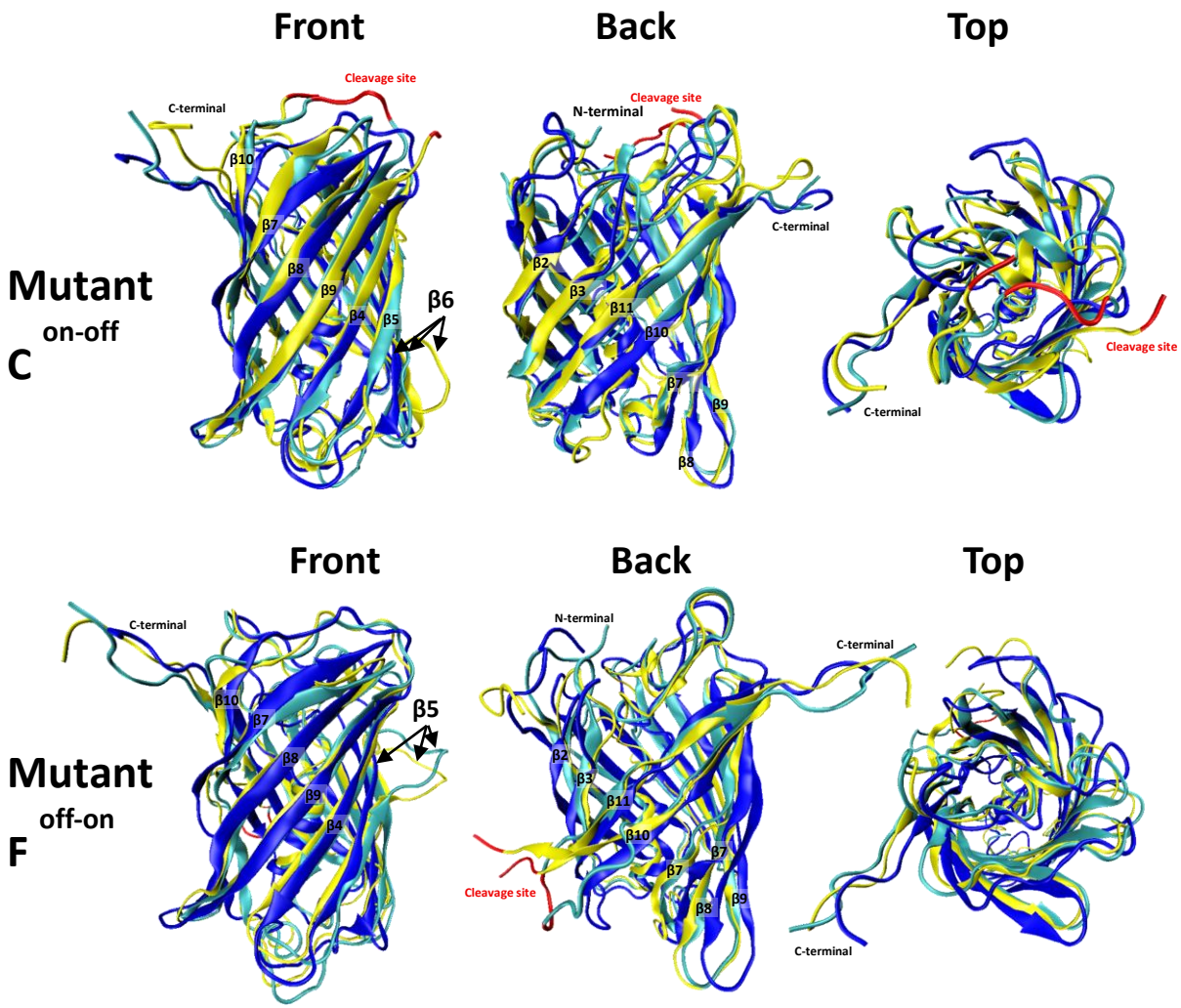


Figure II (b) 9. Conformation of mutant $C^{on\text{-}off}$ and $F^{off\text{-}on}$, before (in cyan) and after cleavage (in yellow), showing front, back and top views. Cleavage peptide is signalled in red. Original ultramarine structure is presented in blue colour. All structures were visualized with VMD 1.9.3 software.

II. (b) 4. Conclusion

This work explores the potential use of chromogenic recombinant proteins as sensors for proteases, in particular for human neutrophil elastase (HNE). We converted the ultramarine chromoprotein into a model substrate for elastase by the inclusion of the HNE-specific cleavage sequence AAPV on ultramarine sequence. Insertions or deletions were strategically made to enlarge or shorten loop regions in order to create switch-off (mutants A, B and C) or switch-on (mutants D, E, F and G) sensors.

A direct relation between the effect of the mutations on ultramarine conformation (analysed by molecular dynamic simulations) and colour generation (evaluated in *in vitro* assays) was found and two of the designed mutants were deeply investigated.

Mutant $C^{on\text{-}off}$ was expressed as a blue coloured protein and incubation with HNE led to a decrease in the absorbance. Mutant $F^{off\text{-}on}$ suffered severe disarrangements in the conformation which impeded the restoration of the complex interaction in the chromophore environment responsible for colour generation, even after incubation with HNE.

The emerging field of molecular biology assisted with molecular dynamics can provide novel approaches for the development of biosensors based in GFP-like proteins. The rationale here described can be investigated for other proteases, for example caspases, thrombin, trypsin, enterokinase, matrix metalloproteinases, collagenase and others, which can contribute to further enzyme-related applications. The development of HNE-specific sensor substrates could be explored in detection systems applied as diagnostic tools in healthcare, as HNE is greatly involved in numerous disorders [114,124,184–188].

The results here obtained (Table II) represent an advance in the field of colour-based sensors with the advantage of the low-cost production of recombinant proteins in comparison with synthetic peptides.

Table II. (b) II. Summary of expected phenotype (rationale) and results obtained from MD simulations and *in vitro* assays. Protein colour is indicated before and after cleavage.

Mutants ID	Expected (Rationale)	Predicted (MD simulations)	Obtained (*In vitro*)	*Comments*
Mutant A	No prediction	**Blue** → Non-colored	Grey → ND	Retrieval of a blue colored protein was unexpected since the mutations introduced flanking the chromophore triad were projected to disarrange the chromophore environment
Mutant B	**Blue** → Non-colored	**Blue** → Non-colored	**Blue** → ND	-
Mutant C	**Blue** → Non-colored	**Blue** → Non-colored	**Blue** → Non-colored	Promising candidate for a switch-off HNE sensor Extinction coefficients of 6057 $M^{-1}cm^{-1}$ (585 nm)
Mutant D	Non-colored → **Blue**	Non-colored → **Blue**	Non-colored → ND	-
Mutant E	Non-colored → **Blue**	Non-colored → **Blue**	Non-colored → **Blue**	-
Mutant F	Non-colored → **Blue**	Non-colored → **Blue**	Non-colored → Non-colored	It was evaluated as a switch-on candidate since mutations did alter the chromophore environment. However, the regeneration of chromophore environment upon HNE cleavage has to be further explored. Extinction coefficients of 666 $M^{-1}cm^{-1}$ (585 nm)
Mutant G	**Blue** → Non-colored	Non-colored → **Blue**	Non-colored → ND	Both *in silico* and *in vitro* results were contradictory with the theoretically expected.

ND – Not determined

II. (b) 5. Supplementary Information

Table II (b) S I. Residues involved in the chromophore and conserved residues in ultramarine protein.

Residues involved in the chromophore		
Chromophore triad		Gln62, Tyr6, Gly64
Interaction with the chromophore triad		Tyr10, Gln38, Ala40, Pro59, Gln60, Ser65, Ile66, Trp89, Arg91, Asn142, Glu144, Asn157, Met159, Thr175, Arg199, Cys215, Glu217
Conserved residues		
Loop regions	Top lid	Val3, Gly36, Tyr71, Pro72, Ile75, Pro84, Glu85, Gly86, P182, Val183, Met185, Pro186
	Bottom lid	Asn19, Gly20, Gly47, Leu50, Pro51, Glu96, Asp97, Ala99, Phe125, Gly129, Val131, Met132, Lys135, Asp209
	Internal loop	Phe52, Trp54, Leu57, Tyr63, Gly64, Phe68, Lys70, Asp77, Tyr 78, Lys80
β-sheets	β1	Met8, Val12, Met14, Gly16, Val18
	β2	His21, Phe23, Val25, Gly27, Asp28, Gly29 and Gly31
	β3	Thr39, Ala40, Lys41, Thr45
	β4	Phe87, Glu90, Arg91, Phe95
	β5	Asp106
	β6	His117, Val118, Gly122, Thr123
	β7	Trp139, Ser143, Leu146, Phe147
	β8	Lys162, Leu163
	β9	Tyr177
	β10	His195, Tyr196, Val197, Val203, Thr204
	β11	Val213, Gln215

Residues are numbered relative to mutant E and adapted from Prescott *et al.*, 2003 [250] and Ong *et al.*, 2011 [284].

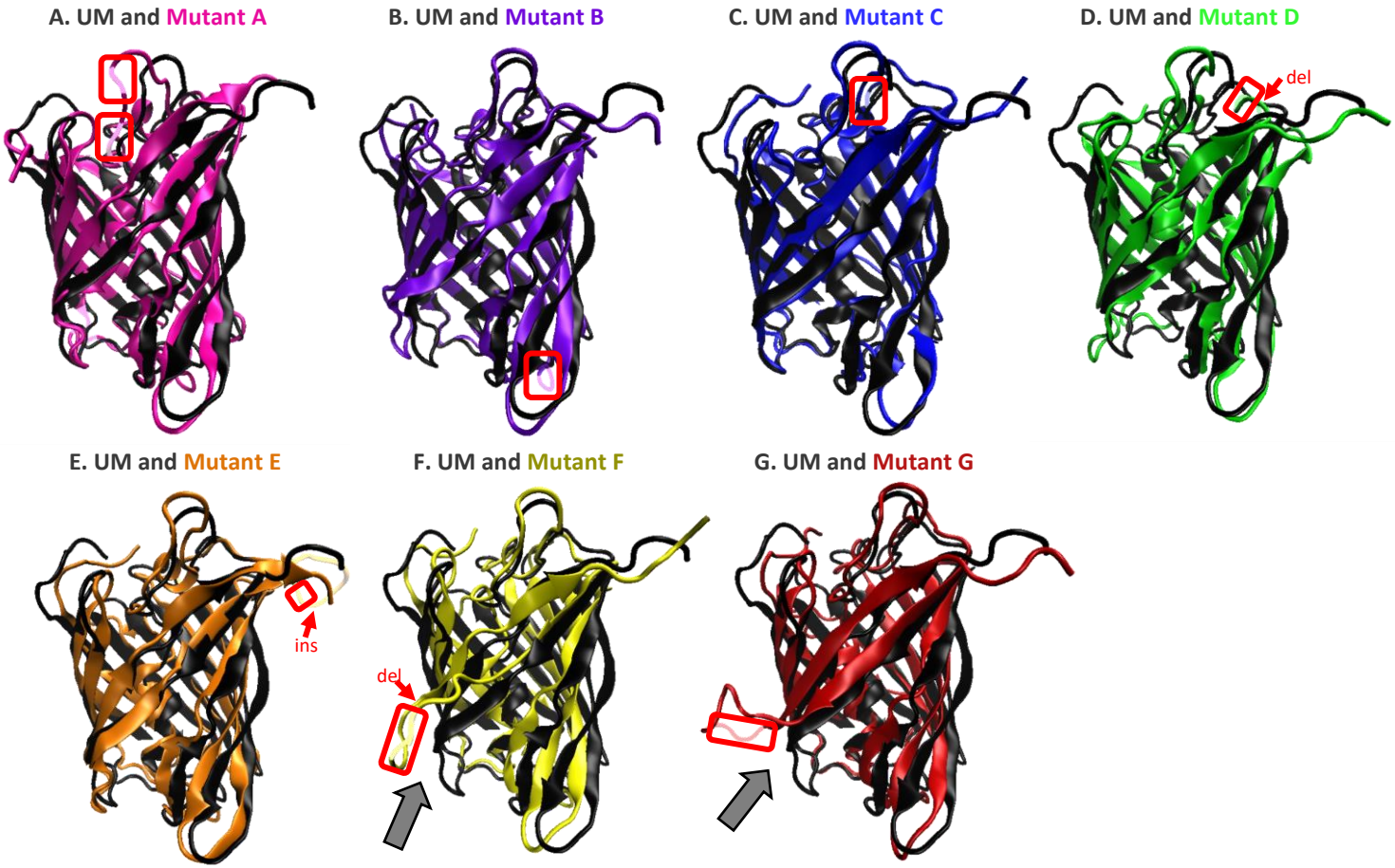


Figure II (b) S 1. β-barrel conformation of each designed variant (A-G), aligned with the original ultramarine protein. All structures were generated by VMD 1.9.3 softwar**e.**

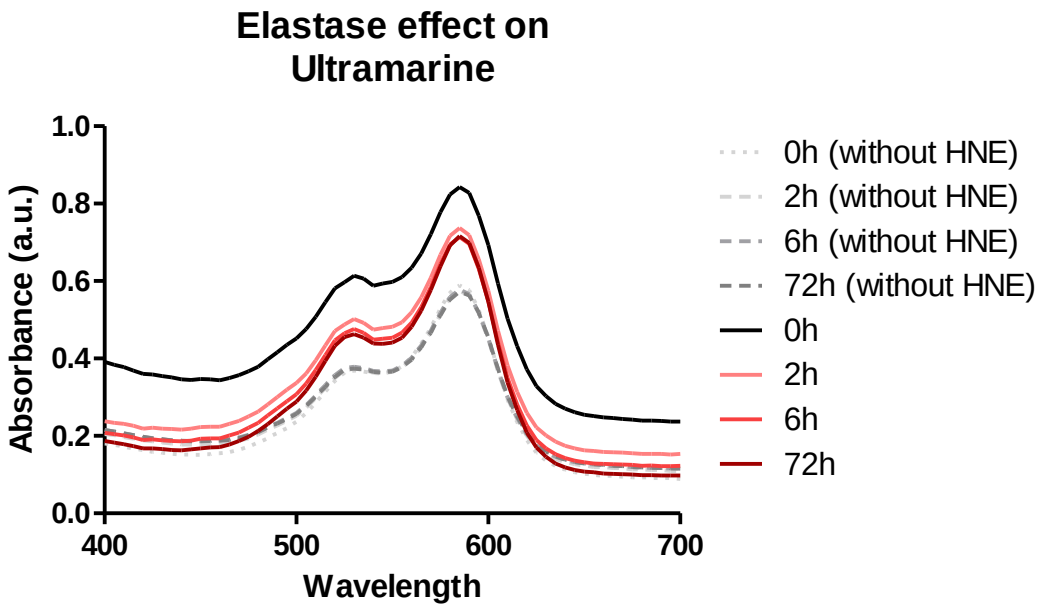


Figure II (b) S 2. Absorbance spectra for ultramarine (1.5 mg/mL) before (dashed line) and after (filled lines) addition of HNE (150 mU) at room temperature (RT) over 0, 2, 6 and 72 hours.

CHAPTER III.

HNE-specific fluorogenic sensors

This chapter is based on the following scientific paper:

Ferreira, A. V., Perelshtein, I., Perkas, N., Gedanken, A., Cunha, J. and Cavaco-Paulo, A. (2015). Detection of human neutrophil elastase (HNE) on wound dressings as marker of inflammation in *Applied Microbiology and Biotechnology*, doi: 10.1007/s00253-016-7889-6.

III. HNE-specific fluorogenic sensors

Abstract

Chronic wound fluids have elevated concentration of human neutrophil elastase (HNE) which can be used as inflammation/infection marker. Our goal is to develop functional materials for fast diagnosis of wound inflammation/infection using HNE as a specific marker. For that, fluorogenic peptides with a HNE-specific cleavage sequence were incorporated into traditional textile dressings, to allow real-time detection of the wound status.

Two different fluorogenic approaches were studied in terms of intensity of the signal generated upon HNE addition: a fluorophore 7-amino-4-trifluormethylcoumarin (AFC) conjugated to a HNE-specific peptide and two fluorophore/quencher pairs (FAM/Dabcyl and EDANS/Dabcyl) coupled to a similar peptide as a Förster resonance energy transfer (FRET) strategy. Also, two immobilization methods were tested: sonochemistry immobilization onto a cotton bandage and glutaraldehyde (GTA)-assisted chemical crosslinking onto a polyamide dressing.

The immobilized fluorogenic AFC-peptide showed an intense fluorescence emission in the presence of HNE. HNE also induced an enhanced fluorescent signal with the EDANS/Dabcyl FRET-peptide which showed to be a more sensitive and effective strategy than the AFC-peptide. However, its chemical immobilization onto the polyamide dressing greatly decreased its detection, mainly due to the more difficult access of the enzyme to the cleavage sequence of the immobilized peptide.

After optimization of the *in situ* immobilization, it will be possible to use these fluorescence functionalized dressings for an effective and specific monitoring of chronic wounds by simply using a portable ultraviolet (UV) light source. We envision that the development of this point-of-care medical device for wound control will have a great impact on patient's life quality and reduction of costs on health care system.

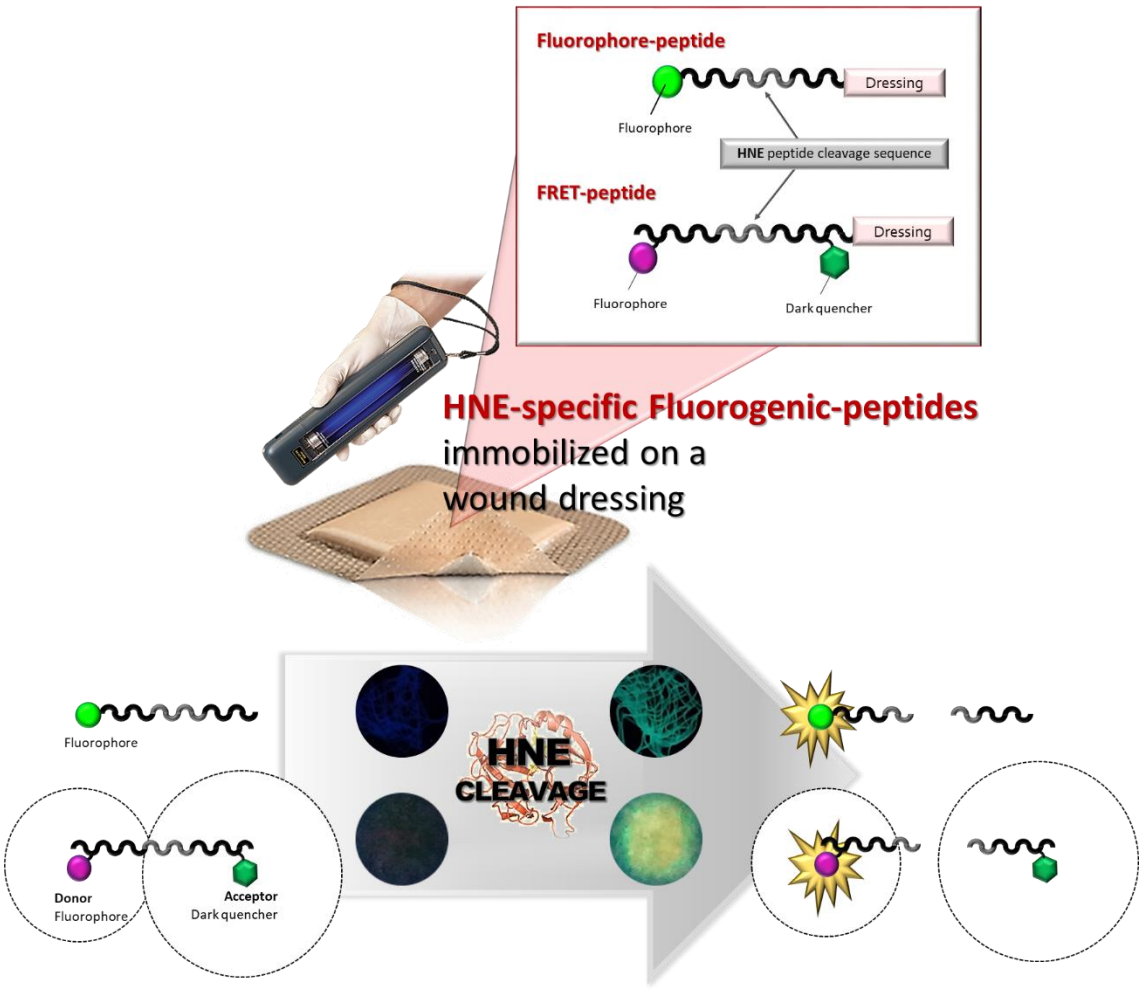


Figure III. 1. Graphical abstract of the chapter. Embedding of fluorogenic peptide sensors with HNE-specific cleavage sequence into a wound dressing material. HNE enzyme present in the chronic wound fluid will recognize and cleave the sensor peptides, leading to visually detectable modification on the dressing, thus discriminating the wound status.

III.1. Introduction

Human neutrophil elastase (HNE) is one of the most abundant neutral proteinases present in chronic wounds [107,183], being significantly active in pressure and diabetic ulcers [105,109,311]. Recent studies have demonstrated that HNE activity is elevated in fluids from chronic wounds (22.97 ± 13.27 U/mL) and reduced in healing wounds (2.89 ± 1.27 U/mL) [208,240–242]. According to this, we intend to use HNE activity as a wound inflammation/infection marker using fluorogenic peptide sensors with HNE-specific cleavage sequence embedded into a dressing material (as schematized in Figure III.1). Briefly, HNE enzyme present in the chronic wound fluid will recognize and cleave the sensor peptides, leading to visually detectable modification on the dressing, thus discriminating the wound status.

Nowadays, fluorescence systems are widely used in many applications in biotechnology fields, being a method of choice for biological and medical diagnosis due to its inherent sensitivity, selectivity, ease of implementation, response time, spatial resolution, and also growing availability of commercial products [312,313]. A possible limitation for the use of fluorogenic substrates is its direct visual assessment, since the human-eye is not a great spectral detector and cannot easily detect fluorescence changes when white light is used as excitation source. To overcome this, we aim to develop a simple method for visual assessment of HNE in wound dressings using a portable ultraviolet (UV) light source (commonly known as black light) to excite the fluorophores and allow the detection of the enzyme's activity on those fluorescent substrates.

In this work, to evaluate HNE activity, we firstly used a commercially available fluorogenic HNE-specific peptide, N-(Methoxysuccinyl)-Alanine-Alanine-Proline-Valine-7-amino-4-trifluormethylcoumarin (MeOSuc-AAPV-AFC), which releases AFC after peptidolysis, leading to the generation of a fluorescent signal. In a second approach, we designed a short peptide comprising a specific HNE cleavage sequence coupled to a fluorescence quenching system based on Förster resonance energy transfer (FRET). As described in literature, the quencher molecule absorbs the light emitted by fluorophore molecule, being this interaction distance-dependent [314,315]. Hence, the quencher and fluorophore molecules were paired at opposite terminals of the HNE-specific peptide sequence. Moreover, the quencher molecule chosen is a dark quencher, meaning that the energy absorbed from the fluorophore is released in the form of heat instead of light [312]. Therefore, it is not necessary to discriminate the wavelength of the light emitted by the system,

since there will only be fluorescence emission when the peptide is cleaved and fluorophore and quencher are not in spatial vicinity.

A variety of immobilization techniques and approaches can be used to incorporate the fluorogenic sensors onto the wound dressing matrix. Sonochemical immobilization method is one of the most used and effective coating methods for textiles [316,317]. Previously, we published several works showing that the deposition of a large variety of nanoparticles (NPs) on different materials using the sonochemical method can be successfully achieved [317–319]. In general terms, when high-intensity ultrasound is applied to the peptide aqueous solution, the peptide molecules are adsorbed on the formed acoustic bubbles [320]. When the cavity collapses, the absorbed molecules are exposed to extreme localized conditions of temperature and pressure. As a consequence, these molecules impact on each other and NPs of the organic compound are produced. In our case, the cavitation occurs not only in liquid, but also in a solid-liquid interface, *i.e.* near textile surface, due to increased nucleation rate in presence of a solid material [321]. After the bubbles collapse, high-speed jets of the liquid throw the generated peptide NPs at high speed toward the textile cotton surface where they remained embedded [319,322]. To achieve a stronger and stable immobilization, covalent binding through chemical reaction is another option [323]. This chemical immobilization process involves two main steps: activation of the support matrixes (in this case, the textile dressing) and coupling of the interest compound (the sensor) to the activated matrices [323,324]. The covalent bonds are normally formed through amide, ether, thio-ether, or carbamate bonds [323,324].

Either through a sonochemical or chemical immobilization method, the embedding of the developed fluorogenic HNE-specific sensors into a functionalized wound dressing material will allow *in situ* and real-time assessment of the wound status at an early stage of inflammation/infection. In contrast to other off-site methods, this novel approach would provide a fast and objective diagnosis, without the need of expensive and long-lasting analytic methods [75].

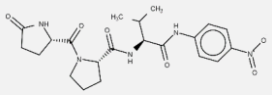
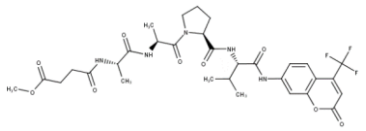
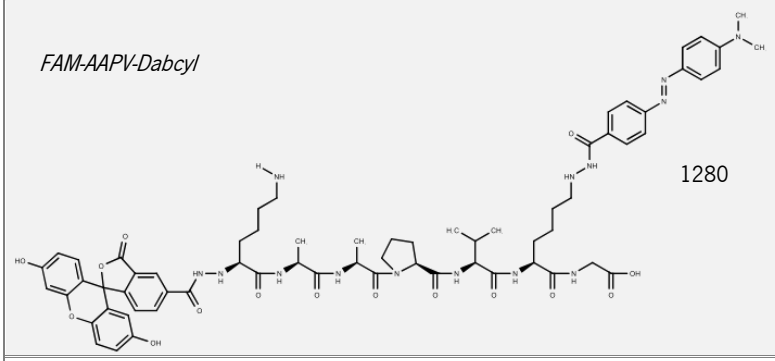
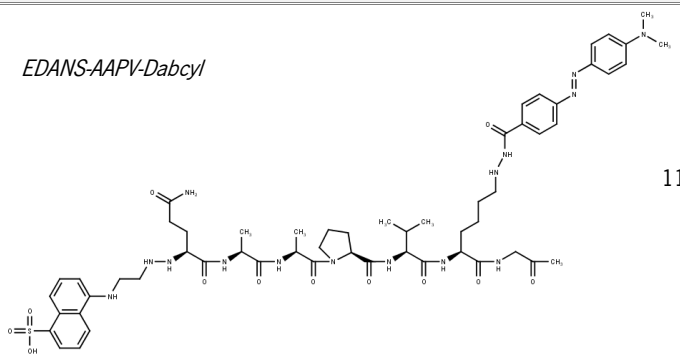
III.2. Materials and Methods

Materials

All chemicals were analytical graded and purchased from Sigma-Aldrich, namely glutaraldehyde (GTA) 50% solution in water, sodium hydroxide (NaOH), hydrochloric acid (HCl), pararosaniline hydrochloride (PS) dye, the enzyme HNE and synthetic HNE substrate pyroglutamate-Proline-Valine-*p*-nitroaniline (Glp-PV-*p*NA). The fluorogenic HNE substrate N-(Methoxysuccinyl)-Alanine-Alanine-Proline-Valine-7-amino-4-trifluormethylcoumarin (MeOSuc-AAPV-AFC) was purchased from Abcam, and FRET-peptides H-(FAM)Lysine-Alanine-Alanine-Proline-Valine-Lysine(Dabcyl)-Glycine-OH (FAM-AAPV-Dabcyl) and H-(EDANS)Glutamine-Alanine-Alanine-Proline-Valine-Lysine(Dabcyl)-Glycine-OH (EDANS-AAPV-Dabcyl) were synthetized by JPT Peptide Technologies GmbH (Germany). The respective molecular weight and structure of the chromogenic and fluorogenic HNE substrates are summarized in Table 1. Commercial cotton gauze with 17g/m2 was used for sonochemical coating. Commercial polyamide 6.6 fabric (nylon), a plain woven structure with 63 g/m2, was supplied by Rhodia (Switzerland).

Table III. 1. Chemical information (structure, molecular weight and spectral properties) of the used HNE substrates, Glp-PV-*p*NA, MeOSuc-AAPV-AFC, FAM-AAPV-Dabcyl and EDANS-AAPV-Dabcyl. All structures were drawn using MarvinSketch (ChemAxon, HU).

*** Determined using the reaction buffer of HNE**

	PEPTIDE STRUCTURE	Molecular Weight (Da)	Spectral properties *
Chromogenic peptide	*Glp-PV-pNA* 	445	λAbs_{max} = 380 nm
Fluorogenic peptide	*MeOSuc-AAPV-AFC* 	681	λEx_{max} = 380 nm λEm_{max} = 460 nm
FRET-peptides	*FAM-AAPV-Dabcyl* 	1280	λEx_{max} = 470 nm λEm_{max} = 492 nm
	EDANS-AAPV-Dabcyl 	1170	λEx_{max} = 475 nm λEm_{max} = 512 nm

Instrumentation

High intensity ultrasonic horn, Ti-horn, 20 kHz, 750W at 30% efficiency, was used for sonochemical coating reactions. The morphology of sonochemically coated cotton was studied by high resolution scanning electron microscope (HRSEM), using a Magellan – FEI, at an accelerating voltage over the range of 5-15 kV. All absorbance and fluorescence measurements were carried out in 96-well microplates using a Synergy Mx reader (Bio-Tek Instruments, Inc., USA) spectrometer and Gen5™ Data Analysis Software. Also, a fluorescence chamber equipped with UV light of 366 nm was used for visual assessment of the FRET system.

Methods

1. HNE activity assessment

HNE activity was evaluated with the synthetic substrates in accordance with the protocol supplied by Sigma-Aldrich. Briefly, the standard HNE activity assay consisted in mixing the enzyme (0.5 U/mL) with 25-1500 µM of substrate, in a final volume of 300 µL of reaction buffer (0.1M HEPES + 0.5M NaCl, pH 7.5). A blank consisting only in buffer and substrate, was also included in these assays. The kinetic constants were determined from the initial rates of hydrolysis by the Lineweaver-Burk method. All enzymatic assays were conducted at 37°C for 10 minutes with triplicates and the absorbance was measured at 405 nm by UV-Vis spectrophotometry.

2. Characterization of synthetic and commercially available HNE substrates and sonochemical immobilization on wound dressings

Commercially available elastase substrates MeOSuc-AAPV-AFC and Glp-PV-*p*NA were dissolved in water at a final concentration of 0.1 g/L, corresponding to a molar concentration of 147 and 225 µM, respectively. Then, the substrates were deposited onto a previously washed cotton bandages (7 x 7 cm^2) for 5 minutes using a high intensity ultrasonic horn. The sonication was carried out in a thermo-stated bath at 16◦C. The coated dressing was dried under vacuum.

The surface of the cotton coated with the HNE commercial substrates was imaged by HRSEM, and fluorescence emission after incubation at 37°C with several concentrations of HNE. The emission was quantified in a fluorimeter and visually detected using an UV light lamp.

3. Characterization of the FRET-peptides and chemical immobilization using GTA crosslinking

To examine the ability of FRET-peptides FAM-AAPV-Dabcyl and EDANS-AAPV-Dabcyl in detecting HNE activity, different peptide concentrations (1-600 µM) were added to a fixed amount of HNE solution (0.5 U/mL). The incubation was carried out at 37 °C, and at determined time points, the fluorescence spectrum (400-700 nm) of the samples was registered in a fluorimeter. As suggested by the supplier, the peptide was dissolved in DMSO to a stock concentration of 2.7 µg/mL and then diluted to the required assay concentrations in the reaction buffer.

Chemical immobilization of FRET-peptides into polyamide dressing consisted in the following steps: (1) surface alkaline treatment of previously washed polyamide dressing in 2 g/L NaOH for 30 minutes at room temperature with agitation assisted with glass beads; (2) GTA crosslinking to FRET-peptide for 2h with vigorous agitation; and (3) reaction of treated polyamide dressing (1 x 1 cm2) with GTA-FRET-peptide under orbital agitation overnight at 4°C (Figure III.2). At the end of each step, treated dressings were washed and dried under vacuum. The dye pararosaniline (PS) was used as a visual control of the immobilization and its GTA crosslinking was adapted from a previously described protocol of [325]. Crosslinking with GTA was performed in the molar ratios of 1:125 for FRET-peptide and GTA and 1:125:1255 for control PS, HCl and GTA.

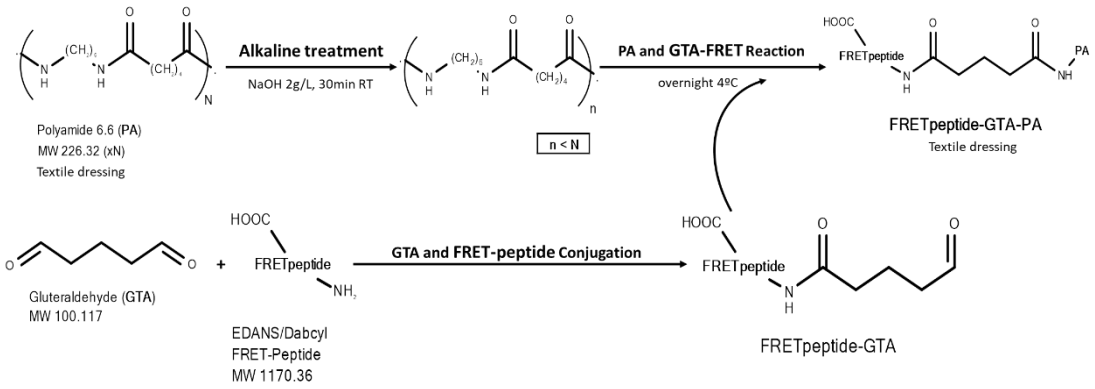


Figure III. 2. Chemical reaction of the EDANS/Dabcyl FRET-peptide immobilization into a polyamide (PA) dressing in three steps: Alkaline treatment of the PA dressing surface; Conjugation of Glutaraldehyde (GTA) and FRET-peptide; and reaction of the PA treated dressing and GTA-FRET-peptide. All structures were drawn using MarvinSketch (ChemAxon, HU).

III.3. Results

In vitro characterization of commercially available fluorogenic HNE substrates sonochemically immobilized on wound dressings

As a fluorogenic substrate we used MeOSuc-AAPV-AFC. Cleavage of this substrate releases the highly fluorescent compound 7-amino-4-trifluormethylcoumarin (AFC) (λExmax = 380 nm; λEmmax = 460 nm) [326]. The chromogenic peptide Glp-PV-*p*NA was used as a negative control of fluorescence. The enzymatic hydrolysis of this substrate releases *p*-nitroaniline (*p*Na), a molecule that can be easily detected with a UV-Vis spectrophotometer by increase in absorbance (λAbsmax) at 400nm which corresponds to the appearance of a light yellow colour detected by naked-eye [327].

These two commercially available peptides specific for HNE were immobilized into a plain and commonly used cotton gauze. Immobilization was accomplished by a sonochemical method using an ultrasonic (US) probe immersed in a solution of the substrate where the dressing was placed.

The morphology of the cotton dressing before and after the sonochemical coating reaction was observed by HRSEM (Figure III.S1 in supplementary data). A dense layer of spherical peptide NPs with an average particle diameter of ~15 nm was observed on the cotton fibres after sonication (Figure III.S1 B-D in supplementary data).

In order to evaluate the availability of the immobilized substrates to the enzyme, the sonochemically treated dressings were incubated with HNE and placed in a dark chamber to be observed under UV light (366 nm) source (Figure III.3).

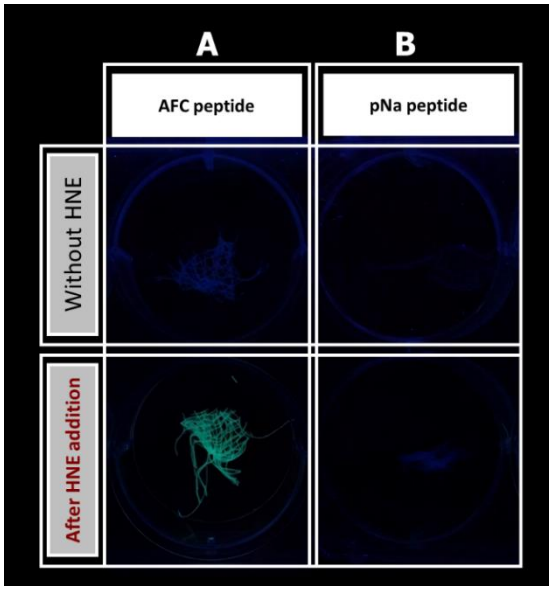


Figure III. 3. Visual assessment of the cotton dressing coated with the HNE substrates **(A)** MeOSuc-AAPV-AFC or **(B)** Glp-PV-*p*NA, after the addition of reaction buffer without HNE and with 150 mU of enzyme (incubation at 37°C, 30 minutes) using UV light with 366nm as excitation source.

Successfully, HNE was able to cleave MeOSuc-AAPV-AFC, as the dressing turned fluorescent after the addition of the enzyme (Figure III.3 A). Glp-PV-*p*Na was also efficiently immobilized and accessible to the enzyme, as a slightly yellow colour was visible after incubation of the dressing with HNE (data not shown). However, this colour change is barely detected by the human-eye. As expected, this substrate didn't develop fluorescence upon cleavage by HNE (Figure III.3 B).

For an estimate quantification of the naked-eye visualizations, the fluorescence spectrum was measured for each dressing (Figure III.4 B). The fluorescence intensity increased proportionally according to the concentration of HNE enzyme (Figure III.4).

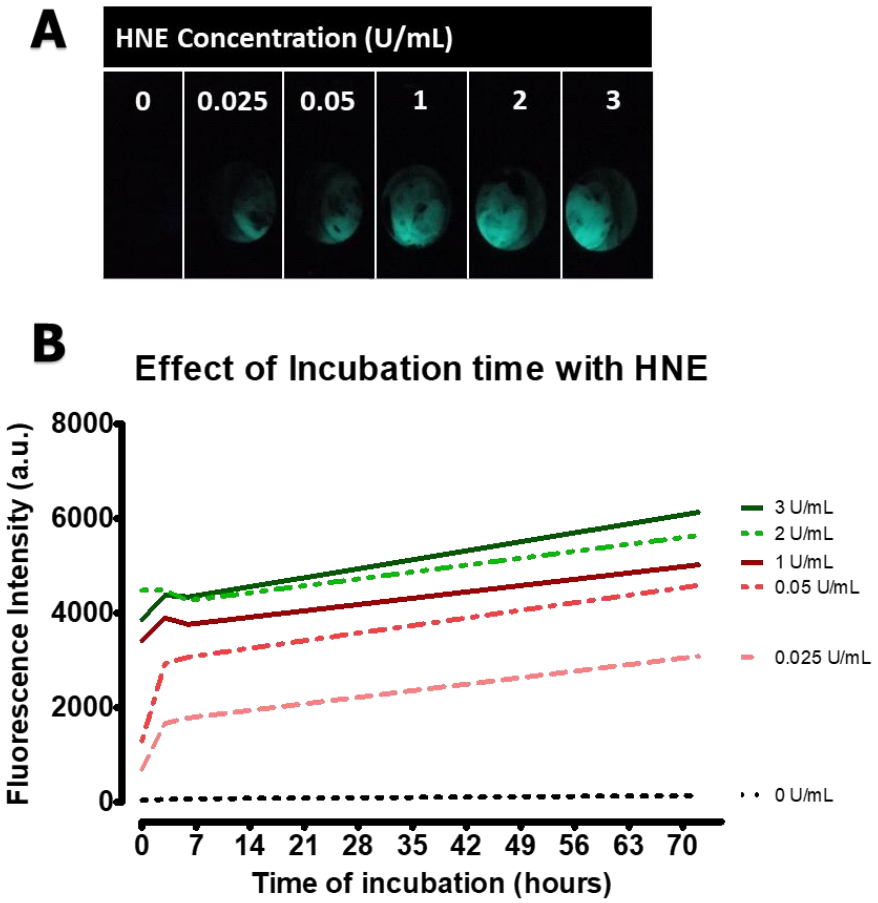


Figure III. 4. Assessment of the sensitivity of the substrate MeOSuc-AAPV-AFC with different concentrations of HNE (0 – 3 U/mL). **(A)** Visual assessment of the fluorescence of the dressing, using UV light (366 nm) as excitation source. **(B)** Fluorescence intensity of the dressing material quantified in a fluorimeter with λEx_{max} = 380 nm and emission λEm_{max} = 460 nm over time of incubation at 37°C. The legend shows the categorization of the fluorescence value in arbitrary units (a.u.).

In vitro characterization of FRET-peptides for HNE detection

Two fluorophore donors, FAM (5(6)-carboxyfluorescein) or EDANS (N-(Aminoethyl)-5-naphthalenamine-1-sulfonic acid), and a quencher acceptor, Dabcyl (4-([4'-dimethulamino)phenyl]azo)benzoyl), were covalently linked on opposite terminals of the HNE-specific peptide sequence, specifically the donor to the N-terminal and the quencher to the C-terminal. To avoid disturbance in the core of the peptide cleavage sequence, some amino acid residues were added to the sequence to serve as anchors through the free amino groups. Namely, FAM and Dabcyl were coupled through a lysine residue and EDANS was coupled through a glutamine residue (Table 1). A glycine residue was also added at C-terminal to improve the synthesis and purification process.

Because there are no previous studies with these substrates for HNE, first we analysed in detail the spectral changes of the donor fluorophore in absence and presence of the HNE to assess the ability of these FRET-peptides to serve as reporter for HNE activity. Several concentrations of each FRET-peptide were tested, and the obtained results are presented in the following Figure III.5 and Figure III.S2 in supplementary data.

For both FRET-peptides, the fluorescence intensity of the donor, FAM or EDANS, at the wavelength for the peak of fluorescence emission (λEmmax of 492 and 512nm, respectively) increased when the enzyme was added (Figure III.S2 in supplementary data). The fluorescence intensity was also higher with the increase of substrate concentrations (Figure III.S2 in supplementary data and Figure III.5). This correlation was expected since the fluorophore donor molecules present in solution increase in number and, therefore, more photons are capable to be released.

Then, the FRET-peptides solutions were placed on a hydrophobic paper surface for visual assessment on a solid surface and the fluorescence changes upon HNE cleavage were visualized using a UV light lamp (Figure III.6). It was possible to visually observe significant differences in the fluorescence intensity of both FRET-peptides in the absence or presence of HNE enzyme, however the fluorescence changes were significantly higher for EDANS/Dabcyl-peptide. For this reason, this FRET-peptide pair was selected for further immobilization into a textile dressing.

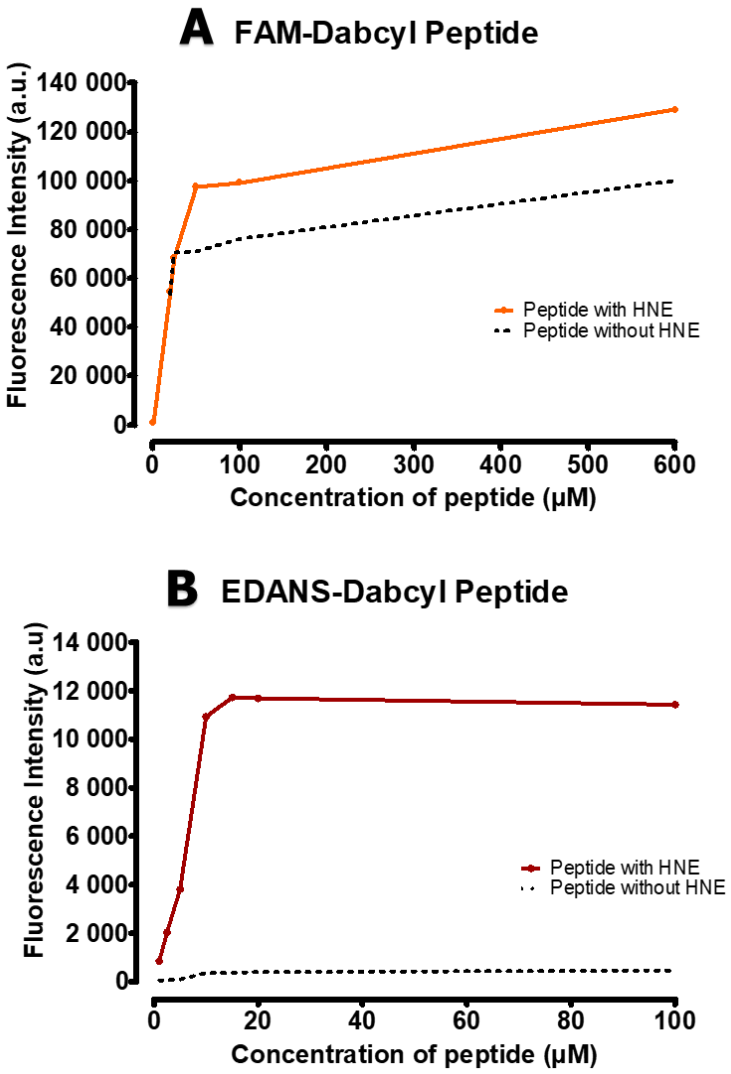


Figure III. 5. Fluorescence intensity of **(A)** FAM/Dabcyl-peptide and **(B)** EDANS/Dabcyl-peptide before (dashed line) and after a 10 minute-incubation at 37°C with HNE (10-600 µM or 1-100 µM, respectively) (filled coloured line). λEm_{max} was chosen accordingly for each fluorophore donor (Table III.1) and the emission spectra were measured. The legend shows the categorization of the fluorescence value in arbitrary units (a.u.).

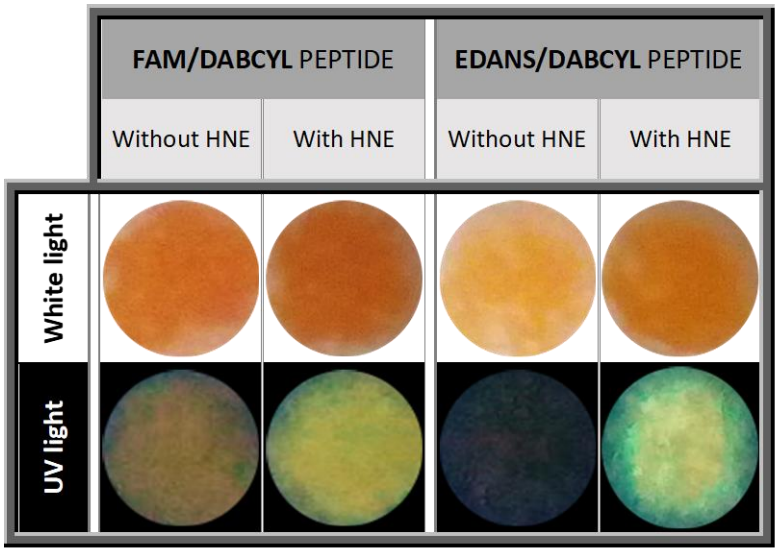


Figure III. 6. FRET-peptides FAM/Dabcyl and EDANS/Dabcyl (100 μM of concentration) solutions after incubation with 150 mU of HNE at 37°C for 10 minutes. The photographs show visualization under white light and UV light from a portable UV device. Sample solutions were placed in a hydrophobic paper surface.

In vitro characterization of EDANS/Dabcyl FRET-peptide for HNE detection chemically immobilized on wound dressings

The FRET-peptide EDANS/Dabcyl was then immobilized into a traditional textile dressing of polyamide based in a methodology described in [328], as schematized in Figure III.2. Photographs of the resulted PA dressings after immobilization are presented in Figure III.7 A. The immobilization efficiencies, calculated as the fraction of the amount of peptide that remained in the dressing after washing compared to the initially immobilized/adsorbed amount, are presented in Figure III.7 B. Statistical significance of the immobilization efficiencies was determined by Student's t-test with a confidence level of 95% and is assigned in the graph.

The immobilization efficiency for PS-HCl dye (used in this work as a control) varied greatly whether or not GTA was used to crosslink it to PA. GTA crosslinking method allowed a significant increase in the immobilization efficiency (P value < 0.0001), changing from 38.32% ± 1.04 to 69.81% ± 0.46.

The solution of EDANS/Dabcyl FRET-peptide has an orange colour (Figure III.6), however after the immobilization process its colour intensity faints to a pale yellow (Figure III.7 A). EDANS/Dabcyl FRET-peptide was successfully immobilized into the polyamide dressing with similar immobilization efficiency of 77.94% ± 2.45 with GTA and 79.62% ± 2.38 without GTA (Figure III.7 B) (ns non-significant, P value of 0.44).

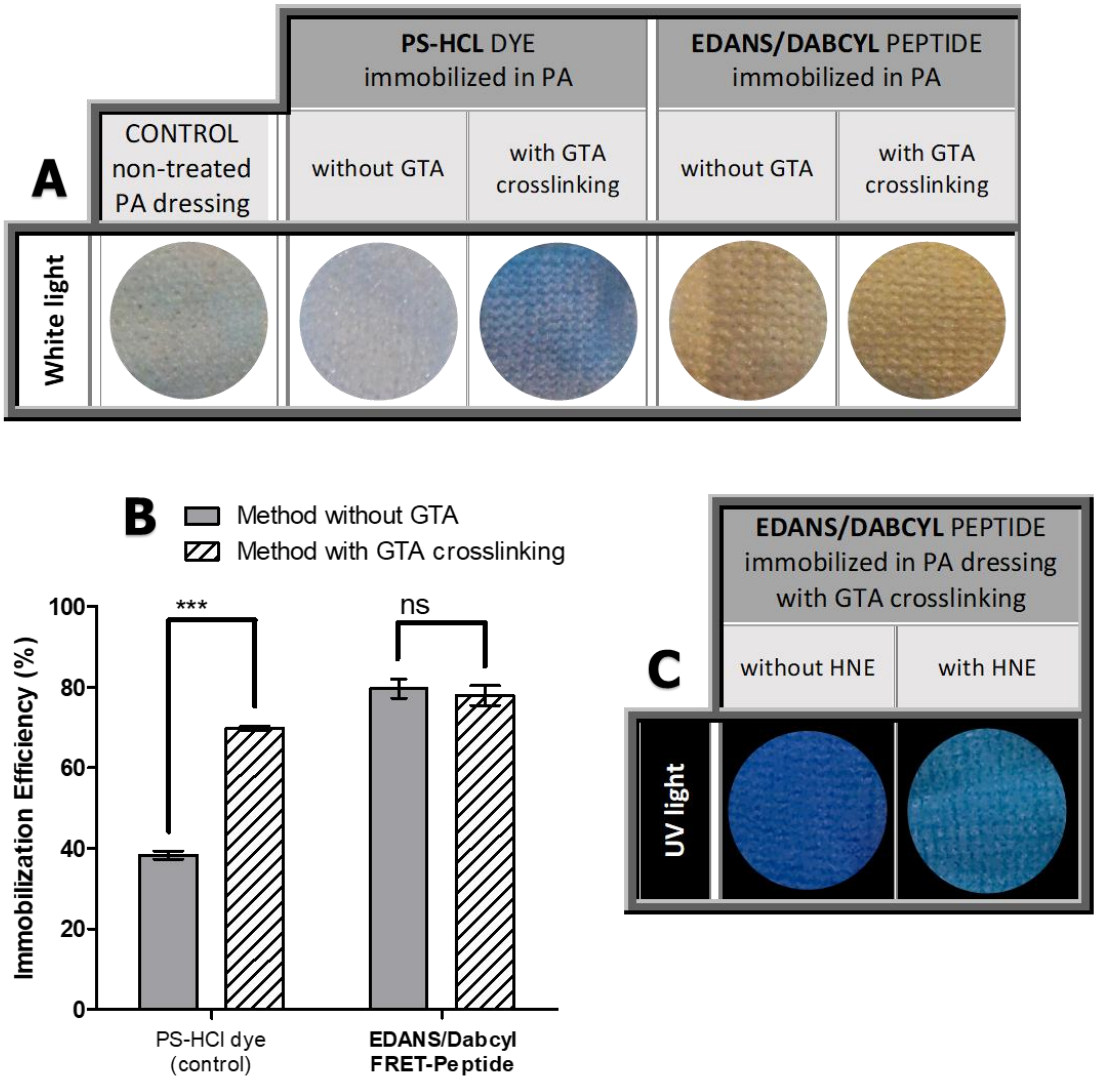


Figure III. 7. (A) Visual assessment under white light of the resulted PA dressings after immobilization without GTA and with GTA of control PS-HCl dye and EDANS/Dabcyl. **(B)** Immobilization efficiencies of PS-HCl dye and EDANS/Dabcyl FRET-peptide with and without GTA crosslinking. **(C)** Visual assessment under UV light of the EDANS/Dabcyl FRET-peptide immobilized on PA dressings with GTA crosslinking method upon incubation with 150 mU of HNE at 37°C for 24 hours.

For the final application of using the treated fabric as a sensor for elastase activity, the dressings functionalized with EDANS/Dabcyl FRET-peptide were incubated with the HNE enzyme (Figure III.7 C). A slight fluorescence signal was detected upon HNE addition after 24 hours of incubation. However, the fluorescence intensity was lower when the substrate was immobilized than when in solution (Figure III.6). It also required an increased incubation time with elastase (24 hours of incubation at 37°C) in comparison to the previous assays in solution (10 minutes).

III.4. Discussion

Analysis of the developed fluorogenic sensors for HNE detection.

In this work, we intend to immobilize fluorogenic substrates on wound dressings to efficiently detect human neutrophil elastase (HNE) present in exudate from chronic wounds.

As a first and straight forward immobilization strategy, we submitted cotton dressings and substrate solutions to an ultrasound treatment leading to the formation of peptide nanoparticles (NPs) which are thrown at the surface of the dressing (Figure III.S1 B-D in supplementary data). The formation of these peptide NPs only occurred as a result of ultrasound irradiation applied on the peptide solution with the dressing, since before sonication the cotton fibres presented a smooth structure (Figure III.S1 A in supplementary data). This result is in accordance with previous publications that report on the sonication of organic solutions leading to the formation of NPs [329,330]. Nevertheless, these do not remain stable in aqueous solution without a stabilizer, and eventually re-dissolve back in the solvent. If one wants to embed organic NPs onto a solid surface, then the use of a sonochemical technique presents itself as a clear benefit, since in a one-step process, the organic peptide NPs are created from the aqueous solution and anchored onto the cotton surface.

Detection of HNE activity with the fluorogenic MeOSuc-AAPV-AFC substrate showed to be very sensitive, since visual detection using a UV light was possible even at low concentrations of the enzyme (Figure III.4). Even so, a second approach using peptides with specific cleavage sequence for HNE were coupled to a fluorescence quenching system was also studied. According to the literature, the use of FRET system allows a more sensitive detection of the peptide cleavage in comparison to colorimetric (and even other fluorescence) methods [312,313].

In this work, two FRET-peptides pairs FAM/Dabcyl and EDANS-Dabcyl were tested. Upon HNE addition, the fluorescence of both FRET-peptides increased (Figure III.S2 in supplementary data). This means that HNE was able to recognize the specific cleavage sequence and the subsequent peptidolysis on the FRET-peptides separated the fluorophore donor and the quencher acceptor molecules. Consequently, Dabcyl was no longer in the necessary spatial vicinity of the donors to quench its fluorescence, and, hence their signal is released to the medium. Dabcyl is a dark quencher, which means that instead of emitting the energy that was transferred from the donor, it releases it as heat [312]. Since the energy emission of the acceptor molecule will not affect the fluorescence measurements, the use of dark quencher enables a more sensible analysis [312], usually from an off-signal to an on-signal.

Analysing in detail, significant differences are seen between the fluorescence profiles of FAM/Dabcyl and EDANS/Dabcyl pairs before and after HNE cleavage (Figure III.5). The basal fluorescence (*i.e.* without HNE) of FAM/Dabcyl pair is much higher than that of EDANS/Dabcyl pair. This then translates on a fluorescence change after HNE addition more evident when using EDANS than FAM as a donor, even with the relative fluorescence intensity of cleaved EDANS/Dabcyl peptide being 10 times lower than cleaved FAM/Dabcyl peptide. The main reason for these results resides in the spectral overlap between the donor and acceptor (Figure III.S3 in supplementary data).

Resonance energy transfer only occurs when the acceptor molecule is able to absorb light in the same spectral range as the donor emission, meaning that the energy of photon emitted by the donor should be as close as possible to the energy absorption ability of the acceptor [331]. In practical terms, this means that the emission spectrum of the donor should overlap the absorption spectrum of the acceptor, being this termed as donor/acceptor pair compatibility [331–334].

As presented in Figure III.S3 A in supplementary data, for FAM/Dabcyl there is not a complete spectral overlap and FAM emission is not entirely absorbed by the quencher Dabcyl. Since the donor fluorescence quenching only occurs at the “overlapping area”, a great amount of fluorescence emission leaks even when the peptide is not cleaved, and for this reason the fluorescence changes without or with HNE are not significant. These results demonstrated the non-compatibility of the FRET pair FAM/Dabcyl despite being commercially available.

For the other FRET pair, EDANS emission is almost fully absorbed by Dabcyl, as showed by the complete spectral overlap (Figure III.S3 B in supplementary data). The basal fluorescence of

EDANS/Dabcyl-peptide is very weak, thus upon peptide cleavage the increase in fluorescence is notable. EDANS/Dabcyl-peptide proved to be very sensitive to HNE activity, as the concentrations tested with HNE were much lower than for the other FRET-peptide (Figure III.5).

The fluorescence visual changes were also significantly higher for EDANS/Dabcyl-peptide (Figure III.6), since the condition without HNE was completely visually off and after the enzyme addition a bright signal appeared. FAM/Dabcyl-peptide showed to be fluorescent even in the absence of HNE, which for our purposes would lead to false positive results of HNE assessment in wound fluids. The evaluation of HNE activity on the dressing must rely on UV excitation and fluorescence visualization, since observation of the dressings under white light revealed no major differences in colour generation after HNE addition.

To enhance and create a stronger embedding, a chemical immobilization method was favoured as an alternative to previously used method of sonochemical immobilization by US probe. The chemical immobilization chosen consisted in the establishment of chemical bonds between the amine groups of the peptide (N-terminal) and free amines from polyamide generated by mild hydrolysis through a glutaraldehyde (GTA) crosslinking conjugation (Figure III.2). GTA is one of the most effective protein crosslinking reagents due to its high reactivity and low cost [335]. Since GTA is extremely reactive to amine groups, a polyamide textile dressing was preferred instead of the previously used cotton bandage. Furthermore, polyamide dressing provides high elasticity and strength, textile uniformity, and cost effectiveness, presenting itself as a great immobilization substrate for wound dressing applications [336].

Pararosaniline (PS) dye was used as a control of the immobilization process since it is described as a reactive dye of polymer fibres with high tinting properties, *i.e.* high immobilization efficiencies [337]. In addition, in our experiment PS also allowed a visual confirmation of the chemical reactions during the immobilization process, since PS is used as main reagent in colorimetric tests for aldehydes [325,337]. In aqueous neutral solution PS colour is bright magenta, but upon acidification with HCl it turns to a pale biscuit colour; after the addition of aldehyde compounds, PS solution results in a purple blue colour [325]. Figure III.7 A confirms these colour changes of PA dressing immobilized with PS-HCl in a direct reaction (control without GTA) and with GTA crosslinking.

A high immobilization efficiency of FRET-peptide without GTA crosslinking was not expected (Figure III.7 B); in fact GTA was initially selected and used to enhance the immobilization process.

According to the findings available in literature, this surprising result might be owed to the initial alkaline treatment of the polyamide dressing. Conventionally, alkaline or acid solvent hydrolysis is used to improve the hydrophilicity and dyeability of textiles [338,339]. By using the initial alkaline treatment with NaOH, the polyamide structure suffered a hydrolysis process on the most outward fibres that improved its absorption properties, allowing an enhanced molecule penetration [338,339], in this case of the EDANS/Dabcyl peptide. On the contrary, immobilization efficiencies with non-treated PA dressings are described to be considerably lower [328,338,339].

Upon HNE cleavage, a slight fluorescence signal was detected (Figure III.7 C), however its intensity was lower in comparison to the observed signal in solution (Figure III.6). This decreased detection might be related to the inaccessibility of the immobilized FRET-peptide. Indeed, substrate-immobilization significantly changes enzymatic reaction parameters, in which the rates and yields of solid-phase reactions are often lower than solution-phase reactions [340,341]. Since HNE active site possesses a hemispherical and hydrophobic deep pocket which is completely buried in the interior of the enzyme, it is likely that HNE is less capable to act on a substrate which is immobilized on a solid surface like our EDANS/Dabcyl FRET-peptide chemically conjugated to the PA dressing [124,341].

Furthermore, the intermolecular quenching phenomenon from Dabcyl on EDANS cannot be excluded as a possible reason for the observed diminished detection [105]. In solution, we recorded that upon HNE cleavage, the full fluorescence quantum yield of EDANS was restored (Figure III.6), since the now released Dabcyl peptide fragment out distanced from EDANS. However this distance detachment may be affected in the solid state. When immobilized, the distance of the cleaved fragments of EDANS and Dabcyl peptide might not significantly increase, since EDANS might be still close to its previously paired Dabcyl or to Dabcyl from molecules in the vicinity [105]. This phenomenon termed as intermolecular quenching could also contribute to the weaker fluorescence observed in Figure III.7 C.

Improvements and future prospects

Although the obtained fluorescent on-signal of EDANS/Dabcyl functionalized dressing was at this stage limited, this is a promising approach for specific detection of elastase on sensor dressings using a UV portable light. Currently, optimization of the immobilization process of the FRET-peptide onto a textile dressing is necessary. The chosen chemical immobilization method

with GTA crosslinking caused some problems and restricted the accessibility of the enzyme to the detection substrate. A popular method that can be applied to improve these issues is the use of polyethylene glycol (PEG) spacers that would increase the substrate accessibility and mobility. As a result, the HNE enzyme could access and catalyse the immobilized FRET-peptide, causing an intense fluorescent on-signal [340,341].

In further development of this work, the immobilization of the HNE-specific FRET-peptide onto the dressing must be optimized taking into consideration not only the method to be applied, but also the conditions and parameters used, including the concentration of the FRET-peptide. At this stage, the in-vitro assays were only performed using 150 mU of commercial HNE enzyme (specifically, 50 µL with 3 U/mL). Since HNE activity in non-infected or infected wound ranges from 2.89 ± 1.27 U/mL to 22.97 ± 13.27 U/mL [208], it is paramount that the HNE-sensor develops a fluorescent signal proportional to the activity of HNE in the wound. For that, in further assays, the concentration of immobilized FRET-peptide in the dressing should be optimized using exudate collected from patients with non-infected and infected wounds, taking into account not only the activity and kinetics of HNE in the exudate, but also the volume of exudate produced by the wound (high or low exudative wounds).

The pH and temperature of a wound are dynamic factors that fluctuate depending the type of wound, local wound factors and systemic factors intrinsic to the patient conditions [342]. Under normal circumstances, the pH value of the skin surface varies between 4 and 6. However, in a wound, this skin's acidic milieu is disturbed and can oscillate to pH values above 7-9 [342]. Additionally, the temperature of a wound varies from 30 to 42 °C [96]. At this stage, evaluation of the developed fluorogenic sensors was performed at the enzyme optimal conditions (pH 7.5 and temperature 37°C) [108]. To ensure the effectiveness of the HNE-sensor and taking into consideration the wound environment, further assays should be performed at wider range of pH (4 - 9) and temperature (30 - 42 °C).

The embedding of chromogenic or naked-eye detection sensors into a wound dressing material will allow in situ and real-time assessment of the wound inflammation/infection at an early stage. In contrast to other off-site methods, this novel approach would provide a fast and objective diagnosis, without the need of expensive and long-lasting analytical methods [1,31,75]. The use of a FRET-peptide with a HNE-specific cleavage applied in a wound dressing can assist the medical

staff in the evaluation of the wound status by fast and easy visualization of the dressing with a portable UV light source (Figure III.1).

Some concerns may be raised regarding the toxicity of fluorogenic substrates used in the sensor, namely the AFC, FAM, EDANS and Dabcyl compounds. Previously published works have tested these compounds in cell-based assays, where it has been proven their safety. Actually, AFC has been extensively used as a viable cell protease marker due its innocuous behaviour on cells [343,344]. Also, previous studies have shown viability rates above 98% of intact THP-1 cells incubated with 5 μM of FAM peptide-substrates [345], as well as concentrations up to 100 μM of EDANS/Dabcyl compounds have shown no cytotoxicity effect on the viability of human rhabdomyosarcoma (RD) cells [346].

Although a proven absence of toxicity can only be evaluated with direct tests to evaluate the effect of these fluorogenic sensors on cells, we may predict that they should be biocompatible and will not lead to cytotoxicity due to the incorporated fluorogenic compounds. Furthermore, at the next stages of this work, the fluorogenic sensors will be placed on top of a dressing with controlled fluid-handling ability, so that the wound fluid will only flow in the direction of the upper surface. This way, the released products upon HNE cleavage would not leak to the wound. The immobilization site containing the fluorogenic sensor will also be protected against light and air-exposure with a removable dark cover, allowing the use of the same dressing for longer periods of time consistent with the typical wound care practice, without the risk of fluorescence bleaching.

Chronic wounds are a significant burden for the health care system, accounting for almost 4% of its total budget, and currently increasing [2,31]. Early detection of incipient infection in chronic wound reduces the severity of the disease and decreases health care expenses [239]. However, currently, it is very difficult, expensive and time consuming to accurately assess a wound status [2,32]. Besides, upon diagnosis, the current treatments strategies follow a trial-and-error approach, which is also inefficient, expensive and time-consuming [1,32].

This work serves as a proof of concept, so to this extend it aims only to demonstrate the feasibility of a fluorogenic sensor for monitoring the activity of HNE, and not to be an early version of a final product. We envisioned that this new functional and diagnostic material will allow a better control of inflammation/infection in chronic wound at an early stage, contributing to the decision on the treatment to be implemented, and consequently, to a better patient's life quality and decrease in the wound care costs.

III.5. Supplementary Information

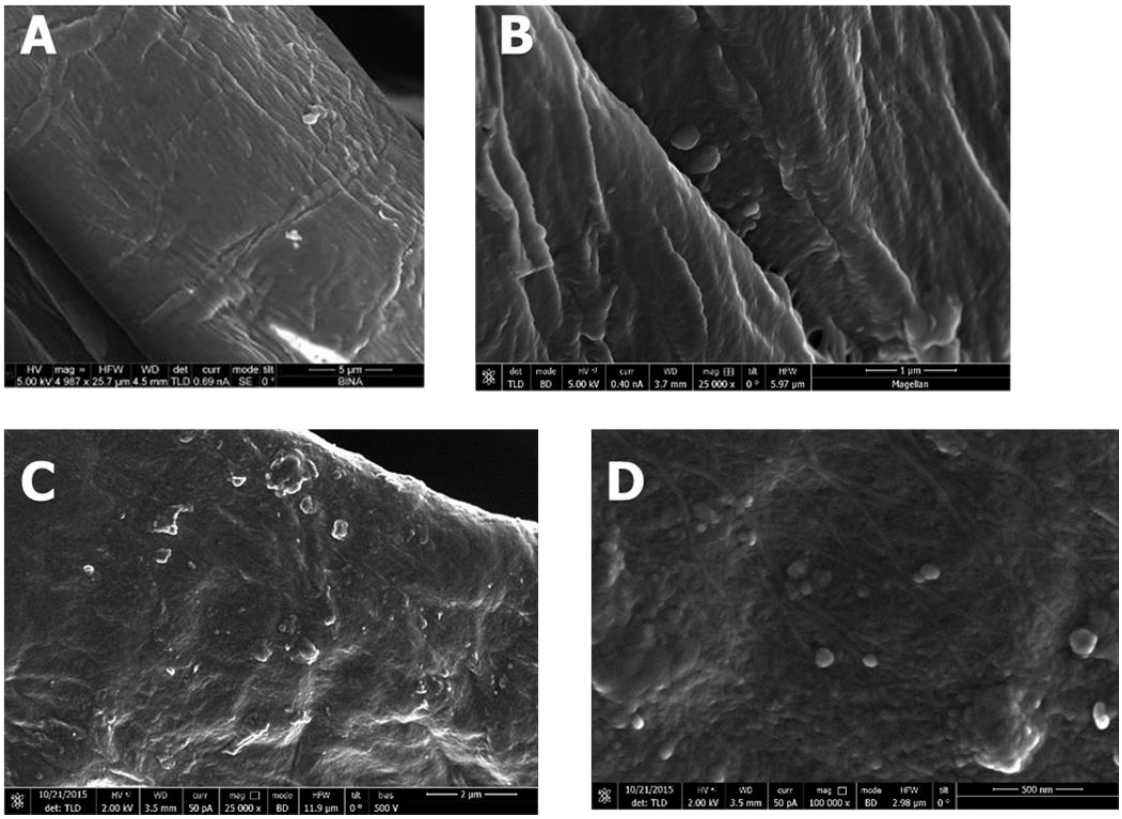


Figure III. S 1. E-SEM images of **(A)** non-treated pristine cotton fabric; and fabrics treated with ultrasonic waves to incorporate elastase substrate **(B)** Glp-PV-*p*NA, or **(C)** MeOSuc-AAPV-AFC peptides (MAG25K). **(D)** A higher magnification (MAGX100K) of C is shown in order to better analyse the morphology of the coated fabric.

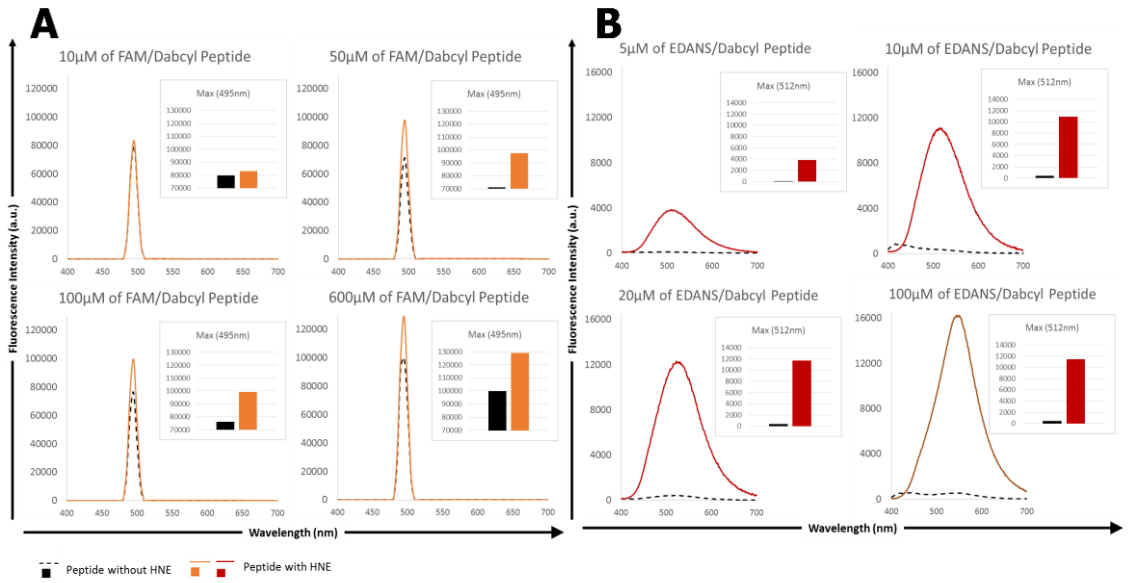


Figure III. S 2. Fluorescence spectrum of **(A)** FAM/Dabcyl-peptide and **(B)** EDANS/Dabcyl-peptide before (dashed line) and after a 10 minute-incubation at 37°C with 150mU of HNE (10-600 µM or 5-100 µM, respectively) (filled coloured line). λEm_{max} was chosen accordingly for each fluorophore donor and the emission spectra were measured. The legend shows the categorization of the fluorescence value in arbitrary units (a.u.).

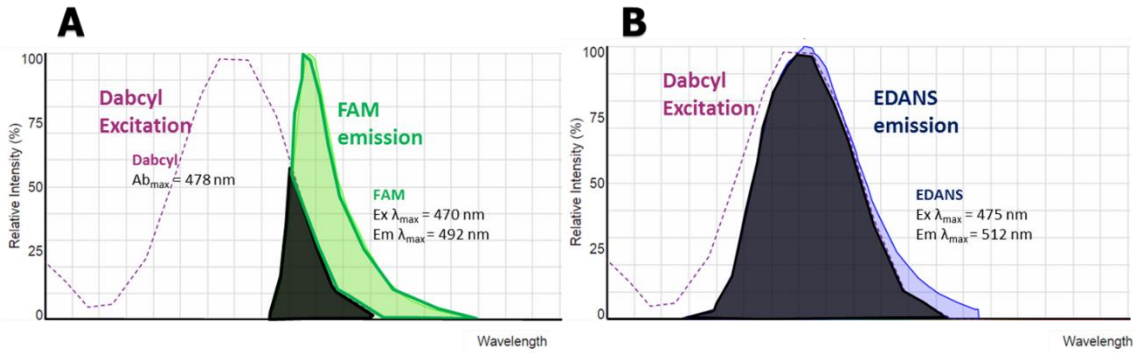


Figure III. S 3. Emission spectrum of donor (filled line) and excitation spectrum of the acceptor (dotted line) of **(A)** FAM/Dabcyl and **(B)** EDANS/Dabcyl FRET pairs, showing the spectral overlap between the two spectra (dark tinted area), adapted from the Thermo Fisher Scientific online tool of Fluorescence SpectraViewer.

CHAPTER IV.
Conclusions

IV. Conclusions

IV.1. Final Remarks

The work developed during this PhD thesis aimed to develop new strategies for monitoring HNE in chronic wounds (state of the art reviewed in chapter I). For that, specific cleavage sequences for HNE were associated to detection systems, either for chromogenic or fluorogenic approaches. We first defined the cleavage sequence with higher affinity for HNE – chapter II (a). Then, the HNE-specific sequence was associated to a colour generating system, using the recombinant GFP-like chromoprotein ultramarine – chapter II (a) and II (b). In a chromogenic sensor, a colour indication would appear in presence of high activity levels of elastase in the wound. Colour generating systems offer an outstanding perception for the user. Even though the sensor is to be placed over the dressing, in the top layer, and the wound fluids will be eluted from the wound surface until they reach the sensor, the colour selection has to consider the wound environment. We established that the signalling colour should be in the range of dark blue, dark green or deep purple – chapter II (a). Not only because these are colours that are easily perceived by the human eye but also because they would be easily discriminated against the colour of the wound environment.

In another approach, the same HNE-specific substrate was associated to a fluorogenic system, namely a FRET-peptide – chapter III. To predict the action of the developed sensors on monitoring wounds status, they were assessed *in vitro* using HNE enzymatic solutions. The most promising sensor, the FRET-peptide, was then incorporated into a commonly used dressing material, being then evaluated *in vitro* regarding its application as a dressing diagnostic tool – chapter III. The specific remarks for each chapter are described below:

Peptide design with specific HNE cleavage sequences

The use of molecular docking simulations allows a better cost and time efficiency in the prediction of the peptides' behaviour. These studies – chapter II (a) –provided the most suitable HNE cleavage sequence (Ala-Ala-Pro-Val; AAPV) and allowed a better understanding of the mechanisms underlying HNE's substrate recognition and cleavage. AAPV was used in the following studies after association to the chromogenic or fluorogenic systems.

Chromogenic sensor for HNE based on UM-split

We developed a split system as described for GFP by Callhan *et al.*, 2010 [1] – chapter II (a). It involved the production of two colourless proteins UM10 and E11, that when combined and in presence of elastase could generate ultramarine's dark blue colour. We were able to obtain an absorbance increase upon HNE addition, but this was a transient effect with limited visual perception. At this stage, we could not fully understood the mechanism of interaction within this split-UM system. We also engineered an *all-in-one* approach and produced the fused protein UM10E11.As with split-UM, this strategy also proved it to be extremely challenging, in particular with the efforts needed to obtain soluble protein. This thesis also provides a summary of the many strategies used to improve the solubility of recombinant proteins (chapter II (a) - supplementary information).

Chromogenic sensor for HNE based on UM-derived mutants

As an alternative to the split-UM approach, we designed 7 variants of ultramarine through site-directed mutagenesis – chapter II (b). With this strategy we explored the use of ultramarine as switch-on or switch-off sensor for HNE. The preparation of the rationale of the work also allowed us to better understand the chemistry involved in the regeneration of the chromophore environment of this protein in particular and of GFP-like proteins in general. *In vitro* studies assisted with molecular dynamic simulations, enabled us to explore the impact of the mutations in certain residues and their effect on the protein's colour. The production of colour requires a network of interactions within the residues from the chromophore triad and the known interacting residues. However, our studies showed that this network is even more complex than the literature describes.

We selected two variants for a deeper analysis, one aimed as a switch-off approach (mutant C) and another aiming a switch-on signal (mutant F). The switch-off variant proved to be more conceivable than the switch-on version. We successfully detected an absorbance decrease accompanied by a colour diming in the presence of elastase, as the enzyme freed the 11th βsheet at the specific cleavage site of the substrate.

The development of a switch-on chromogenic sensor using a non-fluorescent GFP-like protein is explored for the first time within this thesis, reinforcing the original and inventive aspects of this work. In addition, since the mechanisms underlying the properties of GFP-like proteins are not yet

fully understood, this task proves to be even more challenging and inevitable. In sum, the work here described serves as a starting point for other developments regarding the use of chromogenic GFP-like proteins.

Fluorogenic sensor for HNE

To increase the sensitivity of the already existing fluorophore-associated detection systems, we explored an approach based in the coupling of a quenching mechanism into the HNE peptide sequence – chapter III. The internally quenched HNE peptide was assessed for its application as an HNE-monitoring fluorogenic sensor for wounds. The designed FRET-peptide showed to be a more sensitive and effective strategy in comparison to a fluorophore-coupled peptide. Immobilization of these sensors provides advantages for its application associated with friendly handling and allowance of *in-situ* assessment when integrated in bandages or dressings, which makes them suitable for home-care. We successfully impregnated the fluorophore-coupled peptide in dressing material by sonochemistry. Since initial concerns were raised with using the same immobilization method with the FRET-peptide, we explored an alternative based on chemically immobilization. However, the immobilization onto a dressing greatly decreased the detection of HNE by the FRET-peptide. Optimization of the immobilization process will strong benefit the application of this sensor. Functionalized dressing integrating these sensors would allow an effective and specific monitoring of HNE in chronic wounds by simply using a portable UV light source.

IV.2. Future Perspectives

A better biochemical characterization of ultramarine and UM-mutants is needed in addition to a better understanding of the residues that are involved in the chromophore environment, critical for colour appearance. The yield of production of soluble proteins was lower than the desired, even after extensive optimization steps of the experimental set-up. Indeed, this was the major limiting factor along the course of this work. Optimization of the expression conditions is needed not only to allow us to have enough protein amount to experimentally answer the above concerns, but also taking in consideration the economical point of view regarding its final application as an integrative of a wearable sensor.

As previously discussed, the fluorogenic FRET-peptide requires further optimization of the process for its incorporation onto the dressing. Aside from a screening of dressing materials (which may include cellulosic and nanocellulosic matrices, silica gel, polyester or polyurethane), other immobilization processes should be investigated. For example, inkjet printing, sonochemical procedures and other strategies relying on chemical immobilization. It would also be necessary to study the feasibility of using the fluorogenic approach in chronic wounds regarding their efficacy using exudate and their viability for upscaling. At a larger scale, the cost of production might be a limiting factor. A possible solution could be the production of the HNE's substrate peptide coupled to recombinant proteins, followed by its linkage to fluorophores.

In INFACT project, the integration of the developed sensor in the course of the Project into the dressing was thought to be as an addition/attachment to a commercially available dressing. Namely through the immobilization of the sensor onto the top layer of the dressing, ideally with a defined "window" for colour/fluorescence visualization. Briefly, the exudate would be absorbed from the bottom layer contacting with the wound to the top layer in a single direction (and never a down the pathway to the wound), and always assuring safe accumulation and absorption of exudate.

An important factor to take into account for wearable sensors for wounds resides on leaching. Indeed, there is a small possibility for the sensor materials, when used in a wound, to leach into the bottom dressing layer, and possibly to come into direct contact with the wound. Even though, the design of the sensor sets out to avoid this, further testing monitoring the back-flow would be required.

Furthermore, the detection of wound infection using only one marker is valid. Still, a more reliable detection and better prediction of the wound status should comprise the simultaneous assessment of several biomarkers. The strategies explored in this work might be easily applied to other wound biomarkers, for example matrix metalloproteinases and other serine proteases like cathepsin G and proteinase 3.

REFERENCES

References

[1] F. Gottrup, J. Apelqvist, P. P, Outcomes in controlled and comparative studies on non-healing wounds: recommendations to improve the quality of evidence in wound management, J. Wound Care. 19 (2010) 237–268. doi:10.12968/jowc.2010.19.6.48471.

[2] C.K. Sen, G.M. Gordillo, S. Roy, R. Kirsner, L. Lambert, T.K. Hunt, et al., Human skin wounds: a major and snowballing threat to public health and the economy., Wound Repair Regen. 17 (2010) 763–71. doi:10.1111/j.1524-475X.2009.00543.x.

[3] T. Velnar, T. Bailey, V. Smrkolj, The Wound Healing Process: An Overview of the Cellular and Molecular Mechanisms, J. Int. Med. Res. 37 (2009) 1528–1542. doi:10.1177/147323000903700531.

[4] M. Todd, An overview of wound care in the care home population, Nurs. Resid. Care. 19 (2017) 316–320. doi:10.12968/nrec.2017.19.6.316.

[5] K. Järbrink, G. Ni, H. Sönnergren, A. Schmidtchen, C. Pang, R. Bajpai, et al., The humanistic and economic burden of chronic wounds: A protocol for a systematic review, Syst. Rev. 6 (2017) 1–7. doi:10.1186/s13643-016-0400-8.

[6] D. Broszczak, D. Stupar, A. Compay, M. Sharma, T. PArker, G. Shooter, et al., Biochemical profiling of proteins and metabolites in wound exudate from chronic wound environments, Wound Pract. Res. 20 (2012) 62–72.

[7] C. Shi, J.C. Dumville, N. Cullum, Support surfaces for pressure ulcer prevention: A network meta-analysis, PLoS One. 13 (2018) e0192707. doi:10.1371/journal.pone.0192707.

[8] V.N. Obolenskiy, A.A. Ermolov, G. V. Rodoman, Negative pressure wound therapy in the treatment of acute pyo-inflammatory diseases of soft tissues, EWMA J. 16 (2016) 15–21.

[9] J.C. Dumville, B.A. Lipsky, C. Hoey, M. Cruciani, M. Fiscon, J. Xia, Topical antimicrobial agents for treating foot ulcers in people with diabetes, Cochrane Database Syst. Rev. 2017 (2017). doi:10.1002/14651858.CD011038.pub2.

[10] C.M. Jones, A.T. Rothermel, D.R. Mackay, Evidence-Based Medicine, Plast. Reconstr. Surg. 140 (2017) 201e–216e. doi:10.1097/PRS.0000000000003486.

[11] J.S. Boateng, K.H. Matthews, H.N.E. Stevens, G.M. Eccleston, Wound Healing Dressings and Drug Delivery Systems: A Review, J. Pharm. Sci. 97 (2008) 2892–2923. doi:10.1002/jps.21210.

[12] J. Posnett, F. Gottrup, H. Lundgren, G. Saal, The resource impact of wounds on health-care providers in Europe, J. Wound Care. 18 (2009) 154–154. doi:10.12968/jowc.2009.18.4.41607.

[13] C. Dowsett, C. Dowsett, Breaking the cycle of hard-to-heal wounds: balancing cost and care, Wounds Int. 6 (2015) 17–21.

[14] S. Probst, S. Seppänen, V. Gerber, G. Gethin, A. Hopkins, R. Rimdeika, EWMA Document:

Home Care - Wound Care, J Wound Care. 23 (2014) S1–S44.

[15] G. Mosti, Compression therapy in the community, J. Community Nurs. 31 (2017) 36–42.

[16] C. Lindholm, R. Searle, Wound management for the 21st century: combining effectiveness and efficiency, Int. Wound J. 13 (2016) 5–15. doi:10.1111/iwj.12623.

[17] K. Harding, Innovation and Wound Healing, J. Wound Care. 24 (2015) 7–13. doi:10.12968/jowc.2015.24.Sup4b.7.

[18] J.M. Badia, A.L. Casey, N. Petrosillo, P.M. Hudson, S.A. Mitchell, C. Crosby, Impact of surgical site infection on healthcare costs and patient outcomes: a systematic review in six European countries, J. Hosp. Infect. 96 (2017) 1–15. doi:10.1016/j.jhin.2017.03.004.

[19] D.J. Leaper, H. van Goor, J. Reilly, N. Petrosillo, H.K. Geiss, A.J. Torres, et al., Surgical site infection - a European perspective of incidence and economic burden, Int. Wound J. 1 (2004) 247–273. doi:10.1111/j.1742-4801.2004.00067.x.

[20] B. Chan, S. Cadarette, W. Wodchis, J. Wong, N. Mittmann, M. Krahn, Cost-of-illness studies in chronic ulcers: a systematic review, J. Wound Care. 26 (2017) S4–S14. doi:10.12968/jowc.2017.26.Sup4.S4.

[21] R. Brambilla, J. Hurlow, S. Landis, R. Wolcott, Innovations in hard-to-heal wounds, Complex Wounds. (2016) 1–6.

[22] L. Prompers, M. Huijberts, N. Schaper, J. Apelqvist, K. Bakker, M. Edmonds, et al., Resource utilisation and costs associated with the treatment of diabetic foot ulcers. Prospective data from the Eurodiale Study, Diabetologia. 51 (2008) 1826–1834. doi:10.1007/s00125-008-1089-6.

[23] J. Apelqvis, S. Aron, M. Carter, H. Edwards, K. Harding (Chair), D. Margolis, et al., International consensus: Making the case for cost-effective wound management, Wounds Int. (2013) 1–24. doi:10.1007/s13398-014-0173-7.2.

[24] K.G. Harding, H.L. Morris, G.K. Patel, Clinical review Healing chronic wounds, 324 (2002). doi:10.1136/bmj.324.7330.160.

[25] J. Walburn, K. Vedhara, M. Hankins, L. Rixon, J. Weinman, Psychological stress and wound healing in humans: A systematic review and meta-analysis, J. Psychosom. Res. 67 (2009) 253–271. doi:10.1016/j.jpsychores.2009.04.002.

[26] S. Guo, L.A. DiPietro, Factors Affecting Wound Healing, J. Dent. Res. 89 (2010) 219–229. doi:10.1177/0022034509359125.

[27] E.A. Gantwerker, D.B. Hom, Skin: Histology and Physiology of Wound Healing, Clin. Plast. Surg. 39 (2012) 85–97. doi:10.1016/j.cps.2011.09.005.

[28] S.A. Eming, T. Krieg, J.M. Davidson, Inflammation in Wound Repair: Molecular and Cellular Mechanisms, J. Invest. Dermatol. 127 (2007) 514–525. doi:10.1038/sj.jid.5700701.

[29] W.K. Stadelmann, A.G. Digenis, G.R. Tobin, Physiology and healing dynamics of chronic cutaneous wounds., Am. J. Surg. 176 (1998) 26S–38S. http://www.ncbi.nlm.nih.gov/pubmed/9777970.

[30] K.J. Sonnemann, W.M. Bement, Wound Repair: Toward Understanding and Integration of Single-Cell and Multicellular Wound Responses, Annu. Rev. Cell Dev. Biol. 27 (2011) 237–263. doi:10.1146/annurev-cellbio-092910-154251.

[31] T.A. Mustoe, K. O??Shaughnessy, O. Kloeters, Chronic Wound Pathogenesis and Current Treatment Strategies: A Unifying Hypothesis, Plast. Reconstr. Surg. 117 (2006) 35S–41S. doi:10.1097/01.prs.0000225431.63010.1b.

[32] K. Moore, R. McCallion, R.J. Searle, M.C. Stacey, K.G. Harding, Prediction and monitoring the therapeutic response of chronic dermal wounds, Int. Wound J. 3 (2006) 89–98. doi:10.1111/j.1742-4801.2006.00212.x.

[33] R.G. Sibbald, H. Orsted, G.S. Schultz, P. Coutts, D. Keast, International Wound Bed Preparation Advisory Board, et al., Preparing the wound bed 2003: focus on infection and inflammation., Ostomy. Wound. Manage. 49 (2003) 24–51. http://cawc.net/images/uploads/resources/PWB.pdf%5Cnhttp://www.ncbi.nlm.nih.gov/pubmed/14652411.

[34] J. Byrnes, K. Carville, K. Coleman, A. Cowin, D. Findlay, K. May, et al., Wound Management for the Advanced Practitioner, Ip Communications, 2014.

[35] P.M.G. Filius, I.C. Gyssens, Impact of increasing antimicrobial resistance on wound management., Am. J. Clin. Dermatol. 3 (2002) 1–7. http://www.ncbi.nlm.nih.gov/pubmed/11817964.

[36] G. Sussman, Antimicrobial resistance relating to wound management and infection, Wound Pract. Res. J. Aust. Wound Manag. Assoc. 24 (2016) 224–227.

[37] G.S. Lazarus, D.M. Cooper, D.R. Knighton, D.J. Margolis, R.E. Pecoraro, G. Rodeheaver, et al., Definitions and guidelines for assessment of wounds and evaluation of healing., Arch. Dermatol. 130 (1994) 489–93. http://www.ncbi.nlm.nih.gov/pubmed/8166487.

[38] S. Enoch, D.J. Leaper, Basic science of wound healing, Surg. 26 (2008) 31–37. doi:10.1016/j.mpsur.2007.11.005.

[39] J.F. Guest, K. Vowden, P. Vowden, The health economic burden that acute and chronic wounds impose on an average clinical commissioning group/ health board in the UK, J. Wound Care. 26 (2017). doi:10.12968/jowc.2017.26.6.292.

[40] G.C. Gurtner, S. Werner, Y. Barrandon, M.T. Longaker, Wound repair and regeneration, Nature. 453 (2008) 314–321. doi:10.1038/nature07039.

[41] J.E. Janis, R.K. Kwon, D.H. Lalonde, A Practical Guide to Wound Healing, Plast. Reconstr. Surg. 125 (2010) 230e–244e. doi:10.1097/PRS.0b013e3181d9a0d1.

[42] G. Han, R. Ceilley, Chronic Wound Healing: A Review of Current Management and Treatments, Adv. Ther. 34 (2017) 599–610. doi:10.1007/s12325-017-0478-y.

[43] M. Häggström, Medical gallery of Mikael Häggström 2014, WikiJournal Med. 1 (2014). doi:10.15347/wjm/2014.008.

[44] S. Patel, A. Maheshwari, A. Chandra, Biomarkers for wound healing and their evaluation, J. Wound Care. 25 (2016) 46–55. doi:10.12968/jowc.2016.25.1.46.

[45] J.E. Janis, B. Harrison, Wound Healing: Part I. Basic Science, Plast. Reconstr. Surg. 133

(2014) 199e–207e. doi:10.1097/01.prs.0000437224.02985.f9.

[46] P. Martin, Wound Healing - Aiming for Perfect Skin Regeneration, Science (80-.). 276 (1997) 75–81. doi:10.1126/science.276.5309.75.

[47] A.J. Singer, R.A.F. Clark, Cutaneous Wound Healing, N. Engl. J. Med. 341 (1999) 738–746. doi:10.1056/NEJM199909023411006.

[48] T.A. Springer, Traffic signals for lymphocyte recirculation and leukocyte emigration: The multistep paradigm, Cell. 76 (1994) 301–314. doi:10.1016/0092-8674(94)90337-9.

[49] V. Witko-Sarsat, P. Rieu, B. Descamps-Latscha, P. Lesavre, L. Halbwachs-Mecarelli, Neutrophils: molecules, functions and pathophysiological aspects., Lab. Invest. 80 (2000) 617–53. http://www.ncbi.nlm.nih.gov/pubmed/10830774.

[50] F. Diegelmann, Robert, Wound healing: an overview of acute, fibrotic and delayed healing, Front. Biosci. 9 (2004) 283. doi:10.2741/1184.

[51] M.J. Westby, J.C. Dumville, N. Stubbs, G. Norman, J.K. Wong, N. Cullum, et al., Protease activity as a prognostic factor for wound healing in venous leg ulcers, Cochrane Database Syst. Rev. 2017 (2017). doi:10.1002/14651858.CD012841.

[52] N.J. Percival, Classification of Wounds and their Management, Surg. 20 (2002) 114–117. doi:10.1383/surg.20.5.114.14626.

[53] P. Vowden, K. Vowden, The economic impact of hard-to-heal wounds: promoting practice change to address passivity in wound management, Wounds Int. 7 (2016) 10–15.

[54] K. Rahim, S. Saleha, X. Zhu, L. Huo, A. Basit, O.L. Franco, Bacterial Contribution in Chronicity of Wounds, Microb. Ecol. 73 (2017) 710–721. doi:10.1007/s00248-016-0867-9.

[55] J. Apelqvist, C. Willy, A.-M. Fagerdahl, M. Fraccalvieri, M. Malmsjö, A. Piaggesi, et al., EWMA document: Negative pressure wound therapy: Overview, challenges and perspectives, J. Wound Care. 26 (2017) S1–S154. doi:10.12968/jowc.2017.26.Sup3.S1.

[56] P. Martin, S.J. Leibovich, Inflammatory cells during wound repair: the good, the bad and the ugly, Trends Cell Biol. 15 (2005) 599–607. doi:10.1016/j.tcb.2005.09.002.

[57] W. Paul, C.P. Sharma, Advances in Wound Healing Materials: Science and Skin Engineering, Smithers Rapra Technology, United Kingdom, 2015.

[58] S. Gupta, C. Andersen, J. Black, J. de Leon, C. Fife, J.C. Lantis Ii, et al., Management of Chronic Wounds: Diagnosis, Preparation, Treatment, and Follow-up., Wounds a Compend. Clin. Res. Pract. 29 (2017) S19–S36. doi:10.2310/7800.2190.

[59] American Blood Clot Association, Deep vein thrombosis, Blood Clots. (2018). https://www.bloodclot.org/dvt_pe.

[60] TheHolisticCare.com, Varicose veins, HolisticTreatment&Therapeutics. (2018). http://theholisticcare.com/treatment-therapeutics/446-varicose-veins.html.

[61] Drugs.com, Bedsores (Decubitus Ulcers), Harvard Heal. Publ. (2010). https://www.drugs.com/health-guide/bedsores-decubitus-ulcers.html.

[62] Angiologist.com, Peripheral arterial disease schematic, Vasc. Med. (2010). http://www.angiologist.com/arterial-disease/atherosclerosis/.

[63] ConejoFeet, Diabetic foot ulcer, Agoura-Los RoblesPodiatreyCenters. (2016). http://conejofeet.com/diabetic-wounds/.

[64] DiabetesTreatmentGuide.org, Effect of diabetes on feet, DiabetesTreatmentGuide. (2016). http://www.diabetestreatmentguide.org/complications-of-feet-due-to-diabetes/.

[65] I.H. Foundation, Peripherial Arterial Disease, ShermanHeart&VascularBlog. (2010). https://shermanheart.wordpress.com/2010/02/17/an-education-on-peripheral-arterial-disease-and-abi-testing/.

[66] N. Cullum, H. Buckley, J. Dumville, J. Hall, K. Lamb, M. Madden, et al., Wounds research for patient benefit: a 5-year programme of research, Program. Grants Appl. Res. 4 (2016) 1–304. doi:10.3310/pgfar04130.

[67] M.C. Ferreira, P. Tuma Júnior, V.F. Carvalho, F. Kamamoto, Complex wounds, Clinics. 61 (2006) 571–578. doi:10.1590/S1807-59322006000600014.

[68] M.J. Castillo, K. Nakajima, M. Zimmerman, J.C. Powers, Sensitive substrates for human leukocyte and porcine pancreatic elastase: A study of the merits of various chromophoric and fluorogenic leaving groups in assays for serine proteases, Anal. Biochem. 99 (1979) 53–64. doi:10.1016/0003-2697(79)90043-5.

[69] H. Brem, M. Tomic-Canic, Cellular and molecular basis of wound healing in diabetes, J. Clin. Invest. 117 (2007) 1219–1222. doi:10.1172/JCI32169.

[70] R.G. Frykberg, J. Banks, Challenges in the Treatment of Chronic Wounds, Adv. Wound Care. 4 (2015) 560–582. doi:10.1089/wound.2015.0635.

[71] J.E. Grey, K.G. Harding, S. Enoch, Venous and arterial leg ulcers, BMJ. 332 (2006) 347–350. doi:10.1136/bmj.332.7537.347.

[72] P. Astagneau, C. Rioux, F. Golliot, G. Brücker, Morbidity and mortality associated withsurgical site infections: results from the 1997–1999 INCISO surveillance, J. Hosp. Infect. 48 (2001) 267–274. doi:10.1053/jhin.2001.1003.

[73] J.S. Harrop, J.C. Styliaras, Y.C. Ooi, K.E. Radcliff, A.R. Vaccaro, C. Wu, Contributing Factors to Surgical Site Infections, J. Am. Acad. Orthop. Surg. 20 (2012) 94–101. doi:10.5435/JAAOS-20-02-094.

[74] R.J. Snyder, V. Driver, C.E. Fife, J. Lantis, B. Peirce, T. Serena, et al., Using a diagnostic tool to identify elevated protease activity levels in chronic and stalled wounds: a consensus panel discussion., Ostomy. Wound. Manage. 57 (2011) 36–46. http://europepmc.org/abstract/MED/22156177.

[75] K. Harding, D.G. Armstrong, S. Barrett, H. Kaufman, J.L. Lázaro-Martínez, D. Mayer, et al., International Consensus. The role of proteases in wound diagnostics. An expert working group review., London Wounds Int. (2011). http://www.woundsinternational.com/media/issues/419/files/content_9869.pdf.

[76] S.L. Percival, S. McCarty, J.A. Hunt, E.J. Woods, The effects of pH on wound healing, biofilms, and antimicrobial efficacy, Wound Repair Regen. 22 (2014) 174–186.

doi:10.1111/wrr.12125.

[77] J.M. Black, J.H. Hawks, Medical-surgical nursing: clinical management for positive outcomes, 8th Editio, Saunders, St. Louis, 2009.

[78] R. Salcid, Healing by Intention, Adv. Skin Wound Care. 30 (2017) 246–247. doi:10.1097/01.ASW.0000516787.46060.b2.

[79] S. Greatrex-White, H. Moxey, Wound assessment tools and nurses' needs: an evaluation study, Int. Wound J. 12 (2015) 293–301. doi:10.1111/iwj.12100.

[80] J. Fletcher, Wound bed preparation and the TIME principles, Nurs. Stand. 20 (2005) 57–65. doi:10.7748/ns2005.11.20.12.57.c4019.

[81] R.L. Harries, D.C. Bosanquet, K.G. Harding, Wound bed preparation: TIME for an update, Int. Wound J. 13 (2016) 8–14. doi:10.1111/iwj.12662.

[82] A. Halim, T. Khoo, A.. Mat Saad, Wound bed preparation from a clinical perspective, Indian J. Plast. Surg. 45 (2012) 193. doi:10.4103/0970-0358.101277.

[83] A.D. Widgerow, Deconstructing the stalled wound., Wounds a Compend. Clin. Res. Pract. 24 (2012) 58–66. http://www.ncbi.nlm.nih.gov/pubmed/25876241.

[84] J.E. Grey, S. Enoch, K.G. Harding, Wound assessment, BMJ. 332 (2006) 285–288. doi:10.1136/bmj.332.7536.285.

[85] N.X. Landén, D. Li, M. Ståhle, Transition from inflammation to proliferation: a critical step during wound healing, Cell. Mol. Life Sci. 73 (2016) 3861–3885. doi:10.1007/s00018-016-2268-0.

[86] S. Purohit, T. Li, W. Guan, X. Song, J. Song, Y. Tian, et al., Multiplex glycan bead array for high throughput and high content analyses of glycan binding proteins, Nat. Commun. 9 (2018) 258. doi:10.1038/s41467-017-02747-y.

[87] C. Caspell-Garcia, T. Simuni, D. Tosun-Turgut, I.-W. Wu, Y. Zhang, M. Nalls, et al., Multiple modality biomarker prediction of cognitive impairment in prospectively followed de novo Parkinson disease, PLoS One. 12 (2017) e0175674. doi:10.1371/journal.pone.0175674.

[88] E. Lawrence, C. Vegvari, A. Ower, C. Hadjichrysanthou, F. De Wolf, R.M. Anderson, A Systematic Review of Longitudinal Studies Which Measure Alzheimer's Disease Biomarkers, J. Alzheimer's Dis. 59 (2017) 1359–1379. doi:10.3233/JAD-170261.

[89] J. Wu, M. Dong, S. Santos, C. Rigatto, Y. Liu, F. Lin, Lab-on-a-Chip Platforms for Detection of Cardiovascular Disease and Cancer Biomarkers, Sensors. 17 (2017) 2934. doi:10.3390/s17122934.

[90] C.A. Ross, J. Bang, Potential biomarker breakthrough for Huntington's disease, Lancet Neurol. 16 (2017) 573–574. doi:10.1016/S1474-4422(17)30195-3.

[91] F. Werdin, M. Tennenhaus, H.-E. Schaller, H.-O. Rennekampff, Evidence-based Management Strategies for Treatment of Chronic Wounds, Eplasty. 9 (2009) 169–179.

[92] Z.N. Maan, M. Januszyk, R.C. Rennert, D. Duscher, M. Rodrigues, T. Fujiwara, et al., Noncontact, Low-Frequency Ultrasound Therapy Enhances Neovascularization and Wound

Healing in Diabetic Mice, Plast. Reconstr. Surg. 134 (2014) 402e–411e. doi:10.1097/PRS.0000000000000467.

[93] D.A. Jankowska, M.B. Bannwarth, C. Schulenburg, G. Faccio, K. Maniura-Weber, R.M. Rossi, et al., Simultaneous detection of pH value and glucose concentrations for wound monitoring applications, Biosens. Bioelectron. 87 (2017) 312–319. doi:10.1016/j.bios.2016.08.072.

[94] J. Janis, B. Harrison, Wound Healing: Part II. Clinical Applications, Plast. Reconstr. Surg. 133 (2014) 383e–392e. doi:10.1097/PRS.0000000000000077.

[95] G. Han, R. Ceilley, Chronic Wound Healing: A Review of Current Management and Treatments, Adv. Ther. 34 (2017) 599–610. doi:10.1007/s12325-017-0478-y.

[96] V. Dini, P. Salvo, A. Janowska, F. Di Francesco, A. Barbini, M. Romanelli, Correlation Between Wound Temperature Obtained With an Infrared Camera and Clinical Wound Bed Score in Venous Leg Ulcers., Wounds a Compend. Clin. Res. Pract. 27 (2015) 274–8. http://www.scopus.com/inward/record.url?eid=2-s2.0-84945137440&partnerID=tZOtx3y1.

[97] G. Power, Z. Moore, T. O'Connor, Measurement of pH, exudate composition and temperature in wound healing: a systematic review, J. Wound Care. 26 (2017) 381–397. doi:10.12968/jowc.2017.26.7.381.

[98] M. Romanelli, K. Vowden, D. Weir, Exudate management Made Easy, Wounds Int. 1 (2010) 1–6.

[99] K.F. Cutting, R.J. White, Maceration of the skin and wound bed 1: its nature and causes, J. Wound Care. 11 (2002) 275–278. doi:10.12968/jowc.2002.11.7.26414.

[100] N.J. Trengove, M.C. Stacey, S. Macauley, N. Bennett, J. Gibson, F. Burslem, et al., Analysis of the acute and chronic wound environments: the role of proteases and their inhibitors, Wound Repair Regen. 7 (1999) 442–452. doi:10.1046/j.1524-475X.1999.00442.x.

[101] D. Gibson, B. Cullen, R. Legerstee, K. Harding, G. Schultz, MMPs made easy, Wounds Int. 1 (2009) 1–6.

[102] M.E. Davey, George A. O'toole, Microbial Biofilms: from Ecology to Molecular Genetics, Microbiol Mol Biol Rev. 64 (2000) 847–867.

[103] A. Akhmetova, T. Saliev, I.U. Allan, M.J. Illsley, T. Nurgozhin, S. Mikhalovsky, A Comprehensive Review of Topical Odor-Controlling Treatment Options for Chronic Wounds, J. Wound, Ostomy Cont. Nurs. 43 (2016) 598–609. doi:10.1097/WON.0000000000000273.

[104] R.F. Diegelmann, Excessive neutrophils characterize chronic pressure ulcers, Wound Repair Regen. 11 (2003) 490–495. doi:10.1046/j.1524-475X.2003.11617.x.

[105] B. Korkmaz, S. Attucci, M.A. Juliano, T. Kalupov, M.-L. Jourdan, L. Juliano, et al., Measuring elastase, proteinase 3 and cathepsin G activities at the surface of human neutrophils with fluorescence resonance energy transfer substrates, Nat. Protoc. 3 (2008) 991–1000. doi:10.1038/nprot.2008.63.

[106] J.B. Cowland, N. Borregaard, Granulopoiesis and granules of human neutrophils, Immunol. Rev. 273 (2016) 11–28. doi:10.1111/imr.12440.

[107] E. Kolaczkowska, P. Kubes, Neutrophil recruitment and function in health and inflammation, Nat. Rev. Immunol. 13 (2013) 159–175. doi:10.1038/nri3399.

[108] C.A. Owen, E.J. Campbell, The cell biology of leukocyte-mediated proteolysis., J. Leukoc. Biol. 65 (1999) 137–50. http://www.jleukbio.org/content/65/2/137.full.pdf.

[109] S.J. Weiss, J.T. Curnutte, S. Regiani, Neutrophil-mediated solubilization of the subendothelial matrix: oxidative and nonoxidative mechanisms of proteolysis used by normal and chronic granulomatous disease phagocytes., J. Immunol. 136 (1986) 636–41. http://www.ncbi.nlm.nih.gov/pubmed/3484496.

[110] T.N. Mayadas, X. Cullere, C.A. Lowell, The Multifaceted Functions of Neutrophils, Annu. Rev. Pathol. Mech. Dis. 9 (2014) 181–218. doi:10.1146/annurev-pathol-020712-164023.

[111] U. Thormann, Neutrophil granulocytosis, WikiJournal Med. 1 (2005). http://de.wikipedia.org/wiki/Bild:NeutrophilerAktion.png.

[112] Blausen.com staff, Medical gallery of Blausen Medical 2014, WikiJournal Med. 1 (2014). doi:10.15347/wjm/2014.010.

[113] J.G. Wagner, R. a Roth, Neutrophil migration during endotoxemia., J. Leukoc. Biol. 66 (1999) 10–24. http://www.ncbi.nlm.nih.gov/pubmed/10410985.

[114] Y.-F. Tsai, T.-L. Hwang, Neutrophil elastase inhibitors: a patent review and potential applications for inflammatory lung diseases (2010 – 2014), Expert Opin. Ther. Pat. 25 (2015) 1145–1158. doi:10.1517/13543776.2015.1061998.

[115] A.J. O'Donoghue, Y. Jin, G.M. Knudsen, N.C. Perera, D.E. Jenne, J.E. Murphy, et al., Global Substrate Profiling of Proteases in Human Neutrophil Extracellular Traps Reveals Consensus Motif Predominantly Contributed by Elastase, PLoS One. 8 (2013) 1–12. doi:10.1371/journal.pone.0075141.

[116] M. Li, J.A. Norton, A.E. Chang, H.P. Lorenz, M.T. Longaker, Wounds : Biology , Pathology , and Management, (2003) 191–208. doi:10.1007/0-387-22744-X.

[117] P. Mak, J. Pohl, A. Dubin, M.S. Reed, S.E. Bowers, M.T. Fallon, et al., The increased bactericidal activity of a fatty acid-modified synthetic antimicrobial peptide of human cathepsin G correlates with its enhanced capacity to interact with model membranes, Int. J. Antimicrob. Agents. 21 (2003) 13–19. doi:10.1016/S0924-8579(02)00245-5.

[118] K. Le-Barillec, D. Pidard, V. Balloy, M. Chignard, Human neutrophil cathepsin G down-regulates LPS-mediated monocyte activation through CD14 proteolysis., J. Leukoc. Biol. 68 (2000) 209–15. http://www.ncbi.nlm.nih.gov/pubmed/10947065.

[119] N. Beaufort, D. Leduc, J.-C. Rousselle, V. Magdolen, T. Luther, A. Namane, et al., Proteolytic Regulation of the Urokinase Receptor/CD87 on Monocytic Cells by Neutrophil Elastase and Cathepsin G, J. Immunol. 172 (2004) 540–549. doi:10.4049/jimmunol.172.1.540.

[120] M. Baggiolini, U. Bretz, B. Dewald, M.E. Feigenson, The polymorphonuclear leukocyte,

Agents Actions. 8 (1978) 3–10. doi:10.1007/BF01972395.

[121] A. Belaaouaj, Neutrophil elastase-mediated killing of bacteria: lessons from targeted mutagenesis, Microbes Infect. 4 (2002) 1259–1264. doi:10.1016/S1286-4579(02)01654-4.

[122] T. Anderssen, H. Halvorsen, S.P. Bajaj, B. Osterud, Human leukocyte elastase and cathepsin G inactivate factor VII by limited proteolysis., Thromb. Haemost. 70 (1993) 414–7. http://www.ncbi.nlm.nih.gov/pubmed/8259540.

[123] U. Bank, S. Ansorge, More than destructive: neutrophil-derived serine proteases in cytokine bioactivity control., J. Leukoc. Biol. 69 (2001) 197–206. http://www.ncbi.nlm.nih.gov/pubmed/11272269.

[124] B. Korkmaz, T. Moreau, F. Gauthier, Neutrophil elastase, proteinase 3 and cathepsin G: Physicochemical properties, activity and physiopathological functions, Biochimie. 90 (2008) 227–242. doi:10.1016/j.biochi.2007.10.009.

[125] E. Hajjar, T. Broemstrup, C. Kantari, V. Witko-Sarsat, N. Reuter, Structures of human proteinase 3 and neutrophil elastase - so similar yet so different, FEBS J. 277 (2010) 2238–2254. doi:10.1111/j.1742-4658.2010.07659.x.

[126] T. Moreau, K. Baranger, S. Dadé, S. Dallet-Choisy, N. Guyot, M.-L. Zani, Multifaceted roles of human elafin and secretory leukocyte proteinase inhibitor (SLPI), two serine protease inhibitors of the chelonianin family, Biochimie. 90 (2008) 284–295. doi:10.1016/j.biochi.2007.09.007.

[127] C.T.N. Pham, Neutrophil serine proteases: Specific regulators of inflammation, Nat. Rev. Immunol. 6 (2006) 541–550. doi:10.1038/nri1841.

[128] J.E. Swedberg, C.Y. Li, S.J. de Veer, C.K. Wang, D.J. Craik, Design of Potent and Selective Cathepsin G Inhibitors Based on the Sunflower Trypsin Inhibitor-1 Scaffold, J. Med. Chem. 60 (2017) 658–667. doi:10.1021/acs.jmedchem.6b01509.

[129] J.C. Taylor, I.P. Crawford, T.E. Hugli, Limited degradation of the third component (C3) of human complement by human leukocyte elastase (HLE): partial characterization of C3 fragments, Biochemistry. 16 (1977) 3390–3396. doi:10.1021/bi00634a016.

[130] M. Bédard, C.D. McClure, N.L. Schiller, C. Francoeur, A. Cantin, M. Denis, Release of Interleukin-8, Interleukin-6, and Colony-stimulating Factors by Upper Airway Epithelial Cells: Implications for Cystic Fibrosis, Am. J. Respir. Cell Mol. Biol. 9 (1993) 455–462. doi:10.1165/ajrcmb/9.4.455.

[131] D.H. Allen, P.B. Tracy, Human Coagulation Factor V Is Activated to the Functional Cofactor by Elastase and Cathepsin G Expressed at the Monocyte Surface, J. Biol. Chem. 270 (1995) 1408–1415. doi:10.1074/jbc.270.3.1408.

[132] M.J. Janusz, N.S. Doherty, Degradation of cartilage matrix proteoglycan by human neutrophils involves both elastase and cathepsin G., J. Immunol. 146 (1991) 3922–8. http://www.ncbi.nlm.nih.gov/pubmed/8324217.

[133] K. Wu, T. Urano, H. Ihara, Y. Takada, M. Fujie, M. Shikimori, et al., The cleavage and inactivation of plasminogen activator inhibitor type 1 by neutrophil elastase: the evaluation of its physiologic relevance in fibrinolysis., Blood. 86 (1995) 1056–61.

http://www.ncbi.nlm.nih.gov/pubmed/7620159.

[134] D.J. Pipoly, E.C. Crouch, Degradation of native type IV procollagen by human neutrophil elastase. Implications for leukocyte-mediated degradation of basement membranes, Biochemistry. 26 (1987) 5748–5754. doi:10.1021/bi00392a025.

[135] R.E. Jordan, R.M. Nelson, J. Kilpatrick, J.O. Newgren, P.C. Esmon, M.A. Fournel, Inactivation of human antithrombin by neutrophil elastase. Kinetics of the heparin-dependent reaction., J. Biol. Chem. 264 (1989) 10493–500. http://www.ncbi.nlm.nih.gov/pubmed/2732232.

[136] R. Kittelberger, T.J. Neale, K.T. Francky, N.S. Greenhill, G.J. Gibson, Cleavage of type VIII collagen by human neutrophil elastase, Biochim. Biophys. Acta - Mol. Basis Dis. 1139 (1992) 295–299. doi:10.1016/0925-4439(92)90103-T.

[137] H. Tschesche, V. Knäuper, S. Krämer, J. Michaelis, R. Oberhoff, H. Reinke, Latent collagenase and gelatinase from human neutrophils and their activation., Matrix Suppl. 1 (1992) 245–55. http://www.ncbi.nlm.nih.gov/pubmed/1480034.

[138] A. Rice, M.J. Banda, Neutrophil Elastase Processing of Gelatinase A Is Mediated by Extracellular Matrix, Biochemistry. 34 (1995) 9249–9256. doi:10.1021/bi00028a038.

[139] C. Rogalski, U. Meyer-Hoffert, E. Proksch, O. Wiedow, Human Leukocyte Elastase Induces Keratinocyte Proliferation *In vitro* and *In vivo*, J. Invest. Dermatol. 118 (2002) 49–54. doi:10.1046/j.0022-202x.2001.01650.x.

[140] P. Renesto, M. Chignard, Enhancement of cathepsin G-induced platelet activation by leukocyte elastase: consequence for the neutrophil-mediated platelet activation., Blood. 82 (1993) 139–44. http://www.ncbi.nlm.nih.gov/pubmed/8324217.

[141] J.V. Edwards, P.S. Howley, Human neutrophil elastase and collagenase sequestration with phosphorylated cotton wound dressings, J. Biomed. Mater. Res. Part A. 83A (2007) 446–454. doi:10.1002/jbm.a.31171.

[142] A. Wohlkönig, J. Huet, Y. Looze, R. Wintjens, Structural Relationships in the Lysozyme Superfamily: Significant Evidence for Glycoside Hydrolase Signature Motifs, PLoS One. 5 (2010) e15388. doi:10.1371/journal.pone.0015388.

[143] G.S. Bixler, M.Z. Atassi, T-cell recognition and antigen presentation of lysozyme., Adv. Exp. Med. Biol. 225 (1987) 89–101. http://www.ncbi.nlm.nih.gov/pubmed/3502593.

[144] C.A. Clarke, E.M. Scheurwater, A.J. Clarke, The Vertebrate Lysozyme Inhibitor Ivy Functions to Inhibit the Activity of Lytic Transglycosylase, J. Biol. Chem. 285 (2010) 14843–14847. doi:10.1074/jbc.C110.120931.

[145] S.A. Ragland, A.K. Criss, From bacterial killing to immune modulation: Recent insights into the functions of lysozyme, PLOS Pathog. 13 (2017) e1006512. doi:10.1371/journal.ppat.1006512.

[146] G.S. Bixler, T. Yoshida, M.Z. Atassi, Antigen presentation of lysozyme: T-cell recognition of peptide and intact protein after priming with synthetic overlapping peptides comprising the entire protein chain., Immunology. 56 (1985) 103–112.

[147] S. Starling, Innate immunity: A new way out for lysozyme, Nat. Rev. Immunol. 17 (2017)

532–532. doi:10.1038/nri.2017.98.

[148] S. Bel, M. Pendse, Y. Wang, Y. Li, K.A. Ruhn, B. Hassell, et al., Paneth cells secrete lysozyme via secretory autophagy during bacterial infection of the intestine, Science (80-.). 357 (2017) 1047–1052. doi:10.1126/science.aal4677.

[149] H. Nagase, R. Visse, G. Murphy, Structure and function of matrix metalloproteinases and TIMPs, Cardiovasc. Res. 69 (2006) 562–573. doi:10.1016/j.cardiores.2005.12.002.

[150] M.D. Sternlicht, Z. Werb, How Matrix Metalloproteinases Regulate Cell Behavior, Annu. Rev. Cell Dev. Biol. 17 (2001) 463–516. doi:10.1146/annurev.cellbio.17.1.463.

[151] A. Page-McCaw, A.J. Ewald, Z. Werb, Matrix metalloproteinases and the regulation of tissue remodelling, Nat. Rev. Mol. Cell Biol. 8 (2007) 221–233. doi:10.1038/nrm2125.

[152] M. Giannandrea, W.C. Parks, Diverse functions of matrix metalloproteinases during fibrosis, Dis. Model. Mech. 7 (2014) 193–203. doi:10.1242/dmm.012062.

[153] S. Swarnakar, S. Paul, L.P. Singh, R.J. Reiter, Matrix metalloproteinases in health and disease: regulation by melatonin, J. Pineal Res. 50 (2011) 8–20. doi:10.1111/j.1600-079X.2010.00812.x.

[154] R. Visse, Matrix Metalloproteinases and Tissue Inhibitors of Metalloproteinases: Structure, Function, and Biochemistry, Circ. Res. 92 (2003) 827–839. doi:10.1161/01.RES.0000070112.80711.3D.

[155] S. Loffek, O. Schilling, C.-W. Franzke, Biological role of matrix metalloproteinases: a critical balance, Eur. Respir. J. 38 (2011) 191–208. doi:10.1183/09031936.00146510.

[156] M.M. Handsley, D.R. Edwards, Metalloproteinases and their inhibitors in tumor angiogenesis, Int. J. Cancer. 115 (2005) 849–860. doi:10.1002/ijc.20945.

[157] D. Rodríguez, C.J. Morrison, C.M. Overall, Matrix metalloproteinases: What do they not do? New substrates and biological roles identified by murine models and proteomics, Biochim. Biophys. Acta - Mol. Cell Res. 1803 (2010) 39–54. doi:10.1016/j.bbamcr.2009.09.015.

[158] T.-H. Chun, F. Sabeh, I. Ota, H. Murphy, K.T. McDonagh, K. Holmbeck, et al., MT1-MMP–dependent neovessel formation within the confines of the three-dimensional extracellular matrix, J. Cell Biol. 167 (2004) 757–767. doi:10.1083/jcb.200405001.

[159] N. Hiraoka, E. Allen, I.J. Apel, M.R. Gyetko, S.J. Weiss, Matrix Metalloproteinases Regulate Neovascularization by Acting as Pericellular Fibrinolysins, Cell. 95 (1998) 365–377. doi:10.1016/S0092-8674(00)81768-7.

[160] T.B. Rajavashisth, X.-P. Xu, S. Jovinge, S. Meisel, X.-O. Xu, N.-N. Chai, et al., Membrane Type 1 Matrix Metalloproteinase Expression in Human Atherosclerotic Plaques : Evidence for Activation by Proinflammatory Mediators, Circulation. 99 (1999) 3103–3109. doi:10.1161/01.CIR.99.24.3103.

[161] Y. Itoh, Membrane-type matrix metalloproteinases: Their functions and regulations, Matrix Biol. 44–46 (2015) 207–223. doi:10.1016/j.matbio.2015.03.004.

[162] O. Hiller, A. Lichte, A. Oberpichler, A. Kocourek, H. Tschesche, Matrix Metalloproteinases Collagenase-2, Macrophage Elastase, Collagenase-3, and Membrane Type 1-Matrix

Metalloproteinase Impair Clotting by Degradation of Fibrinogen and Factor XII, J. Biol. Chem. 275 (2000) 33008–33013. doi:10.1074/jbc.M001836200.

[163] S. Sugiyama, Hypochlorous Acid, a Macrophage Product, Induces Endothelial Apoptosis and Tissue Factor Expression: Involvement of Myeloperoxidase-Mediated Oxidant in Plaque Erosion and Thrombogenesis, Arterioscler. Thromb. Vasc. Biol. 24 (2004) 1309–1314. doi:10.1161/01.ATV.0000131784.50633.4f.

[164] R.M. Roman, A.E. Wendland, C.A. Polanczyk, Mieloperoxidase e doença arterial coronariana: da pesquisa à prática clínica, Arq. Bras. Cardiol. 91 (2008) e12–e19. doi:10.1590/S0066-782X2008001300015.

[165] W.M. Nauseef, Myeloperoxidase in human neutrophil host defence, Cell. Microbiol. 16 (2014) 1146–1155. doi:10.1111/cmi.12312.

[166] S.J. Klebanoff, A.J. Kettle, H. Rosen, C.C. Winterbourn, W.M. Nauseef, Myeloperoxidase: a front-line defender against phagocytosed microorganisms, J. Leukoc. Biol. 93 (2013) 185–198. doi:10.1189/jlb.0712349.

[167] M.J. Davies, Myeloperoxidase-derived oxidation: mechanisms of biological damage and its prevention, J. Clin. Biochem. Nutr. 48 (2010) 8–19. doi:10.3164/jcbn.11-006FR.

[168] R. Zhang, M.-L. Brennan, Z. Shen, J.C. MacPherson, D. Schmitt, C.E. Molenda, et al., Myeloperoxidase Functions as a Major Enzymatic Catalyst for Initiation of Lipid Peroxidation at Sites of Inflammation, J. Biol. Chem. 277 (2002) 46116–46122. doi:10.1074/jbc.M209124200.

[169] A. Uehara, S. Sugawara, K. Muramoto, H. Takada, Activation of Human Oral Epithelial Cells by Neutrophil Proteinase 3 Through Protease-Activated Receptor-2, J. Immunol. 169 (2002) 4594–4603. doi:10.4049/jimmunol.169.8.4594.

[170] S. Robache-Gallea, V. Morand, J.M. Bruneau, B. Schoot, E. Tagat, E. Réalo, et al., *In vitro* Processing of Human Tumor Necrosis Factor-α, J. Biol. Chem. 270 (1995) 23688–23692. doi:10.1074/jbc.270.40.23688.

[171] J.E. Gabay, R.W. Scott, D. Campanelli, J. Griffith, C. Wilde, M.N. Marra, et al., Antibiotic proteins of human polymorphonuclear leukocytes., Proc. Natl. Acad. Sci. 86 (1989) 5610–5614. doi:10.1073/pnas.86.14.5610.

[172] P. Renesto, L. Halbwachs-Mecarelli, P. Nusbaum, P. Lesavre, M. Chignard, Proteinase 3. A neutrophil proteinase with activity on platelets., J. Immunol. 152 (1994) 4612–7. http://www.ncbi.nlm.nih.gov/pubmed/8157974.

[173] J.J. Yang, G.A. Preston, W.F. Pendergraft, M. Segelmark, P. Heeringa, S.L. Hogan, et al., Internalization of Proteinase 3 Is Concomitant with Endothelial Cell Apoptosis and Internalization of Myeloperoxidase with Generation of Intracellular Oxidants, Am. J. Pathol. 158 (2001) 581–592. doi:10.1016/S0002-9440(10)64000-X.

[174] N. V Rao, N.G. Wehner, B.C. Marshall, W.R. Gray, B.H. Gray, J.R. Hoidal, Characterization of proteinase-3 (PR-3), a neutrophil serine proteinase. Structural and functional properties., J. Biol. Chem. 266 (1991) 9540–8. http://www.ncbi.nlm.nih.gov/pubmed/2033050.

[175] A. Heinz, M.C. Jung, G. Jahreis, A. Rusciani, L. Duca, L. Debelle, et al., The action of

neutrophil serine proteases on elastin and its precursor, Biochimie. 94 (2012) 192–202. doi:10.1016/j.biochi.2011.10.006.

[176] A. McLister, A. Mathur, J. Davis, Wound diagnostics: Deploying electroanalytical strategies for point of care sensors and smart dressings, Curr. Opin. Electrochem. 3 (2017) 40–45. doi:10.1016/j.coelec.2017.05.002.

[177] J. Skokowa, D.C. Dale, I.P. Touw, C. Zeidler, K. Welte, Severe congenital neutropenias, Nat. Rev. Dis. Prim. 3 (2017) 17032. doi:10.1038/nrdp.2017.32.

[178] D.S. Grenda, M. Murakami, J. Ghatak, J. Xia, L.A. Boxer, D. Dale, et al., Mutations of the ELA2 gene found in patients with severe congenital neutropenia induce the unfolded protein response and cellular apoptosis, Blood. 110 (2007) 4179–4187. doi:10.1182/blood-2006-11-057299.

[179] G. Hansen, H. Gielen-Haertwig, P. Reinemer, D. Schomburg, A. Harrenga, K. Niefind, Unexpected Active-Site Flexibility in the Structure of Human Neutrophil Elastase in Complex with a New Dihydropyrimidone Inhibitor, J. Mol. Biol. 409 (2011) 681–691. doi:10.1016/j.jmb.2011.04.047.

[180] L. Hedstrom, Serine protease mechanism and specificity, Chem. Rev. 102 (2002) 4501–4523. doi:10.1021/cr000033x.

[181] L. Feng, X. Liu, W. Zhu, F. Guo, Y. Wu, R. Wang, et al., Inhibition of human neutrophil elastase by pentacyclic triterpenes, PLoS One. 8 (2013) 1–11. doi:10.1371/journal.pone.0082794.

[182] A. V. Nemukhin, I.A. Topol, S.K. Burt, Energy profiles for the rate-limiting stage of the serine protease prototype reaction, Int. J. Quantum Chem. 88 (2002) 34–40. doi:10.1002/qua.10076.

[183] J.I. Weitz, S.L. Landman, K.A. Crowley, S. Birken, F.J. Morgan, Development of an assay for *in vivo* human neutrophil elastase activity. Increased elastase activity in patients with alpha 1-proteinase inhibitor deficiency., J. Clin. Invest. 78 (1986) 155–162. doi:10.1172/JCI112545.

[184] K. Sugino, Y. Nakamura, Y. Muramatsu, Y. Hata, K. Shibuya, S. Homma, Analysis of blood neutrophil elastase, glutathione levels and pathological findings in postoperative acute exacerbation of idiopathic pulmonary fibrosis associated with lung cancer: Two case reports, Mol. Clin. Oncol. 5 (2016) 402–406. doi:10.3892/mco.2016.993.

[185] T. Sato, S. Takahashi, T. Mizumoto, M. Harao, M. Akizuki, M. Takasugi, et al., Neutrophil elastase and cancer, Surg. Oncol. 15 (2006) 217–222. doi:10.1016/j.suronc.2007.01.003.

[186] C. Carmona-Rivera, P.M. Carlucci, E. Moore, N. Lingampalli, H. Uchtenhagen, E. James, et al., Synovial fibroblast-neutrophil interactions promote pathogenic adaptive immunity in rheumatoid arthritis, Sci. Immunol. 2 (2017) eaag3358. doi:10.1126/sciimmunol.aag3358.

[187] K. Tanaka, K. Yamada, M. Matsushima, T. Izawa, S. Furukawa, Y. Kobayashi, et al., Prediction of spontaneous preterm delivery in asymptomatic twin pregnancies using cervical length and granulocyte elastase, Taiwan. J. Obstet. Gynecol. 56 (2017) 188–191.

doi:10.1016/j.tjog.2016.07.014.

[188] A. Reinhardt, G. Haidl, W.B. Schill, Granulocyte elastase indicates silent male genital tract inflammation and appropriate anti-inflammatory treatment, Andrologia. 29 (1997) 187–192. http://www.ncbi.nlm.nih.gov/entrez/query.fcgi?cmd=Retrieve&db=PubMed&dopt=Citation&list_uids=9263568.

[189] J. Davis, A. McLister, Chapter One - Introduction to Wound Management, Elsevier Inc., 2016. doi:http://dx.doi.org/10.1016/B978-0-12-803762-1.00001-1.

[190] T.R. Dargaville, B.L. Farrugia, J.A. Broadbent, S. Pace, Z. Upton, N.H. Voelcker, Sensors and imaging for wound healing: A review, Biosens. Bioelectron. 41 (2013) 30–42. doi:10.1016/j.bios.2012.09.029.

[191] J. McNeill, D. Sen, Y. Mendelson, M. Crivello, S. Mazumder, A. Agdeppa, et al., Wearable wireless sensor patch for continuous monitoring of skin temperature, pressure, and relative humidity, in: 2017 IEEE Int. Symp. Circuits Syst., IEEE, 2017: pp. 1–4. doi:10.1109/ISCAS.2017.8050898.

[192] Y. Yamamoto, D. Yamamoto, M. Takada, H. Naito, T. Arie, S. Akita, et al., Efficient Skin Temperature Sensor and Stable Gel-Less Sticky ECG Sensor for a Wearable Flexible Healthcare Patch, Adv. Healthc. Mater. 6 (2017) 1700495. doi:10.1002/adhm.201700495.

[193] S. Nakata, T. Arie, S. Akita, K. Takei, Wearable, Flexible, and Multifunctional Healthcare Device with an ISFET Chemical Sensor for Simultaneous Sweat pH and Skin Temperature Monitoring, ACS Sensors. 2 (2017) 443–448. doi:10.1021/acssensors.7b00047.

[194] T.Q. Trung, S. Ramasundaram, B.-U. Hwang, N.-E. Lee, An All-Elastomeric Transparent and Stretchable Temperature Sensor for Body-Attachable Wearable Electronics, Adv. Mater. 28 (2016) 502–509. doi:10.1002/adma.201504441.

[195] A. Giuliani, M. Placidi, F. Di Francesco, A. Pucci, A new polystyrene-based ionomer/MWCNT nanocomposite for wearable skin temperature sensors, React. Funct. Polym. 76 (2014) 57–62. doi:10.1016/j.reactfunctpolym.2014.01.008.

[196] N. Calisi, A. Giuliani, M. Alderighi, J.M. Schnorr, T.M. Swager, F. Di Francesco, et al., Factors affecting the dispersion of MWCNTs in electrically conducting SEBS nanocomposites, Eur. Polym. J. 49 (2013) 1471–1478. doi:10.1016/j.eurpolymj.2013.03.029.

[197] N. Calisi, P. Salvo, B. Melai, C. Paoletti, A. Pucci, F. Di Francesco, Effects of thermal annealing on SEBS/MWCNTs temperature-sensitive nanocomposites for the measurement of skin temperature, Mater. Chem. Phys. 186 (2017) 456–461. doi:10.1016/j.matchemphys.2016.11.018.

[198] P. Salvo, V. Dini, A. Kirchhain, A. Janowska, T. Oranges, A. Chiricozzi, et al., Sensors and Biosensors for C-Reactive Protein, Temperature and pH, and Their Applications for Monitoring Wound Healing: A Review, Sensors. 17 (2017) 2952. doi:10.3390/s17122952.

[199] P. Salvo, B. Melai, N. Calisi, C. Paoletti, F. Bellagambi, A. Kirchhain, et al., Graphene-

based devices for measuring pH, Sensors Actuators B Chem. 256 (2018) 976–991. doi:10.1016/j.snb.2017.10.037.

[200] P. Salvo, N. Calisi, B. Melai, V. Dini, C. Paoletti, T. Lomonaco, et al., Temperature- and pH-sensitive wearable materials for monitoring foot ulcers, Int. J. Nanomedicine. Volume 12 (2017) 949–954. doi:10.2147/IJN.S121726.

[201] P. Salvo, N. Calisi, B. Melai, B. Cortigiani, M. Mannini, A. Caneschi, et al., Temperature and pH sensors based on graphenic materials, Biosens. Bioelectron. 91 (2017) 870–877. doi:10.1016/j.bios.2017.01.062.

[202] J. Davis, A. McLister, Sensors for Detecting and Combating Wound Infection, in: Smart Bandage Technol., Elsevier, 2016: pp. 195–227. doi:10.1016/B978-0-12-803762-1.00006-0.

[203] D. Sharp, S. Forsythe, J. Davis, Carbon Fibre Composites: Integrated Electrochemical Sensors for Wound Management, J. Biochem. 144 (2008) 87–93. doi:10.1093/jb/mvn045.

[204] D. Sharp, P. Gladstone, R.B. Smith, S. Forsythe, J. Davis, Approaching intelligent infection diagnostics: Carbon fibre sensor for electrochemical pyocyanin detection, Bioelectrochemistry. 77 (2010) 114–119. doi:10.1016/j.bioelechem.2009.07.008.

[205] J. Zhou, A.L. Loftus, G. Mulley, A.T.A. Jenkins, A Thin Film Detection/Response System for Pathogenic Bacteria, J. Am. Chem. Soc. 132 (2010) 6566–6570. doi:10.1021/ja101554a.

[206] J. Zhou, T.N. Tun, S. Hong, J.D. Mercer-Chalmers, M. Laabei, A.E.R. Young, et al., Development of a prototype wound dressing technology which can detect and report colonization by pathogenic bacteria, Biosens. Bioelectron. 30 (2011) 67–72. doi:10.1016/j.bios.2011.08.028.

[207] D.R. Yager, B.C. Nwomeh, The proteolytic environment of chronic wounds, Wound Repair Regen. 7 (1999) 433–441. doi:10.1046/j.1524-475X.1999.00433.x.

[208] A. Hasmann, U. Gewessler, E. Hulla, K.P. Schneider, B. Binder, A. Francesko, et al., Sensor materials for the detection of human neutrophil elastase and cathepsin G activity in wound fluid, Exp. Dermatol. 20 (2011) 508–513. doi:10.1111/j.1600-0625.2011.01256.x.

[209] R. Hoffman, J. Noble, M. Eagle, The use of proteases as prognostic markers for the healing of venous leg ulcers, J. Wound Care. 8 (1999) 273–276. doi:10.12968/jowc.1999.8.6.25885.

[210] J.M. Herrmann, J.R. Gonzáles, R.H. Boedeker, J. Vonholdt, J. Meyle, Microassay for the detection of elastase activity in the gingival crevice., J. Clin. Periodontol. 28 (2001) 31–7. http://www.ncbi.nlm.nih.gov/pubmed/11142664.

[211] A.J. O'Donoghue, Y. Jin, G.M. Knudsen, N.C. Perera, D.E. Jenne, J.E. Murphy, et al., Global Substrate Profiling of Proteases in Human Neutrophil Extracellular Traps Reveals Consensus Motif Predominantly Contributed by Elastase, PLoS One. 8 (2013) e75141. doi:10.1371/journal.pone.0075141.

[212] L. Ottonello, N. Arduino, M. Bertolotto, P. Dapino, M. Mancini, F. Dallegri, *In vitro*

inhibition of human neutrophil histotoxicity by ambroxol: evidence for a multistep mechanism, Br. J. Pharmacol. 140 (2003) 736–742. doi:10.1038/sj.bjp.0705497.

[213] G. Zhang, Protease Assays, 2004. http://www.ncbi.nlm.nih.gov/pubmed/22553874.

[214] G. de la Rebière de Pouyade, T. Franck, A. Salciccia, G. Deby-Dupont, S. Grulke, L. Vander Heyden, et al., Development of an enzyme-linked immunosorbent assay for equine neutrophil elastase measurement in blood: Preliminary application to colic cases, Vet. Immunol. Immunopathol. 135 (2010) 282–288. doi:10.1016/j.vetimm.2009.10.023.

[215] T.L. Dunn, W.D. Blackburn, W.J. Koopman, L.W. Heck, Solid-phase radioimmunoassay for human neutrophil elastase: a sensitive method for determining secreted and cell-associated enzyme., Anal. Biochem. 150 (1985) 18–25. http://www.ncbi.nlm.nih.gov/pubmed/3853449.

[216] Y. Bai, H. Wang, Q. Zhao, Detection of human neutrophil elastase by aptamer affinity capillary electrophoresis coupled with laser-induced fluorescence using specified site fluorescently labeled aptamer, Anal. Bioanal. Chem. 409 (2017) 6843–6849. doi:10.1007/s00216-017-0645-7.

[217] V.E. J, Protease Biosensors Based on Peptide-Nanocellulose Conjugates: From Molecular Design to Dressing Interface, Int. J. Med. Nano Res. 3 (2016). doi:10.23937/2378-3664/1410018.

[218] M.R. Wardell, Methods for using Human Neutrophil Elastase as an indicator of active wound infection, WO2010022281, 2010.

[219] G.S. Schultz, D.J. Gibson, Rapid bed-side measurement of neutrophil elastase activity in biological fluids, WO2010151878A2, 2010.

[220] A. Schröter, A. Walther, K. Fritzsche, J. Kothe, A. Rösen-Wolff, G. Gerlach, Infection Monitoring in Wounds, Procedia Chem. 6 (2012) 175–183. doi:10.1016/j.proche.2012.10.144.

[221] S. Pasche, S. Angeloni, R. Ischer, M. Liley, J. Luprano, G. Voirin, Wearable Biosensors for Monitoring Wound Healing, Adv. Sci. Technol. 57 (2008) 80–87. doi:10.4028/www.scientific.net/AST.57.80.

[222] M. Ochoa, R. Rahimi, B. Ziaie, Flexible Sensors for Chronic Wound Management, IEEE Rev. Biomed. Eng. 7 (2014) 73–86. doi:10.1109/RBME.2013.2295817.

[223] J. Davis, A. McLister, Wound Diagnostics and Diagnostic Dressings, in: Smart Bandage Technol., Elsevier, 2016: pp. 145–193. doi:10.1016/B978-0-12-803762-1.00005-9.

[224] T.E. Serena, Development of a Novel Technique to Collect Proteases from Chronic Wounds, Adv. Wound Care. 3 (2014) 729–732. doi:10.1089/wound.2013.0463.

[225] T.E. Serena, B.M. Cullen, S.W. Bayliff, M.C. Gibson, M.J. Carter, L. Chen, et al., Defining a new diagnostic assessment parameter for wound care: Elevated protease activity, an indicator of nonhealing, for targeted protease-modulating treatment, Wound Repair Regen. 24 (2016) 589–595. doi:10.1111/wrr.12431.

[226] Systagenix Wound Management, WOUNDCHEK™ Protease Status Point of Care (POC) Diagnostic Test, `ClinicalTrials.gov Identifier: NCT01537003. (2012).

https://clinicaltrials.gov/ct2.

[227] J. Edwards, S. Caston-Pierre, A.F. Bopp, W. Goynes, Detection of human neutrophil elastase with ethoxylate acrylate resin analogs, J. Pept. Res. 66 (2005) 160–168. doi:10.1111/j.1399-3011.2005.00284.x.

[228] T.G. Henares, M. Takaishi, N. Yoshida, S. Terabe, F. Mizutani, R. Sekizawa, et al., Integration of multianalyte sensing functions on a capillary-assembled microchip: Simultaneous determination of ion concentrations and enzymatic activities by a "drop-and-sip" technique, Anal. Chem. 79 (2007) 908–915. doi:10.1021/ac061245i.

[229] Y. Wang, D. V. Zagorevski, J.A. Stenken, In situ and multisubstrate detection of elastase enzymatic activity external to microdialysis sampling probes using LC-ESI-MS, Anal. Chem. 80 (2008) 2050–2057. doi:10.1021/ac702047w.

[230] J.L. Stair, M. Watkinson, S. Krause, Sensor materials for the detection of proteases, Biosens. Bioelectron. 24 (2009) 2113–2118. doi:10.1016/j.bios.2008.11.002.

[231] A. Hasmann, E. Wehrschuetz-Sigl, G. Kanzler, U. Gewessler, E. Hulla, K.P. Schneider, et al., Novel peptidoglycan-based diagnostic devices for detection of wound infection, Diagn. Microbiol. Infect. Dis. 71 (2011) 12–23. doi:10.1016/j.diagmicrobio.2010.09.009.

[232] J.V. Edwards, N. Prevost, K. Sethumadhavan, A. Ullah, B. Condon, Peptide conjugated cellulose nanocrystals with sensitive human neutrophil elastase sensor activity, Cellulose. 20 (2013) 1223–1235. doi:10.1007/s10570-013-9901-y.

[233] J.V. Edwards, N.T. Prevost, A.D. French, M. Concha, B.D. Condon, Kinetic and structural analysis of fluorescent peptides on cotton cellulose nanocrystals as elastase sensors, Carbohydr. Polym. 116 (2015) 278–285. doi:10.1016/j.carbpol.2014.04.067.

[234] J.V. Edwards, K.R. Fontenot, N.T. Prevost, N. Pircher, F. Liebner, B.D. Condon, Preparation, Characterization and Activity of a Peptide-Cellulosic Aerogel Protease Sensor from Cotton, Sensors (Basel). 16 (2016) 1–19. doi:10.3390/s16111789.

[235] K.R. Fontenot, J.V. Edwards, D. Haldane, E. Graves, M.S. Citron, N.T. Prevost, et al., Human neutrophil elastase detection with fluorescent peptide sensors conjugated to cellulosic and nanocellulosic materials: part II, structure/function analysis, Cellulose. 23 (2016) 1297–1309. doi:10.1007/s10570-016-0873-6.

[236] K.R. Fontenot, J.V. Edwards, D. Haldane, N. Pircher, F. Liebner, B.D. Condon, et al., Designing cellulosic and nanocellulosic sensors for interface with a protease sequestrant wound-dressing prototype: Implications of material selection for dressing and protease sensor design, J. Biomater. Appl. 32 (2017) 622–637. doi:10.1177/0885328217735049.

[237] C. Schulenburg, G. Faccio, D. Jankowska, K. Maniura-Weber, M. Richter, A FRET-based biosensor for the detection of neutrophil elastase, Analyst. 141 (2016) 1645–1648. doi:10.1039/C5AN01747E.

[238] G. Faccio, S. Salentinig, Enzyme-Triggered Dissociation of a FRET-Based Protein Biosensor Monitored by Synchrotron SAXS, Biophys. J. 113 (2017) 1731–1737. doi:10.1016/j.bpj.2017.08.044.

[239] L. Macgregor, S. Calne, K. Day, J. Jones, A. Pugh, Wound Infection in Clinical Practice.,

Int. Wound J. 5 (2008) iii-11. doi:10.1111/j.1742-481X.2008.00488.x.

[240] A. Vasconcelos, A.P. Pêgo, L. Henriques, M. Lamghari, A. Cavaco-Paulo, Protein Matrices for Improved Wound Healing: Elastase Inhibition by a Synthetic Peptide Model, Biomacromolecules. 11 (2010) 2213–2220. doi:10.1021/bm100537b.

[241] A. Vasconcelos, N.G. Azoia, A.C. Carvalho, A.C. Gomes, G. Güebitz, A. Cavaco-Paulo, Tailoring elastase inhibition with synthetic peptides, Eur. J. Pharmacol. 666 (2011) 53–60. doi:10.1016/j.ejphar.2011.05.056.

[242] S.C. Barros, R.O. Louro, N.M. Micaêlo, J.A. Martins, J.C. Marcos, A. Cavaco-Paulo, NMR and molecular modelling studies on elastase inhibitor-peptides for wound management, React. Funct. Polym. 73 (2013) 1357–1365. doi:10.1016/j.reactfunctpolym.2013.02.011.

[243] O. V. Stepanenko, O. V. Stepanenko, I.M. Kuznetsova, V. V. Verkhusha, K.K. Turoverov, Beta-Barrel Scaffold of Fluorescent Proteins, in: 2013: pp. 221–278. doi:10.1016/B978-0-12-407699-0.00004-2.

[244] S. Cabantous, T.C. Terwilliger, G.S. Waldo, Protein tagging and detection with engineered self-assembling fragments of green fluorescent protein., Nat. Biotechnol. 23 (2005) 102–107. doi:10.1038/nbt1044.

[245] B.P. Callahan, M.J. Stanger, M. Belfort, Protease Activation of Split Green Fluorescent Protein, ChemBioChem. 11 (2010) 2259–2263. doi:10.1002/cbic.201000453.

[246] G.L. Hansen, E.M. Sparrow, J.Y. Kokate, K.J. Leland, P.A. Iaizzo, Wound status evaluation using color image processing, IEEE Trans. Med. Imaging. 16 (1997) 78–86. doi:10.1109/42.552057.

[247] G. Tegl, A. Rollett, J. Dopplinger, C. Gamerith, G.M. Guebitz, Chitosan based substrates for wound infection detection based on increased lysozyme activity, Carbohydr. Polym. 151 (2016) 260–267. doi:10.1016/j.carbpol.2016.05.069.

[248] D. Schiffer, G. Tegl, R. Vielnascher, H. Weber, A. Herrero-Rollett, E. Sigl, et al., Myeloperoxidase-responsive materials for infection detection based on immobilized aminomethoxyphenol, Biotechnol. Bioeng. 113 (2016) 2553–2560. doi:10.1002/bit.26025.

[249] A. Pettikiriarachchi, L. Gong, M.A. Perugini, R.J. Devenish, M. Prescott, Ultramarine, a Chromoprotein Acceptor for Förster Resonance Energy Transfer, PLoS One. 7 (2012) e41028. doi:10.1371/journal.pone.0041028.

[250] M. Prescott, M. Ling, T. Beddoe, A.J. Oakley, S. Dove, O. Hoegh-Guldberg, et al., The 2.2 Å Crystal Structure of a Pocilloporin Pigment Reveals a Nonplanar Chromophore Conformation, Structure. 11 (2003) 275–284. doi:10.1016/S0969-2126(03)00028-5.

[251] C.T. Chung, S.L. Niemela, R.H. Miller, One-step preparation of competent Escherichia coli: transformation and storage of bacterial cells in the same solution., Proc. Natl. Acad. Sci. 86 (1989) 2172–2175. doi:10.1073/pnas.86.7.2172.

[252] L. Schrödinger, The PyMOL Molecular Graphics System, (n.d.).

[253] G.M. Morris, R. Huey, W. Lindstrom, M.F. Sanner, R.K. Belew, D.S. Goodsell, et al.,

AutoDock4 and AutoDockTools4: Automated docking with selective receptor flexibility, J. Comput. Chem. 30 (2009) 2785–2791. doi:10.1002/jcc.21256.

[254] O. Trott, A.J. Olson, AutoDock Vina: Improving the speed and accuracy of docking with a new scoring function, efficient optimization, and multithreading, J. Comput. Chem. (2009) NA-NA. doi:10.1002/jcc.21334.

[255] S. Cabantous, G.S. Waldo, *In vivo* and *in vitro* protein solubility assays using split GFP, Nat. Methods. 3 (2006) 845–854. doi:10.1038/nmeth932.

[256] A. Yasutake, J.C. Powers, Reactivity of Human Leukocyte Elastase and Porcine Pancreatic Elastase toward Peptide 4-Nitroanilides Containing Model Desmosine Residues. Evidence That Human Leukocyte Elastase Is Selective for Cross-Linked Regions of Elastin, Biochemistry. 20 (1981) 3675–3679. doi:10.1021/bi00516a002.

[257] I. Schechter, Reprint of "On the Size of the Active Site in Proteases. I. Papain," Biochem. Biophys. Res. Commun. 425 (2012) 497–502. doi:10.1016/j.bbrc.2012.08.015.

[258] G.D. Virca, G. Metz, H.P. Schnebli, Similarities between human and rat leukocyte elastase and cathepsin G., Eur. J. Biochem. 144 (1984) 1–9. http://www.ncbi.nlm.nih.gov/pubmed/6566611.

[259] S.C. Tyagi, Reversible inhibition of neutrophil elastase by thiol-modified alpha-1 protease inhibitor., J. Biol. Chem. 266 (1991) 5279–85. http://www.ncbi.nlm.nih.gov/pubmed/2002060.

[260] K. Nakajima, J.C. Powers, B.M. Ashe, M. Zimmerman, Mapping the extended substrate binding site of cathepsin G and human leukocyte elastase. Studies with peptide substrates related to the alpha 1-protease inhibitor reactive site., J. Biol. Chem. 254 (1979) 4027–32. http://www.ncbi.nlm.nih.gov/pubmed/312290.

[261] P. Artimo, M. Jonnalagedda, K. Arnold, D. Baratin, G. Csardi, E. de Castro, et al., ExPASy: SIB bioinformatics resource portal, Nucleic Acids Res. 40 (2012) W597–W603. doi:10.1093/nar/gks400.

[262] X. Du, Y. Li, Y.-L. Xia, S.-M. Ai, J. Liang, P. Sang, et al., Insights into Protein–Ligand Interactions: Mechanisms, Models, and Methods, Int. J. Mol. Sci. 17 (2016) 144. doi:10.3390/ijms17020144.

[263] N. Brooijmans, I.D. Kuntz, Molecular Recognition and Docking Algorithms, Annu. Rev. Biophys. Biomol. Struct. 32 (2003) 335–373. doi:10.1146/annurev.biophys.32.110601.142532.

[264] V. V Verkhusha, K.A. Lukyanov, The molecular properties and applications of Anthozoa fluorescent proteins and chromoproteins, Nat. Biotechnol. 22 (2004) 289–296. doi:10.1038/nbt943.

[265] O. V Stepanenko, V. V Verkhusha, I.M. Kuznetsova, V.N. Uversky, K.K. Turoverov, Fluorescent proteins as biomarkers and biosensors: throwing color lights on molecular and cellular processes., Curr. Protein Pept. Sci. 9 (2008) 338–69. doi:10.1016/j.neuron.2009.10.017.A.

[266] A. Hense, K. Nienhaus, G.U. Nienhaus, Exploring color tuning strategies in red fluorescent proteins, Photochem. Photobiol. Sci. 14 (2015) 200–212. doi:10.1039/C4PP00212A.

[267] D. E., Y.-M. Huang, D. J., C. Schenkelberg, K. Fraser, S. Macari, et al., GFP-Based Biosensors, in: State Art Biosens. - Gen. Asp., InTech, 2013. doi:10.5772/52250.

[268] S.M. Singh, A.K. Panda, Solubilization and refolding of bacterial inclusion body proteins, J. Biosci. Bioeng. 99 (2005) 303–310. doi:10.1263/jbb.99.303.

[269] G.L. Rosano, E.A. Ceccarelli, Recombinant protein expression in Escherichia coli: Advances and challenges, Front. Microbiol. 5 (2014) 1–17. doi:10.3389/fmicb.2014.00172.

[270] H.P. Sørensen, K.K. Mortensen, Soluble expression of recombinant proteins in the cytoplasm of Escherichia coli., Microb. Cell Fact. 4 (2005) 1. doi:10.1186/1475-2859-4-1.

[271] H. Yamaguchi, M. Miyazaki, Refolding techniques for recovering biologically active recombinant proteins from inclusion bodies, Biomolecules. 4 (2014) 235–251. doi:10.3390/biom4010235.

[272] L.A. Palomares, S. Estrada-Mondaca, O.T. Ramírez, Production of Recombinant Proteins: Challenges and Solutions, Recomb. Gene Expr. 267 (2004) 1–39. doi:10.1385/1-59259-774-2:015.

[273] R.R. Burgess, Chapter 17 Refolding Solubilized Inclusion Body Proteins, 1st ed., Elsevier Inc., 2009. doi:10.1016/S0076-6879(09)63017-2.

[274] T.R. Butt, S.C. Edavettal, J.P. Hall, M.R. Mattern, SUMO fusion technology for difficult-to-express proteins, Protein Expr. Purif. 43 (2005) 1–9. doi:10.1016/j.pep.2005.03.016.

[275] K.Y. Han, J.A. Song, K.Y. Ahn, J.S. Park, H.S. Seo, J. Lee, Enhanced solubility of heterologous proteins by fusion expression using stress-induced Escherichia coli protein, Tsf, FEMS Microbiol. Lett. 274 (2007) 132–138. doi:10.1111/j.1574-6968.2007.00824.x.

[276] A. Singh, V. Upadhyay, A.K. Upadhyay, S.M. Singh, A.K. Panda, Protein recovery from inclusion bodies of Escherichia coli using mild solubilization process, Microb. Cell Fact. 14 (2015) 41. doi:10.1186/s12934-015-0222-8.

[277] I. Palmer, P.T. Wingfield, Preparation and Extraction of Insoluble (Inclusion-Body) Proteins from Escherichia coli, in: Curr. Protoc. Protein Sci., John Wiley & Sons, Inc., Hoboken, NJ, USA, 2004: p. 6.3.1-6.3.18. doi:10.1002/0471140864.ps0603s38.

[278] S. Gräslund, P. Nordlund, J. Weigelt, B.M. Hallberg, J. Bray, O. Gileadi, et al., Protein production and purification, Nat. Methods. 5 (2008) 135–146. doi:10.1038/nmeth.f.202.

[279] H. Tao, W. Liu, B.N. Simmons, H.K. Harris, C. Cox, M.A. Massiah, Benchmarks Purifying natively folded proteins, (2010) 61–63. doi:10.2144/000113304.

[280] M.M.H.M. Zimmer, B. Li, R. Shahid, P. Peshkepija, M.M.H.M. Zimmer, Structural consequences of chromophore formation and exploration of conserved lid residues amongst naturally occurring fluorescent proteins, Chem. Phys. 429 (2014) 5–11. doi:10.1016/j.chemphys.2013.11.015.

[281] U. Shimanovich, D. Pinotsi, K. Shimanovich, N. Yu, S. Bolisetty, J. Adamcik, et al.,

Biophotonics of Native Silk Fibrils, Macromol. Biosci. 1700295 (2018) 1700295. doi:10.1002/mabi.201700295.

[282] U. Shimanovich, T.C.T. Michaels, E. De Genst, D. Matak-Vinkovic, C.M. Dobson, T.P.J. Knowles, Sequential Release of Proteins from Structured Multishell Microcapsules, Biomacromolecules. 18 (2017) 3052–3059. doi:10.1021/acs.biomac.7b00351.

[283] F.T.S. Chan, G.S. Kaminski Schierle, J.R. Kumita, C.W. Bertoncini, C.M. Dobson, C.F. Kaminski, Protein amyloids develop an intrinsic fluorescence signature during aggregation, Analyst. 138 (2013) 2156. doi:10.1039/c3an36798c.

[284] W.J.-H. Ong, S. Alvarez, *I.E.* Leroux, R.S. Shahid, A. a Samma, P. Peshkepija, et al., Function and structure of GFP-like proteins in the protein data bank, Mol. Biosyst. 7 (2011) 984. doi:10.1039/c1mb05012e.

[285] B. Li, R. Shahid, P. Peshkepija, M. Zimmer, Water diffusion in and out of the β-barrel of GFP and the fast maturing fluorescent protein, TurboGFP, Chem. Phys. 392 (2012) 143–148. doi:10.1016/j.chemphys.2011.11.001.

[286] G. Flores-Ramírez, M. Rivera, A. Morales-Pablos, J. Osuna, X. Soberón, P. Gaytán, The effect of amino acid deletions and substitutions in the longest loop of GFP, BMC Chem. Biol. 7 (2007) 1. doi:10.1186/1472-6769-7-1.

[287] W. Humphrey, A. Dalke, K. Schulten, VMD: visual molecular dynamics., J. Mol. Graph. 14 (1996) 33–8, 27–8. http://www.ncbi.nlm.nih.gov/pubmed/8744570.

[288] E. Lindahl, B. Hess, D. van der Spoel, GROMACS 3.0: A package for molecular simulation and trajectory analysis., J. Mol. Model. (2001) 306–317.

[289] H.J.C. Berendsen, D. van der Spoel, R. van Drunen, GROMACS: A message-passing parallel molecular dynamics implementation, Comput. Phys. Commun. 91 (1995) 43–56. doi:10.1016/0010-4655(95)00042-E.

[290] W.R.P. Scott, P.H. Hünenberger, I.G. Tironi, A.E. Mark, S.R. Billeter, J. Fennen, et al., The GROMOS Biomolecular Simulation Program Package, J. Phys. Chem. A. 103 (1999) 3596–3607. doi:10.1021/jp984217f.

[291] N. Schmid, A.P. Eichenberger, A. Choutko, S. Riniker, M. Winger, A.E. Mark, et al., Definition and testing of the GROMOS force-field versions 54A7 and 54B7, Eur. Biophys. J. 40 (2011) 843–856. doi:10.1007/s00249-011-0700-9.

[292] W. Huang, Z. Lin, W.F. van Gunsteren, Validation of the GROMOS 54A7 Force Field with Respect to β-Peptide Folding, J. Chem. Theory Comput. 7 (2011) 1237–1243. doi:10.1021/ct100747y.

[293] B. Hess, H. Bekker, H.J.C. Berendsen, J.G.E.M. Fraaije, LINCS: A linear constraint solver for molecular simulations, J. Comput. Chem. 18 (1997) 1463–1472. doi:10.1002/(SICI)1096-987X(199709)18:12<1463::AID-JCC4>3.0.CO;2-H.

[294] S. Miyamoto, P.A. Kollman, Settle: An analytical version of the SHAKE and RATTLE algorithm for rigid water models, J. Comput. Chem. 13 (1992) 952–962. doi:10.1002/jcc.540130805.

[295] J. Hermans, H.J.C. Berendsen, W.F. Van Gunsteren, J.P.M. Postma, A consistent

empirical potential for water-protein interactions, Biopolymers. 23 (1984) 1513–1518. doi:10.1002/bip.360230807.

[296] H.J.C. Berendsen, J.P.M. Postma, W.F. van Gunsteren, A. DiNola, J.R. Haak, Molecular dynamics with coupling to an external bath, J. Chem. Phys. 81 (1984) 3684–3690. doi:10.1063/1.448118.

[297] G. Bussi, D. Donadio, M. Parrinello, Canonical sampling through velocity rescaling, J. Chem. Phys. 126 (2007) 14101. doi:10.1063/1.2408420.

[298] M. Parrinello, A. Rahman, Polymorphic transitions in single crystals: A new molecular dynamics method, J. Appl. Phys. 52 (1981) 7182–7190. doi:10.1063/1.328693.

[299] S. Nosé, M.L. Klein, Constant pressure molecular dynamics for molecular systems, Mol. Phys. 50 (1983) 1055–1076. doi:10.1080/00268978300102851.

[300] P.E. Smith, W.F. van Gunsteren, Consistent dielectric properties of the simple point charge and extended simple point charge water models at 277 and 300 K, J. Chem. Phys. 100 (1994) 3169–3174. doi:10.1063/1.466407.

[301] T. Beddoe, M. Ling, S. Dove, O. Hoegh-Guldberg, R.J. Devenish, M. Prescott, et al., The production, purification and crystallization of a pocilloporin pigment from a reef-forming coral, Acta Crystallogr. - Sect. D Biol. Crystallogr. 59 (2003) 597–599. doi:10.1107/S0907444902023466.

[302] B.T. Andrews, M. Roy, P.A. Jennings, Chromophore Packing Leads to Hysteresis in GFP, J. Mol. Biol. 392 (2009) 218–227. doi:10.1016/j.jmb.2009.06.072.

[303] B.R. Branchini, A.R. Nemser, M. Zimmer, A computational analysis of the unique protein-induced tight turn that results in posttranslational chromophore formation in green fluorescent protein, J. Am. Chem. Soc. 120 (1998) 1–6. doi:10.1021/ja973019j.

[304] B.L. Grigorenko, A.I. Krylov, A. V. Nemukhin, Molecular Modeling Clarifies the Mechanism of Chromophore Maturation in the Green Fluorescent Protein, J. Am. Chem. Soc. 139 (2017) 10239–10249. doi:10.1021/jacs.7b00676.

[305] J. Petersen, P.G. Wilmann, T. Beddoe, A.J. Oakley, R.J. Devenish, M. Prescott, et al., The 2.0-Å Crystal Structure of eqFP611, a Far Red Fluorescent Protein from the Sea Anemone Entacmaea quadricolor, J. Biol. Chem. 278 (2003) 44626–44631. doi:10.1074/jbc.M307896200.

[306] T.D. Craggs, Green fluorescent protein: structure, folding and chromophore maturation, Chem. Soc. Rev. 38 (2009) 2865. doi:10.1039/b903641p.

[307] J.L. Fu, T. Kanno, S.-C. Liang, A.J.M. Matzke, M. Matzke, GFP Loss-of-Function Mutations in Arabidopsis thaliana., G3 (Bethesda). 5 (2015) 1849–55. doi:10.1534/g3.115.019604.

[308] J. Chen, B. Shen, Computational Analysis of Amino Acid Mutation: A Proteome Wide Perspective, Curr. Proteomics. 6 (2009) 228–234. doi:10.2174/157016409789973734.

[309] N. Nagasundaram, H. Zhu, J. Liu, V. Karthick, C. George Priya Doss, C. Chakraborty, et al., Analysing the effect of mutation on protein function and discovering potential

inhibitors of CDK4: Molecular modelling and dynamics studies, PLoS One. 10 (2015) 1–21. doi:10.1371/journal.pone.0133969.

[310] M. Alaraby Salem, A. Brown, Two-photon absorption of fluorescent protein chromophores incorporating non-canonical amino acids: TD-DFT screening and classical dynamics, Phys. Chem. Chem. Phys. 17 (2015) 25563–25571. doi:10.1039/C5CP03875H.

[311] S.E. Herrick, P. Sloan, M. McGurk, L. Freak, C.N. McCollum, M.W. Ferguson, Sequential changes in histologic pattern and extracellular matrix deposition during the healing of chronic venous ulcers., Am. J. Pathol. 141 (1992) 1085–95. http://www.pubmedcentral.nih.gov/articlerender.fcgi?artid=1886678&tool=pmcentrez&rendertype=abstract.

[312] J.R. Lakowicz, Principles of Fluorescence Spectroscopy, Springer US, Boston, MA, 2006. doi:10.1007/978-0-387-46312-4.

[313] S. Adhikari, A. Ghosh, S. Mandal, A. Sengupta, A. Chattopadhyay, J. Sanmartín Matalobos, et al., Visible light excitable ON fluorescence and naked eye detection of Cu^{2+} via hydrolysis of rhodamine-thiophene conjugate: human breast cancer cell (MCF7) imaging studies., Dalton Trans. 43 (2014) 7747–51. doi:10.1039/c4dt00002a.

[314] A.K. Carmona, M.A. Juliano, L. Juliano, The use of Fluorescence Resonance Energy Transfer (FRET) peptides for measurement of clinically important proteolytic enzymes., An. Acad. Bras. Cienc. 81 (2009) 381–92. http://www.ncbi.nlm.nih.gov/pubmed/19722010.

[315] H. Fan, X. Jiang, T. Zhang, Q. Jin, Peptide-induced fluorescence quenching of conjugated polyelectrolyte for label-free, ultrasensitive and selective assay of protease activity, Biosens. Bioelectron. 34 (2012) 221–226. doi:10.1016/j.bios.2012.02.006.

[316] A. Gedanken, Using sonochemistry for the fabrication of nanomaterials, Ultrason. Sonochem. 11 (2004) 47–55. doi:10.1016/j.ultsonch.2004.01.037.

[317] N. Perkas, G. Amirian, S. Dubinsky, S. Gazit, A. Gedanken, Ultrasound-assisted coating of nylon 6,6 with silver nanoparticles and its antibacterial activity, J. Appl. Polym. Sci. 104 (2007) 1423–1430. doi:10.1002/app.24728.

[318] V.G. Pol, A. Gedanken, J. Calderon-Moreno, V. Palchik, M. a Slifkin, a M. Weiss, Deposition of Gold Nanoparticles on Silica Spheres: A Sonochemical Approach., Chem. Mater. 15 (2003) 3402–3402. doi:10.1021/cm033005e.

[319] I. Perelshtein, G. Applerot, N. Perkas, E. Wehrschetz-Sigl, A. Hasmann, G.M. Guebitz, et al., Antibacterial properties of an in situ generated and simultaneously deposited nanocrystalline ZnO on fabrics, ACS Appl. Mater. Interfaces. 1 (2009) 361–366. doi:10.1021/am8000743.

[320] D. Sunartio, K. Yasui, T. Tuziuti, T. Kozuka, Y. Iida, M. Ashokkumar, et al., Correlation between Na* Emission and “Chemically Active” Acoustic Cavitation Bubbles, ChemPhysChem. 8 (2007) 2331–2335. doi:10.1002/cphc.200700426.

[321] A. Mersmann, Crystallization Technology Handbook, A. Mersman, CRC Press, 2001.

[322] I. Perelshtein, A. Lipovsky, N. Perkas, T. Tzanov, M. Arguirova, M. Leseva, et al., Making the hospital a safer place by sonochemical coating of all its textiles with antibacterial

nanoparticles, Ultrason. Sonochem. 25 (2015) 82–88. doi:10.1016/j.ultsonch.2014.12.012.

[323] B. Brena, P. González-Pombo, F. Batista-Viera, Immobilization of Enzymes: A Literature Survey, in: Immobil. Enzym. Cells Third Ed., 2013: pp. 15–31. doi:10.1007/978-1-62703-550-7_2.

[324] M.D. Trevan, Enzyme Immobilization by Covalent Bonding, in: New Protein Tech., Humana Press, New Jersey, 1988: pp. 495–510. doi:10.1385/0-89603-126-8:495.

[325] T.M. Monro, R.L. Moore, M.C. Nguyen, H. Ebendorff-Heidepriem, G.K. Skouroumounis, G.M. Elsey, et al., Sensing free sulfur dioxide in wine, Sensors (Switzerland). 12 (2012) 10759–10773. doi:10.3390/s120810759.

[326] S. Scharpé, I. De Meester, G. Vanhoof, D. Hendriks, M. van Sande, K. Van Camp, et al., Assay of dipeptidyl peptidase IV in serum by fluorometry of 4-methoxy-2-naphthylamine., Clin. Chem. 34 (1988) 2299–301. http://www.ncbi.nlm.nih.gov/pubmed/2902942.

[327] R. Bru, P. Walde, Product inhibition of alpha-chymotrypsin in reverse micelles., Eur. J. Biochem. 199 (1991) 95–103. http://www.ncbi.nlm.nih.gov/pubmed/1712303.

[328] C. Silva, C.J. Silva, A. Zille, G.M. Guebitz, A. Cavaco-Paulo, Laccase immobilization on enzymatically functionalized polyamide 6,6 fibres, Enzyme Microb. Technol. 41 (2007) 867–875. doi:10.1016/j.enzmictec.2007.07.010.

[329] S. Kiel, O. Grinberg, N. Perkas, J. Charmet, H. Kepner, A. Gedanken, Forming nanoparticles of water-soluble ionic molecules and embedding them into polymer and glass substrates, Beilstein J. Nanotechnol. 3 (2012) 267–276. doi:10.3762/bjnano.3.30.

[330] I. Perelshtein, E. Ruderman, A. Francesko, M.M. Fernandes, T. Tzanov, A. Gedanken, Tannic acid NPs – Synthesis and immobilization onto a solid surface in a one-step process and their antibacterial and anti-inflammatory properties, Ultrason. Sonochem. 21 (2014) 1916–1920. doi:10.1016/j.ultsonch.2013.11.022.

[331] I. Medintz, N. Hildebrandt, FRET - Förster Resonance Energy Transfer, Wiley-VCH Verlag GmbH & Co. KGaA, Weinheim, Germany, 2013. doi:10.1002/9783527656028.

[332] B.R. Masters, Paths to Förster's resonance energy transfer (FRET) theory, Eur. Phys. J. H. 39 (2014) 87–139. doi:10.1140/epjh/e2013-40007-9.

[333] J. Szöllosi, S. Damjanovich, L. Mátyus, Application of fluorescence resonance energy transfer in the clinical laboratory: routine and research., Cytometry. 34 (1998) 159–79. doi:10.1002/(SICI)1097-0320(19980815)34:4<159::AID-CYTO1>3.0.CO;2-B.

[334] S. Tabassum, W.M. Al-Asbahy, M. Afzal, F. Arjmand, R. Hasan Khan, Interaction and photo-induced cleavage studies of a copper based chemotherapeutic drug with human serum albumin: spectroscopic and molecular docking study, Mol. Biosyst. 8 (2012) 2424. doi:10.1039/c2mb25119a.

[335] I. Migneault, C. Dartiguenave, M.J. Bertrand, K.C. Waldron, Glutaraldehyde: behavior in aqueous solution, reaction with proteins, and application to enzyme crosslinking., Biotechniques. 37 (2004) 790–6, 798–802. doi:10.2144/3705A0790.

[336] C. Byrne, Technical textiles market – an overview, in: A.R. Horrocks, S.C. Anand (Eds.),

Handb. Tech. Text., Elsevier, Boca Raton Boston New York Washington, DC, 2000: pp. 1–23. doi:10.1533/9781855738966.1.

[337] J.S. Bowers, Toluidines, in: Ullmann's Encycl. Ind. Chem., Wiley-VCH Verlag GmbH & Co. KGaA, Weinheim, Germany, 2000: pp. 119–126. doi:10.1002/14356007.a27_159.

[338] M.P. Gashti, J. Willoughby, P. Agrawal, Surface and Bulk Modification of Synthetic Textiles to Improve Dyeability, Text. Dye. 18 (2011) 927–929. doi:10.5772/800.

[339] S. Begum, J. Wu, C.M. Takawira, J. Wang, Surface Modification of Polyamide 6 , 6 Fabrics with an Alkaline Protease – Subtilisin, J. Eng. Fiber. Fabr. 11 (2016) 64–74. http://www.jeffjournal.org/papers/Volume11/V11I1.9 J. Wang.pdf.

[340] N. Laurent, R. Haddoub, S.L. Flitsch, Enzyme catalysis on solid surfaces, Trends Biotechnol. 26 (2008) 328–337. doi:10.1016/j.tibtech.2008.03.003.

[341] C.J. Gray, M.J. Weissenborn, C.E. Eyers, S.L. Flitsch, Enzymatic reactions on immobilised substrates, Chem. Soc. Rev. 42 (2013) 6378. doi:10.1039/c3cs60018a.

[342] L.A. Schneider, A. Korber, S. Grabbe, J. Dissemond, Influence of pH on wound-healing: a new perspective for wound-therapy?, Arch. Dermatol. Res. 298 (2007) 413–420. doi:10.1007/s00403-006-0713-x.

[343] A.L. Niles, R.A. Moravec, T.L. Riss, *In vitro* Viability and Cytotoxicity Testing and Same-Well Multi-Parametric Combinations for High Throughput Screening, Curr. Chem. Genomics. 3 (2009) 33–41. doi:10.2174/1875397300903010033.

[344] A.L. Niles, R.A. Moravec, P. Eric Hesselberth, M.A. Scurria, W.J. Daily, T.L. Riss, A homogeneous assay to measure live and dead cells in the same sample by detecting different protease markers, Anal. Biochem. 366 (2007) 197–206. doi:10.1016/j.ab.2007.04.007.

[345] M. Alvarez-Iglesias, G. Wayne, K.P. O'Dea, A. Amour, M. Takata, Continuous real-time measurement of tumor necrosis factor-α converting enzyme activity on live cells, Lab. Investig. 85 (2005) 1440–1448. doi:10.1038/labinvest.3700340.

[346] L. Shang, S. Zhang, X. Yang, J. Sun, L. Li, Z. Cui, et al., Biochemical Characterization of Recombinant Enterovirus 71 3C Protease with Fluorogenic Model Peptide Substrates and Development of a Biochemical Assay, Antimicrob. Agents Chemother. 59 (2015) 1827–1836. doi:10.1128/AAC.04698-14.

[347] K. Turcic, A. Pettikiriarachchi, J. Battad, P.G. Wilmann, J. Rossjohn, S.G. Dove, et al., Amino acid substitutions around the chromophore of the chromoprotein Rtms5 influence polypeptide cleavage, Biochem. Biophys. Res. Commun. 340 (2006) 1139–1143. doi:10.1016/j.bbrc.2005.12.118.

[348] P.S. Langan, D.W. Close, L. Coates, R.C. Rocha, K. Ghosh, C. Kiss, et al., Corrigendum to "Evolution and Characterization of a New Reversibly Photoswitching Chromogenic Protein, Dathail" [J. Mol. Biol., 428, (2016), 1776–89], J. Mol. Biol. 428 (2016) 4244. doi:10.1016/j.jmb.2016.08.024.

[349] K.P. Kent, S.G. Boxer, Light-Activated Reassembly of Split Green Fluorescent Protein, J. Am. Chem. Soc. 133 (2011) 4046–4052. doi:10.1021/ja110256c.

[350] J.M. Battad, D. a K. Traore, E. Byres, J. Rossjohn, R.J. Devenish, S. Olsen, et al., A Green Fluorescent Protein Containing a QFG Tri-Peptide Chromophore: Optical Properties and X-Ray Crystal Structure, PLoS One. 7 (2012) 1–14. doi:10.1371/journal.pone.0047331.

APPENDIX

APPENDIX

Scientific publications

In the scope of this dissertation:

Ferreira, A. V., Perelshtein, I., Perkas, N., Gedanken, A., Cunha, J. and Cavaco-Paulo, A. (2015). Detection of human neutrophil elastase (HNE) on wound dressings as marker of inflammation *in Applied Microbiology and Biotechnology*, doi: 10.1007/s00253-016-7889-6.

In other scientific fields:

Volkov, V., **Ferreira, A. V.** and Cavaco-Paulo, A. (2015). On the Routines of Wild-Type Silk Fibroin Processing Toward Silk-Inspired Materials: A Review *in Macromolecular Materials and Engineering*, doi: 10.1002/mame.201500179.

Ferreira, A. V., Volkov, V., Abreu, A. S., Azoia, N., Botelho, C. M. and Cavaco-Paulo, A. (2015). Orange IV stabilizes silk fibroin microemulsions *in Engineering in Life Sciences*, doi: 10.1002/elsc.201400190.

Publications in Scientific Meetings

In the scope of this dissertation:

Ferreira, A. V., Cunha, J. and Cavaco-Paulo, A., Monitoring human neutrophil elastase (HNE) in chronic wounds. Oral presentation. *Designer Biology: From Proteins and Cells to Scaffolds & Materials.* Vienna, Austria, June 7-9, 2017.

Ferreira, A. V., Cunha, J. and Cavaco-Paulo, A., Monitoring human neutrophil elastase (HNE) in chronic wounds. Oral presentation at the CELL Division (Cellulose and Renewable Materials) in the Special Issue of Biomedical & Drug Delivery Applications of Polysaccharide-Based Materials, CELL 325. *ACS – 251st American Chemical Society National Meeting & Exposition*. San Diego, United States of America, May 13-17, 2016.

In other scientific fields:

Ferreira, A. V., Volkov, V., Vasconcelos, A., Abreu, A. S., Azoia, N., Botelho, C. M. and Cavaco-Paulo, A., Silk Fibroin Nanoparticles for Drug Delivery purposes: Stabilization, Incorporation and Release Design. Oral presentation. *IPFB2014 - 8th International Conference on Polymer and Fiber Biotechnology.* Braga, Portugal, May 25-27, 2014.

Poster Communications

In other scientific fields:

J.M. Ribeiro; J.C. Dias; **A.V. Ferreira**; A.P. Bettencourt and M.D. Geraldo, Quantification of antioxidants in foodstuff by LC-MS. Poster presentation *in* 2nd *Portuguese Young Chemists Meeting*, University of Aveiro, April 21-23, 2010.

Other Communications

In the scope of this dissertation:

A.V. Ferreira and Cavaco-Paulo, A., High-Tech Health: Dressing that detects early infected wounds "*Saúde High-Tech: Penso deteta precocemente feridas infetadas*". Oral presentation *in Evento CEB Talk*, November 27, 2015.

A.V. Ferreira and Cavaco-Paulo, A., Dressings that detect infection. Oral presentation *in XVIII Symposium of Biological Engineering*, November 25, 2015.

A.V. Ferreira and Cavaco-Paulo, A., Dressings that detect when a chronic wound is infected, "*Pensos rápidos que detetam quando uma ferida crónica está infetada*". Reportage *in SIC*, January 26, 2015.

A.V. Ferreira and Cavaco-Paulo, A., University of Minho' innovative dressings detect infection in wounds, "*Pensos inovadores da UMinho detetam infeções em feridas*". Reportage *in Porto Canal*, January 30, 2015.

“ **Cat:** Where are you going?

Alice: Which way should I go?

Cat: That depends on where you are going.

Alice: I don’t know.

Cat: Then it doesn’t matter which way you go. ”

Lewis Carroll
***in* Alice in Wonderland**

